AN EXPERIMENTAL INVESTIGATION OF DROPWISE AND FILMWISE CONDENSATION OF LOW PRESSURE STEAM IN TUBE BANKS

BY

GRANT CUTHBERTSON

Volume 1 of 2

SUBMITTED FOR THE DEGREE OF

DOCTOR OF PHILOSOPHY

AT HERIOT-WATT UNIVERSTIY

ON COMPLETION OF RESEARCH IN THE

DEPARTMENT OF MECHANICAL

AND CHEMICAL ENGINEERING

JULY 1999

DECLARATION

I hereby declare that the work presented in this thesis was carried out by myself at Heriot-Watt University, Edinburgh, except where due acknowledgement is made, and that this thesis nor any part of it, has been or is being concurrently submitted in candidature for any degree at any other university.

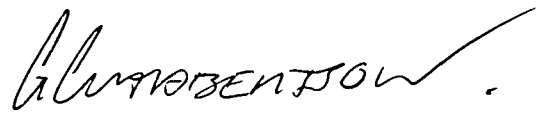

Grant Cuthbertson (Candidate)

Dr. D. A. McNeil (Supervisor)

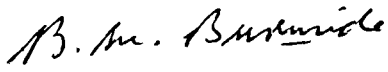

Dr. B. M. Burnside (Co-Supervisor)

ACKNOWLEDGEMENTS

The candidate wishes to express his thanks and appreciation to the project supervisors, Dr D. A. McNeil and Dr. B. M. Burnside for their knowledge and experience which they generously imparted, and for their continued guidance, without which this project would not have been possible.

Thanks are also due to Prof. J. I. B. Wilson of the Department of Physics for all his knowledge and assistance in the preparation of the tube coatings.

Special thanks are due to Mr R. Kinsella, for his invaluable effort and commitment to the apparatus manufacture, and for his continued encouragement throughout the entire project.

Finally thanks are also due to the industrial collaborators especially Dr. P. J. Shechter at Hick Hargreaves & Co., Bolton, for his assistance and knowledge and to National Power for their generously donated data logging equipment.

ABSTRACT

Research to date has highlighted a number of conditions where dropwise condensation may offer heat transfer enhancements over filmwise condensation. Previous studies have shown at pressures above or around atmospheric, dropwise condensation offers significant benefit over filmwise. However, some of this research suggests that as the system pressure is reduced below atmospheric, the benefits of dropwise condensation diminish rapidly, to the extent that, at pressures around 50mbar the benefits of dropwise over filmwise are minimal.

This thesis details a series of experiments which were conducted to investigate the heat transfer and pressure drop distributions in tube bundles during both dropwise and filmwise condensation of steam. The primary objective of the work was to determine the design implications associated with switching the mode of condensation of a electricity generating steam turbine condenser from the current filmwise mode, to dropwise. Experimental data were obtained from a new purpose build apparatus containing seventy-five, 150mm long titanium tubes, arranged in an in line configuration of five columns and fifteen rows. Dropwise and filmwise data were recorded from each row at test cell inlet pressures down to 50mbar using both pure steam and steam air mixtures.

Filmwise heat transfer data indicated that, under most conditions, heat transfer coefficients were generally in agreement with those obtained by previous workers.

Heat transfer data obtained during dropwise condensation suggested that the benefits of dropwise condensation are not significantly diminished at low pressure, and that, unlike filmwise condensation, inundation has little or no effect in a fifteen row bundle.

The data also indicated that the pressure drop characteristics and effects of air are, within experimental error, identical during both modes of condensation and in line with models and theories proposed by previous workers.

NOMENCLATURE

NOMENCLATURE

A_{mv}	Mean void area or volume	m^2 or m^3
A_r	Area of a tube row	m^2
Cd	Tube bundle drag coefficient	-
Cp	Specific heat at constant pressure	J/kg K
D	Diameter tube	m
De	Equivalent tube hydraulic diameter	m
D_ρ	Air stream diffusion coefficient	$(kg/ms)/(N/m^2)$
E	Energy	J
F	Defined by equation 2.23	-
Fr	Froude number (U_∞^2/gD_o)	-
G	Shell side mass flux	kg/m^2s
g	Gravitational acceleration	m/s^2
h	Enthalpy	J/kg
h_{fg}	Specific heat of vaporisation	J/kg
Ja	Jakob number	-
k	Thermal conductivity	W/m K
L	Tube length	m
m	Mass flow rate	kg/s
$\dot{m}$	Mass flux of vapour condensing at surface	kg/m^2s
$\dot{m}_c$	Mass flux of condensate draining from tube	kg/m^2s
$\dot{m}_o$	Mass flux of condensate produced at first row conditions	kg/m^2s
n	Number of tube rows or nth tube row	-
N	Index for inundation equations	-
Nu	Nusselt number (h D/k)	-
Nu_{Nu}	Nusselt number predicted by Equation 2.2	kW/m^2K
P	Pressure	mbar
Pr	Prandtl number	$\mu c_p/k$
P_t	Tube pitch	m
Q	Power	W
q	Heat flux	W/m^2
R	Specific gas constant	J/kgK
Re	Reynolds number $(\rho UD/\mu)$	-
Re_{tp}	Two phase Reynolds number $(\rho_c UD/\mu_c)$	-
T	Temperature	^oC
TPM	Two phase multiplier	-
U	Velocity	m/s
V	Voltage	V
W	Non-condensable gas mass fraction	-
x	Vapour quality	-

GREEK NOMENCLATURE

γ	Ratio of specific heats	-
α	Heat transfer coefficient	kW/m^2K
ν	Specific volume	m^3/kg
θ	Tube angular position or flat plate angle of inclination	Radians

υ	Kinematic viscosity	m^2/s
ρ	Density	kg/m^3
α	Heat transfer coefficient	kW/m^2K
α_{Nu}	Heat transfer coefficient predicted by Nusselt equation	kW/m^2K
ΔT	Temperature difference	K
μ	Dynamic Viscosity	kg/m s
τ	Shear stress	N/m^2
Ψ	Mass transfer coefficient	$(kg/m^2s)/(N/m^2)$
δ	Condensate film thickness	m

SUBSCRIPTS

1, 2, 3, ..	Row number
a	Air or air film
b	Bulk
b	Bulk
c	Condensate
ci	Cooling water inlet
co	Cooling water outlet
cvi	Condensate vapour interface
cw	Cooling water
d	Dropwise condensation droplet diameter.
e	Equivalent
f	Condensate film
G	Gas Phase
GO	Gas only
I	Tube inside
in	Inlet
ins	Insert
L	Liquid Phase
LO	Liquid only
mix	Steam air mixture
n	nth tube row
o	Tube outside
ov	Overall value
r	Tube row
ref	Reference
s	Steam
sat	Saturation
ss	Shell side
tp	Two phase
w	Tube wall - condensate interface

GREEK SUBSCRIPTS

∞	At infinity
θ	Tube angular location

CONTENTS

LIST OF TABLES

LIST OF PHOTOGRAPHS

LIST OF FIGURES

CHAPTER 1

1.1 INTRODUCTION

As the commercial pressures on manufacturing industries increase, companies are being forced to both refine their products and cut costs. Various methods are available to address one or both these issues, from reducing labour, overheads and capital through efficiency increases and material reductions, to the use of new technology and improved design methods. Of the systems available, a significant proportion are based and rely solely on the efficient management of people and resources. Others, such as those that rely on new technology or methods of design, are different since, before they can be adopted, they must first be created and developed. This is the area of engineering expertise to which this project contributes.

Manufacturing industry can produce more economic products though process intensification. The intensification of a process can be achieved by either a new technology and/or an improved design. New technology offers the potential for both evolutionary and step changes, while improved design allows systems or conditions to be optimised within an existing technology.

The process of condensation occurs when the temperature of a vapour is reduced below the saturation value and results in a change of phase from a vapour to a liquid. Condensation can occur within the vapour due to a change in saturation temperature creating a homogeneous two phase flow. However, industrially, it is more common for condensation to occur due to the presence of a cold or cooled surface. The surface may be a solid surface or a liquid surface in the form of droplets or a film, these two condensation processes are termed surface condensation and direct contact condensation respectively. When condensation occurs on a solid surface one of two modes of condensation occurs, either filmwise or dropwise. The mode of condensation is dependant on the combination of condensing vapour properties and the chemistry of the

condensing surface. In general, when the surface energy of the condensing surface is relatively high, filmwise condensation occurs. During filmwise condensation the condensing vapour wets and forms a thin liquid film on the condensing surface. In this case the surface is termed hydrophilic. If the surface energy of the condensing surface is sufficiently low, the liquid created by the condensing vapour is unable to wet the condensing surface. Under these condition the condensate forms in small liquid beads on the condensing surface and the condensing surface is termed hydrophobic. Focusing on metallic compounds, all but a few precious metals will, in an untreated state, tend to promote filmwise condensation, this is why industrial condensers currently operate filmwise. With suitable promoters or surface treatments, most metals, including those with high surface energies, can promote dropwise condensation, e.g. copper, stainless steel, titanium.

Dropwise condensation has been of interest to engineers and designers for a number of years since compared with filmwise condensation, dropwise can offer significantly higher heat transfer coefficients. These higher coefficients occur since, hydrophobic surfaces prevent the build-up the liquid film which occurs during filmwise condensation and which can under certain circumstances can represent a significant resistance to heat transfer.

Since the early pioneering work of Nusselt [1] (1916), our understanding of the process of filmwise condensation has gradually improved. During this time, filmwise theories and models have become increasingly accurate and are now applicable to a wider range of conditions. The process of dropwise condensation has also been the subject of considerable research. Workers have started to model the process and quantify the potential benefits of the change in condensation mode, however, in terms of our understanding of the mechanisms, dropwise condensation lags significantly behind filmwise.

Modelling of filmwise condensation has developed significantly over the years, early workers considered the case shown in Figure 1.1 (a) where stagnant steam condensed on a horizontal tube. These workers modelled the condensate film and predicted the heat resistance transfer caused by the condensate film thickness around the tube. These analyses assumed that the steam flowed radially towards the tube and that the resulting condensate film was laminar and unaffected be the vapour surrounding it. The results of these workers were, in general, found to well represent the case considered. However, in industrial applications, cases where the vapour is stagnant are unusual, and, as a result, workers continued to develop film models where the vapour velocity results in significant shear force on the condensate film. This case is depicted by Figure 1.1 (b).

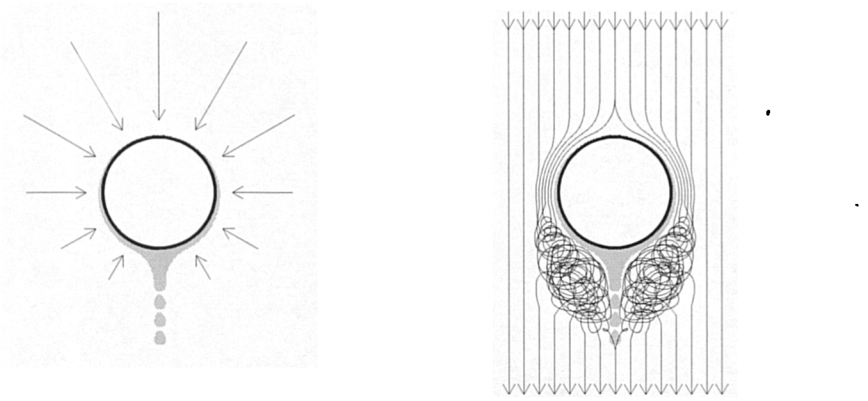

Figure 1.1 Typical steam flows around an isolated tube

Workers modelled the condensate film using a number of assumptions, the most significant of which was the circumferential velocity profile. Most of these models were very rigorous in their development up to the vapour boundary layer separation point at around 109^{O} from the stagnation point. Beyond this separation point the behaviour of the vapour was uncertain and as a result significant uncertainty was introduced into the liquid film behaviour predictions. However, since the results of these analyses indicted that most of the heat was transferred through the upper half of the tube, the errors due to

uncertainties beyond the separation point introduced only minor errors into the final solutions. As with the stagnant steam case the isolated tube models with vapour shear have been shown to be representative and produce accurate heat transfer predictions. Industrially, the two cases depicted in Figure 1.1 have no real applications since modern condensers contain large numbers of closely packed tubes and operate with significant vapour velocities. This case is illustrated in Figure 1.2. To date, the modelling of this type of arrangement has been considerably less rigorous than the two cases described above. This is primarily due to the numerous interactions and uncertainties which occur when the tubes are assembled in a bundle configuration.

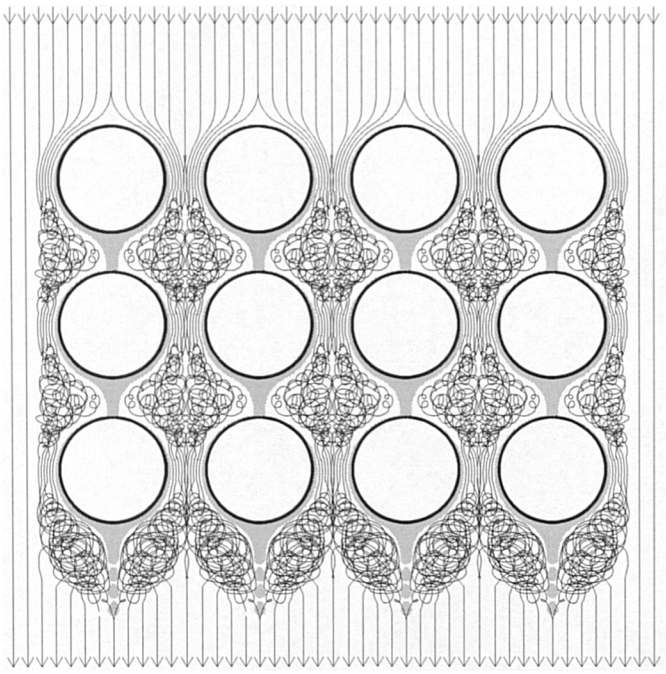

Figure 1.2 Typical steam flow in a tube bundle

Models, correction factors and correlations do exist to estimate the performance of tube bundles, however, the uncertainties and unknowns involved are reflected in the accuracy and confidence levels of the predictions. For filmwise condensation this is currently the state of the art.

In the UK electricity industry, the costs of both capital and operational efficiently, makes the accurate design of turbine exhaust condensers critical. During the period of rapid expansion and investment in the electricity industry, the size of plant increased rapidly to achieve higher efficiencies. This inherently led to requirements for new and larger condensers. Rowe [2] (1983) discussed the performance of these new plant and stated that thermodynamic performance of a number of these units was poor. Rowe presented a list of the problem areas and stated that the majority were outwith the scope of the design codes available.

The design of box condensers, of the type found in modern steam cycle power plant, presents a number of problem areas. A significant number of these problems arise since the bulk of the design information available pertains to single phase, industrial shell and tube heat exchangers, while a number of the procedures described can be used to design specific sections of a condenser, for example the cooling water-side, the design of the steam-side geometry of a condenser is driven by significantly altered criteria. The low operating pressures, and often high steam velocities in condensers, force the design of the shell-side geometry to be dominated by pressure drop considerations. Pressure drop is critical, since, under condenser conditions, a pressure loss normally considered to be small can represent a significant proportion of the upstream pressure. In addition, pressure loss can significantly reduce the vapour saturation temperature, which, due to the practical limitations on cooling water temperature, can cause serious reductions in the heat transfer performance. Condenser designs have evolved to accommodate pressure drop requirements and, as a result, modern condenser steam-side geometries are no longer remotely similar to that of the typical shell and tube heat exchanger.

Overall, even after over 100 years of research, current filmwise condenser design methods are still less than ideal, which, considering the potentially high costs associated with condenser performance shortfalls, vindicates continued research.

The modelling of dropwise condensation has, to date, only undergone limited development. Research into dropwise condensation has mainly focused on work with flat plates. The experimental work has shown that under certain conditions dropwise condensation can offer significant heat transfer improvement over filmwise. Previous workers have shown that during dropwise condensation all the heat transfer occurs through the liquid droplets. Using this fact in conjunction with estimated droplet size and distributions, models to estimate heat transfer coefficients during dropwise condensation have been produced. Under a limited range of conditions, these models have been shown to accurately predict the heat transfer coefficients which occur during dropwise condensation. However, these models only describe simplistic flat plate cases and considerable uncertainty surrounds the effects of vapour pressure and steam velocity. In terms of the cases shown in Figure 1.1, dropwise condensation theory has still to developed to the type of case shown by (a). The implications and performance associated with the design of a complete tube bundle condensing dropwise and operating with significant steam velocities are virtually unknown, as are additional complications such as the effects of air.

To date, a large quantity of experimental data has been obtained for both modes of condensation. Unfortunately, many of these data have been obtained under simplistic laboratory conditions. As a result, the applicability of it to real condensers is uncertain because of the unknowns generated, or, in the case of dropwise condensation, because of the impractical or short lived surface promoters used. From a design prospective, for a filmwise condenser, uncertainty still surrounds issues such as representative flow areas for both pressure drop and heat transfer modelling, the effects of tube spacing and layout. All of these uncertainties exist for dropwise condensers, however, the added uncertainty of the effect of inundation and non-condensables, especially at low pressure has yet to be investigated.

1.2 AIMS AND OBJECTIVES

With the above issues in mind, the objectives of this work were two fold. Firstly, to investigate a selection of current condenser design correlations and compare their predictions with new experimental bundle data, using pure steam and steam air mixtures. Where these correlations were produced for the case of an isolated tube the applicability and the corrections required for bundle modelling are investigated. The second objective was to investigate the implications for the heat transfer and fluid flow design caused by the technology step change associated with switching the mode of condensation from filmwise to dropwise at low steam pressures.

This has been achieved through the design, manufacture and commissioning of a new condenser test facility, and an extensive test and analysis programme. The research was aimed primarily at the power generation industry, hence, within practical limits, every effort was made to duplicate the conditions typical of these environments. Heat transfer and pressure drop data were obtained during both the filmwise and dropwise condensation of steam. Test condenser inlet steam conditions included pressures down to 50mbar, velocities up to 35m/s and air concentrations up to 1% by mass. The apparatus consisted of a 75 tube test condenser, with 5 columns and 15 rows arranged in an inline configuration. Titanium tubes were used with an outside diameter and wall thickness of 19.05mm and 0.5mm respectively. The tubes used in both the dropwise and filmwise tests were identical, except, that the tubes used to promote dropwise condensation were coated with ultra thin Hexamethyldisiloxane (HMDSO) plasma polymer films, using a process supplied by Heriot-Watt University's Physics Department.

CHAPTER 2

LITERATURE REVIEW

2.1 FILMWISE CONDENSATION

2.1.1. FREE CONVECTION CONDENSATION ON HORIZONTAL TUBES

Condensation heat transfer has been the subject of investigation for over a century. Fujii [3] (1991) reports the following early work. Joule of 1861 performed an experiment with condensation inside a vertical tube and substantiated the existence of thermal resistance in the condensate, and obtained data for the design of a surface condenser. Reynolds in 1873 conducted a series of experiments involving mixing a small amount of air in vapour and concluded that the condensation rate was drastically reduced in comparison to condensing pure vapour.

The earliest publication of significance on laminar film condensation was that of Nusselt [1] (1916) which considered the condensation of a pure saturated stationary vapour on a vertical and inclined plate and on a horizontal tube. Nusselt, with the following idealising assumptions, generated equations for predicting the average heat transfer coefficients α_{Nu}. He assumed a stagnant pure vapour was condensed in the absence of air or any other inert, non-condensable gas. Momentum changes in the liquid film and the resistance to mass transfer at the vapour liquid interface were neglected. The vapour was assumed to be saturated and no account was taken of any temperature distributions or heat removed by sub-cooling the film in the condensate film. The cooling wall temperature was assumed to be uniform. The flow in the condensate film was laminar. The physical properties of the condensate film were at the mean film temperature and the condensate film thickness was significantly less than the tube diameter.

The equations for the average heat transfer coefficients from Nusselts analysis are as follows:

For an inclined plate,

$$\alpha_{Nu} = 0.943\left[\frac{g \sin\theta k_f^3 \rho_f (\rho_f - \rho_s) h_{fg}}{\mu_f (T_{sat} - T_w) L}\right]^{\frac{1}{4}}$$

Equation 2.1

where L is the distance from the top edge of the condensing surface and θ is the angle of inclination. For a horizontal cylinder,

$$\alpha_{Nu} = 0.725\left[\frac{g k_f^3 \rho_f (\rho_f - \rho_s) h_{fg}}{\mu_f (T_{sat} - T_w) D_o}\right]^{\frac{1}{4}}$$

Equation 2.2

These expressions describe the fundamentals of the condensation process and hence, even today, some eighty years on, are still applicable to simple cases where steam or organics are condensing and often form the basis of modern more refined correlations.

Rose [4] (1988) discussed the Nusselt model and stated that inertia and vapour shear stresses act to retard the flow of the condensate film, causing the Nusselt theory to overestimate the heat transfer rate, while convection and sub-cooling enhanced the heat transfer, giving an underestimate of the heat transfer rate. Errors in the Nusselt theory were therefore, to some degree, self compensating.

Rohsenow [5] (1956) considered the effect of sub-cooling in the liquid film. Using mass and energy balances on an element of the film, Rohsenow proposed a modification to Nusselt's result. This replaced, the enthalpy of vaporisation, h_{fg}, in Nusselts equation with h^*_{fg}, an equivalent value defined by

$$h^*_{fg} = h_{fg}\left(1 + 0.68Cp\Delta T / h_{fg}\right)$$

Equation 3.3

Sparrow and Gregg [6] (1956) & [7] (1959) addressed the same problem as Nusselt for both a flat plate and a horizontal tube, however, unlike Nusselt, they included the effects of inertia and convection in their analysis. Sparrow and Gregg compared their solution with that of Nusselt for a range of Prandtl numbers, Pr, between 0.1 and 10. The two solutions were in close agreement for water with a T_{sat}-T_w < 110K, the difference being less than 4% for Jakob numbers, Ja, defined by, Equation 2.4 of less than 0.2

$$Ja = Cp\left(T_{sat} - T_w\right) / h_{fg}$$

Equation 2.4

This covered the normal condenser operating range. For fluids with low Prandtl numbers, i.e. less than about 0.03, the difference in the two solutions was significant, i.e. greater than 10% for Jakob numbers greater than 0.05. The results from the solution of Sparrow and Gregg are shown in Figure 2.1.

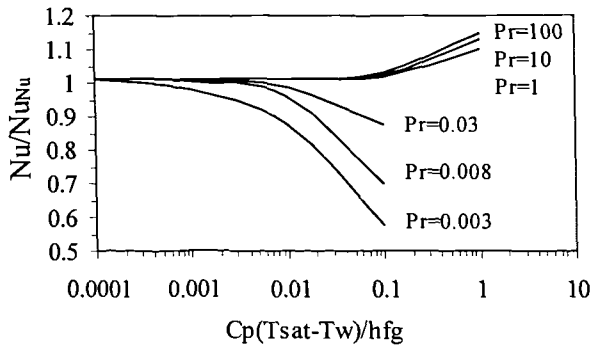

Figure 2.1 Local heat transfer predictions of Sparrow and Gregg [7] (1959)

Chen [8] (1961) continued with the same analysis technique as Sparrow and Gregg, but included the effect of vapour shear created by the velocity difference between the falling liquid film and the stationary vapour. Chen presented the results of his solution in the form shown in Figure 2.2. This shows the ratio of the tube average Nusselt number predicted from his solution to that predicted by Nusselt against an acceleration parameter $k_f(T_w - T_{sat})/\mu_f h_{fg}$, for a range of fluid Prandtl numbers. Chen concluded that for fluids with Prandtl numbers between 1 and 10, the Nusselt number predicted by his analytical solution was higher than that predicted by the Nusselt theory, although the improvement was not as large as that predicted by Sparrow and Gregg. It was suggested that this was due to the increased film thickness caused by the shear forces acting between the moving film and the stationary vapour.

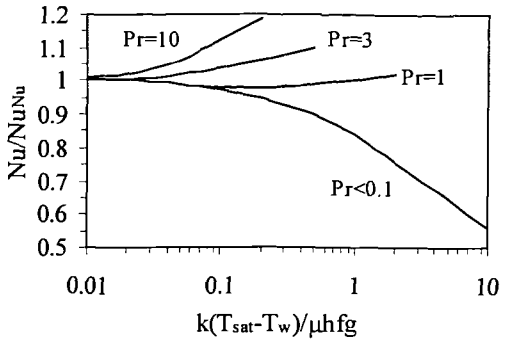

Figure 2.2 Theoretical heat transfer results Chen [8] (1961)

Chen also proposed that the results of his analysis for a single tube could be approximated to within 1% by Equation 2.5.

$$\frac{Nu}{Nu_{Nu}} = \frac{1 + 0.68Ja + 0.02Ja^2\,Pr^{-1}}{1 + 0.95Ja\,Pr^{-1} - 0.15Ja^2\,Pr^{-1}}$$

Equation 2.5

SUMMARY

To date the work on free convection condensation has shown that the assumptions made in Nusselts analysis were generally justifiable and that his solution was accurate over a wide range of conditions. However in terms of real applications the assumptions inherent in Nusselt analysis, particularly the requirement for stationary steam limits this model to either a first, usual conservative estimate or to cases where the vapour is virtually stationary.

2.1.2 FORCED CONVECTION FILM CONDENSATION ON A HORIZONTAL TUBE

The analyses discussed above in section 2.1.1 were based on the assumption of stationary vapour. Thus, the shear force acting at the vapour liquid interface was negligible. This is not the case for most industrial condensers where vapour velocities are often high and shear forces significant.

Shekriladze and Gomelauri [9] (1965) analysed the heat transfer to a plate and horizontal tube with flowing vapour. The analysis assumed that the rate of suction was sufficient to prevent the transition of a laminar boundary layer to a turbulent one and produced shear stresses on the surface that depended mainly on the momentum transferred by the suction mass removed. Hence they used the asymptotic surface shear stress expression of Equation 2.6,

$$\tau = \dot{m}(U_\infty - U_f)$$

Equation 2.6

where $\dot{m}$ is the mass flux of condensate produced per unit area and U_f is the film velocity.

The flat plate analysis assumed a uniform wall temperature and initially neglected the effects of inertia and convection, in addition they also covered the case of uniform heat flux. Using the previous assumptions and fundamental equations of heat and fluid flow, Shekriladze and Gomelauri derived Equation 2.7 for the average heat transfer coefficient. Two correction equations were given to account for the effects of inertia and convection. The authors pointed out that these corrections were so close to unity for ordinary liquids that they may be neglected.

$$\alpha = \sqrt{\left(\frac{\varepsilon}{\varepsilon+1} \cdot \frac{\rho_f h_{fg} U_\infty k_f}{\Delta T \cdot L}\right)}$$

Equation 2.7

where L is the distance along the plate and ε is defined by

$$\varepsilon = \frac{k_f \cdot \Delta T}{h_{fg} \mu_f}$$

Equation 2.8

The analysis was extended to a single horizontal tube in transverse flow. As with the flat plate work, it assumed that the condensate film remained laminar, that inertia effects and the pressure gradient along the tube periphery could be neglected and that outside the vapour boundary layer, potential flow theory for flow around a cylinder could be applied, see Equation 2.9. They also assumed that the film velocity U_f was much less than U_θ and hence neglected U_f in Equation 2.6.

$$U_\theta = 2U_\infty \sin\theta$$

Equation 2.9

Shekriladze and Gomelauri first considered the case of a horizontal cylinder with the vapour flow vertically downward in the absence of body forces. For this case an exact

analytical solution was possible, giving the local angular heat transfer coefficient distribution as

$$\alpha_\theta = \frac{\sin\theta}{\sqrt{1-\cos\theta}} \cdot \sqrt{\frac{k_f^2 \rho_f U_\infty}{\mu_f D_o}}$$

Equation 2.10

and the average the heat transfer coefficient as

$$\alpha = 0.9 \cdot \sqrt{\frac{k_f^2 \rho_f U_\infty}{\mu_f D}}$$

Equation 2.11

The gravitational body force was then included in the analysis. A solution for the mean condensate velocity in the liquid film was given. Including gravity terms made it impossible to obtain an explicit solution for the heat transfer coefficient, however by making suitable approximations and assuming that boundary layer separation did not occur, they obtained the following expression for the mean heat transfer coefficient,

$$\alpha = 0.64 \sqrt{\frac{k_f^2 \rho_f U_\infty}{\mu_f D}} \times \sqrt{\left[1 + \sqrt{\left(1 + 1.69 \frac{D_o g}{U_\infty^2 \varepsilon}\right)}\right]}$$

Equation 2.12

where ε is given by Equation 2.8

Figure 2.3 shows the dependence of Equation 2.12 of the average heat transfer coefficient on the driving temperature for steam, using T_{sat}=40^{O}C, for various vapour velocities.

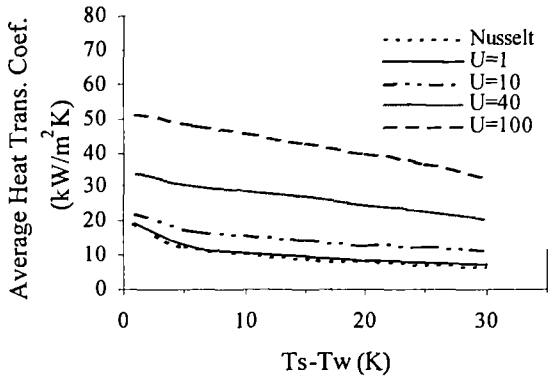

Figure 2.3 Theoretical heat Transfer coefficients of

Shekriladze and Gomelauri [9] (1965)

Shekriladze and Gomelauri also estimated the effect of boundary layer separation. They calculated that even in a flow without separation, only 35% of the total heat transfer would occur at the surface lying beyond the angle $\theta=82^{O}$, the minimum angle at which they expected separation to occur. They presented the following equation for the average heat transfer coefficient, assuming that no heat was transferred from the surface beyond the $\theta=82^{O}$ angle, where ε is given by Equation 2.8

$$\alpha = 0.42\sqrt{\frac{k_f^2 \rho_f U_\infty}{\mu_f D}} \times \sqrt{\left[1+\sqrt{\left(1+1.69\frac{D_o g}{U_\infty^2 \varepsilon}\right)}\right]}$$

Equation 2.13

They stated that under real conditions separation would begin at some point between 82^{o} to 180^{o}. Equation 2.12 and Equation 2.13 would therefore yield upper and lower limits for the mean heat transfer coefficient for condensation on a horizontal tube under the conditions of vapour flow with a separated boundary layer.

Denny and Mills [10] (1969) generated an analytical solution for laminar film condensation with a flowing vapour on a horizontal cylinder which accounted for the

effects of gravity. The authors stated that an explicit solution for condensation in a gravitational field was impossible, and that their aim was to demonstrate that a satisfactory solution could be obtained. Denny and Mills assumed that the effects of fluid acceleration and energy convection were negligible and evaluated the fluid film properties at a reference temperature T^*, given by Equation 2.14

$$T^* = T_w + 0.33(T_{sat} - T_w)$$

Equation 2.14

The analysis produced complicated expressions for the local film thickness and heat transfer coefficient, and their evaluation requires reference to a table of averaged angle functions. The equation presented for the local heat transfer coefficient was compared with an exact numerical solution as a function of θ, the angle around the tube. For angles less than 140^O, the discrepancy was less than 2% but increased significantly as the angle approached 180^O. This increasing discrepancy was thought to be due to the assumptions made, particularly neglecting inertial effects, as these are significant as the angle approached 180^O.

Fujii et al. [11] (1972) solved the liquid and vapour boundary layer equations for filmwise condensation of flowing vapour on a horizontal cylinder, using, the corrected approximate method of Jacobs [12] (1966). This method relied on the assumptions that inertia, convection and pressure gradient terms could be omitted from the momentum equation for the condensate film and that the vapour flow outside the boundary layer could be treated as a potential flow. However, they matched the shear stress and stream wise velocity at the vapour condensate interface rather than adopting the approximate expression for τ given by Equation 2.6 which neglects frictional effects. The expression for the average tube Nusselt number which they obtained was,

$$Nu = \chi\left(1+\frac{0.276}{\chi^4 Fr\cdot H}\right)^{\frac{1}{4}} Re^{\frac{1}{2}}$$

Equation 2.15

where,

$$\chi = 0.9\left(1+\frac{1}{RH}\right)^{\frac{1}{3}}$$

Equation 2.16

$$R = \left(\frac{\rho_f \mu_f}{\rho_s \mu_s}\right)^{\frac{1}{2}}$$

Equation 2.17

and,

$$H = \frac{C_p\left(T_{sat} - T_w\right)}{Pr\cdot h_{fg}}$$

Equation 2.18

The authors compared this result with a numerical solution and found a maximum difference of about 5%. They also compared it with their experimental results. The average coefficients of heat transfer were found to be in fairly good agreement. As with the analysis of Shekriladze and Gomelauri, Fujii et al [11] (1972) assumed that there was no boundary layer separation and that the wall temperature was constant. Figure 2.4 shows the dependence of Equation 2.15 on the driving temperature for various steam velocities at $T_{sat}=40^{O}$.

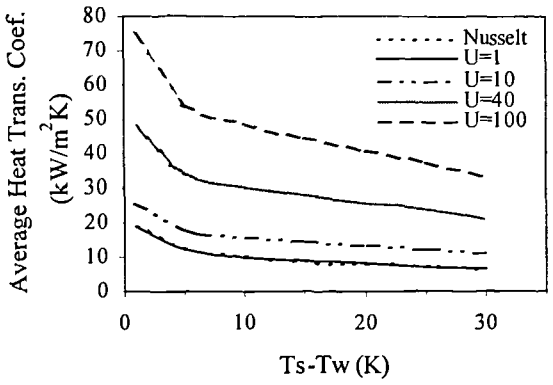

Figure 2.4 Theoretical heat Transfer coefficients of Fujii et al. [11] (1972)

Nicol and Wallace [13] (1974) analysed a single tube under the influence of vapour shear caused by both vapour flowing from above and below. Unlike the previous work, they assumed that separation occurred and predicted an angle of 108.8^{O}. They assumed a shear stress distribution on the film surface on the upper half of the cylinder from 0^{O} around to the angle of separation, and Nusselt type condensation conditions on the lower half to an angle of 180^{O}. In their analysis they assumed that potential flow existed outside the vapour boundary layer up to the point of separation and that the wall temperature was uniform. They also made allowances for the additional contribution to the shear stress on the surface of the film, caused by momentum changes as the vapour condensed, and used a modified value for the enthalpy of condensation to account for the sub-cooling in the condensate film. For vapour down-flow they derived the following expression for the film thickness, δ, as a function of angular position, θ,

$$\frac{d\delta}{d\theta} = \frac{e - \delta^4 \cos\theta - \frac{3}{2}\rho_f C\delta^3 \frac{d\tau_v}{d\theta} - 3\beta \frac{k_f \Delta T}{h^*_{fg}} \rho_f C\delta^2 U_\infty \cos\theta}{3\sin\theta\delta^3 + 3\tau_v \rho_f C\delta^2 + 3\beta C \frac{k_f \Delta T}{h^*_{fg}} \rho_f \delta U_\infty \sin\theta}$$

Equation 2.19

In Equation 2.19 the β variable is the fraction of the momentum change contributing to the shear force on the surface of the film and e is constant. The value of β had to be determined before Equation 2.19 could be integrated. Nicol and Wallace referred to previous work to obtain a value for β, and found that the recommended values ranged from 0.5 to 1. Integrating and evaluating Equation 2.19 with β in this range resulted in an over-prediction of the average heat transfer coefficient by up to a factor of 5 or 6 times that found in their experiments. To resolve this problem Nicol and Wallace referred to papers by Denny & Mills [10] (1969) and Denny and South [14] (1972). In their subsequent analysis Nicol and Wallace assumed that the surface shear stress was equal to that with suction without phase change. They found that in both cases the predicted heat transfer coefficient was comparable to their analysis if β=0, i.e. with no contribution from the momentum term, and hence decided to evaluate the film thickness δ from Equation 2.19 with β=0. The evaluation of Equation 2.19 requires numerical integration. The values predicted for film thickness around the tube show that the film is thinner than Nusselt on the top half of the tube i.e. up to the separation point, and thicker on the lower half.

Nobbs and Mayhew [15] (1976) studied the effect of downward vapour velocity on condensation rates on a horizontal tube both experimentally and theoretically. They generated a model for the local film thickness that included terms for shear forces at the vapour liquid interface and in the liquid film, as well as gravity forces and pressure forces around the tube. Their preliminary experimental work suggested that the wall temperature was not uniform. As a result they also generated an equation which specified a cooling water temperature together with an equation for the cooling water side, heat transfer coefficient and allowed the temperature distribution around the tube

to be estimated. Nobbs and Mayhew also suggested a refinement for boundary layer separation. This refinement assumed separation would occur at an angle of 109^{O} as per the Blasius shear stress distribution. The model generated by Nobbs and Mayhew operated up to this point, while beyond this the Nusselt model was adopted. Numerical integration generated a local film thickness value which allowed the heat transfer coefficient to be calculated. The experimental results obtained were compared with the theoretical values without separation and, on the whole, agreed well except at angles approaching 180^{O}. This was reported to be due to neglecting peripheral conduction in the tube wall, however, the overall effect was relatively small because the heat transfer at angles near 180^{O} was small. They concluded that peripheral temperature variations around the wall of the tube had a marked effect on the heat transfer rate and that predictions based on a uniform wall temperature theory tended to be over optimistic.

Fujii et al. [16] (1979) conducted an experimental and theoretical investigation into the influence of vapour velocity and thermal boundary conditions at the tube wall. They stated that their were two possible boundary conditions, uniform heat flux and uniform surface temperature. They reported that previous experimental work showed that the magnitude of the circumferential variations in tube wall temperature were comparable with the difference between the steam and the average tube temperature. This, under appropriate conditions, invalidates the constant wall temperature assumptions. If the thermal resistance of the steam-side is much smaller than the water-side, the possibility exists for the condensation process to occur under uniform heat flux conditions rather than uniform surface temperature. Fujii et al. generated differential equations to represent both uniform surface temperature and uniform heat flux conditions and solved these numerically for local and average Nusselt number, assuming potential or Roshko mainstream velocity distributions. The experimental investigation was conducted with a

horizontal tube with a horizontal vapour flow. The range of pressures and velocities were 0.03 to 0.125 bar and 0.5 to 80 m/s. Fujii et al. reported three types of condensation; laminar film, wrinkled film and dropwise. They found that the experimental data for laminar film condensation agreed fairly well with the theoretical results for the uniform heat flux model. The two other reported types of condensation resulted in higher than predicted values for the average heat transfer coefficient. The models created by Fujii et al. were not restricted to a vapour flow direction. This allowed an investigation of the effect of the direction of the oncoming vapour on the average heat transfer coefficient. They concluded that variations were not significant except in the region where combined body force and forced convection dominated the condensation process.

Gaddis [17] (1979) also solved the boundary layer equations for laminar film condensation. He discussed the assumptions made by previous workers and stated that a method was required for solving the full two phase boundary layer equations. He modelled the process by including terms for gravity, momentum, pressure gradient, an energy balance in the condensate film and did not assume that U_f was much less than U_∞ i.e. he included U_f in Equation 2.6. The partial differential equations generated were transformed into a number of ordinary differential equations, depending on the required solution accuracy. He solved the resulting equations numerically and compared his solution with a range of experimental data and existing equations for flowing and stationary vapour. For the case of stationary vapour, Gaddis compared his predictions for local and mean Nusselt number with the Nusselt equations and found that they agreed for water. For flowing vapour he assumed that separation did not occur and compared the local Nusselt numbers for water, liquid metal and a viscous liquid at three Reynolds numbers 10^3, 10^4 and 10^5. His results indicated that the local Nusselt number

increased as the Reynolds number increased and as ΔT decreases. The dependence of the local Nusselt number as a function of the angular position, θ, was significant for water especially at high Reynolds numbers.

Berman [18] (1979) investigated the effect of vapour velocity on filmwise condensation. His analysis led to an expression, Equation 2.20, for the ratio of the average heat transfer coefficient for a tube in stationary vapour, α_{stat}, to that of a tube in a vapour crossflow, α.

$$\frac{\alpha}{\alpha_{stat}} = a + b \log \Pi$$

Equation 2.20

were α_{stat} would be calculated using the Nusselt equation and

$$\Pi = \frac{k_f \Delta T U_\infty^2}{g D_o \mu_f h_{fg}}$$

Equation 2.21

and a and b were empirical constants. Values of a and b are generally in the range 1.2 to 1.5 and 0.1 to 0.3 respectively, which he obtained using his experimental data. Berman compared his data with Equation 2.12 and Equation 2.15. He found that both Equation 2.12 and Equation 2.15 predicted the data only at low values of Π, i.e. less than about 5. At higher values of Π, both Equation 2.19 and Equation 2.15 over-predicted the data. Berman suggested that this over prediction may have be due to the assumptions of Equation 2.12 and Equation 2.15, particularly uniform tube temperature and neglecting the effect of pressure gradients.

Theoretical studies of film condensation prior to 1984 have assumed negligible pressure gradients around the tube. Rose [19] (1984) and Rose [20] (1988) reported on the effect of pressure gradient on forced convection film condensation on a horizontal tube. Rose included a pressure gradient term in the momentum equation. He then solved the resulting equation for the local film thickness and found that the thickness was reduced on the upper half of the tube and increased on the lower half. Solutions of his model were dependent on the relative values of parameters P and F defined by Equation 2.23 and Equation 2.25 below. If 0 <P < F/8 the film thickness could be evaluated at all locations around the tube. If P > F/8, the film thickness could only be determined up to a critical angle where the pressure gradient became negative. Rose proposed that the average Nusselt number could be approximated if it was assumed that all the heat transfer occurred up to this separation point, with any small quantities of heat transferred from the lower areas of the tube being negligible.

Rose [19] (1984) finally proposed Equation 2.22 for obtaining a conservative estimate of the Nusselt number for the whole tube.

$$Nu\,Re^{-\frac{1}{2}} = \frac{0.64(1+1.81A)^{0.209}\left(1+G^{-1}\right)^{\frac{1}{3}} + 0.728F^{\frac{1}{2}}}{\left(1+3.51F^{0.53}+F\right)^{\frac{1}{4}}}$$

Equation 2.22

where

$$F = \frac{gD_o\mu_f h_{fg}}{U_\infty^2 k_f \Delta T}$$

Equation 2.23

$$G = \left(\frac{\Delta T k_f}{\mu_f h_{fg}}\right)\left(\frac{\rho_f \mu_f}{\rho_s \mu_s}\right)$$

Equation 2.24

and

$$A = \frac{\rho_s h_{fg} \mu_f}{\Delta T k_f}$$

Equation 2.25

Figure 2.5 shows the dependence of Equation 2.22. on the driving temperature for various steam velocities and for T_{sat}=40^{O}.

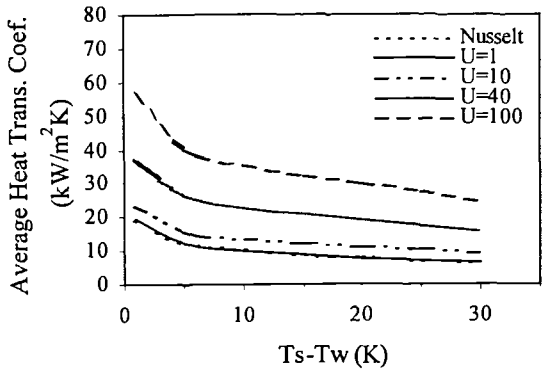

Figure 2.5 Theoretical heat Transfer coefficients of Rose [19] (1984)

Lee et al. [21] (1984) conducted an experimental investigation into the effect of vapour velocity on film condensation on a horizontal tube. For this work R113 and ethanediol were condensed on a single copper tube, i.d. 7.5 mm o.d. 12.5 mm, containing six pairs of embedded thermocouples. Tests with R113 were conducted at atmospheric pressures and with vapour velocities in the range 1 to 6 m/s, while with ethanediol velocities from 7 to 100 m/s were achievable at pressures down to 0.0126 bar absolute. The data they recorded were compared to Equation 2.15 and the empirical correlation of Fujii et al. [16] (1979) Equation 2.26, where F is defined by Equation 2.23 as per previous workers.

$$Nu\, Re^{-\frac{1}{2}} = 0.96 F^{\frac{1}{5}}$$

Equation 2.26

Lee et al. reported that for R113, previous workers using the same apparatus, but with a larger diameter tube, obtained data that agreed satisfactorily with Equation 2.26. The new data demonstrated an unexpected upturn in $Nu\,Re^{-\frac{1}{2}}$ with decreasing values of F, i.e. high vapour velocities. In contrast, the data obtained for ethanediol was comparable with that obtained by previous workers, less than that predicted by Equation 2.15 and greater than that predicted by Equation 2.22. Lee et al. suggested that the higher than predicted, heat transfer coefficients for the R113 data at the higher vapour velocities may be due to the onset of turbulence in the film. This in turn, may be associated with a reverse pressure gradient beyond the tube separation angle, or, the variation of vapour pressure and the corresponding saturation temperature around the periphery of the tube. The thermocouples embedded in the tube wall measured only a small variation in temperature for R113, but, for ethanediol, the variations were significant, being approximately four times greater than those for R113. This, Lee et al. suggested, may be the explanation for the lower than predicted heat transfer coefficients, as the assumptions in both models of uniform surface temperature were being violated. It was also shown for ethanediol at high vapour velocities, above 80 m/s, that there was an abrupt thickening of the condensate film on the lower half of the tube. This tended to lower the tube mean heat transfer coefficient.

Memory and Rose [22] (1986) conducted an experimental investigation into filmwise condensation of high velocity, ethylene glycol on a single, horizontal tube. The apparatus utilised was a closed loop system and was capable of operating at pressures within the range 0.01 to 0.2 bar with vapour velocities of up to 135 m/s. The data which they obtained were compared with the models proposed by Shekriladze and Gomelauri [9] (1966), Equation 2.12, and also with a modified version of this equation proposed by

Rose [19] (1984), based on the integral solution of Fujii et al. [11] (1972), which did not invoke the asymptotic shear stress approximation. Memory and Rose proposed Equation 2.27 for the evaluation of the condensate film heat transfer coefficient,

$$Nu\,Re^{-\frac{1}{2}} = \frac{0.9\left(1+G^{-1}\right)^{\frac{1}{3}} + 0.728F^{\frac{1}{2}}}{\left(1+3.44F^{\frac{1}{2}}+F\right)^{\frac{1}{4}}}$$

Equation 2.27

where the parameter F is as per Equation 2.23 and G as per Equation 2.25.

When evaluating these models Memory and Rose assumed a reference temperature T^*, given by Equation 2.14 for estimation of condensate film properties, except the enthalpy of vaporisation h_{fg}, which were evaluated at T_{sat}. The experimental results and theory was found to agree satisfactorily, except at low values of F, which occurred at low pressure and high vapour velocity. At low F values the experimental results were lower than those predicted by theory. Memory and Rose corrected their data to account for pressure variations around the tube. By adopting a corrected mean condensate pressure and corresponding saturation temperature, the corrected pressure was calculated using

$$P_{Corrected} = P - \Delta P_1 - \Delta P_2$$

Equation 2.28

where an approximation of the pressure drop between the bulk and the interface is given by,

$$\Delta P_1 = a\left(\frac{\rho_s U_\infty}{2}\right)$$

Equation 2.29

and the interphase mass transfer pressure drop, as proposed by Rahbar and Rose [23] (1984) is given by,

$$\Delta P_2 = \frac{bq(\gamma+1)\sqrt{RT_{sat}}}{4h_{fg}(\gamma-1)}$$

Equation 2.30

Values for a and b were 0.7 and 0.8 respectively. The corrected saturation temperature was used to calculate a corrected temperature drop across the film. The data were reprocessed and were found to compare well with the predictions of Equation 2.12 and Equation 2.25 throughout the range of F, including the previously low values of heat transfer coefficient at low F values. Memory and Rose accounted for the remaining small discrepancies by proposing that they were due to property variations, notably the viscosity, as well as the variations in the tube wall temperature that violated the assumptions of both models.

Memory et al. [24] (1993) studied the effect of surface temperature variations. They used the same approach and assumptions as Shekriladze and Gomelauri [9] (1966) except that they adopted the cosine surface temperature distribution given by Equation 2.31.

$$T_\theta = d\cos\theta + c$$

Equation 2.31

Memory et al., using a numerical technique, solved the resulting condensate film equations and compared the result with the constant surface temperature model of Equation 2.12. They evaluated their solution for a range of values of d. When d=0 the two solutions were identical. As the value of a was increased the predicted tube average, heat transfer coefficient increased above the prediction of Equation 2.12. The increase was most marked at low values of F. Increasing d in Equation 2.31 from 0 to 1 resulted in an increase in heat transfer coefficient of approximately 10%.

Zhou and Rose [25] (1996) analysed the effect of two dimensional heat conduction in the condensate film for laminar film condensation on a horizontal tube with variable wall temperature. They generated and solved equations that accounted for both radial and stream wise conduction in the condensate film for a tube with variable wall temperature. Zhou and Rose concluded that one and two dimensional conduction had a negligible effect on heat transfer over a practical range of operating conditions.

SUMMARY

The analyses on forced convection have shown for most common circumstances that inertia and convection have a small effect, particularly at low condensation rates i.e. when the condensate film is thin. The assumption of uniform surface temperature has generally been adopted by most of the workers, and is only violated significantly at angles approaching 180^{O} where heat transfer rates are small. Memory et al. [24] (1993) included a tube wall temperature distribution which resulted in an increase in the predicted, average, heat transfer coefficient. Uniform heat flux models also exist but have been less widely utilised since the assumption is violated on the forward area of the tube, where most of the heat transfer takes place. For the uniform heat flux model, theoretical predictions were less than those for a uniform surface temperature model. Pressure gradients around the tube were neglected by most of the investigators. Rose [19] (1984) included terms to account for the pressure gradient and demonstrated that this enhances the heat transfer over the forward portion of the tube but can, due to the potential for boundary layer separation lead to uncertainties over the rear of the tube. Modelling forced convection on a single tube, Rose [4] (1988) recommended the approximate result of Equation 2.22 which accounts for vapour shear, gravity and pressure gradients in the condensate film. This expression approaches the Nusselt value

at low vapour velocities and is conservative, but not overly so, at high velocities, since heat transferred beyond the angle of separation is ignored.

2.1.3 FREE CONVECTION WITH NONCONDENSABLES

Sparrow and Eckert [26] (1961) investigated the effect of non-condensable gases on laminar film condensation. They modelled on a flat plate the condensation of a stationary vapour containing a non-condensable component. Their analysis was derived from first principles and included terms for momentum and energy conservation and gas diffusion. They neglected the free convection within the vapour phase and hence stated their analysis was qualitative rather than quantitative. Using their solution, Sparrow and Eckert evaluated an example where pure steam with a saturation temperature of 90 ^{O}C, condensed on a wall at 60 ^{O}C. They then evaluated a second case where the conditions were identical except that the bulk steam contained 2% air by mass. They predicted that with no air the liquid vapour interface temperature would be 90 ^{O}C and with 2% air this temperature would fall to 60.16 ^{O}C, reducing the driving temperature across the film to only 0.166 K and resulting in a reduction in heat transfer of approximately 97.8%. They compared their predictions with experimental results and noted that the predicted reductions in heat transfer was substantially greater than that measured. Sparrow and Eckert suggested that a significant part of this discrepancy was due to neglecting free convection in the analysis. They concluded that their expression qualitatively indicated the importance of non-condensables and that free convection must be included in the analysis to achieve more accurate quantitative predictions.

Sparrow and Lin [27] (1964) studied the same problem as Sparrow and Eckert [26] (1961) but they included terms for the effect of fluid motion caused by natural convection. Using numerical techniques they evaluated their solution for air

concentrations up to 5% and with steam air mixture temperatures from 49 ^{O}C to 100 ^{O}C. They generated plots of interfacial non-condensable concentration and partial pressures. The plots show that, for stationary vapour, very high concentrations of non-condensables may build up at the interface, even when there are very small amounts of non-condensable in the bulk. The trend of the results showed that the interfacial mass fraction of non-condensables increased with condensation rate. This was accentuated when the bulk concentration of the non-condensable was greater. Sparrow and Lin also compared their analytically predicted, heat transfer reductions with experimental results and found, with the exception of one data point, good agreement.

Minkowycz and Sparrow [28] (1966) conducted a wide ranging investigation of laminar film condensation on a flat plate in stationary vapour. They included in their analysis the effect of non-condensables, interfacial resistance, superheat, variable properties, buoyancy and diffusion. Using their solution, Minkowycz and Sparrow predicted the heat transfer rate for a steam air mixture at various concentrations, pressures and temperatures and generated a range of figures to demonstrate this behaviour. As suggested by previous workers, the presence of a small quantity of non-condensable gas had a dramatic effect. For example, they predicted reductions in heat transfer rate of more than 50% when the bulk contained 0.5% air by mass. The figures also showed that heat transfer reductions increased as the condensation rate increased and/or the system pressure was reduced. Superheat, which has a negligible effect on heat transfer rate for a pure vapour, was shown to lessen the heat transfer reduction caused by non-condensables, e.g., the heat transfer reductions from a vapour containing 0.5% air at a saturation temperature of 100 ^{O}C condensing on a wall at 80 ^{O}C is approximately 55% of that under saturation conditions, but with 220 K superheat, this is only 45%. This behaviour is most apparent at high saturation temperatures, small driving temperatures

and low air concentrations. The analysis also demonstrated that interfacial resistance affected the heat transfer rate. With saturated vapour, reductions in heat transfer of up to 25% were predicted at low driving temperatures, while, with superheat, heat transfer prediction ranged from a 5% increase for a saturation temperature of 100 ^{O}C to a 25% reduction at a saturation temperature of 27 ^{O}C. These variations were most evident at low driving temperatures. Minkowycz and Sparrow attempted to compare their solution with experimental data. Due to the differences in the physical system and the interpolation required to generate comparative data, only one set of data at a driving temperature of 11 K was available. They found that the level of agreement was about as good as could have been hoped for.

Rose [29] (1969) studied the work of Sparrow and co-workers [26] (1961) & [27] (1964) and noted that while solutions may be found using the approach of [26] (1961) & [27] (1964), the evaluation of the equations required the use of numerical techniques that required significant computing time. Rose stated that the case solved by Sparrow and Lin [27] (1964) has been shown to be representative and hence he generated an approximate solution given by Equation 2.32, where Sc is the velocity parallel to the plate divided by the diffusion coefficient.

$$10SpSc\left(\frac{\mu_f\rho_f}{\mu_{mix}\rho_{mix}}\right)\left(\frac{W_\infty}{w_0}\right)^2\left(\frac{20}{21}+\frac{W_{cvi}}{W_\infty}Sc\right)$$

$$+\frac{8}{Sp^2Sc}\left(\frac{\mu_{mix}\rho_{mix}}{\mu_f\rho_f}\right)\left(\frac{w_0}{W_{cvi}}\right)^2\left(\frac{5}{28}Sp-\frac{Xw_0}{3}\right)$$

$$=\frac{100}{21}\frac{W_\infty}{W_{cvi}}-2\frac{w_0}{W_{cvi}}+8Sc$$

Equation 2.32

where

$$Sp = \frac{(T_{cvi} - T_w)k_f}{h_{fg}\mu_f}$$

Equation 2.33

and

$$w_0 = W_{cvi} - W_\infty$$

Equation 2.34

where W_{cvi} and W_∞ are the air concentrations at the condensate vapour interface and the bulk vapour respectively.

Equation 2.32 was evaluated and compared with the solution of Sparrow and Lin [27] (1965). The difference in interfacial gas concentration between the two solutions depended on the condensation rate. At low condensation rates the discrepancy approached zero, while at higher condensation rate, Equation 2.32 over predicted by up to 25%. Rose also compared Equation 2.32 with the solution of Minkowycz and Sparrow [28] (1966) for a range of concentrations of non-condensables. From the comparative plot, Figure 2.6 it was clear that the results of Equation 2.32 for the condensate vapour interface concentration W_{cvi}, follow the same trend as the exact solution.

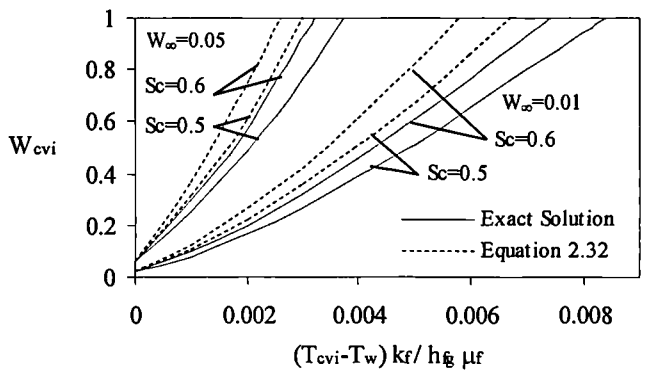

Figure 2.6 Non condensable interface concentration solutions of Sparrow [28] (1966)

Rose calculated the effect on heat transfer caused by the differences between Equation 2.32 and the exact solution. At low non-condensable concentrations, 0.1% and high driving temperatures, Equation 2.32 was shown to under predicted the exact solution by up to 8%, while at higher concentrations, e.g. 1%, the solutions practically coincided. Rose [29] (1968) concluded that the approximate result would be satisfactory in many practical circumstances, or as a first approximation.

Slegers and Seban [30] (1970) conducted an experimental investigation into the condensation of steam containing small concentrations of air on a vertical copper surface. Results were obtained for three saturation temperatures, 66, 46 and 26 ^{O}C, with pure steam and with air concentrations ranging from 0.01% to 1% by mass.

Slegers and Seban found their pure steam data was about 15% above the prediction of the Nusselt solution, Equation 2.1 for pure steam. They compared the data obtained for steam-air mixtures with an integral solution for mass fractions from 0.00001 to 0.001 and with an exact solution by Minkowycz when the mass fractions were in the range 0.001 to 0.01. They found the data to be in the range of slightly below to 30% above the theory, with a tendency towards higher scatter at lower concentrations. To account for the differences between the theories and the experimental results, Slegers and Seban suggested that the air concentration may not have been uniform or that a forced vapour flow may have been present because of the position of the boiler inlet. They investigated both these possibilities and noted that a non-uniform air concentration would act to reduce the heat flux. This was the opposite effect to that observed. They therefore concluded that the increased heat flux was due to non-stagnant steam.

Summary

The effects of air on free convection condensation has been well researched by a number of workers. Today a number of models have been produced each of which have developed with a different set of assumptions. Theory and the experimental work have shown dramatic reductions in heat transfer due to the presence of air. As a result free convection condensation heat transfer with non condensables has no industrial applications. The main product of the research has been an understanding of the mechanisms and the production of theoretical models which can be developed to cover the case of forced convection condensation.

2.1.4 FORCED CONVECTION WITH NONCONDENSABLES

Chisholm and McFarlane [31] (1964) presented a complete method for predicting the performance of a condenser. They detailed methods for the prediction of all the heat transfer resistances associated with a condenser design, including those due to the presence of air. Chisholm and McFarlane presented Equation 2.35 as a means of predicting the mass transfer coefficient Ψ, where D_ρ is the diffusion coefficient, π is the difference between the steam partial pressure in the bulk and the condensate surface, divided by the mixture pressure, and ε_v is the ratio of the air volume to the total mixture volume.

$$\frac{\psi D_o}{D_\rho} = a \cdot Re_{mix}^{0.5}\, \pi^{-\frac{1}{3}} \varepsilon_v^{-0.6}$$

Equation 2.35

This solution for the mass transfer coefficient was then combined with the Clausius-Clapeyron equation, Equation 2.36, which provided a relationship between pressure

difference driving the mass transfer to the temperature difference driving the heat transfer.

$$\frac{dP}{dT_{sat}} = \frac{h_{fg}}{T_{sat}(v_s - v_f)}$$

Equation 2.36

Chisholm and McFarlane based the Reynolds number on the cross sectional flow area of the condenser in the absence of tubes and provided values of the constant, a, for a range of Reynolds numbers and bundle depths.

Sparrow et al [32] (1967) investigated, analytically, the effect of non-condensable gases on the laminar boundary layer in forced convection condensation. Their work focused on modelling a flat horizontal plate and the resulting differential equations. The effect of interfacial resistance was also investigated. They investigated the problem by subdividing the task into smaller, logical sub-problems. Firstly, they analysed the liquid boundary layer by assuming constant fluid properties at a reference temperature, secondly they simplified the equations by neglecting the inertia and convection contributions. Sparrow et al then analysed the vapour gas boundary layer. They modelled the process using the following conservation equations, mass of the mixture, species for one of the components, and momentum. They neglected the energy conservation equation and stated that this was valid since, "the energy transferred to the interface due to convection and conduction in the vapour gas boundary layer was very small relative to that liberated as latent heat". They then solved these equations using suitable boundary conditions, by both an numerical and integral techniques. When the results were compared they found close agreement.

Finally, they addressed the problem of species diffusion in the vapour gas boundary layer. They generated a diffusion, differential equation using a binary diffusion

coefficient and assuming species conservation for the non-condensable. Again they applied suitable boundary conditions and solved the equations both numerically and by an integral method. The two solutions were in close agreement. These solutions allowed Sparrow et al to estimate the gas mass fraction at the interface. These results together with the values of the temperature and concentrations of the mixture, allowed the interface temperature and hence heat flux to be estimated using an iterative process.

Sparrow et al then proceeded with further analysis that was specific to a steam air mixture, they calculated the ratio of the heat flux with non-condesables, q, to that without, q_o, over a range of conditions.

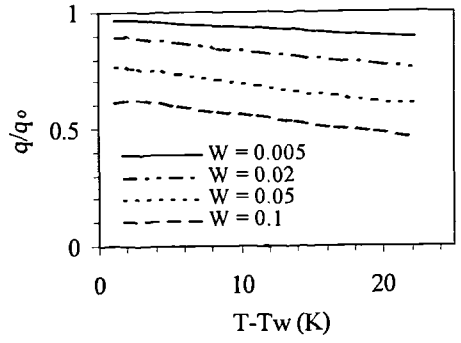

Figure 2.7 Predicted ratio of heat transfer rate with pure steam and steam air mixtures, Sparrow et al [32] (1967)

Figure 2.7 shows the results of the analysis of Sparrow et al for a steam air mixture with a saturation temperature of 46 ^{O}C and air mass fractions from 0.005 (0.5%) to 0.1 (10%). Sparrow et al also generated results at higher saturation temperatures (65, 83 & 100 ^{O}C) and found that the trends were of a similar form, but with the values of q/q_o increased as the saturation temperature increased; up to 10% at 100 ^{O}C. They also compared their result with a solution for gravity driven flow and noted that the general trends were essentially the same. However, there was one dramatic difference. The heat transfer reductions for air mass fractions in the range 0.005 to 0.1 gave values of q/q_o

between 0.95 and 0.45 for forced convection flows and 0.3 and 0.05 for gravity driven flows.

Sparrow et al analysed the effect of interfacial resistance on condensation heat transfer. They stated that the value of the condensation coefficient, σ, which for water has been the subject of a number of investigations, was still uncertain. Values ranging from 0.04 to 1 have been reported. Sparrow et al stated that the most recent measurements available to them suggest that σ is at least 0.35 and probably unity. To quantify the effect of interfacial resistance they calculated the ratio q/qo over a range of σ values. The heat transfer rate was calculated for a pure vapour at a saturation temperature of 26 ^{O}C. The ratio q/q_o was estimated to be 0.997, 0.987 and 0.873 for σ values of 1, 0.35 and 0.04 respectively. They concluded that only if the σ values were 0.04, or less would interfacial resistance lead to a non-negligible reduction in heat transfer. However, their evidence suggested that $\sigma = 1$ for steam. They therefore concluded that interfacial resistance had a negligible effect on forced convection condensation.

Rose [33] (1980) investigated the problem of forced convection condensation with non-condensable gases on both a flat plate and a horizontal tube. He generated approximate, theoretically based equations, relating the mass flux of vapour to the condensing surface to the free stream and condensing surface conditions. Rose qualified the use of approximate equations by stating, "In practice, however, approximate results giving relatively simple relations between the surface parameters are often adequate, owing to the non-ideal geometry or imprecisely known property values". Rose simultaneously solved the momentum, energy and diffusion equations for the vapour layer and the momentum and energy equations for the condensate film. With these solutions, together with an approximate equation which related the local surface heat and mass transfer

parameters, Rose produced a solution for the case of a flat plate. The solutions were compared to the results of a number of other investigators and close agreement was found to exist. The analysis was extended to the case of a horizontal tube. In this case he neglected gravity and included a radial surface velocity profile. Once the appropriate boundary conditions were applied, Rose solved the equations and generated three unknown constants a, b & c. He stated that these could only be obtained by comparing the result with accurate experimental data over a wide range of conditions, with steam air mixtures being the only mixture with sufficient data. However, since good agreement was found when a = b = c = 1, further refinement of the values was postponed. Equation 2.37 is one form of the solution for ω, the ratio between the air concentration in the bulk and that at the vapour condensate interface, designed to be correct for high and low condensation rates

$$\omega = \left\{1 + 1.75\beta \cdot Sc^{2/3}\left(1 + \beta \cdot Sc\right)\right\}^{-1}$$

Equation 2.37

were Sc is the Schmidt number and

$$\beta = \left(\frac{\dot{m}}{\rho U_{\infty}}\right) Re^{1/2}$$

Equation 2.38

Equation 2.37 allows the air concentration at the interface to be estimated and therefore, with knowledge of the system pressure, the interface saturation temperature can be estimated. The heat transfer rate may then be calculated in conjunction with an appropriate gas law and condensate film equations. Rose stated such equations and calculated the heat fluxes over a range of air concentrations. He compared his solution for horizontal tubes with available experimental data for steam air mixtures covering wide ranges of velocity, composition, condensation rate and pressure. Excellent

agreement was found. He suggested that this indicated that Equation 2.37 would also be satisfactory for other vapour gas combinations.

Lee and Rose [34] (1984) investigated, experimentally, forced convection film condensation on a horizontal tube with and without non-condensing gases. Their objective was to obtain condensation heat transfer data over a wide range of conditions. To this end they condensed steam and R113 with air and hydrogen as the non-condensable. They operated at pressures from 4 to 124 kPa, heat fluxes from 12 to 455 kW/m2, vapour velocities from 0.3 to 26 m/s and non-condensable gas mass fractions from 0.02 to 32%.

Lee and Rose compared their data with a number of models, including two equations originally proposed by Rose [33] (1980), which they rewrote as Equation 2.39 and Equation 2.40,

$$\frac{\dot{m}D_o}{\rho_{mix}D_\rho} = 0.5\,Re^{\frac{1}{2}} \times \left\{ \left[1 + 2.28Sc^{1/3} \frac{W_{cvi} - W_\infty}{W_\infty} \right]^{1/2} - 1 \right\}$$

Equation 2.39

and,

$$\frac{\dot{m}D_o}{\rho_{mix}D_\rho} = 0.455\,Re^{\frac{1}{2}} \frac{(W_{cvi} - W_\infty)^{2/3}(1 - 0.378W_\infty)^{0.933}}{W_\infty^{0.6}(1 - 0.378W_{cvi})^{2/3}}$$

Equation 2.40

Equation 2.39 was generated without experimental data and Equation 2.40 originated from a steam air correlation by Berman [35] (1969). For pure steam and pure R113 vapour at moderate velocities, they found good agreement with theory. They attributed the discrepancies at high velocities to the violated uniform wall temperature assumption. For vapour gas mixtures, Equation 2.39 was found to be in excellent agreement with

their data over a wide range of bulk composition, velocity, pressure and heat flux. Equation 2.40 was also compared with the new data and Equation 2.39, and was found to agree quite well.

Briggs et al [36] (1992) conducted an experimental investigation into the condensation of steam air mixtures on a small bundle of horizontal tubes. The bundle consisted of 45, 18.7 mm outside diameter tubes arranged in 10 staggered rows. The horizontal and vertical pitch of the tubes was 26.2 and 22.7 mm respectively and 272 mm of the tube length was exposed to the steam. Briggs et al obtained results with concentrations of air up to 12% by mass. At atmospheric pressure the vapour velocities were less than 1.5 m/s, and at 0.09 bar, the velocities were less than 12 m/s. In both cases they assumed that the pressure drop down through the bundle was negligible. Briggs et al used a Wilson plot technique to calculate the steam-side heat transfer coefficient from their data. They found that at atmospheric pressure the vapour-side heat transfer coefficient decreased down through the bundle due to the vapour velocity decreasing and the air mass fraction increasing. At low pressures the vapour-side heat transfer coefficient trends were similar. However decreases were less marked and the values were smaller than those for the high pressure data. They compared their data with a theory proposed Rose [33] (1980) Equation 2.40 for steam air mixtures. For steam air mixtures the experimental results for the first five rows were in fair agreement with Equation 2.40 with the data falling in a narrow band. Further down the bundle the results fell significantly below the predictions of Equation 2.40. Briggs et al suggested that this was due to the air concentrations in the bundle being higher than those calculated on the basis of condensation rates. Reductions may also be partially due to inundation effects. Briggs et al suggested, in their concluding comments, that some of the remarks were somewhat speculative and that the paper should be regarded as an interim report.

Abdullah et al [37] (1995) reported on an experimental investigation into the condensation of steam and R113 on a bank of horizontal tubes in the presence of a non-condensing gas. Their work was a continuation of the work of Briggs et al [36] (1992) and used the same apparatus. They condensed pure vapours and mixtures containing air as a non-condensable. Experiments were conducted at atmospheric pressure, with up to 10% of air by mass and at vapour velocities of up to 3.3 m/s. The vapour-side, heat transfer coefficients were estimated using a modified Wilson plot technique. Their conclusions were very similar to those of Briggs et al [36] (1992). Abdullah et al concluded that the nominally pure vapour data was in fairly good agreement with the single tube theory, Equation 2.41, at the top of the bundle. However, the data showed a more rapid decrease in the vapour-side, heat transfer coefficient than was expected as a result of inundation or reductions in vapour velocity. They attributed these discrepancies to air build up. For both cases, pure vapour and for the air vapour mixtures, one further possibility exists to explain the low experimental heat transfer coefficient values. They assumed that the pressure drop down through the bundle was negligible, this may not be justifiable, and would account, to some degree, for the low, heat transfer coefficient values found. In closing, Abdullah et al stated that "the combined influence of vapour velocity, condensate inundation, and non-condensing gas on the condensation process in industrial condensers is still not properly understood".

Summary

The condensation of steam containing air has been investigated by a number of prominent workers. Currently there exists both a number of models for predicting the effects of air during the condensation of steam and a range of experimental data. Good agreement has generally been reported between the published models and the

experimental data. However, few of the investigators have focused on the effects of air in a tube bundle and hence there remains uncertainly regarding interactions with inundation, the effect of bundle geometry and the calculation of the mixture velocity and Reynolds number.

2.1.5 FORCED CONVECTION CONDENSATION IN TUBE BUNDLES

Michael et al [38] (1989) investigated the effect of vapour velocity on the condensation of steam and R113 on a single tube. The test tube was 19.05 mm in diameter and was placed in a rectangular channel 31.6 x 157.6 mm to simulate the conditions in a bundle with a tube pitch to diameter ratio of 1.25. Steam data were recorded at 0.116 bar over a range of velocities from 4.8 to 31.5 m/s. The data were compared with the correlation of Rose [19] (1984), Equation 2.41, and a correlation proposed by Fujii et al [16] (1979), Equation 2.26. Both theses equations were developed for the case of an isolated tube.

$$Nu = \frac{0.9 + 0.728F^{\frac{1}{2}}}{\left(1 + 3.44F^{\frac{1}{2}} + F\right)^{\frac{1}{4}}} \times Re^{\frac{1}{2}}$$

Equation 2.41

Michael et al computed the results of their experiments using steam velocities corresponding to the maximum and minimum cross sectional areas. Figure 2.8 is a reproduction of their data, where the light and dark symbols are, respectively the results based on the minimum and maximum cross sectional area. Michael et al did not draw any real conclusions relating to the vapour velocity options, however Figure 2.8 suggests that their data was best represented by Equation 2.41 with a vapour velocity corresponding to the maximum flow area. Michael et al stated that Equation 2.26 had been found to lie close to a number of previous experimental workers and suggested that

the significantly higher experimental results found may be due to the tube diameter to channel width blockage ratio.

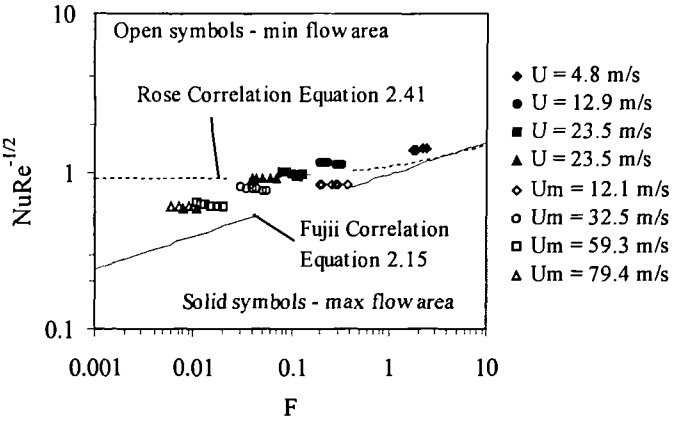

Figure 2.8 Condensation heat transfer coefficient predictions with the experimental data of Michael et al [38] (1989)

Aoune and Burnside [39] (1990) conducted a theoretical investigation into the effect of tube spacing on condensation heat transfer. They investigated, using a finite element method, the velocity distributions around a 19.1 mm diameter tube with pitch to diameter ratios of 1.25 and 1.5. Figure 2.9 is a reproduction of the dimensionless distributions which they obtained.

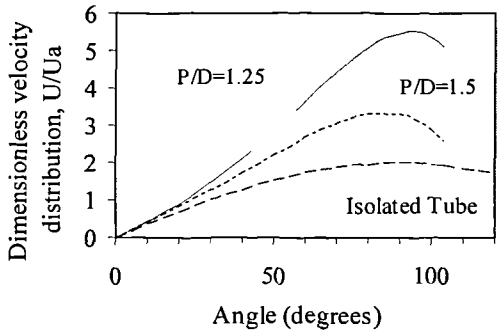

Figure 2.9 Theoretical tube circumferential velocity distribution Aoune and Burnside [39] (1990)

Aoune and Burnside, using the new velocity distributions, solved the boundary layer equations by, in general, the same methods as Fujii [40] (1981). They produced three solutions, one for an isolated tube and pair for tubes with pitch to diameter ratios of 1.25 and 1.5 and compared the results. They concluded that the tube spacing has a strong effect on the condensing film Nusselt numbers, and that the effect increases with approach velocity. Typical values of the increase in $Nu/Re^{1/2}$ compared to an isolated tube were from 4 up to 35%.

Briggs et al [36] (1992) conducted an experimental investigation into the condensation of steam air mixtures on a small bundle of horizontal tubes. In addition to tests with air they conducted a series of experiments with pure steam to investigate the applicability of single tube theories to bundle conditions. Briggs et al compared their data with Equation 2.41 proposed by Rose [19] (1984) for a single tube. They evaluated Equation 2.41 using three definitions for the vapour velocity to replace the free stream velocity required by the single tube theory, the minimum and total flow area and also the mean void flow area proposed Nobbs [41] (1972). Briggs et al. defined the mean void area for his configuration by Equation 2.42 which is a function of the area upstream of the bundle, the total area of the test section and the minimum flow area between the tubes.

$$A_{mv} = 5L\left[P_t - \frac{\pi D_o^2}{2\sqrt{3P_t}}\right]$$

Equation 2.42

Figure 2.10 and Figure 2.11 are reproductions of the atmospheric and low pressure pure steam data respectively. They are complete with the single tube theory trends. The trends are, (A) based on minimum flow area, (B) mean void area, (C) total flow area and (D) Nusselts theory, Equation 2.2, with 0.728 replacing the original 0.725 multiplier.

At atmospheric pressure, these results with pure steam at the top row gave fair agreement with single tube forced convection theory, Equation 2.41. Subsequent rows lie below all the theories, including the Nusselt theory, Equation 2.2. Briggs et al stated that this was unexpected and suggested that this indicated that air effects were significant below the first row and that since the maximum velocity was only 1.5 m/s for the atmospheric tests, air re-circulation may have been occurring. This explanation is somewhat confusing since Briggs et al stated that these results were for pure steam.

The results for the low pressure steam, 0.09 bar, were concentrated into a narrower band, Figure 2.11. These tests were conducted at higher velocities, approximately 10-12 m/s. The results were generally in agreement with the Nusselt theory, however Briggs et al stated that the heat transfer coefficient remained constant at about 10 kW/m^2K for the first four rows in the bank, then increased to approximately 15 kW/m^2K.

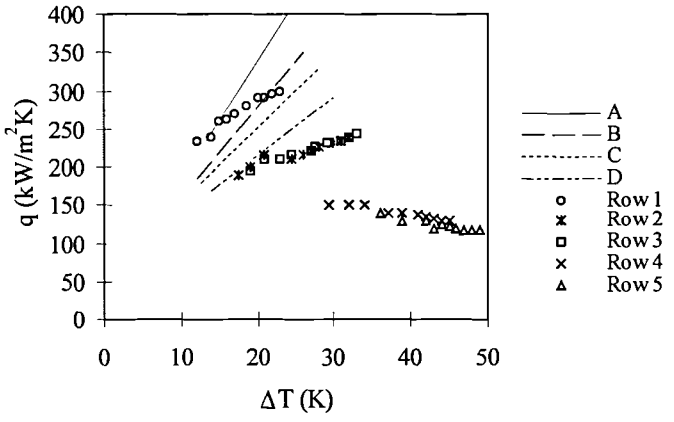

Figure 2.10 Condensation heat transfer coefficient predictions

with the experimental data of Briggs et al [36] (1992)

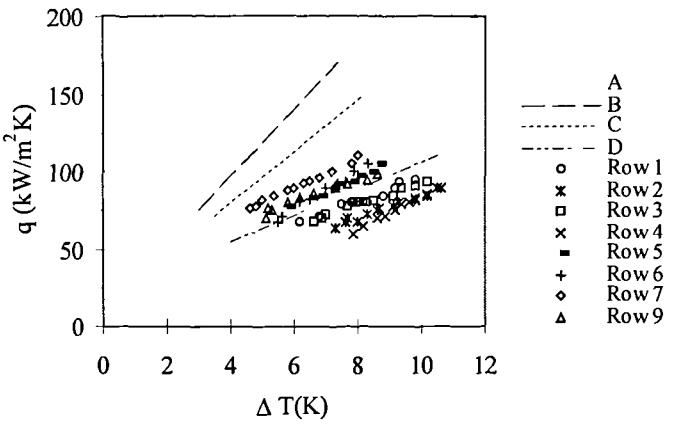

Figure 2.11 Condensation heat transfer rate predictions

with the experimental data of Briggs et al [36] (1992)

Michael et al [42] (1992) reported on heat transfer measurements for the condensation of steam flowing down through a small staggered tube bundle. They obtained data at approximately atmospheric pressure with steam approach velocities from 6 to 23 m/s. They compared their data with Equation 2.41, using three definitions of area for the estimation of the vapour velocity. The definitions were mean void area, the total test section area and minimum flow area between the tubes. These definitions were identical to that of Briggs et al [36] (1992) except Michael et al., due to a different bundle geometry, used Equation 2.43 to calculate the mean void volume.

$$A_{mv} = 4L\left(P_t - \frac{\pi D_o^2}{2\sqrt{3}P_t}\right)$$

Equation 2.43

Michael presented Figure 2.12 as a comparison between their data and Equation 2.41. Figure 2.12 includes data from all the bundle rows. As a result, most of the vertical scatter on each data set can be attributed to inundation and variations in vapour shear.

Michael et al stated that the best overall agreement was found using Equation 2.41 when the vapour velocity is based on the mean void area, with the data being predicted to within ±35%. They concluded their results were generally in agreement with Fujii et al [43] (1972) and Nobbs [41] (1975) but noted that the results of Fujii were for near horizontal steam flow, and that Nobbs had used a single condensing tube in a dummy bank.

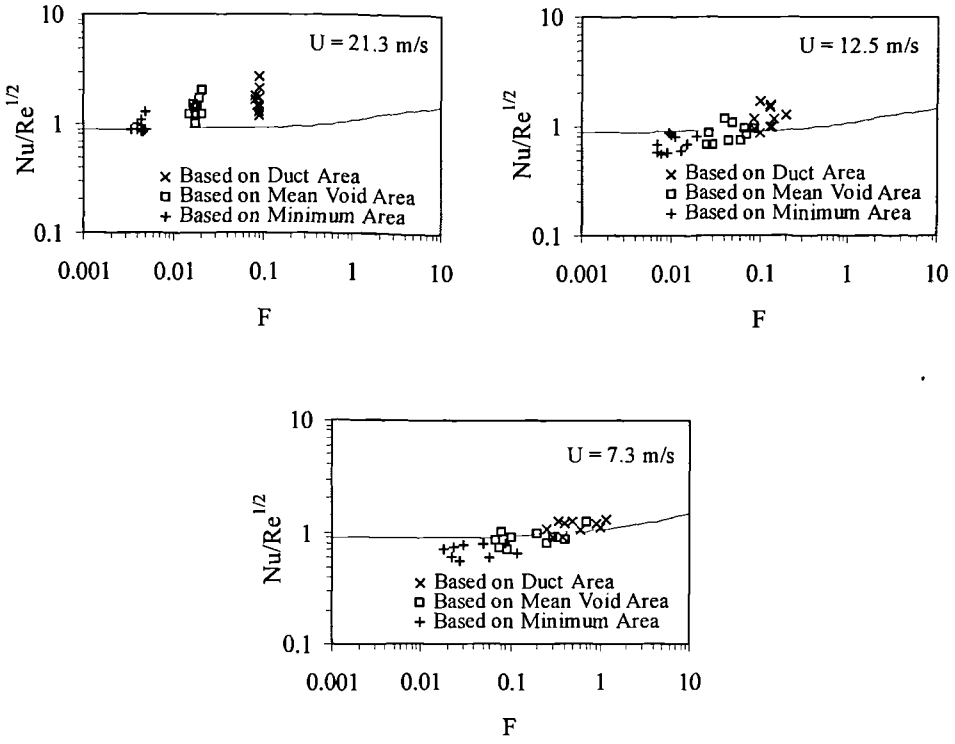

Figure 2.12 Condensation heat transfer coefficient predictions

with the experimental data of Michael et al [42] (1992)

Summary

Recently their have been a few studies of the condensation heat transfer in tube bundles. The main focus of this work has been to determine the applicability of established single tube theories to bundle flow. It has been shown that, due to the velocity distributions of

the steam, the heat transfer is greater in a bundle than for an isolated tube. Very little analytical work has been published which investigates this behaviour. Most workers in this area have instead investigated this area by comparing experimental data with established theories using various definitions for the steam flow area and hence velocity. Currently no satisfactory solution has been presented, although the literature indicates that the use of a mean void area definition produces a moderate degree of agreement. The issue is still unclear and requires further research.

2.1.6 INUNDATION EFFECTS DURING FILMWISE CONDENSATION

Nusselt [1] (1916) was the first to address the problem of condensate inundation in tube bundles. Nusselt extended his single tube analysis to include the effects of condensate inundation. In addition to the usual Nusselt assumptions the inundation analysis assumed that the condensate flowed from one tube to the next in a continuous sheet, and that the condensate does not gain any momentum as it falls.

Nusselt proposed Equation 2.44 as a simple method of predicting the ratio of the heat transfer on the nth tube row in a bundle to that on the first row.

$$\frac{\alpha_n}{\alpha_1} = n^{-\frac{1}{4}}$$

Equation 2.44

Short and Brown [44] (1951) studied the condensation of Freon 11 and steam on a vertical column of 20 horizontal tubes. They discussed the assumptions made by Nusselt [1] (1916) in deriving his inundation model and stated that the majority were reasonably close to the actual conditions. However they noted that the assumptions of, a continuous sheet failing between the tubes and no disturbance of the condensate film by the

preceding tube were considered to be over simplifications. Short and Brown suggested the above as potentially the main inaccuracies in Nusselts model. They conducted their tests with stagnant vapour and determined the condensate film heat transfer coefficient by conducting batches of tests in which only the cooling water velocity was altered. Short and Brown then analysed their data and suggested that the ratio of heat transfer coefficients on an un-inundated tube and inundated tube was proportional to the condensate flow rate leaving a tube to some power less than 0.333. Short and Brown presented their data graphically on two main plots with correlating groups on each of the axes. Derivation of the various groups was not discussed. Comparison with the experimental data indicated good correlation with both group pairs. However it was stated that of the two plots the correlating group pair described by Equation 2.45 demonstrated the best agreement.

$$\frac{\alpha_n}{C_P \dot{m}_{dn}}\left(\frac{3\mu_f \dot{m}_c}{\rho_f^2 \cdot g}\right)^{\frac{1}{3}}\left(\frac{C_P \mu_f}{k_f}\right)^{\frac{2}{3}} = \left(\frac{4\dot{m}_c}{\mu_f}\right)^{-1}$$

Equation 2.45

Fuks [45] (1957) investigated experimentally the effects of condensate inundation using a staggered bundle of 19mm diameter tubes. The bundle contained 11 rows with 7 and 6 tubes in alternate rows. To simulate high inundation rates Fuks recycled a controlled flow rate of condensate from a hot well to a distributor tube in the first row. He conducted a series of experiments during which he measured the heat transfer rate on the vertical column below the outlet over a range of inundation flows. Fuks proposed Equation 2.46 as a means of predicting the heat transfer performance of an inundated tube, with a value of –0.07 for the exponent N.

$$\frac{\alpha_n}{\alpha_1} = \left(\frac{\dot{m}_c}{\dot{m}}\right)^N$$

Equation 2.46

Based on his experience, Kern [46] (1958), proposed a correction to Equation 2.44 and proposed Equation 2.47 as a correlation for predicting the performance of tubes in the nth row.

$$\frac{\alpha_n}{\alpha_1} = n^{-\frac{1}{6}}$$

Equation 2.47

Chen [8] (1961) conducted a study into condensation on single and a column of horizontal tubes. Chen stated that heat transfer results for lower tubes in horizontal bundles have been found to be consistently higher than Nusselts theory. He suggested that this was largely due to both the momentum gained by condensate sheet as a result of condensation on the sheet between tube rows. Chen developed a solution which included these additional boundary conditions, but neglected the unpredictable effects of splashing and ripples. Evaluation of the exact theoretical solution was not practical. As a result Chen proposed an approximate solution, Equation 2.48 which he stated would predict the theoretical result to within 1%.

$$\frac{\alpha_n}{\alpha_1} n^{\frac{1}{4}} = \left[1 + 0.2\zeta(n-1)\right]\left(\frac{1 + 0.68\zeta + 0.02\zeta\xi}{1 + 0.95\xi - 0.15\zeta\xi}\right)$$

Equation 2.48

where

$$\zeta = \frac{C_P \Delta T}{h_{fg}}$$

Equation 2.49

and

$$\xi = \frac{k_f \Delta T}{\mu_f h_{fg}}$$

Equation 2.50

Chen compared his result with a range of experimental data and concluded that condensation between the tubes could be accounted for by the approximate theory and that higher experimental results were due to splashing, intermittent dripping and local dripping, rather than the continuous condensate sheet which he assumed.

Grant and Osment [47] (1968) conducted a series of experiments to study the effects of inundation on condensation of steam. Their experimental condenser consisted of approximately 139, ¾ inch diameter tubes in a staggered configuration. To simulate high inundation rates they recycled condensate from a hot well to a row of 11 distribution tubes positioned directly above the bundle. The effect of inundation was then estimated by measuring the performance of a tube in the centre of the first row over a range of inundation rates. Grant and Osment analysed their results and found that their data could be well represented by Equation 2.46 if the exponent N was set to –0.223.

Nobbs [41] (1975) investigated the effects of vapour velocity and inundation on the condensation of steam. Just as previous workers, Nobbs analysed his data using Equation 2.46 and studied the dependence of the exponent N on the shell-side, two phase Reynolds number (Re_{tp}). Nobbs stated that the exponent N varied from –0.22 to –

0.095 as the two phase Reynolds, Re_{tp}, number increased from $1x10^5$ to $9x10^5$. Nobbs reported very good agreement with the value –0.223 proposed by Grant and Osment [47] (1968) at low Reynolds numbers but stated that the value of N was always smaller than the value –0.07 suggested by Fuks [45] (1957).

Nobbs suggested that the variations in the exponent n may be due to entrainment but concluded that the two phase Reynolds number was probably not the best correlating parameter.

Fujii [40] (1981) re-analysed the high heat flux in-line bundle data of Nobbs [41] (1975) and presented Equation 2.51 as an experimental correlation which included a two phase Reynolds number term.

$$\frac{\alpha_n}{\alpha_1} = \left(\frac{Re_{tp}}{2\times10^6} \right)^{0.071\left(\frac{\dot{m}_c - m_o}{m_o} \right)^{0.65}}$$

Equation 2.51

Fujii examined graphically the applicability of Equation 2.51, the results of which suggested that the accuracy of the equation limited its use to cases where, $\dot{m}_c / \dot{m} < 18$ and $\alpha_n/\alpha_1 > 0.35$.

Butterworth [48] (1992) proposed Equation 2.52 for predicting the amount of condensate produced by a tube in the nth row. He then combined Equation 2.2, Equation 2.45 and Equation 2.52 to derived Equation 2.53.

$$\dot{m} = \frac{\pi D_o \alpha_n (T_{sat} - T_w)}{h_{fg}}$$

Equation 2.52

$$\frac{\alpha_n}{\alpha_1} = \left(\frac{\dot{m}_c}{\dot{m}}\right)^{-\frac{1}{4}}$$

Equation 2.53

Butterworth pointed out that this solution was in agreement with the experimental results of Grant and Osment [47] (1968) who found an exponent value of -0.223. He stated that while it was not exactly –0.25, it was so close that the difference need not be a concern.

Summary

The literature details a number of correlations and refers to a selection of experimental data from previous work. All the theories reviewed indicate that inundation reduces the heat transfer. However, the range of both experimental results and theoretical predictions suggest that either the mechanisms of inundation are not fully understood, the assumptions are too simplistic or data which have been previously compared was not comparable. For example, comparing results with and without vapour shear, from in-line and staggered bundles, bundles with different tube diameters and pitch diameter ratios or laminar, turbulent or unknown condensate films.

2.2 DROPWISE CONDENSATION

2.2.1 DROPWISE CONDENSATION ON FLAT PLATES

Le Fevre and Rose [49] (1965) conducted an experimental study of heat transfer during dropwise condensation. They conducted a series of experiments using steam at atmospheric pressure condensing on a flat vertical surface. They obtained dropwise data, using four different promoters, over a range of heat fluxes from 0.3-1.8 MW/m^2 and driving temperatures from approximately 2 to 8 K. They observed that with stagnant

steam, the condensing surface temperature was unstable. The instability was attributed to air. As a result Le Fevre and Rose included a venting system to ensure "gas free steam". They then conducted a series of tests and concluded that the moderate steam velocities caused by venting had no effect on the steam to surface temperature difference. They then obtained heat transfer data using each of the four promoters at distances of 25.4, 28.4 and 101.6 mm from the top of the condensing surface. Figure 2.13 is a reproduction of their data obtained from each of the four promoters, where each trend includes data from all three vertical positions. Le Fevre and Rose concluded that heat transfer coefficients up to 0.3 MW/m^2K could be achieved and that there was no evidence of dependence on plate height.

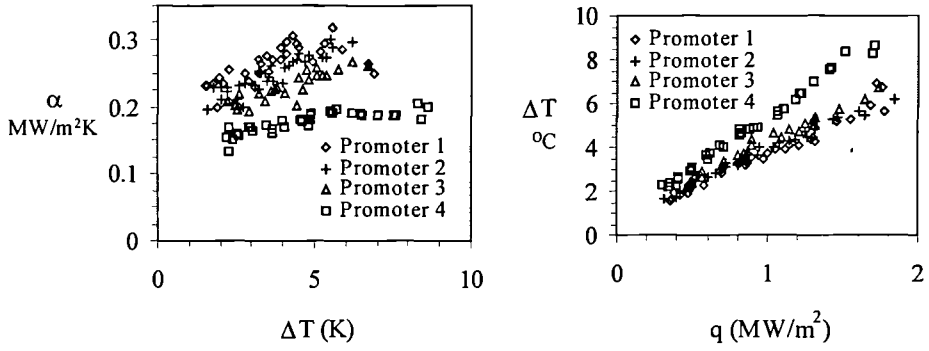

Figure 2.13 Experimental dropwise data of Le Fevre and Rose [49] (1965)

Tanner et. al. [50] (1965) studied experimentally the effects of heat flux, steam velocity and non-condensable gas concentration on dropwise condensation of steam at atmospheric pressure. They discussed their results generally and stated that, the heat transfer coefficients of dropwise condensation were 2-3 times greater than filmwise values and increased with increasing heat flux. They presented few data but concluded that, increasing the steam velocity past the condensing surface increases the heat transfer coefficient, reductions in heat transfer were greater for steam containing CO_2 than with N_2 and with increasing heat flux.

Umur and Griffith [51] (1965) studied the mechanism of dropwise condensation. They discussed two opposing theories. The first theory suggested that during dropwise condensation a very thin film develops on the surface breaking into droplets at a critical thickness, followed by the re-development of a new film on exposed areas. The second theory proposed that dropwise condensation develops from randomly distributed nucleation sites. They also stated that it was not clear whether or not condensation takes place on the area between the drops. Umur and Griffith conducted a series of experiments with monochromatic light. They measured the reflected light intensity since optical theory stated that the intensity would increase if reflected through a film and decrease if scattered by a surface covered with liquid droplets. Umur and Griffith also conducted a theoretical analyses of droplet formation. They developed a model for the heat transfer coefficient at the liquid vapour interface. The model indicated.that this was a function of vapour pressure, hence, when applied to drop growth predictions, a significant pressure dependency was found. Umur and Griffith did, however, state that if the liquid vapour interface heat transfer coefficient was infinite, the drop growth rate would be virtually independent of pressure. They concluded that the area between the drops does not have a liquid film thicker than a monolayer, that no net condensation takes place on the area between the droplets, that the most probable drop nucleation sites were wetted pits and grooves in the surface and that the growth rate of small droplets was significantly dependent on vapour pressure.

McCormick and Westwater [52] (1965) conducted an experimental study of nucleation sites during dropwise condensation. They conducted a series of experiments on horizontal copper surfaces treated to promote dropwise condensation, and operated with surface subcoolings from 0.02 to 6K. They investigated the nucleation of droplets by

both filming and photographing the process using high magnification cameras, achieving magnifications of up to 400 times. From their results McCormick and Westwater observed that drops repeatedly formed at the same locations. They continued their study by selecting 37 potential nucleation sights and conducted eight re-condensation tests. Of these sites, twenty one were effective in all eight tests, four were effective in seven of the tests and six did not nucleate. From these results and from tests with manufactured nucleation sites, McCormick and Westwater concluded that dropwise condensation was a nucleation process and that drops were nucleated at particular preferred sites.

Le Fevre and Rose [53] (1966) developed a new theory for heat transfer by dropwise condensation from stagnant steam. They analysed the heat transfer through a single hemispherical drop, then, by assuming a droplet distribution, predicted the heat transfer for a condensing surface. Le Fevre and Rose compared their theory with experimental data over a wide range of heat fluxes and found good agreement. The theory indicated that the rate of heat transfer was almost a linear function of driving temperature, with heat transfer coefficients being of the order of 340 kW/m^2K at atmospheric pressure. The theory also indicated that the heat transfer coefficient was dependent on the system pressure, with significant reductions indicated as the pressure was reduced below atmospheric. Le Fevre and Rose concluded the dominant factors controlling dropwise condensation were surface tension, interphase matter transfer, pressure drop and conduction in the liquid.

Tanner et. al. [54] (1968) reported on an experimental investigation into the dropwise condensation of stagnant low pressure steam. Two different promoters were used and data were obtained at pressures of 20, 38 and 76 mmHg with heat fluxes from 10 to 100

kW/m^2. They also conducted tests with filmwise condensation. Results indicated that the heat transfer coefficients during dropwise condensation were 200-600% higher than filmwise values and that the at low pressures the coefficients were independent of heat flux. The values of the dropwise heat transfer coefficients found by Tanner et. al. were between 40 to 80 kW/m^2K, depending of the promoter and the pressure. These compared to values of around 18 kW/m^2K for filmwise condensation. Tanner et. al. also obtained dropwise condensation data when the bulk steam contained up to approximately 1.0% Nitrogen. They compared their data with and without a non-condensable gas and demonstrated that the heat transfer coefficient may be reduced by a factor of up to 10 and stated that the magnitude of the reduction was dependent on heat flux, concentration and steam pressure.

Citakoglu and Rose [55] (1968) investigated experimentally the influence of air and venting on dropwise condensation heat transfer. They studied a number of results and stated that precise and repeatable measurements of steam to surface temperature can only be achieved when special precautions are taken to eliminate the effects of non-condensing gasses. Citakoglu and Rose assumed that venting was the best method of removing air from the condensing surface. They proceeded to conduct a series of experiments to determine the effect of venting on heat transfer coefficient over a range of heat fluxes, steam pressures and vent positions. Using their results, they determined for each steam and cooling surface condition the optimum configuration which most effectively removed non-condensables with the minimum effect on heat transfer. They then concluded that the presence of a few parts per million of a non-condensing gas can lead to very serious errors in the measurement of steam to surface temperature. With the apparatus configuration optimised, they investigated the effect of time on the dropwise heat transfer coefficient. Their investigation found that the heat transfer coefficient

increased to a maximum value after 3 hours, then remained stable for 4 hours, after which the value gradually decreased. With the precise characteristics of their apparatus known, Citakoglu and Rose proceeded to investigate the effect of vapour to surface temperature difference on heat flux. They conducted their experiments at 1.07 bar and concluded that the steam-side heat transfer coefficient increased with heat flux, Figure 2.14, and that it was highly probable that the presence of non-condensing gases, and the failure to realise that even minute concentrations may lead to serious errors, had been the major cause of the wide range of published dropwise heat transfer data.

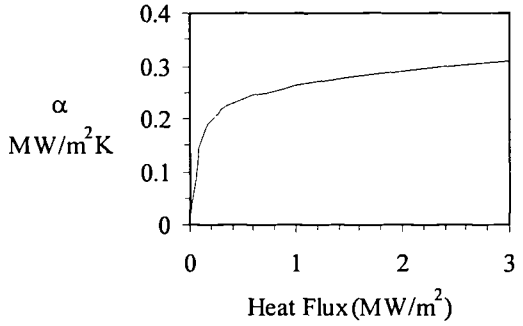

Figure 2.14 Trend of experimental dropwise condensation heat transfer coefficient Citakoglu and Rose [55] (1968)

Wilmshurst and Rose [56] (1970) presented heat transfer results for dropwise condensation. They utilised two surface promoters, dioctadecl disulphide and PTFE, and obtained data over a range of pressures from 0.05-1.0 bar. They stated that their results were in line with those of previous workers and that satisfactory agreement was found with the correlation presented by Le Fevre and Rose [53] (1966). Figure 2.15 is a reproduction of data at a heat flux of 0.35 MW/m^2 and indicates the variation of steam-side heat transfer coefficient with pressure.

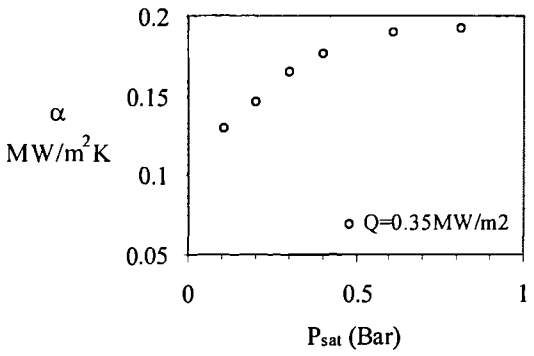

Figure 2.15 Experimental dropwise condensation heat transfer coefficient Wilmshurst and Rose [56] (1970)

Tanasawa and Ochiai [57] (1973) conducted an experimental study into dropwise condensation of steam on flat surfaces. They acknowledged previous workers who had highlighted the importance of eliminating air and elected to minimise the effects by testing with steam flowing at a velocity of 4.0 m/s. Tanasawa and Ochiai selected this steam velocity by conducting a series of tests with steam velocities from 0.5 to 8.0m/s. These indicated than 4.0m/s was sufficient to prevent air accumulation but low enough for the heat transfer not to be enhanced by vapour shear. They then conducted a series of experiments where they measured the heat transfer coefficient and critical drop radius on their surface over a range of inclination angles. When their surface was vertical, Tanasawa and Ochiai measured steam-side heat transfer coefficients around 0.2 MW/m^2K and observed that the critical drop radius of 1mm showed little change when the steam velocity varied between 3-7m/s. Tanasawa and Ochiai also presented a theoretical analysis, however, their predicted heat transfer coefficient of 0.64 MW/m^2K was considered to be inaccurate due to their selection of two empirical constants.

Tanaka [58] (1975) conducted a theoretical study of dropwise condensation of stagnant steam. Tanaka considered statistical and geometrical aspects to derive and solve a series

of fundamental equations describing the transient process of droplet growth and hence produced a universal model for the drop size distribution. Tanaka then introduced a model for the cycle of drop departure and derived a general expression, Equation 2.54, for the heat transfer coefficient during dropwise condensation.

$$\alpha = 5300 \cdot k \cdot \frac{D_d^{-0.3}}{Z^{0.7}}$$

Equation 2.54

Where, for steam at atmospheric pressure, the mean distance between neighbouring nucleation sites, Z, is approximately 0.0033 mm.

Rose [59] (1976) analysed theoretically the process of dropwise condensation on a vertical flat plate. He incorporated the result of Le Fevre & Rose [53] (1966) for the dependence of heat transfer on maximum drop size in a new analysis. The solution demonstrated the dependence of the droplet sweeping frequency and the heat transfer coefficient on the distance down the plate. His solutions indicated that the sweeping frequency and the heat transfer coefficient were proportional to the plate height raised to the power 4/11 and 1/11 receptively, suggesting the heat transfer would increase with distance down the surface. Rose compared his result with two sets of experimental data both of which he found to display no dependence of heat transfer coefficient on plate height.

Tanasawa et al [60] (1978) conducted an experimental study into the effect of maximum drop size on the dropwise condensation heat transfer coefficient of steam. In a series of experiments they measured the heat transfer while controlling the maximum droplet size with a wiper. They conducted both steady state and transient experiments measuring

heat transfer and drop growth rate. Tanasawa et al conducted experiments at atmospheric pressure and heat fluxes of 0.74 and 0.41 MW/m^2. Their data indicated that the drop diameter growth rate could be described by Equation 2.55, where D is the drop diameter in mm, and t time in seconds

$$D = 2.1 \cdot t^{0.87}$$

Equation 2.55

Tanasawa et al also presented a relationship that described the diameter of the largest drop (maximum drop diameter) which occurred as a function of wiping frequencies. They proposed Equation 2.56 where D_{max} is the maximum drop diameter and τ the sweeping frequency.

$$D_{max} = 1.8 \cdot \tau^{0.83}$$

Equation 2.56

Tanasawa et al discussed the differences between the coefficients values of 1.8 & 2.1 and the indices of 0.83 & 0.87 in Equation 2.55 and Equation 2.56. They stated that while the values were not identical, the differences were not thought to be of great significance when considering the scatter and accuracy of the data. They then stated that the relationship between the maximum drop size and the drop growth rate could be considered to be identical. The heat transfer coefficient was found to be proportional to the maximum drop diameter to the power –0.22 and was dependent on heat flux. Tanasawa et al noted that the exponent was different from the value, -0.31, found in their previous work [61] (1976). They suggested that this may have been be due to the difference between maximum drop size and departing drop size, differences in droplet size distributions or the effect of the finite wiper sweeping time. Tanasawa et al did not draw any direct conclusions, however, they demonstrated that the heat transfer

coefficient reached a maximum value of 1.1MW/m^{2}K, 5ms after the surface had been swept.

Tanasawa [62] (1978) discussed dropwise condensation and the way forward to practical applications. He reviewed a large body of work, commenting on important factors or issues, areas where there are gaps in knowledge, the mechanisms of dropwise condensation and the historical trend of results. Tanasawa commented on a large number of issues which influence the heat transfer coefficient of dropwise condensation. However with regard to the then current research he made a number of comments. Four of these are as follows.

1. The relationship between the heat transfer and maximum drop size and the heat transfer rate should be studied more extensively.

2. The effect of material thickness and thermal properties requires more reliable and accurate measurements for ultimate verification.

3.Much more work is necessary to quantify the relationship between heat transfer coefficient and the non-condensable gas concentration.

4. Dropwise condensation is not so much a heat transfer problem as a problem of surface chemistry or surface treatment. Looking forward to practical applications, Tanasawa stated in his final paragraphs his personal opinion that the most promising of all the method for promoting dropwise condensation was the use of polymer films, followed by the continuous injection techniques.

Tanasawa and Utaka [63] (1983) conducted a series of experiments to measured the heat transfer during dropwise condensation of steam. They discussed the existence of the boiling curve and stated that their objective was to measure the equivalent "condensation curve". Tanasawa and Utaka studied previous work and noted the

requirement for measurement accuracy. An apparatus was constructed containing a conical copper heat transfer block with a concave spherical condensing surface. The conical configuration was chosen to remove any heat transfer rate limitations imposed by the cooled surface, in this work the area ratio of the condensing surface to the cooled surface was 1:176. Within the block there were imbedded four constantan wires which operating as thermocouples allowing both the heat flux and surface temperature to be predicted. They conducted their tests using steam at atmospheric pressure, velocities up to 100m/s and sub-cooling of 0.5-180K. In addition a small quantity of data was obtained with non-condensable gas concentrations up to 483 parts per million (p.p.m.). Tanasawa and Utaka analysed their data and demonstrated the dependence of the data on mean final drop size, surface subcooling and air content. Their data indicated that over the range of heat flux of 0.59-4.7MW/m^2, the heat transfer coefficient was dependent on the mean final droplet diameter, D_d in mm, as per Equation 2.57.

$$\alpha = 293 \cdot D_d^{-0.29}$$

Equation 2.57

Tanasawa and Utaka [63] generated two condensation curves demonstrating the effect of subcooling on both the heat flux and the heat transfer coefficient. The figures presented indicated that for values of subcooling of up to 10K, the dependence of heat flux on subcooling was linear, i.e. the heat transfer coefficient was constant. Beyond subcooling values of 10K the rate of increase of heat flux decreased, with maximum values found to be between 9.3 and 12.2 MW/m^2. Correspondingly the heat transfer coefficients decreased from of 1.0-0.3MW/m^{2}K down to below 0.13MW/m^{2}K. They measured the concentration of air contained in the steam at approximately 30 p.p.m.. They then conducted tests with air concentrations of 126, 255 and 483 p.p.m. and obtained a relationship between heat flux and air concentration. They extrapolated their

data back to 30 p.p.m. and concluded that the effects of this concentration of air was relatively small. To quantify this, Tanasawa and Utaka quoted heat flux reduction figures of 4-5% at a steam velocity of 5m/s and 3-4% at 13 & 27m/s.

Nagata and Tanasawa [64] (1986) carried out an experimental investigation into the dropwise condensation of steam with low surface subcooling. They noted that the measurement of surface temperature was one of the main factors determining the accuracy of heat transfer results at low subcoolings. They manufactured a thin film resistance surface temperature sensor to measure the temperature directly. During the experiments they found that the surface temperature fluctuated violently at a frequency corresponding to the behaviour of the surface droplets. Nagata and Tanasawa did not define the term "behaviour of surface droplets", however, it has been assumed that frequency referred to was that corresponding to the rate of droplet departure. As a result, the median, and not the average value, of the fluctuation was taken as the surface temperature. Nagata and Tanasawa conducted both steady state and quasi steady measurements and found no substantial difference and hence chose to present the results simultaneously and without discrimination. They presented results over a range of subcoolings from 0.04-2.0K. These indicated that above subcoolings of 0.3K the relationship between heat flux and surface subcooling was approximately linear. In terms of heat transfer coefficient, the value of the results increased rapidly up to subcoolings of approximately 0.3K, after which the value remained constant at around 80kW/m^{2}K. Nagata and Tanasawa discussed their results and stated that the trends found were similar to those of previous workers although the values of heat transfer coefficient were some 25-30% lower. They concluded that the temperature of the surface could be measured with very high accuracy using a thin film sensor and

attributed their lower results to the titanium substrate used having a considerably lower thermal conductivity than the copper used by previous workers.

Tanasawa [65] (1991) studied the dropwise condensation data of a number of previous workers. He found that there was little difference between the results of the individual workers, and that all the data showed a tendency of decreasing heat transfer coefficient with decreasing pressure. Utilising his own earlier experimental data, Tanasawa et. al. [61] (1976), he showed the dependence of dropwise heat transfer coefficient on the departing drop diameter. The data were obtained using gravitational, centrifugal and steam shear forces to change the droplet departure size. Tanasawa stated that, no matter what kind of force was used to promote drop departure, the heat transfer coefficient is proportional to the departing drop diameter to the power of approximately –0.3. The data were well represented by Equation 2.58 over a range of departing drop diameters from 0.1-3.0mm, which corresponds to heat transfer coefficients of 0.5-0.2 MW/m^2K.

$$\alpha = 240 \cdot D_d^{-0.31}$$

Equation 2.58

Tsuruta et. al. [66] (1991) conducted an experimental investigation of constriction resistance theory with dropwise condensation. They conducted a series of experiments with steam condensing dropwise on surfaces with a range of thermal conductivities. Quarts glass, stainless steel and carbon steel were employed as condensing surfaces, treated with Oleic acid to promote dropwise condensation. Tsuruta et. al. accurately measure the heat transfer coefficients utilising thin film thermometers to measure the surface temperature. Their results demonstrated that the surface temperature fluctuated significantly due to the formation and departed of condensate droplets. As a result of the fluctuations, Tsuruta et. al. calculated a mean value of the surface temperature and used

the result to estimate the heat transfer coefficient. They obtained result from the three surfaces and concluded that the heat transfer coefficients were dependant on the condensing surface thermal conductivity. They attributed this dependence to the fact that during dropwise condensation, heat is only transferred through the area under the droplets. The called this channelling of heat through the droplets and the dispersion into the surface, constriction resistance. Tsuruta et. al. concluded that, as the surface thermal conductivity decreases, the constriction resistance will increase.

Summary

From the research to date, it is clear that dropwise condensation offers the potential for significantly higher heat transfer coefficients than filmwise. However, the actual values of heat transfer coefficients during dropwise condensation are still uncertain. The situation is further confused by most of what little data exists being obtained at atmospheric pressure. Many theories suggests that the benefits of dropwise condensation diminish as the pressure is reduced. Currently, the best correlating parameter for the prediction of dropwise condensation heat transfer is the droplet departure diameter. However, due to the complex interactions between fluids, condensing surface and local conditions, methods of predicting this diameter remain undeveloped. The modelling of dropwise condensation is also further complicated by the rate and effect of departing droplets sweeping over the surface and the influence of vapour shear.

2.2.2 DROPWISE CONDENSATION ON A HORIZONTAL TUBE

Bonnar [67] (1997) developed and tested ultra thin hydrophobic plasma polymer films to promote dropwise condensation of steam. The films were deposited onto 0.75inch diameter tubes. A series of tests were conducted to determine the relative performance of dropwise to filmwise condensation. Bonnar conducted experiments at 100 &

200mbar and presented overall heat transfer coefficient results. He found that by changing the mode of condensation to dropwise the value of overall heat transfer coefficient increased by around 25-30% at high steam velocities and 30-40% at low velocities. The data from the two test pressures indicated that the heat transfer enhancement was not related to the pressure. Bonnar concluded that the dropwise heat transfer resistance was sufficiently low as to render the value as negligible compared with the other resistances.

Summary

Little information exists for the case of an isolated tube condensing dropwise with flowing vapour. However, flat plate work suggests that the process of dropwise condensation does not develop or change with height or position. As a result, it is likely that in practical situations their will be little difference between the results from flat plate and isolated tubes. But it should be noted that the uncertainties outlined in the section 2.2.1 summary also apply to the case horizontal tube.

2.2.3 DROPWISE CONDENSATION IN TUBE BUNDLES

Furman and Hampson [68] (1959) conducted an experimental investigation into film and dropwise condensation of steam, with and without non-condesables. They utilised only a single tube, however, the arrangement of the surrounding ducting produced a configuration more representative of a bundle than an single tube. They conducted their tests at atmospheric pressure with steam velocities and nitrogen concentrations up to 45m/s and 6% (by mass) respectively. The paper presented only overall heat transfer coefficients, however, the data indicated that the rate of heat transfer during dropwise condensation of steam was dependent on the steam velocity, the heat flux and the air concentration. With regard to the effect of air, Furman and Hampson presented data

indicating that the overall heat transfer coefficient could be reduced significantly by the presence of nitrogen, e.g. with 1% nitrogen reduction of 30-35% and 2-3% were measured at the extremes of velocity, at 6% nitrogen these figures increased to over 60% and approximately 10% respectively.

Fujii et al [43] (1972) conducted experiments to measure the heat transfer during the condensation of low pressure steam. The tests were conducted with vertical steam flow over an inline and staggered tube bundle at pressure of 0.01 – 0.07 bar and with velocities from 10 to 40 m/s. The bundle contained 15 rows of 14 mm diameter tubes pitched at 22 mm centres. They made no attempt to promote dropwise condensation, merely observing the behaviour and measuring the heat transfer during the first few days of their apparatus operation. They observed that the drops coalesced up to sizes of approximately 5 mm before being blown off the tube and into the steam flow. Fujii et al concluded that the heat transfer coefficient of dropwise condensation in forced flow of low pressure steam may be of the same order of magnitude as that in quiescent steam. They also concluded that for low pressure steam the heat transfer coefficients for filmwise and dropwise condensation were comparable to each other.

Tanasawa and Saito [69] (1987) conducted an experimental investigation of the effects of inundation in tube bundles. They conducted tests with a single condensing tube above which there was placed a dripping tube. Saturated water was pumped to the dripping tube simulating condensate inundation. Two dripping tubes were used, one to simulate drainage from a dropwise tube and one for a filmwise tube which were designed to generate inundation flow distributions representative of a complete bundle. They conducted their experiments using steam at near atmospheric pressure with vapour velocities from 0.6 to 8.4m/s. Results were obtained for the dependence of departing

drop diameter on steam velocity, the variation of heat transfer coefficient with bundle depth, circumferential distribution of departing drop diameter and surface temperature. The discussion of Tanasawa and Saito remained qualitative rather than quantitative. However they did compare their data with Equation 2.59 and found good agreement.

$$\alpha = 115 \cdot U_s^{0.33}$$

Equation 2.59

Tanasawa and Saito presented a figure demonstrating the inundation effects during film and dropwise condensation. Figure 2.16 is a reproduction of the extremes of the presented data. The filmwise results showed that the ratio of the heat transfer coefficient compared to the first row decreased as the bundle depth increase up to an approximately constant value of 0.7-0.8. For dropwise condensation the data indicated that the ratio of heat transfer coefficients increased up to a maximum at the fifth or sixth row, after which the ratio slowly decreased. This behaviour was dependent on heat flux and was most noticeable at low heat fluxes. Tanasawa and Saito noted that none of the dropwise results with inundation fell below the value of an un-inundated tube. They concluded the heat transfer coefficient of dropwise condensation would not deteriorate due to inundation up to at least the tenth row.

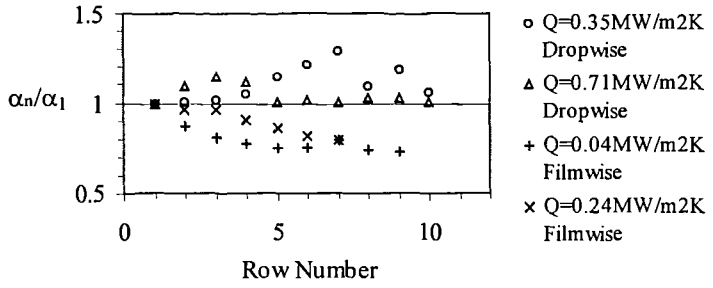

Figure 2.16 Ratio of 1st to nth row experimental heat transfer coefficients Tanasawa and Saito [69] (1987)

Burnside and Zhao [70] (1995) reported on a series of experiments with a small 5 row by 3 column bundle. They tested at a pressure of 0.2 bar using two sets of tubes, one set treated by Magnetron Sputter Ion Plating to promote dropwise condensation, and one untreated filmwise set. They analysed their data from a global perspective by comparing the average bundle heat fluxes over a range of velocities from 6-54m/s and overall driving temperatures from 5-30K. The data from both the dropwise and filmwise tests is reproduced in Figure 2.17, where solid and open symbols represent filmwise and dropwise condensation respectively. They concluded that compared with the untreated bundle the overall heat transfer coefficient during dropwise condensation was between 60-80% higher at low steam velocity and between 50-60% higher at high steam velocity steam. They stated that the results also indicated that no inundation effects were deduced to have occurred in the bundle condensing dropwise.

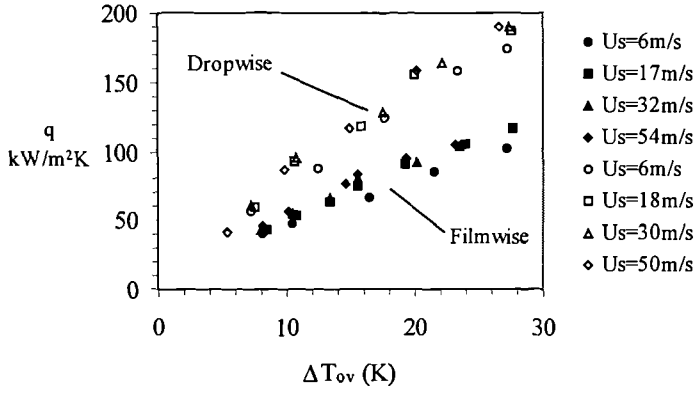

Figure 2.17 Measured heat flux values during dropwise and filmwise condensation Burnside and Zhao [70] (1995)

Summary

Experimental data for dropwise condensation in tube bundles is very scarce. The work undertaken has tended to present qualitative rather than quantitative results. However, even at a qualitative level, the current data is not conclusive, particularly with respect to issues such as the effect of inundation, air, tube material and pressure.

2.3 PRESSURE DROP THROUGH BANKS OF TUBES

2.3.1 SINGLE PHASE FLOW PRESSURE DROP

Pierson [71] (1937) conducted an experimental investigation into pressure drops through tube bundles. He conducted tests on a wide range of configurations and tube sizes using a bundle of electrically heated tubes and air as a working fluid. The results of this work were a series of design curves for Nusselt number, friction factor and bundle depth effects. Pierson defined a friction factor by Equation 2.60 where n is the number of rows crossed and G is the mass velocity.

$$f = \frac{10.84 \times 10^{-8} \rho \cdot \Delta P}{n \cdot G^2}$$

Equation 2.60

For 1.25 inch diameter tubes in an inline configuration, Pierson found values of friction factors, f, in the range 0.065-0.08 over a range of Reynolds number. Figure 2.18 is a reproduction of the results for shallow bundles which demonstrates the friction factor corrections required for shallow bundles.

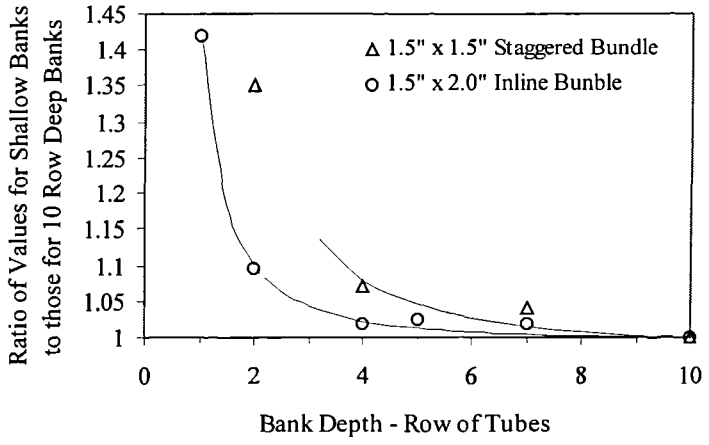

Figure 2.18 Variation of drag coefficient with bundle depth Pierson [71] (1937)

The Engineering Sciences Data Unit (ESDU) have published items [72] (1974) and [73] (1979) which describe a procedure for predicting pressure losses through tube bundles. [73] (1979) describes the irrecoverable pressure loss through a bundle in the form of Equation 2.61,

$$\frac{dp_f}{dn} = -C\frac{\rho U^2}{2D_o}$$

Equation 2.61

where U is the stream velocity based on the flow area calculated ignoring the area occupied by the tubes, and C is calculated using Equation 2.62

$$C = C'\phi_1\phi_2\phi_3$$

Equation 2.62

C′ is a reference coefficient obtained either using charts or can be predicted from a series of correlations. ϕ_1 is the viscosity ratio factor, ϕ_2 is the flow inclination factor and ϕ_3 is the tube external surface roughness factor. For a simple configuration which complies with the reference conditions, correction factors $\phi_1 = \phi_2 = \phi_3 = 1$.

Kakac et al [74] (1987) stated that little research has been performed on shell-side, two phase flow with condensation and recommended the use of a single phase correlation of the form of Equation 2.63

$$\Delta P = 4f \cdot n \cdot \rho \cdot \frac{U_{max}^2}{2}$$

Equation 2.63

where n is the number of tubes crossed and U_m is the maximum velocity based on the minimum flow area. Kakac also stated that for a limited range of Reynolds numbers the

single phase friction factor in a tube bundle may be expressed by Equation 2.64 were x is the Blasius exponent, typically around 0.2 and a was a geometry factor.

$$f = \frac{a}{Re^{x}}$$

Equation 2.64

Taborek [75] (1990) also detailed a method for predicting single phase pressure drops through tube banks. He defined an ideal tube bank friction factor in the form of Equation 2.65

$$f = \left(10^{3}\right)\frac{\Delta P \cdot \rho}{2 \cdot G^{2} \cdot n}\left(\Phi_{s}\right)^{r}$$

Equation 2.65

where n is the number of rows crossed G, is the mass velocity and ϕ_s is a viscosity correction factor. Taborek stated that for a gas being cooled $(\Phi_s)^r = 1$.

Branan [76] (1994) reported on a method of calculating single phase shell-side pressure drop. He recommended Equation 2.63 and Equation 2.64 with x=0.21 and also included a series of tables to determine the friction factor for various bundle geometries and depths.

Table 2.1 details the friction factor corrections for less than 5 tube rows, referenced to a bundle of ten rows.

Number of rows	1	2	3	4
Correction factor	1.3	1.3	1.15	1.07

Table 2.1 Row number friction factor correction Branan [76] (1994)

Summary

Fluid flow through banks of tubes is a highly complex phenomenon even for a single phase flow. Their are many factors which influence the pressure loss including, bundle geometry and construction, tube type, fluid properties and property variations. Due to the complex nature of these flows, calculation techniques for predicting pressure drops through tube banks are highly empirical, with the correlations often requiring reference to charts and graphs to facilitate evaluation. However, single phase flow pressure drops, through tube bundles have been the subject of a considerable amount of research, and today estimates can be calculated with reasonable accuracy.

2.3.2 TWO PHASE FLOW PRESSURE DROP

Calculating the pressure drop in a condenser tube bundle is subject to all the complications found with single phase flows, but is further complicated by condensation suction and by the presence of the two phase flow which is generated. Together these factors create a formidable challenge when predicting the pressure drop in condenser tube bundles. To date their have been few papers published on two phase flow pressure drops through tube bundles and very little published work on pressure drops in condensers.

Diehl [77] (1957) obtained new data from a series of experimental tests and presented an empirical method for correlating two phase pressure drops in condensers, by generating graphs of $\frac{\Delta P_{tp}}{\Delta P_{G*}}$ against $\frac{LVF}{(\rho_G/\rho_L)(Re_{G*})^n}$, where LVF is defined as the liquid volume fraction and G* indicates a fictitious gas only flow, equal to the flow which would occur if the total flow was in the gas phase.

The data were obtained in two test units. The first unit operated with only air/liquid systems at atmospheric pressure and was not capable of any heat transfer. In this unit Diehl studied both inline and staggered tube configurations. The staggered bundle contained 32 tubes in four columns and the inline unit had five tube columns each containing 17 tubes. In the second unit, a vaporisation and condensation pilot plant, adiabatic two phase flow data at different pressures were obtained as well as pressure drop data during condensation in the staggered bundle.

Diehl and Unruh [78] (1958) reported a study of pressure drop for horizontal cross flow of two phase gas liquid mixtures through tube banks. They reported three types of experimental tests, single phase calibration, adiabatic two phase and condensation pressure drop tests. They used the same equipment as Diehl [77] (1957) but analysed their data differently. They proposed that Re_{*G} which had been presented in the previous paper [77] (1958) was not a correlating parameter. Diehl and Unruh produced three plots of $\frac{\Delta P_{tp}}{\Delta P_{G*}}$ against $\frac{LVF}{(\rho_G/\rho_L)}$ for the various configurations and compared the trends with a correlation of Chenoweth and Martin [79] (1955) for two phase flow in pipes, see Figure 2.19. Over a fairly wide range of flow conditions the two phase multiplier was predicted well by this correlation.

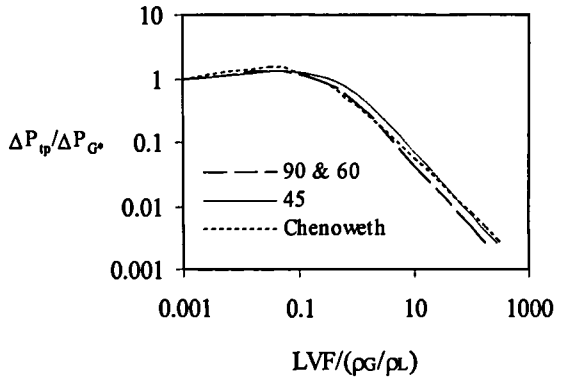

Figure 2.19 Ratio of two phase to gas only pressure drop Diehl and Unruh [78] (1958)

Fujii et al [43] (1972) conducted a series of experiments with low pressure steam flowing through banks of tubes and reported on both the heat transfer and pressure drop behaviour which they observed. The tube banks were in-line and staggered configurations and contained 15 rows of 14 mm diameter tubes with 22 mm spacing. Fujii stated that the prediction of pressure drop through condensers was fundamental to the design and that despite this there was little experimental information available on pressure drops.

Fujii et al analysed the pressure drop behaviour by applying Newton's second law to the steam flow between the ith and jth row. They neglected the momentum of the condensate and derived Equation 2.66, where ζ is the ratio of the maximum to minimum flow area, η is the number of rows crossed in the control volume, ξ is the ratio of squared mass velocities based on the maximum and mean flow areas, G_{mean} is the average mass velocity between the ith and jth rows, $\overline{\rho}$ is the steam density at a particular row and $\overline{\rho}_{mean}$ is the average steam density between the ith and jth rows.

$$P_i - P_j = C_D \frac{2(\zeta G_{mean})^2 \eta}{\overline{\rho}_{mean}} - \left\{ \left(\frac{\xi G^2}{\overline{\rho}} \right)_i - \left(\frac{\xi G^2}{\overline{\rho}} \right)_j \right\}$$

Equation 2.66

Fujii et al then proposed Equation 2.67 for calculating pressure drop distributions through tube bundles, this equation can be evaluated with reference to Figure 2.20 provided the inlet steam conditions are known. where j is the jth row, G_0 is the bundle inlet mass velocity and β is the number of rows required for complete condensation, i.e. the inlet mass flow of steam divided by the local condensation rate.

$$P_j - P_{j-1} = \frac{2G_0^2}{\overline{\rho}_{j-1}} \left\{ C_D \zeta^2 \left(1 - \frac{j-1}{\beta} \right)^2 - \frac{1}{\beta} \left(1 - \frac{j-0.5}{\beta} \right) \right\}$$

Equation 2.67

Shown in Figure 2.20 is the relationship and values of C_D against $Re\zeta x10^{-3}$ for staggered and in line tube bundles with separate values for the first row and remainder of the bundle, where,

$$\overline{Re}_\zeta = \frac{\zeta G D_o}{\overline{\mu}}$$

Equation 2.68

and ζ is as defined above.

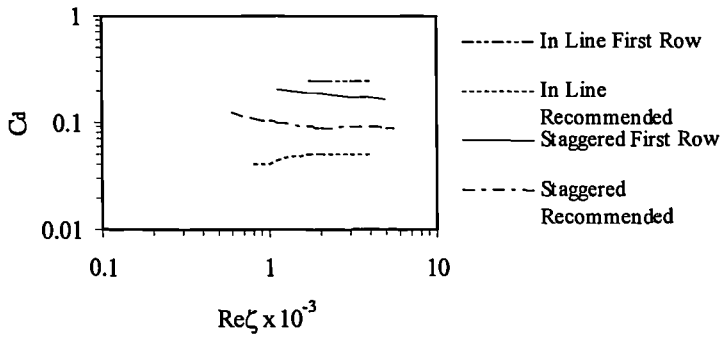

Figure 2.20 Tube bundle drag coefficients proposed by Fujii et al [43] (1972)

They also produced a simplified version of Equation 2.67 which contained a number of additional assumptions. This simplified equation will not be discussed here since compared with the data of Fujii et al the errors were up to approximately 3 times greater than the prediction of Equation 2.67 and Figure 2.20.

Grant and Murray [80] (1972) reported an investigation into pressure drop on the shell-side of a segmentally baffled shell and tube heat exchanger with vertical two phase flow. They conducted a series of experiments on a heat exchanger slice constructed from a rectangular Perspex shell containing thirty nine, 19 mm O/D tubes and measured both crossflow and window flow pressure drops. The tubes were arranged in an equilateral triangle configuration, with three baffles plates to generate four vertical crossflow passes in the tube bank. They generated a number of models which were generally based on homogeneous flow theory to predict the two phase multiplier. These models assume that the two phase flow friction factor was the same function of Reynolds number as single phase flow. They then proposed Equation 2.69,

$$\frac{\Delta P_{tp}}{\Delta P_{LO}} = \left(\frac{\mu_{tp}}{\mu_L}\right)^{\eta} \frac{\rho_L}{\rho_{TP}}$$

Equation 2.69

Equation 2.69 required a two phase viscosity. Grant and Murray defined two equations for two phase viscosity, these were,

$$\frac{1}{\mu_{tp}} = \frac{x}{\mu_G} + \frac{1-x}{\mu_L}$$

Equation 2.70

and

$$\mu_{tp} = x \cdot \mu_G + (1-x)\mu_L$$

Equation 2.71

Substituting μ_{tp} from Equation 2.70 & Equation 2.71 into Equation 2.69 Grant and Murray obtained Equation 2.72 and Equation 2.73 respectively.

$$\frac{\Delta P_{tp}}{\Delta P_{LO}} = \left\{1 + x\left(\frac{\rho_L}{\rho_G} - 1\right)\right\}\left\{1 + x\left(\frac{\mu_L}{\mu_G} - 1\right)\right\}^{-\eta}$$

Equation 2.72

They compared Equation 2.73 with their experimental data and stated that up to qualities around 0.5 this homogeneous correlation generally over estimated the pressure drop, while with qualities greater that 0.5 the prediction under estimated the pressure drop.

$$\frac{\Delta P_{tp}}{\Delta P_{LO}} = \left\{1 + x\left(\frac{\rho_L}{\rho_G} - 1\right)\right\}\left\{1 + x\left(\frac{\mu_G}{\mu_L} - 1\right)\right\}^{\eta}$$

Equation 2.73

The exponent η was 0.37 for both Equation 2.72 and Equation 2.73. However, it should be noted that Grant and Murray found that, due to gravity effects, the data for flow up through in a segment was different to that down through the next segment. They attempted to account for these differences by correcting the data but never achieved completely satisfactory agreement.

Grant and Murray then, as an interim measure, presented a correlation, Equation 2.74, for predicting crossflow pressure drops which fitted their data, see Figure 2.21.

$$\frac{\Delta P_{tp}}{\Delta P_{LO}} = 1 + \left(\Gamma^2 - 1\right)\left(x + 0.15x^{1/2} - 0.15x^{400}\right)$$

Equation 2.74

where,

$$\Gamma^2 = \left(\frac{\mu_G}{\mu_L}\right)^{0.37} \frac{\rho_L}{\rho_G}$$

Equation 2.75

and

$$\xi = \frac{\frac{\Delta P_{tp}}{\Delta P_{LO}} - 1}{\Gamma^2 - 1}$$

Equation 2.76

and x is the flow quality by mass.

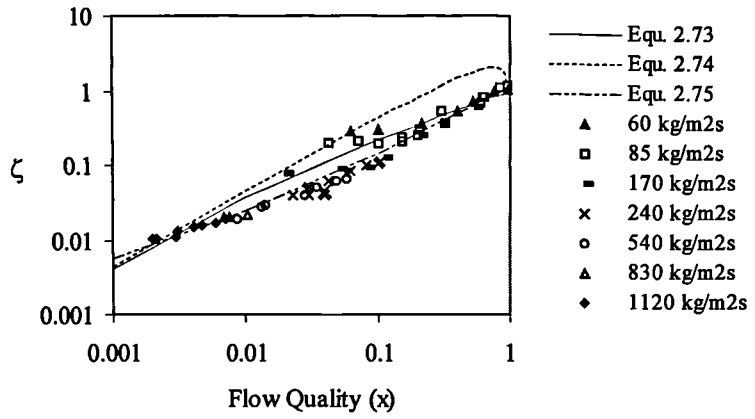

Figure 2.21 Experimental pressure drop data and theoretical prediction of Grant and Murray [80] (1972)

They concluded that the two phase cross flow multiplier was predicted well by Equation 2.74 and stated that it was also be valid when a change of phase is taking place.

Grant and Murray [81] (1974) reported on the pressure drops on the shell-side of a segmentally baffled shell and tube heat exchanger with horizontal two phase flow. They obtained experimental data from the same apparatus as [80] (1972) but with the

exchanger rotated to generated horizontal flow around the baffles. They analysed and compared their data with correlations for flow in pipes (Lockhart & Martinelli), and correlations based on homogenous flow and zero interface shear (Baroczy). They stated that, compared to their data, the correlations based on two phase flow in pipes overestimated the pressure drop, as did the models based on homogeneous flow. Figure 2.22 shows their horizontal crossflow data and the correlations discussed were the vertical axis is presented in the form of the non-dimensional group described by Equation 2.77

$$\varphi = \frac{\frac{\Delta P_{TP}}{\Delta P_{LO}} - 1}{\Gamma^2 - 1}$$

Equation 2.77

and Γ is given by Equation 2.78 below.

$$\Gamma = \left(\frac{\Delta P_{GO}}{\Delta P_{LO}} \right)^{\frac{1}{2}}$$

Equation 2.78

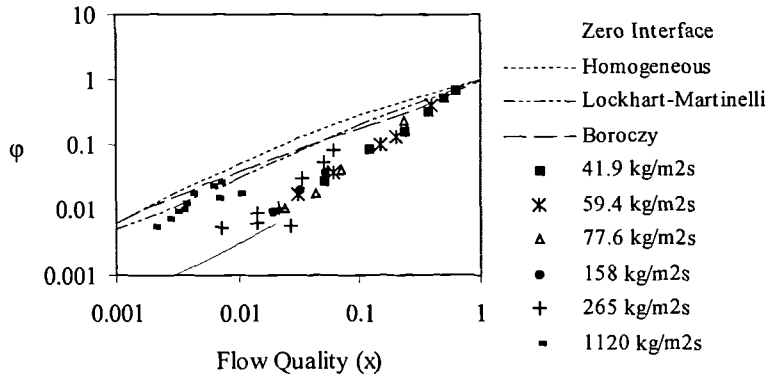

Figure 2.22 Comparison of experimental data of Grant and Murray [81] (1974) with theory

They concluded that for design purposes, Equation 2.79 should be used to estimate the pressure drop.

$$\frac{\Delta P_{tp}}{\Delta P_{LO}} = 1 + \left(\Gamma^2 - 1\right)\left\{ B x^{\frac{2-\eta}{2}} \left(1-x\right)^{\frac{2-\eta}{2}} + x^{2-\eta} \right\}$$

Equation 2.79

With B=1 for vertical up and down spray flow, B=0.75 for horizontal side to side spray and bubbly flow, B=0.25 for horizontal side to side stratified spray flow. Experimentally η was found to be 0.37, x is the fluid quality and Γ is given by Equation 2.78. With B=1 and η=0.37 Equation 2.79 predicted their experimental data very closely over a wide range of flow quality

Grant and Chisholm [82] (1977) reviewed the work of [80] (1972) & [81] (1974). They refined the correlations for predicting the pressure drops in tube banks both for window and crossflow zones. Equation 2.79 was presented with confirmed values for B and η depending on the flow and configuration. This equation has been evaluated and plotted for an air water system at 1 atmosphere for a selection of B and η values, see Figure 2.23.

$$\varphi = B x^{(2-\eta)/2} \left(1-x\right)^{(2-\eta)/2} + x^{(2-\eta)}$$

Equation 2.80

They compared their data with Equation 2.80 and found good agreement with their vertical flow data when B=1, η=037 and,

$$\varphi = \frac{\dfrac{\Delta P_{tp}}{\Delta P_{GO}} - \dfrac{1}{\Gamma^2}}{1 - \dfrac{1}{\Gamma^2}} \text{ or } \frac{\dfrac{\Delta P_{tp}}{\Delta P_{LO}} - 1}{\Gamma^2 - 1}$$

Equation 2.81

and

$$\Gamma^2 = \frac{\rho_L}{\rho_G}$$

Equation 2.82

Grant and Chisholm stated that for condensation when Γ^2 is very large Equation 2.81 can be rewritten in the form of Equation 2.83 below,

$$\varphi = \frac{\Delta P_{tp}}{\Delta P_{GO}}$$

Equation 2.83

They also compared Equation 2.80 with the correlation by Diehl and Unruh [78] (1958) good agreement was only found at qualities above 0.6. See Figure 2.23.

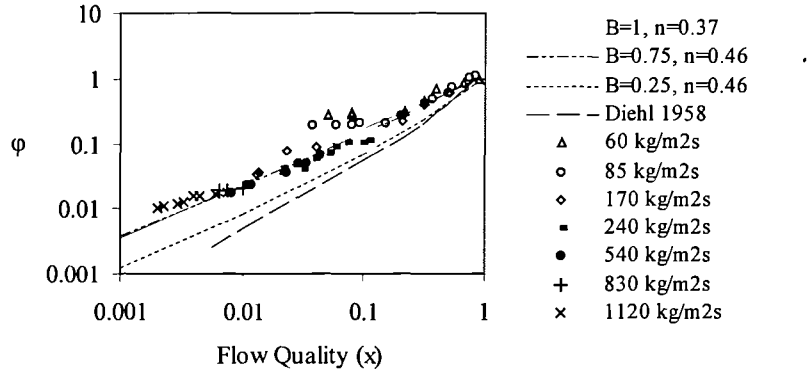

Figure 2.23 Comparison of experimental data of Grant and Chisholm [82] (1977) with theoretical predictions

Nicol et. al [83] (1982) conducted an experimental investigation into the condensation and pressure drop of steam in a tube bundle. They measured condensing and dry pressure losses through their bundle and concluded that the drag coefficients measured with condensation were less than the dry values and that values for the first row were significantly higher than subsequent rows. Nicol et. al also stated that the effect of

condensation rate was investigated and they stated that, once condensation had been established and the vapour separation point delayed, any further change in the condensation rate caused little or no change to the drag or separation point. Nicol et. al compared they results with data of Fujii et al [43] (1972) and noted that for the condensing case their pressure drop data was an order of magnitude lower. Nicol et. al suggested that this may be due to the low pressures at which their data was obtained. However, after studying their data, they concluded that no definite trend for drag coefficient with pressure was observed.

Summary

Publications relating to shell-side two phase pressure drops are relatively scarce. Shell-side two phase pressure drop is a highly complex phenomena and as a result most correlations available are highly empirical. Ishihara et. al. [84] (1980) conducted a critical review of two phase pressure drops and concluded that individual workers found good agreement when comparing their correlation with the data used for the construction, however, comparison with other workers demonstrated significant discrepancies. Ishihara suggested that one possible explanation for the range of data was that investigators had utilised different apparatus geometries and configurations, hence their data was not comparable. Currently, no universally applicable model exists, instead a number of solutions exist, each of which are only representative of certain geometries and flow conditions. In addition to uncertainties associated with two phase flow pressure drops, the situation is further complicated when condensation occurs due to suction which can change the boundary layer separation angle.

2.4 WILSON PLOT ANALYSIS TECHNIQUES

Wilson [85] (1915) conducted an investigation into the design method of heat transfer apparatus. He studied the available literature and stated that due to wide variations of published results, the choice of a suitable design method was unclear. He concluded that while tube-side heat transfer had been shown to be an exponential function of water velocity, the variations between previous workers were a result of neglecting one or more significant variables. To investigate the variations in the literature, Wilson conducted a series of experiments. His work focused on isolating the effects of water velocity and viscosity during heat transfer. Wilson achieved this by conducting heat transfer experiments over a range of cooling water velocities with different cooling water temperatures. From his results, Wilson found that, for a given velocity, the heat transfer coefficient increased with increasing water temperature. Wilson proposed a correction for the effects of temperature which reduced higher temperature data to a standard temperature result. Using this correction which was effectively Reynolds number, Wilson found that his data reduced to a single line on a heat transfer coefficient vs. corrected velocity plot. The information available from this plot was discussed, and it was highlighted that if the trend of the data was projected back to intercept the heat transfer coefficient axis, the intercept value was equal to the sum of the shell side and tube wall resistances. Wilson concluded that an expression based on the cooling water velocity, water temperature and tube diameter should be used for design.

While the primary objective of Wilson's work was to develop a rational basis for the design of heat transfer equipment, a number of workers, Briggs and Young [86] (1969), Khartabil et. al. [87] (1988) and Shah [88] (1990), have developed his basic method as a means of deducing unknown shell-side heat transfer coefficients from overall values. These workers have focused on the Wilson plot technique as a means of determining unknown heat transfer resistances and have improved the original method by using

improved correlations for the cooling water-side characteristics and including modelling of the shell-side to relax the requirements for constant shell-side conditions. Of these workers, Khartabil et. al. [87] (1988) and Shah [88] (1990), considered only single phase heat exchangers. Briggs and Young [86] (1969) presented a modified Wilson plot method for single phase, boiling and condensing heat exchangers. For the condensation case, Briggs and Young used the correlations of Nusselt [1] (1916) to characterise the film and Sieder and Tate [89] (1936) for the water-side. Briggs and Young compared their method with the basic Wilson method using two sets of R114 condensation data obtained at $190^{O}F$ and $168^{O}F$. On the Wilson plot constructed, using the traditional method the data obtained at $190^{O}F$ was parallel to, but clearly separated from, that obtained at $168^{O}F$. In contrast the same data on a Wilson plot, generated using the new method, all lay on a single line. Briggs and Young did not draw any conclusions specific to the condensation case or to the fact that the data had reduced to a single line. Instead they only concluded in general, stating that techniques had been developed and successfully used to determine the individual heat transfer coefficients from an overall coefficient for many types of heat transfer processes.

Summary

A number of Wilson plot type analyses have been developed each of which has applications which depend on the type of heat transfer occurring. However, the methods which include characteristic models for both the water and shell-sides require iterative solutions and are therefore less straight forward to solve than methods which characterise only the cooling water-side. Methods which characterise only the cooling water-side assume that shell-side heat transfer coefficient remains constant as the cooling water coefficient is varied. Obtaining suitable data while maintaining a constant shell-side coefficient can present a significant difficulty. Hence, if data with a constant

or near constant shell-side value is available, then the basic method using in conjunction with an accurate cooling water correlation may be adequate. However, if data of this type is not available, the more complex iterative method should be used.

2.5 LITERATURE REVIEW SUMMARY

Due to the long history of research into condensers there exists a large quantity of published work, both in the form of theoretical models and experimental data. Currently sufficient knowledge exists to permit the design of industrial condensers, however their remains considerable room for improvement in both methods and models. M. Rowe [2] (1983) states that there are still gaps in our knowledge, how is condensate distributed within the tube bank for example.

While some areas e.g. single tube theories have become highly refined, the majority of issues such as the applicability of single tube models to bundles, condensate inundation effects, pressure drop and the benefits of dropwise condensation are still the subjects of on going debate.

The filmwise results of previous workers are directly relevant to this work as they offer, scope to validate the apparatus, methods in the form of dimensionless groups and correlations which can be used as tools to analyse data, especially where due to inherent interactions multiple parameters varied. Compared to filmwise, information relating to realistic industrial applications dropwise condensation is very scarce.

There is therefore considerable scope for a new contribution to the field, from new data obtained under typical industrial conditions which would aid designers in realising the potential of dropwise condensation or improving filmwise modelling methods, addressing these are objectives of this work.

CHAPTER 3

EXPERIMENTAL APPARATUS

3.1 APPARATUS DESIGN SPECIFICATION

The experimental apparatus utilised for this work was designed and built as part of an EPSRC research contract (GR/K82475). The purpose of the facility was to duplicate the steam conditions found in UK, power station steam turbine condensers. To achieve this the following requirements were set as the design specifications:

I. A 75 tube bundle comprising of 5 columns and 15 rows with uncooled half tubes at the shell walls
II. Test pressures in the range 0.05 to 0.1 bar absolute
III. Steam approach velocities of up to 50 m/s.
IV. 19.05mm outside diameter by 150mm long titanium tubes with 0.5 mm wall thickness
V. Dry saturated inlet steam
VI. Inlet air concentrations of up to 8000 ppm.

With the exception of the 50 m/s approach velocity these design criteria were successfully achieved by the manufactured apparatus. The maximum steam velocity achieved in the test programme was 33m/s.

3.2 APPARATUS DESIGN

A simple condensation heat transfer apparatus was build in the Department by Azzeddine Aoune in 1990. Full details of the design can be found in [90] (1991). This apparatus originally contained a bundle of tubes with five rows and three columns.

Aoune's original design has remained substantially unchanged, except for a few modifications to the tube nest, e.g. recently, single tube tests have been undertaken and the instrumentation has been simplified. The operational limitations of this apparatus, and the requirements of further research, highlighted the need for a new, more sophisticated test facility.

The design process for the new facility was undertaken after, personal experience operating Aoune's apparatus, close consultation with previous users and reference to Fujii [91] (1992).

The apparatus for this work was assembled in the Department laboratory area on the site of a redundant steam turbine which had been previously removed and stored. This conveniently left the turbine ancillaries including: the boiler and steam piping, the exhaust condenser and cooling water system, the air and condensate pumps and the laboratory floor area available for this project.

3.2.1 DESIGN CALCULATIONS

3.2.1.1 Steam requirements

The steam supply to the apparatus was from the departmental package boiler. This had a maximum output of 900 kg/hr of dry saturated steam. The steam requirements for the test facility were calculated for a range of test conditions. These are tabulated in Table 3.1.

The steam inlet flow area for the tube bundle was $0.15 \times 0.1524 = 0.02286\ m^2$

	Steam Velocity				
Pressure	10 m/s	20 m/s	30 m/s	40 m/s	50 m/s
50 mbar	30 kg/hr	60 kg/hr	88 kg/hr	117 kg/hr	147 kg/hr
75 mbar	43 kg/hr	85 kg/hr	128 kg/hr	171 kg/hr	214 kg/hr
100 mbar	56 kg/hr	114 kg/hr	168 kg/hr	224 kg/hr	280 kg/hr

Table 3.1 Steam mass flow requirements

3.2.1.2 Heat load estimation

To allow the cooling water system to be designed, the maximum heat loads to the test cell and dump condenser were estimated. Details of the calculations can be found in Appendix A1. The maximum heat loads were estimated to be 80kW for the test cell and 150kW for the dump condenser.

3.2.1.3 Water side, heat transfer coefficients

In a attempt to prevent the overall heat transfer from being dominated by the water-side heat transfer resistance, a high water-side heat transfer coefficient of 10 kW/m^2K was specified. The water flow rate required to achieve this without a tube insert was calculated and found to be very high. This generated two significant difficulties. Firstly, the size and cost of the pumping equipment, and secondly, the resulting temperature rise of the cooling water flow through a tube would be very low, and therefore difficult to measure. The calculations were repeated with a 14mm diameter insert in the centre of the tube, see Appendix A2. This created an annulus for the water flow. The configuration generated the required tube-side, heat transfer coefficients with a water velocity of 2.75m/s. This corresponded to a mass flow rate of 0.28 kg/s per row. At

maximum row-heat-load conditions, this resulted in a cooling water temperature rise of 4.5K.

3.2.1.4 Choking nozzle flow

To fix the mass flow through the cell and reduce the steam pressure, a choking nozzle was included in the apparatus design, upstream of the test cell. The calculations to estimate the required nozzle diameter that provided sufficient dry saturated steam for the cell inlet conditions of 40 m/s at 50, 75 and 100 mbar can be found in Appendix A3. The results are summarised in Table 3.2.

Cell Pressure	50 mbar	75 mbar	100 mbar
Mass Flow required (kg/s)	32.43×10^{-3}	47.53×10^{-3}	62.32×10^{-3}
Less 7% for spray water evaporation	30.16×10^{-3}	44.20×10^{-3}	57.96×10^{-3}
Nozzle area required (mm^2)	40.1	50.78	77.07
Diameter (mm)	7.15	8.65	9.9

Table 3.2 Choking nozzle diameter calculation summary

Three nozzles were manufactured with diameters of 7, 8.6 and 10mm. Following initial operating experience, one additional nozzle with a diameter of 5mm was also manufactured. This was required to achieve the lowest pressure and velocity conditions without exceeding the maximum pressure drop across the pressure regulator.

3.2.1.5 Air flow requirements

The proposed experimental programme included a number of tests with steam containing a non-condensable gas.

For ease of design and use, air was chosen. The required mass and volume flow rates of air were calculated and are tabulated in Table 3.3.

Cell Pressure	50 mbar	75 mbar	100 mbar
Steam flow @ 40 m/s(kg/min)	1.95	2.85	3.73
Required air flow (kg/min) $\dot{m}_{air} / \dot{m}_s = 5000$pmm	9.75×10^{-3}	14.25×10^{-3}	18.65×10^{-3}
Air volume flow @ STP. (l/min) $\dot{m}_{air} / \dot{m}_s = 5000$pmm	8.125	11.87	15.54
Required air flow (kg/min) $\dot{m}_{air} / \dot{m}_s = 10{,}000$pmm	19.5×10^{-3}	28.5×10^{-3}	37.3×10^{-3}
Air volume flow @ STP. (l/min) $\dot{m}_{air} / \dot{m}_s = 10{,}000$pmm	16.25	23.75	31.08

Table 3.3 Air flow requirement calculation summary

For the air flow measurement a metric series rotameter, size 10 unit, was selected. This had two float options to provide the required range and sensitivity. The two floats were Duralumin and Koranite. A metric 10 rotameter with Duralumin float has a capacity of 20 l/min, the Koranite float 38 l/min, of air at standard pressure and temperature.

3.3 STEAM CIRCUIT.

3.3.1 GENERAL

The apparatus was designed to investigate the heat transfer and pressure drop behaviour of steam condensing both filmwise and dropwise, at conditions typical of a UK electricity utility, turbine condenser. To achieve this objective, a supply of low pressure dry saturated steam was required. This was achieved by generating high pressure steam and reducing this to the required conditions using the apparatus shown in photographs 1 & 2 and Figure 3.1.

Photograph 1, General apparatus view.

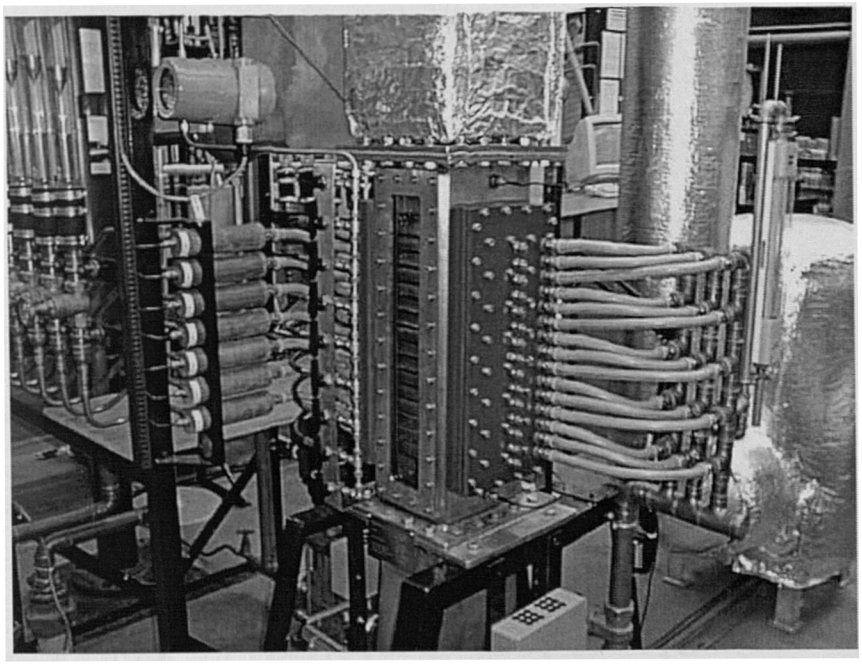

Photograph 2, Front view of test cell.

Referring to Figure 3.1, all apparatus components, from the 3 inch control valve, 4, through to the dump condenser control valve, 15, were manufactured from 316L stainless steel or non-ferrous materials, generally Tufnol, copper or brass. Manufacturing from corrosion resistant materials was chosen after studying the fouling

and discoloration which had occurred during previous work within the Department. Figure 3.1 is a scaled drawing of the apparatus which shows the size and relative proportions of the components.

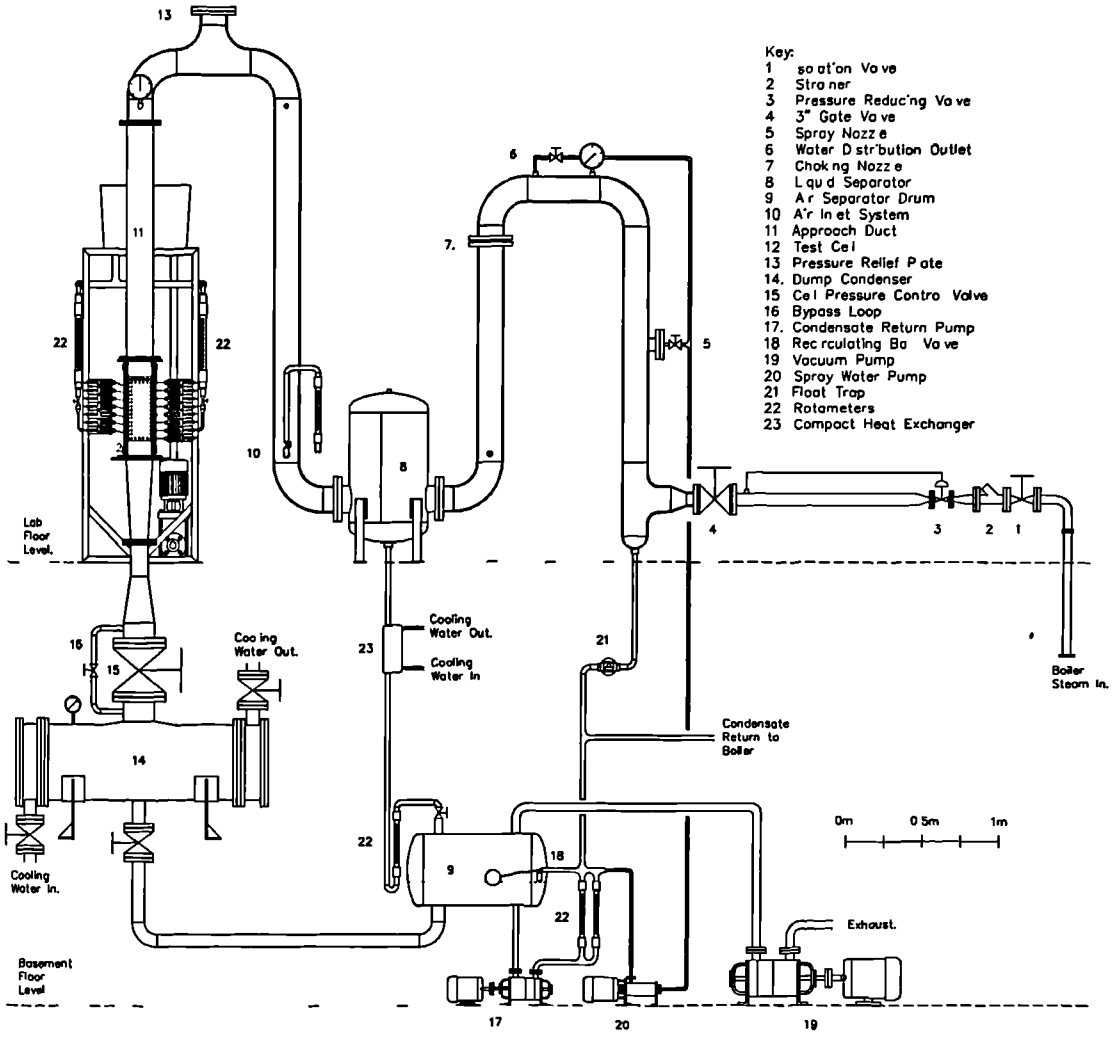

Figure 3.1 Apparatus steam and condensate circuit

3.3.2 STEAM CIRCUIT DESCRIPTION

Dry saturated steam was supplied from the departmental package boiler at approximately 11 bar. The apparatus was connected to this supply via an isolation valve, 1, and strainer, 2. The 11 bar steam passed through the Spirax Sarco self regulating pressure reducing valve, 3, which reduced the pressure to between 2.5 and 5 bar. The steam passed through the 3 inch gate valve, 4, and entered the stainless steel apparatus

section, where de-superheating spray water was injected. Spray water was injected through a water distribution outlet 6. This discharged 4 radial jets, directly above the choking nozzle and operated at a pressure of between 5–10 bar. The two-phase flow generated passed through choking nozzle, 7, where the water droplets flashed and desuperheated the steam to the saturation temperature. The steam thereafter flowed to the purpose built liquid separator, 8, where any excess water was removed and returned to the air separator drum 9. After the exit from the liquid separator, the air inlet system, 10, was included to allow non-condensables to be added to the steam flow. This consisted of a size 10 rotameter, a manual control valve and a spray bar to distribute the air uniformly in the steam. The steam was subsequently piped to the test condenser approach duct, 11, which was a 1.5 meter long, 150 x 153 mm rectangular section leading to the test cell. The final 150 mm of the approach duct contained a flow straighter. This was a honey-comb type device containing approximately 225, 10 x 10 mm square channels 150 mm long. The steam entered the test cell, 12 (also photographs 2,3,4 & 5), where it flowed vertically downwards in crossflow across the bundle of 75 tubes. An O-ring sealed pressure relief plate, 13, ensured that the pressure at the approach to the test cell could not exceed atmospheric.

A proportion of the steam was condensed in the test section, the remainder passed out of the cell through a duct to the dump condenser, 14, where it was condensed. The duct directly below the cell included a gate valve, 15, to control the flow to the dump condenser. This also provided a means of controlling the cell pressure. This valve was fitted with a ¾ inch bypass loop, 16, to ensure a condensate flow path, even when the main valve was closed.

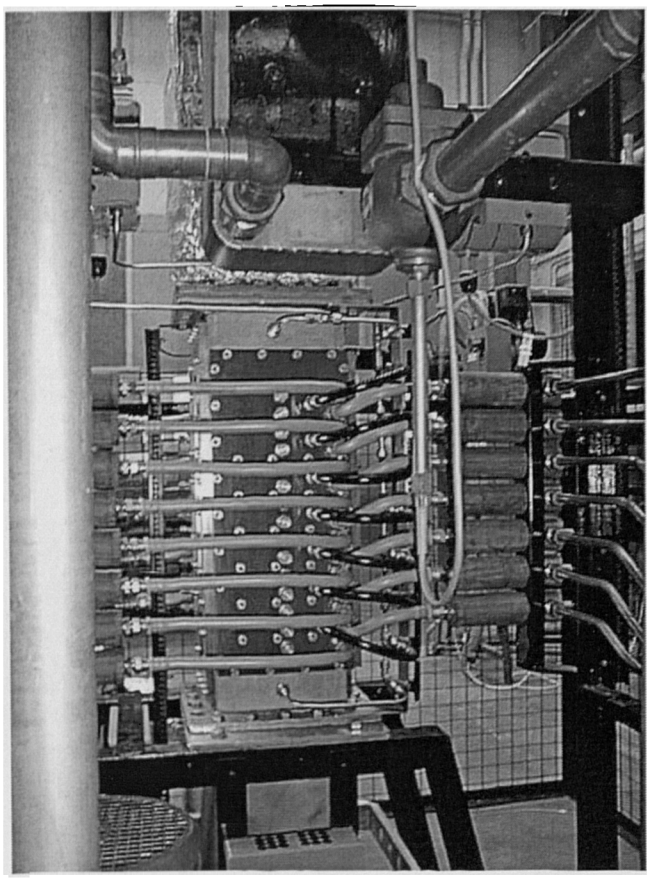

Photograph 3, Rear view of test cell.

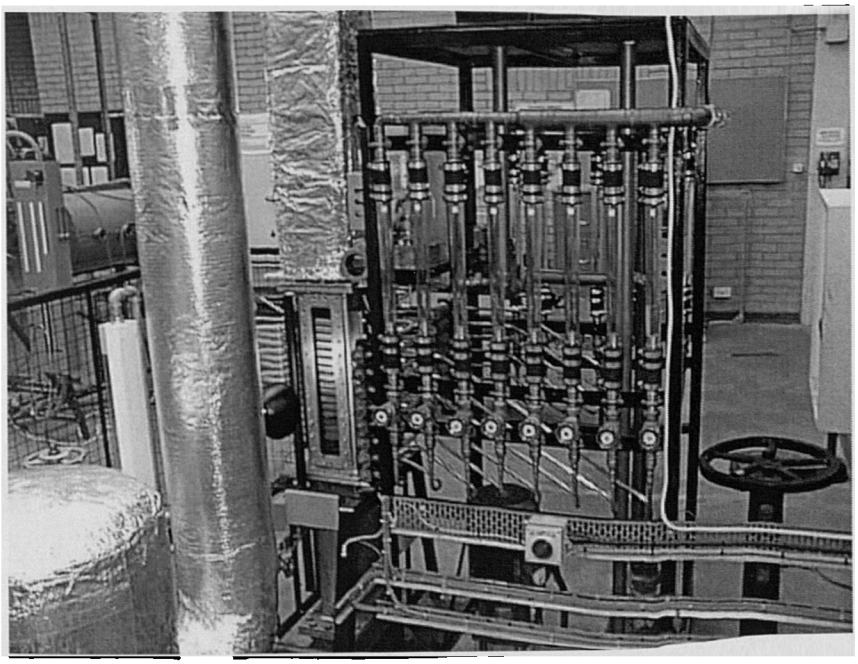

Photograph 4, Test cell and flow rotameters.

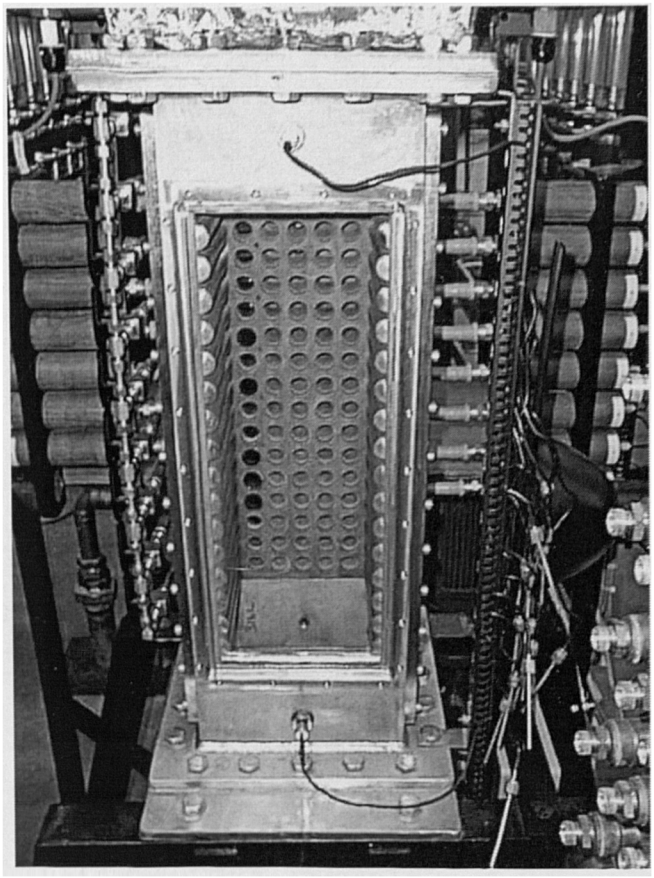

Photograph 5, Open test cell ready to accept tube bundle.

The condensate from the dump condenser flowed by gravity to the air separator drum, 9, where it recombined with the separator outflow. The level in this vessel, which included a level sight glass, was maintained by the condensate return pump, 17, and the three way re-circulating ball valve, 18, which, as required, returned the condensate back to the boiler feed tank. Air was removed from the air separator drum by a vacuum pump ,19, and exhausted to atmosphere.

3.4 COOLING WATER CIRCUIT.

The apparatus operated with two independent cooling water circuits, the Departmental cooling water circuit, which contained a number of additives and impurities, and the test cell cooling water circuit, which contained only clean mains water. The latter is shown in Figure 3.2.

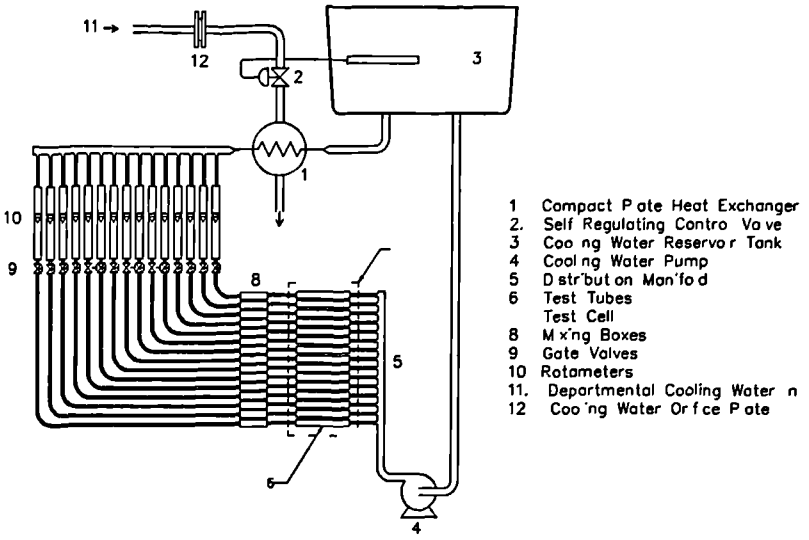

Figure 3.2 Cooling water circuit

The Departmental cooling water circuit included a force draught cooling tower which was located outside the building. Under normal conditions this was capable of supplying up to 130 gal/min of water at 10 - 15 ^{o}C. This cooling water was used to cool both the dump condenser, via a manually operated gate valve, and the cell cooling water through the compact plate heat exchanger, 1, shown in Figure 3.2. A Spirax Sarco self regulating control valve, 2, was used to control the Departmental cooling water supply to the compact heat exchanger. The cell cooling water circuit was a dedicated clean independent system, manufactured using only non-ferrous components to minimise tube side fouling. The water flowed from a reservoir tank, 3, into the cooling water pump, 4. This pump discharged into the distribution manifold, 5. Each of the 15 manifold outlets was connected to a row of tubes in the test cell using a short flexible hose. A test cell row is shown in Figure 3.3. A row flow entered the tube plate at 2, passed over resistance thermometer, 3, before entering the first of the five test tubes. The flow passed through all five tubes before discharging at 7. All the tubes contained 14 mm diameter Tufnol inserts, 4. These were located centrally to create an annulus 18.05 mm

O/D and 14 mm I/D in which the cooling water flowed. The five tubes in each row were connected in series by including cooling water return passages , 5, in the tube plates.

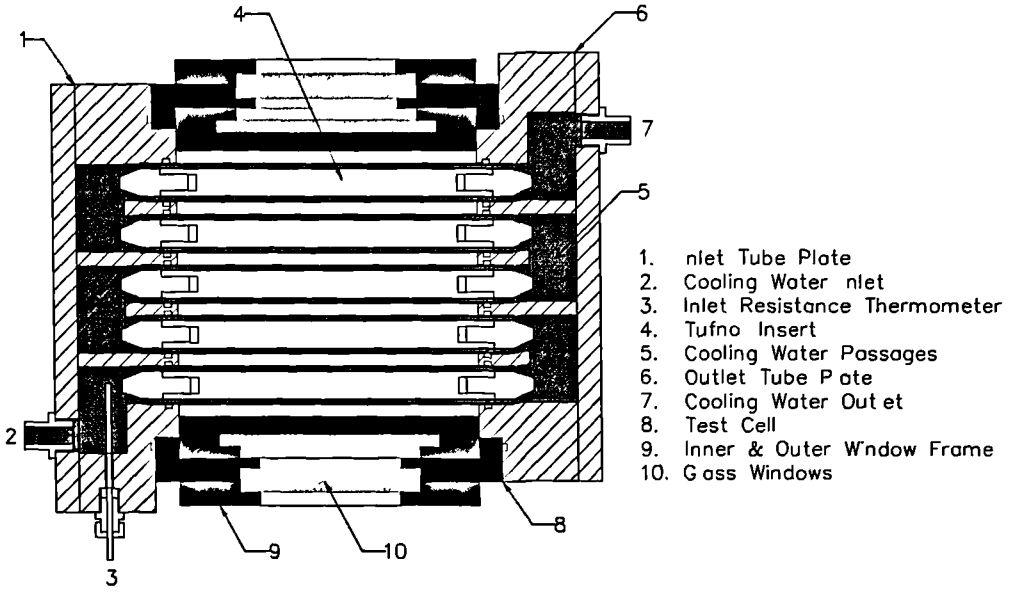

Figure 3.3 Test cell, horizontal cross section

Subsequent to leaving the test cell at, 7, via the outlet tube plate, 6, the flow passed through a short flexible hose that was connected to a Tufnol mixing box, 8 in Figure 3.2. The mixing box design, shown in Figure 3.4, physically disrupted and mixed the flow to ensure a uniform temperature. Water entered through a central inlet distributor containing 40, 3 mm diameter radial holes, photograph 6. The disrupted flows then recombined in the chamber, and passed over a resistance thermometer before leaving radially at the opposite end.

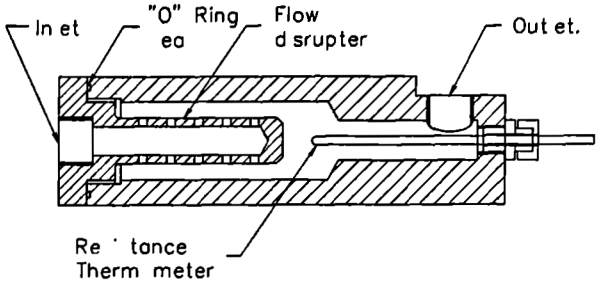

Figure 3.4 Mixing box design

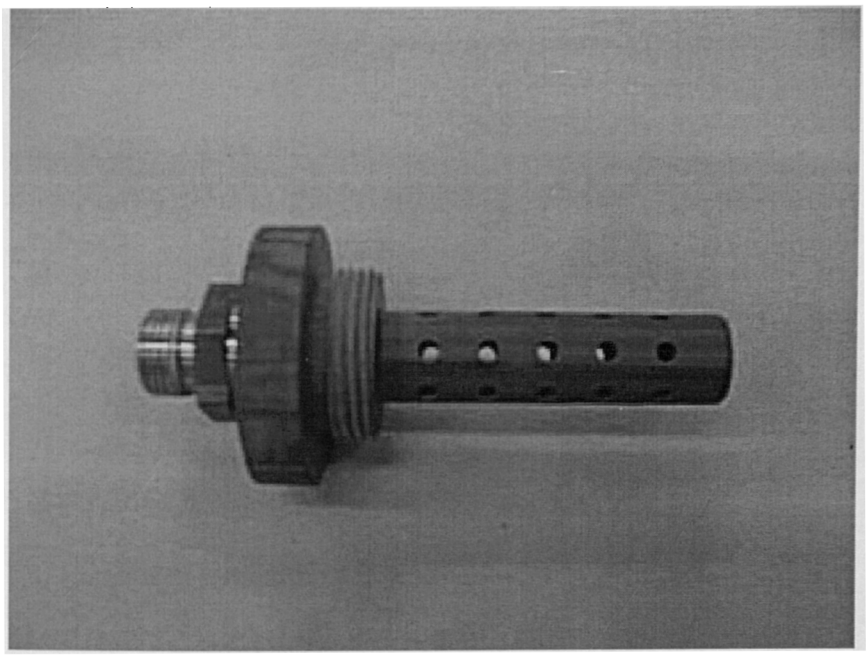

Photograph 6, Mixing box flow disrupter.

The 15 individual tube row flows passed through gate valves, 9 Figure 3.2, and rotameters, 10, before recombining and entering the compact heat exchanger, 1, where the flow was cooled to a controlled temperature before returning to the header reservoir tank, 3.

3.4.1 COOLING WATER OPERATIONAL CONSIDERATIONS

The project required accurate measurements of heat transfer from the steam to the cooling water. To maximise this accuracy, the cooling water circuit was designed to

ensure that any extraneous heat loss or gain by the cooling water was negligible. This was achieved by using low thermal conductivity materials. Tufnol was used for the tube plates and mixing boxes and thick wall rubber hose for the inter-connecting pipe work. The length of all flow passages and pipes was also minimised by locating the cooling water temperature rise PRTs as close to heat source as possible. Heat loss was further minimised since the cooling water temperature was similar in value to the surrounding air temperature.

3.5 TEST CELL

The test cell, photographs 2,3,4 & 5 and item 1, Figure 3.1, was central to the apparatus and contained a bundle of 75 tubes. The tubes were manufactured from titanium with an outside diameter of 19.05mm and an inside diameter of 18.05mm. Each tube was 170mm in length of which 150mm was exposed to steam. High and low surface energy tubes were used to promote either filmwise or dropwise condensation. Steam condensed on the outer tube surfaces. The mechanical finish for the filmwise tubes was as produced during manufacture. The dropwise tubes, photograph 7, were identical to the filmwise except that they were coated with a 1-2 μm thick plasma polymer as described in [67] (1997). These tubes were arranged in five columns and 15 rows with an in-line square configuration and a pitch diameter ratio of 1.33.

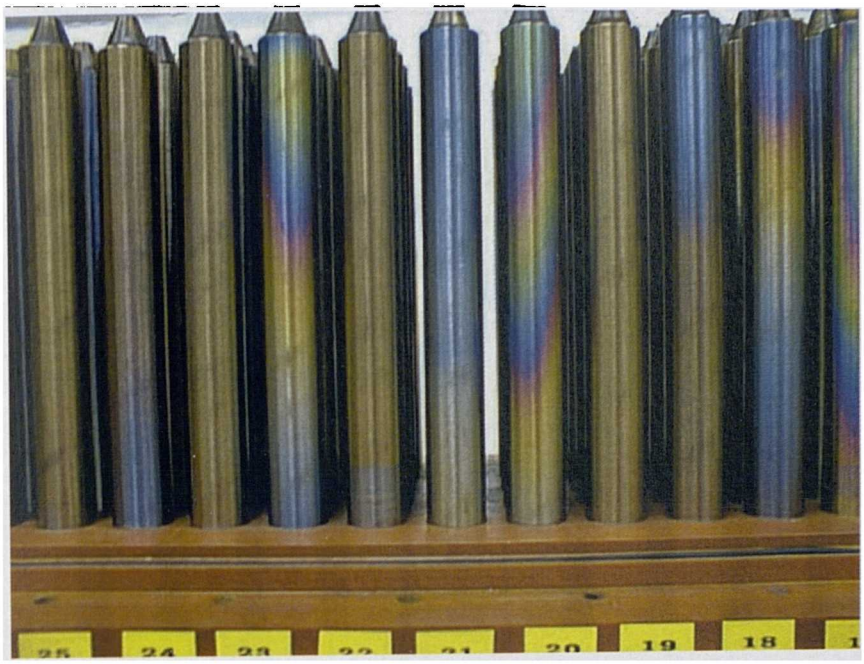

Photograph 7, New plasma polymer coated tubes.

The test cell, Figure 3.3, consisted of a number of major components. The shell was the basic structure. This consisted of a welded 316L stainless steel flanged square tubular shell, and was designed to accept and support all other components and to produce a pressure tight unit. It contained two toughened glass windows, 10. The outer window provided a pressure tight seal with the shell, while the inner window and frame, together with the half tubes, were included to create a boundary geometry representative of a complete bundle, see Figure 3.5. The windows allowed condensation throughout the bundle to be observed, however, due to the bundle configuration, observations into the core of the bundle were somewhat restricted by the geometry and uncooled half tubes.

The shell was also fitted with two tubeplates, 1 & 6 Figure 3.3 and photographs 8 & 9. These were manufactured from Carp brand Tufnol and were designed to position the 75 test tubes, supply cooling water to each tube via a series of passages, provide pressure tapping locations and locate the inlet cooling water resistance thermometers. Appendix A4 contains the tube plate manufacturing drawings.

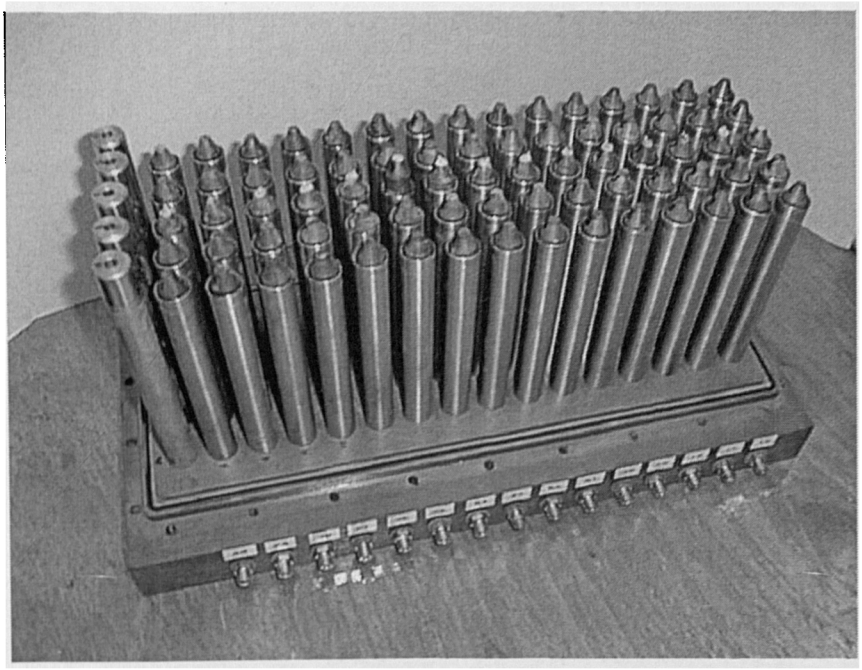

Photograph 8, Tube bundle ready for installation into cell.

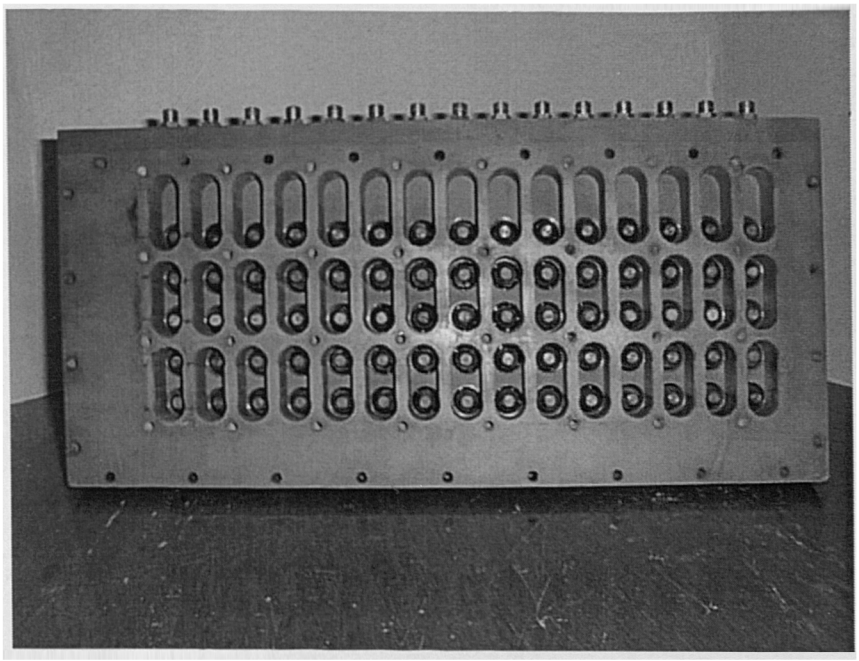

Photograph 9, Tube plate with tubes fitted.

A row of dummy tubes was fitted above the bundle and a column of uncooled half tubes was located on each wall, as shown in Figure 3.5 and photographs 5 & 8. The dummy tubes were fitted both as protection for the first row and to generate representative bundle flow conditions at the first condensing row. The steam inlet to the test cell was

via the duct and flow straightener described in section 3.3.2. These components were aligned directly above the cell providing a smooth transition for the steam into the cell, the flow cross section of which was 152.4 mm by 150 mm.

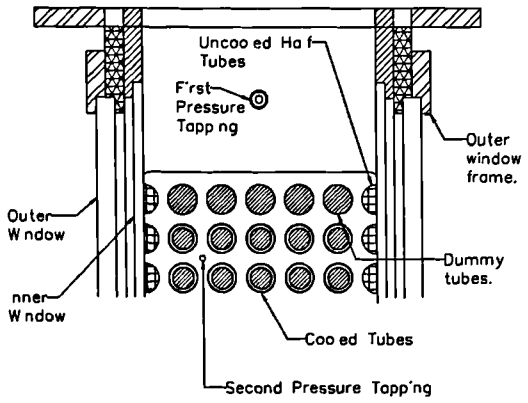

Figure 3.5 Test cell internal details

The shell also provided locations for up and down stream pressure and temperature measurements as shown in Figure 3.6. Nine pressure tapping were included in the design, two of which were in the cell walls, one 65 mm above the bundle and one 65 mm below. The outlet cell tube plate contained the other seven pressure tappings, these were located between every second row of tubes. Each pressure tapping was connected to a dedicated isolation valve via a flexible hose and a through nine-way manifold to the Rosemount pressure transmitters. All pressure tappings were manufactured to be perpendicular and flush with the cell wall. The diameter of the tappings were 4 mm in the cell wall and 5 mm in the tube plate.

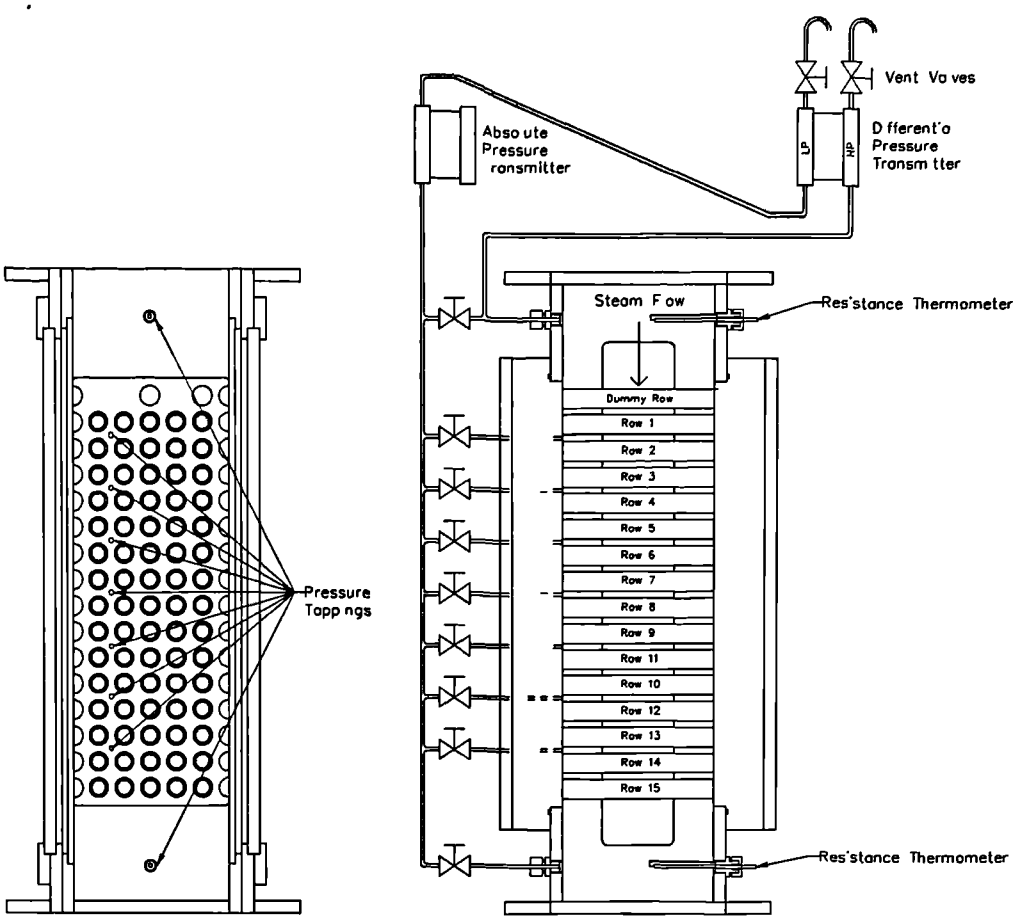

Figure 3.6 Test cell pressure tapping locations

3.6 INSTRUMENTATION

The operation of the apparatus required accurate measurements of a number of temperatures, pressures and flows. This was achieved by including between the test and dump condenser, 35 platinum resistance thermometers, 19 flow rotameters, 2 orifice plates and 3 Rosemount pressure transmitters. The calibration details of these instruments can be found in Appendix A5

3.6.1 TEMPERATURE MEASUREMENT

Temperature measurements of the steam and cooling water were made using platinum resistance thermometers (PRTs). These units consisted of a platinum film resistance element, nominally 100 Ω at 0^{o}C, with a temperature coefficient of approximately 0.385

$\Omega/^{O}C$. The platinum resistance film element was mounted on a ceramic base and fitted into the end of a sealed 3 mm diameter, 150 mm long stainless steel sheath. The units utilised 4-wire sensor operation. One pair of wires were current connections and the second pair were the voltage sense connections. All of the current connections of the PRTs and the high precision Tinsley standard 100 ohm resistor were connected in series, with voltage sensing connections wired directly to the data logger as shown in Figure 3.7

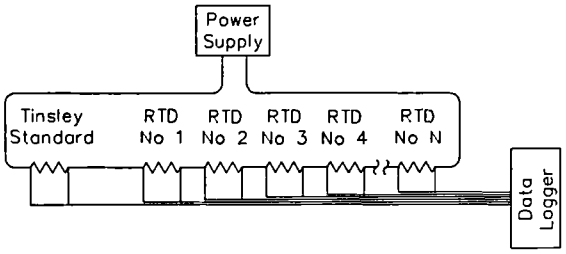

Figure 3.7 Resistance thermometer wiring details

In all installations the PRTs were inserted directly into the flow through a compression fitting gland seal. Of the 35 PRTs installed, 15 were fitted into the inlet tube plate to measure the row inlet cooling water temperatures, 15 were located in the mixing boxes to measure the row outlet cooling water temperatures, see Figure 3.4. A further two were installed in the test cell to measure the steam inlet and outlet temperatures and another three were fitted in the dump condenser to measure the inlet cooling water, the outlet cooling water and the condensate temperatures.

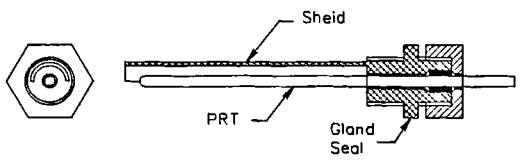

Figure 3.8 Resistance thermometer shield details

The inlet and outlet steam PRTs in the test cell were protected by a condensate shield, as shown in Figure 3.8. This shield was designed to prevented the sensor temperature being depressed by saturated or sub-cooled liquid from above.

The PRT current circuit was powered by a stabilised 7 VDC power supply, which supplied a sensor current of approximately 2.5 mA. This current was as recommended by the manufacturer and was sufficiently low to render the self heating effects negligible. The sensitivity and accuracy of the PRTs based on the data logger sensitivity and the inspection of data were respectively ± 0.005 and ± 0.05 K

3.6.2 FLOW MEASUREMENT

The measurement of flow was achieved using either orifice plates or KDG Mobey rotameters. A range of rotameters and float materials were utilised depending on the application. These are summarised in Table 3.4. Eight of the tube row rotameters are shown in photograph 4.

Duty	Size / model	Floats	Range (l/min)
Cell row cooling water flow	24	Stainless steel	0-20
Separator outflow	7	Stainless steel	0-1
Condensate outflow (1)	18x	Duralumin	0-2.2
Condensate outflow (2)	14	Stainless steel	0-5
Air inlet system	10	Duralumin Korannite	0-21 0-34

Table 3.4 Rotameter duties and details

The accuracy and discrimination of all rotameters were 2.5% of full scale and 1 mm respectively. Table 3.5 details the performance of each unit calculated as per the manufacturers procedure.

Size / model	Floats	Range (l/min)	Accuracy (l/min)	Discrimination (l/min)
24	Stainless steel	20	0.5	0.072
7	Stainless steel	1	0.025	0.0033
18x	Duralumin	2.2	0.055	0.0077
14	Stainless steel	5	0.125	0.018
10	Duralumin Korannite	21 34	0.525 0.85	0.5 0:5

Table 3.5 Rotameter accuracy and discrimination

The dump condenser flow was measured by an orifice plate with corner tapings that were connected to a mercury manometer with a calibrated scale. The range of this system was 20-200 gal/min on a square root scale. Above 40 gal/min the discrimination was 2 gal/min.

The cell plate heat exchanger flow was measured using a standard orifice plate, item 12 in Figure 3.2, as per BS 1042 with tappings positioned one diameter up and downstream of the plate (not the normal D and D/2). The differential pressure generated was measured by a model E1151 Rosemount pressure transmitter. The supply pipe and orifice diameters were 68 mm and 40 mm respectively. A full analysis of this system was not conducted since this system was only included as an indication of cooling water

flow. However, the flow rate corresponding to a selection of differential pressures were calculated and are tabulated in Table 3.6.

D/P (mbar)	1	2.5	5	10	20	40	60	80	100
$\dot{m}$ (kg/sec)	0.387	0.603	0.845	1.187	1.67	2.352	2.875	3.315	3.703

Table 3.6. Cooling water orifice plate flow vs. pressure drop characteristics

3.6.3 PRESSURE MEASUREMENT

Three stainless steel Rosemount pressure transmitters were used, a model 1151 smart absolute transmitter and two differential units, one model 1151 smart and one E1151. The absolute pressure transmitter was supplied with a calibrated range of 0-760 inches of H_2O and was installed to measure the pressure in the test cell. This unit was connected to the nine pressure tappings via a series of ball valves, see Figure 3.6.

The two differential pressure transmitters had the manufacturer's calibrated range of 0-30 inches H_2O. The first was used to measure the pressure drops through the tube bundle and as a check on the range of the absolute transmitter. The high pressure side of this unit was always connected to the pressure above the bundle. The low pressure side could be connected to any one of the nine pressure tapping via the same system of ball valves used by the absolute pressure transmitter. During operation the pressure lines to the transmitters were purged with air by simultaneously opening the two vent valves above the differential pressure transmitter for a short period of time (>0.25s). This process was completed before every pressure measurement. This ensured that the pressure lines were liquid free.

The second differential unit (E1151) measured the pressure drop across the orifice plate, 12 in Figure 3.2, to estimate the flow of departmental cooling water through the compact plate heat exchanger.

The outputs from these pressure transmitters were 4-20 mA analogue signals. However, the two units measuring the cell pressures also incorporated low accuracy, visual digital output indicators. The transmitters were energised by 2, 24 VDC stabilised power supplies as shown in Figure 3.9. These included 250Ω, 0.1% resistors to convert the 4-20 mA outputs to 1-5 volt signals which could be accepted by the data logging system.

The accuracy of the Rosemount pressure transmitters was ±0.25% and ±0.1% of their calibrated range for the absolute and differential units respectively. The sensitivity was not specified but was less than 1 mbar for the absolute transmitter and 0.05 mbar for the two differential units. Appendix A5 gives details of the full transmitter specifications. The accuracy of the measured cell pressures was limited by the turbulent stability of the flow rather than by the transmitters. The steam entering the test cell was at dry saturated conditions. This was checked by viewing into the test cell where an occasional fog could be observed as pressure variations occurred. As a check, the inlet pressure was compared with the saturation pressure based on the inlet temperature. Any discrepancies were generally less than 1 mbar.

3.6.4 DATA ACQUSITION SYSTEM

The experimental apparatus used in this research included an electronic data acquisition system for the measurement, recording and storage of data. The system comprised an Elonex Pentium 100 personal computer, a Hewlett Packard (HP) 75000 Series B mainframe with an HP1326 5 ½ digit internal multimeter and four 16 channel relay multiplexer cards as shown in Figure 3.9. The system also included one HP E1347A, 16 channel thermocouple multiplexer and three HP E1345A, 16 channel multiplexers. The

HP E1347A had a cold junction compensation option. For this application the cold junction was not used and the card performed in an identical manner to the HP E1345A cards.

The voltmeter was configured as a scanning unit and controlled all of the multiplexer card switches. The resolution of this instrument was dependent on the voltage range selected. Two ranges were used, 0.91V and 7.27V, resulting in resolutions of 0.953μV and 7.629μV respectively. The sample time for both of these reading ranges was 65ms.

The mainframe housed the voltmeter, the multiplexer cards and a power supply and also provided a communications interface between the internal components and the controlling computer. The mainframe and its contents are and will be referred to as the data logger.

The system computer was fitted with an HP-IB interface card. This allowed communication with the data logger, via a connecting RS-232 type cable. Communications were as per the IEEE Standard 488.2-1987 IEEE Standard Codes, Formats, Protocols and Common Commands. The computer was installed with the Windows NT-4 operating system and the Hewlett Packard Visual Engineering Environment (HP VEE) software. This software allowed the computer to control the data logging equipment and store data. Windows NT provided a 32 bit operating system and HP VEE offered a convenient instrument user interface. HP VEE was a graphical programming language. This allowed programs to be generated by connecting together standard icons, blocks and objects. Using HP VEE communication between the computer and the data logger occurred through a to/from object. This is instrument specific and is the only object that required user installation/configuration, as detailed in APPENDIX A6.

Connections between the data logger and the resistance thermometers were via 4, 15 and 25 core screened cables. The pressure transmitters were connected via 2 core un-screened cables.

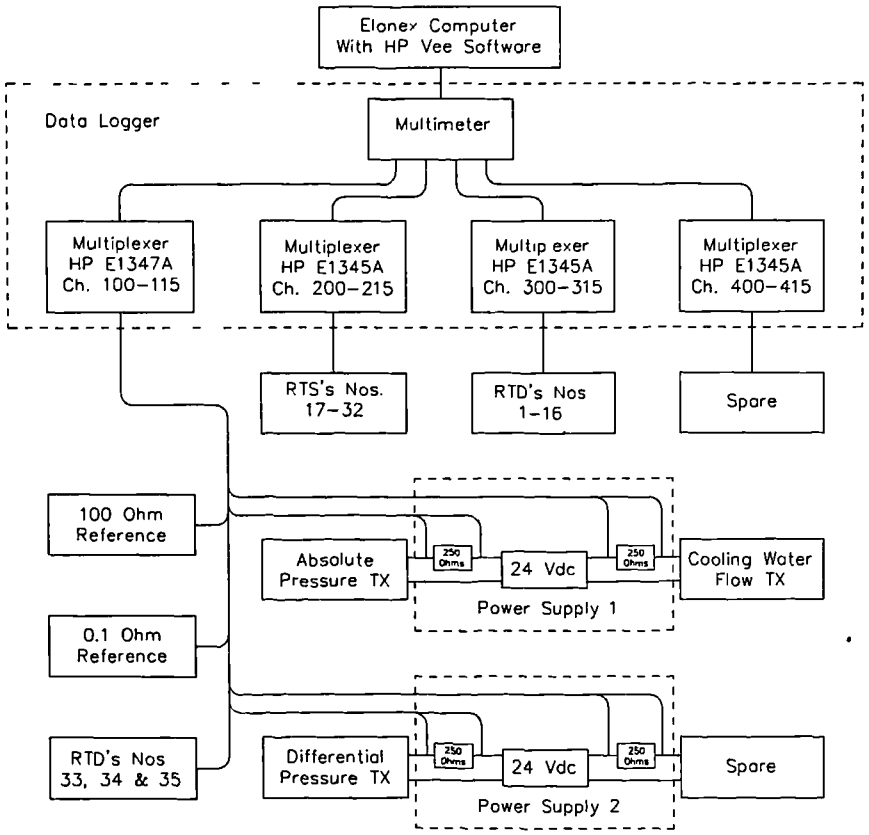

Figure 3.9 Data logging system wiring details

3.6.5 THE DATA LOGGING PROGRAMME

Two computer programs were generated to assist with the collection of data. A display program that provided real time indications of all of the apparatus variables was written. This allowed the system to be monitored during start up and between tests, Appendix A7 screen 1 is a print of the computer screen and shows the information available. A data logging program was also written. This is described below. Appendix A7 screen 2, shows the screen output after the process of logging a set of data has been completed.

The data logging programme was written in HPVEE and was developed throughout the apparatus commissioning period. The final version included on-screen instructions. With the HPVEE software running and the programme file opened, the procedure to log a data set was as follows. The first stage was to enter a name for the new data file. Once entered, the program was run and the computer prompted the user to check that only the top pressure tapping valve was open. When the OK icon was clicked, the data logger proceeded to scan channels 100-115, 200-215, 300-315 & 400-415, (details of the instruments connected to the various channels can be found in Appendix A8). This recorded all the temperature and the inlet pressure data. Once completed the system instructed the user to open the second pressure tapping valve only. When the OK icon was clicked, the data logger proceeded to scan pressure transmitter channels 100 & 101. The process of opening pressure transmitter valves and logging the pressure data was repeated for valves three through to nine. Once all of the data had been collected, the computer completed the program by writing the channel number and data to the file specified. Data file names were generated sequentially and were of the form T059.DAT. The numerical portion corresponds to the test number. The process of logging one data set, as described above, was completed in approximately 30 seconds. Appendix A8 contains the contents of a typical data file. Channel descriptions have been added to aid interpretation.

3.7 APPARATUS COMMISSIONING

The apparatus was commissioned over a 6 week period between April and June 1998. During commissioning, 36 sets of data were recorded. This allowed the capabilities of the apparatus to be found and areas for improvements to be highlighted. A summary of the commissioning difficulties and solutions follows.

During the first batch of tests, T004-T012, the spray water pump was found to be generating very little output pressure. The pump was returned to the manufacture who supplied a replacement unit. During these tests an absolute maximum steam velocity of approximately 45 m/s was found. The second batch of tests, T013-T016, were completed with an operational spray water pump. This provided a flow of de-superheating spray water, the excess of which was removed by the liquid separator. The water removed by the separator was piped into the basement where the flow rate was measured before discharging into the air separator drum. The temperature and pressure of this water caused it to flash. The resulting two phase flow passed through the rotameter, invalidating any measurements. A compact plate heat exchanger, item 23 in Figure 3.1, was fitted to cool the separator outflow and prevent flashing. Tests T017-T023 were conducted with the new heat exchanger located horizontally on the lab floor. The heat exchanger successfully cooled the outflow, however, under conditions where the pressure difference between the liquid separator and air separator was very low, a vapour lock was generated and a flow could not be established. The adjoining pipe work and heat exchanger location were redesigned. The new redesigned pipe work configuration was such that the water flowed under gravity alone.

Tests T024-T030 were completed. These highlighted the fact that controlling the cell pressure using the 6" gate valve in the duct below the test cell was unsatisfactory. These tests were at lower flow rates and proved that the desired cell pressure could only be achieved when the dump condenser gate valve was fully closed. This prevented condensate returning to the air separator and thus prevented measurements of the flow. A bypass loop, 16 in Figure 3.1, was included to prevent condensate accumulation and tests T031-T032 were completed. During these tests the steam de-superheating system failed to operate. The fault was traced to an air lock in float trap 21, in Figure 3.1. As a result the unit was removed and fitted with an addition thermostatic valve. This ensured

that the trap was adequately purged with steam at all times. The apparatus was again run and tests T033-T040 were completed. These tests highlighted an error in the energy balance calculation. An examination of the system revealed that the cell row cooling water rotameters had been incorrectly supplied by the manufacturer and hence that the calibration charts were invalid. New calibration charts were produced and all previous data were recalculated. The commissioning tests demonstrated that the apparatus was readily capable of producing energy balance errors of less than ± 10 %. The heat balance calculation compared the total heat absorbed by the test cell and the dump condenser with the theoretical heat load required to both condense the steam and sub-cool the condensate to the test conditions. Since an error value of ± 10 % was readily attainable, an error limit of ± 5 % was set for the test programme. Any data set found with an error above this value was deleted and the conditions re-run.

With the apparatus operating satisfactorily, a leak test was conducted on the circuit vacuum sections, between the choking nozzle and the outlet from the dump condenser. For the purpose of the pressure test, the system was pumped down to a pressure of approximately 200 mbar and isolated. The pressure in the apparatus was then monitored and recorded. Over a period of 40 hours, the pressure rose from 193 mbar to 198 mbar for build 1, as shown in Figure 3.10. Neglecting fluctuations produced by temperature variations, a leak rate of 0.125 mbar/hr was measured for build 1. This corresponds to an air leak rate of approximately 0.15 grams per hour. This process of leak testing was repeated each time the apparatus was rebuilt. Figure 3.10 shows the leak rate for each build and Appendix A9 gives details of which tests were completed for each build.

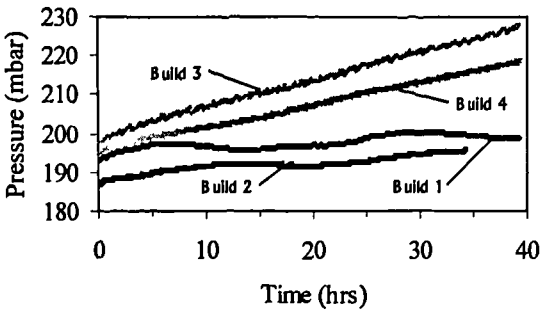

Figure 3.10 Pressure test results

3.8 EXPERIMENTAL PROCEDURE

During the experimental testing period, the data logger remained switched on since, during commissioning, maximum accuracy and repeatability were only achieved when the operating temperature of the data logger was approximately constant.

3.8.1 STARTING PROCEDURE FROM COLD

The following procedure was followed each time the apparatus was started from cold.

The day before, if required, the boiler was warmed to reduce the start up time. The required choking nozzle was fitted and the cell cooling water tank was filled with tap water.

On the day of the test, the boiler was started up and allowed time to reach the 11 bar operating pressure. Once steam was available, the cooling water supply valves to the dump condenser, the cell heat exchanger and the separator outlet heat exchanger were opened to establish the required flow. The cell cooling water pump was then started and the cooling water temperature and flows through the tubes rows were set. The system was pumped down to the limit of the vacuum pumps, approximately 30 mbar, and steam was admitted into the test section.

Superheated steam was allowed to flow for approximately 20 minutes to warm the pipe work. Subsequently the spray water pump was started and the required flow rate set. The out flow from the separator drain was checked.

With all these parameters set, a further 30 minutes was allowed to stabilise temperatures within the apparatus before attempting to set specific flow conditions.

3.8.2 PROCEDURE TO OBTAIN DATA AT SPECIFIC STEAM CONDITIONS

Once the apparatus had warmed through sufficiently and all systems were operating satisfactorily, data were collected using the following procedure.

I. The required steam mass flow rate through the test cell was established by adjusting the pressure upstream of the choking nozzle.
II. The temperature and flow rate of the cell cooling water were set to generate the necessary overall driving temperature and the desired tube-side, heat transfer coefficient.
III. When the cooling water conditions were stable, the steam pressure in the test cell was set. This was done either by adjusting the cell pressure control valve, the flow rate of the dump condenser cooling water, or by isolating the cooling water from a number of the lower tube rows in the test cell.

This procedure was repeated until the required test conditions were reached.

Once the conditions were achieved and the apparatus had stabilised, two sets of data were obtained. The procedure for the logging of data is described in section 3.6.5.

After a set of data was collected, it was processed by a Fortran program which included an energy balance calculation. Any data set found with an energy balance error greater than 5% was deleted and the data re-sampled, this was a rare occurrence, e.g. typically

only 1 in 30 data sets were deleted. With satisfactory data taken, the apparatus was run without any adjustments for a further 10–15 minutes. A second set of data was then taken, producing a pair of results.

For each set of data taken, a record sheet was completed with the manual data inputs, the apparatus settings, the nozzle size and the allocated filename. Appendix A10 contains an example of a typical sheet.

3.8.3 APPARATUS STABILITY.

The apparatus stability was analysed by comparing the variations in pairs of results from T041 to T150. The average change and standard deviation of a range of variables taken at a 10-15 minutes interval are listed below in Table 3.7. The average change is the average value of change from one test to the next, and the standard deviation is that of the average change. Since the average change values are significantly less than that standard deviation, this indicates that the data were distributed evenly around a mid value, with the extent of the spread being quantified by the value of the standard deviation.

Variable	Average change		Standard deviation	
	%	Units	%	Units
Cooling water inlet temperature (^{O}C)	0.05	0.014	0.287	0.074
Cooling water outlet temperature (^{O}C)	0.08	0.02	0.378	0.1
Steam velocity (m/s)	-0.368	-0.082	2.56	0.639
Inlet temperature (^{O}C)	0.347	0.118	1.29	0.447
Inlet pressure (mbar)	0.151	0.05	1.55	0.914
Overall heat transfer coefficient (kW/m^{2}K)	-0.591	-0.048	2.96	0.231

Table 3.7 Apparatus stability calculation summary

CHAPTER 4

DATA PROCESSING

4.1 GENERAL

The data collected for this work was measured and stored using the computer controlled data logging system described in sections 3.6.4 and 3.6.5. For each data set recorded this system created a sequential disk file containing 80 voltage entries, see Appendix A9. Each of these voltages corresponded to one of the apparatus temperature or pressure measurements. Since these output files contained only raw voltages, data processing was required before any analysis work could be undertaken. Due to the quantity of data obtained, a Fortran program was developed. This program was fully automated, and the final code processed the raw data, calculated the overall row heat transfer coefficient, the local shell-side flow conditions, performed an energy balance, predicted the shell side heat transfer coefficient for each row, conducted an error analysis and calculated a range of heat transfer and pressure drop predictions. A typical output print is contained in Appendix B1.

4.2 DATA PROCESSING PROGRAM

The operational details of the data processing program are discussed below. For further details and the program sequence see Appendix B2. For data storage array locations see Appendix B3. Throughout the program, whenever physical properties of water or steam are required, they were obtained by calling the properties subroutine FASTWS in program PROPS. The subroutine FASTWS being a program developed by the National Engineering Laboratory. The data processing program produced an output file for each data set obtained.

4.2.1 RAW DATA PROCESSING

The primary purpose of the data processing program is to convert the raw voltage contents of a data file into meaningful temperatures and pressures. Before this was completed the processing program requested a number of manual inputs. Details of these complete with typical values can be found in Appendix B4. This manual input was automated by creating input disk files for each test and transferring the information to the data processing program using DOS piping techniques.

The program processed the raw data in the subroutine "RAWPRO" the main input of which was two arrays CALC and DATA. Array CALC contained the calibration constants for each instrument, where the values had been previously obtained from the calibration constants disk file CAL.DAT by subroutine GETDAT. Calibration constants were obtained by the method described in Appendix A5. Array DATA was also generated by the subroutine GETDAT in this case the contents of the specified raw data file were read and stored in array DATA. Using the calibration constants and raw data, subroutine RAWPRO calculated the individual temperatures and pressures, writing the results to the third column of array DATA. Array DATA was then passed to subroutine DMAN which reordered the temperature data into columns of cooling water inlet, outlet and temperature rise and stored the results in array TEMPS. Steam inlet and outlet temperatures were also written to this array.

Throughout the program the row numbers are referred to as IROW numbers, this terminology refers to the bundle position rather than condensing row number. i.e. the dummy row is IROW=1 and the first condensing row is IROW=2. Data contained in an output file at a specific IROW number correspond to the variables at the row, i.e. cooling water temperatures, heat flux etc., or to the row approach conditions i.e. steam velocity, pressure, temperature, quality etc.

The array DATA was then transferred to subroutine PRESS. This routine reordered the pressure results from both the absolute and differential transmitters. The reordered data was then stored in three columns of array PRES, where the columns correspond to the three results and the rows to bundle depth.

The results of this processing can be seen under the heading "Experimental data" in the sample output print contained Appendix B1.

4.2.2 OVERALL HEAT TRANSFER COEFFICIENT AND LOCAL CONDITIONS

With the raw data processed and manipulated, the program continued to calculate the overall heat transfer coefficient for each row. Before this could be accomplished the local shell side steam conditions were required.

Since the apparatus design only included a pressure tapping after every second row of tubes, the first step in calculating the local conditions was to predict and recalculate the pressure distribution through the bundle. Subroutine FITLN performed this task. The routine calculated a least mean squares error quadratic curve fit for the pressure data from IROW=3, i.e. the second pressure tapping, to the last tapping within the cooled portion of the bundle. Data from the first and last pressure tapping were never included in the curve fit since, due to bundle entrance and exit effects, these measurements were likely to be unrepresentative of the distribution within the bundle. The routine generated and solved three simultaneous equations to calculate the quadratic coefficients. The results were then used to re-compute the pressures at all locations within the condensing portion of the bundle. FITLN stored these results and transferred directly, the bundle inlet and outlet pressures into the first column of array ALOC.

The main program then calls subroutine LOCAL, which predicted the row local shell side flow conditions. LOCAL first calculated the air concentration and the corresponding steam partial pressure storing the results in array ALOC. The routine

proceeded to calculate the mixture properties and check that the saturation pressure based on the pressure transmitter was not greater than the value corresponding to the temperature measured by the inlet steam resistance thermometer. The code normally calculated a saturation temperature based on the measured pressure. However, if the above check finds a physically incompatible result,. i.e. the saturation temperature based on the pressure transmitter was greater than the temperature sensed by the resistance thermometer, a pressure correction factor was calculated and the program was instructed to return the subroutine beginning. If a pressure correction factor was computed the program applied the result to the pressure distribution values before proceeding with each of the row calculations. The flow conditions at the approach to the remaining rows were calculated, with or without the correction factor, using the same procedure except that, for each row the condensate flow was calculated from the sum of the heat adsorbed by the rows above. The calculated conditions and heat flux etc. were stored in array ALOC. Where the measured conditions were not physically possible the temperature value was given precedence since its theoretical accuracy was greater

With both the water-side and steam-side local conditions known, or estimated, the main program called subroutine HTC. This subroutine calculated a log mean temperature difference and estimated the overall experimental heat transfer coefficient for each row. The results were stored in array HTCOEF.

The last subroutine called before the major theoretical and analysis subroutine was HBAL. This routine conducted an energy balance on the system by summing the heat absorbed by the rows of the test cell, adding the energy absorbed by the dump condenser and comparing the result with the theoretical condensing load. The theoretical condensing load was estimated from the known mass flow of saturated steam through the system and the estimated enthalpy of the inlet steam and outlet sub-cooled

condensate. The result of an energy balance can be seen on the sample output in Appendix B1.

4.2.3 SHELL-SIDE HEAT TRANSFER COEFFICIENT PREDICTIONS

Up to this point, data processing only involved the computation and manipulation of experimental data. Using only experimental data, analysis of the bundle was limited to that described above.

The main focus of the work was the analysis of the shell-side heat transfer performance. However, due to the failure of the direct tube temperature measurement system, the evaluation of the steam-side heat transfer coefficient requires further detailed data analysis. This analysis work was completed in subroutine THEORY. The function of this routine can be divided into two categories. The first section of the routine used theoretical predictions to permit further analysis of the experimental data. The second section evaluated established heat transfer theories and correlations purely for comparative purposes. Details of the theory relating to further analysis is described below. That for comparative purposes is described in Section 4.2.5.

The subroutine THEORY calculated an experimental shell side heat transfer coefficient by predicting values of the water-side and tube wall heat transfer coefficients. Details of the tube-side heat transfer coefficient are given in section 5.2 The tube-wall, heat transfer coefficient was estimated assuming radial conduction based on the outside diameter. The equation used is given in Appendix B2. These results were used in conjunction with the inside and outside wall experimental heat fluxes to calculate the shell-side temperature difference and heat transfer coefficient. The calculated heat transfer coefficients and corresponding temperature differences were stored in array HTCOEF.

The final data processing task performed by the program was the calculation of an experimental $Nu/Re^{1/2}$ value and the parameter F, as defined by Rose [4] (1988) and Equation 2.23.

4.2.4 ERROR ANALYSIS

A subroutine named ERRORS was included in the data processing program. The purpose of this routine was to use a small error analysis techniques to, calculate an estimated percentage error in the following measurements: heat flux, overall heat transfer coefficient, tube outside wall to steam bulk temperature difference and heat transfer coefficient. The routine evaluated errors for each row using the predicted the test conditions and the measured experimental variables and stored the results in array ERROR. The error differential equations used in this routine are shown in Appendix B5. Results from this analysis can be found in the output prints in Volume 2 in the section Experimental Data Analysis, an example of which can be found in Appendix B1.

4.2.5 THEORETICAL PREDICTIONS

As a result of the experimental programme and the apparatus configuration, the only shell side flow conditions which were fully within the operators control were those at the approach to the first condensing row. The flow conditions at all other rows were dependent on the heat transferred by the rows above. At these locations this dependence complicated the analysis of the shell side heat transfer coefficient. Due to these variable conditions, the most convenient analysis tool available was the comparison of data with established theoretical prediction methods. A range of heat transfer and pressure drop predictions were investigated, and, where required, the most representative model was utilised to further reduce and analyse the experimental data. Heat transfer predictions

were evaluated in subroutine THEORY and pressure drop predictions in DROPCAL. The various models are discussed below.

4.2.5.1 Heat transfer

To validate the apparatus and as a tool for processing the results, a number of established filmwise heat transfer correlations were evaluated The correlations used were those of Nusselt [1] (1916), Rose [4] (1988), Shekriladze & Gomelauri [9] (1966) and Fujii et al [11] (1972). These correlations were chosen for evaluation since they are, in the case of Nusselt, the classical theoretical solution, or, in the remaining cases are correlations based on analyses of the physical principles, and a large quantity of experimental data. Additionally, all these correlations are in such a form that, for practical design purposes, their evaluation is a reasonable proposition. The predictions of each of the correlations can be seen in the output prints in the section Heat Transfer and Inundation Predictions. An example of which can be found in Appendix B1. During processing, the results were stored in array AHTC. Comparison between the experimental data and these predictions are discussed in Chapter 5. The dimensionless groups $Nu/Re^{1/2}$ and F, Equation 2.23, were adopted as an analysis tool from these workers. The experimental data were processed in terms of these groups and, as before, the result can be found in the output prints in Volume 2, an example of which can be found in Appendix B1

No dropwise condensation heat transfer coefficients predictions were calculated.

4.2.5.2 Inundation

In a 15 row bundle, such as that used for this work, the effects of condensate inundation can be significant. These effects have been investigated and compared with a number of published models. Using the experimental conditions the completed computer program

evaluated a number of models. The models used were published by Nusselt [2] (1916), Kern [46] (1958), Fuks [45] (1957), Grant & Osment [47] (1968), Fujii [40] (1981) and Chen [8] (1961). These models covered a wide range of assumptions and simplifications, from the ideal case of Nusselt, through the experience based modifications by Kern, to correlations based on detailed experimental work investigating the effects of inundation rate and steam velocity. Comparison between the experimental data and these predictions is discussed in Chapter 5. The predictions of Kern, Fuks and Grant & Osment can be seen in the output prints in Volume 2 in the section Heat Transfer & Inundation Predictions, an example of which can be found in Appendix B1. During processing, the results of all models were stored in array AHTC.

4.2.5.3 Effect of air

The effect of air during the condensation of steam have been investigated and the results have been compared using the prediction method proposed by Chisholm and McFarlane [31] (1964). This publication describes a compete method for the prediction of condenser performance. However, for the purpose of this work, only the method of predicting the mass transfer coefficient and hence the air resistance has been used. Results from this solution can be found in the output prints of Volume 2 in the section Heat Transfer & Inundation Predictions, under the column labelled "hair", an example of which can be found in Appendix B1. The results are discussed fully in Chapter 5.

4.2.5.4 Pressure drops

The pressure drops through the condensing portion of the bundle have been measured and predicted using both the single phase methods published in The Heat Exchanger Design Handbook [75] (1992), and the method developed for two phase flow presented by Grant & Chisholm [82] (1977). The single phase predictions required by the two

phase method have been evaluated using the method described in [75]. Results from these predictions can be found in the output prints of Volume 2 in the section Pressure Drop Predictions, an example of which can be found in Appendix B1.

Results of previous pressure drop investigations have either been described in terms of a drag/loss coefficient for single phase work, or a two phase multiplier for multi phase flow. This type of analysis, i.e. reducing the data using these dimensionless groups, has been applied to the current data. The experimental drag coefficients and two phase multipliers based on the measurements from the differential transmitter and the predicted bundle pressure distribution can be found on the output prints in Volume 2, an example of which can be found in Appendix B1. Results based on the absolute pressure transmitter were also evaluated. However, since these results are so similar to those based on the differential transmitter, these were omitted.

The results are discussed in Chapter 5.

CHAPTER 5

DATA ANALYSIS

5.1 GENERAL

The following analysis is based on 186 data sets obtained over a range of steam and cooling water conditions typical of a turbine exhaust condenser. The independent variables and the target values are tabulated in Table 5.1. A summary of the test conditions can be found in Appendix C1.

Variable	Filmwise tests	Dropwise tests
Steam pressure	50, 75 and 100mbar	50mbar
Steam velocity	10, 20 and 33m/s	10, 20 and 33m/s
Cooling water subcooling	5, 10 and 15K	5, 10 and 15K
Air content by mass	0 and 1%	0 and 1%

Table 5.1 Test condition summary

Each data set was processed by the computer program described in Chapter 4, which produced an output data file for each data set. A sample output file can be seen in Appendix B1. All other output can be found in Volume 2.

5.2 WILSON PLOT ANALYSIS

To determine the steam-side, heat transfer resistance, an accurate value of the tube outside surface temperature was required. Two options were available, either measuring the tube surface temperature directly, or predicting the temperature from knowledge of the cooling water flow conditions and tube wall properties. Direct measurement of the tube surface temperature was the first choice. However, with only 0.5mm thick tube

walls, sensor options very were limited. The original apparatus design included electrical connections to each end of the centre column of tubes. These connections were included to convert these tubes into 15 resistance thermometers. In operation, the system failed to display the necessary repeatability, possibly due to variable contact resistance, and was eventually abandoned.

Without a direct value of the tube surface temperature, evaluation of the steam side resistance required the prediction of both the waterside and tube wall resistances.

The tube wall resistance was evaluated using the radial conduction equations stated in Appendix B2, while the heat transfer characteristics of the tube side were determined using the modified Wilson plot analysis detailed in section 5.2.1.

5.2.1 WILSON PLOT GENERAL

The original Wilson plot technique and a number of published modifications were reviewed in Chapter 2. Inline with the literature it was decided to initially construct Wilson plots using established correlations to characterise the cooling water circuit and neglect steam-side variations. Then if any differences were detected and attributed to neglecting the steam-side characteristics, then the plots would be reconstructed with both steam and water-side equations. This decision was mainly influenced by the results of Briggs an Young [86] (1969), who compared results obtained using the original Wilson plot method, [85] (1915), with results obtain from their new modified method. In the original Wilson plot approach, the water-side characteristics were described by the cooling water Reynolds number only, i.e. variations in steam-side resistance were neglected. The method of Briggs and Young was considerably more sophisticated, modelling the cooling water characteristics using the Reynolds number, the Prandtl number and a wall to bulk viscosity ratio. They also included Nusselts equation [1] (1916) to model the steam-side resistance. Briggs and Young found that, in contrast to

the original Wilson plot, their method reduced the data to a single line. Briggs and Young considered their method to be successful and an improvement on the original technique. While the validity of the method is not in doubt, the improvements obtained may be almost entirely attributable to the improved water-side modelling, rather than the inclusion of a steam-side model. Based on these considerations, and the simplifications to the calculation method which results, the plots were initially constructed with only cooling water resistance modelling.

5.2.2 MODELLING THE COOLING WATER SIDE CHARACTERISTICS

In the original Wilson plot method [85] (1915), the water-side characteristics were described by the cooling water Reynolds number only. For this work, the accuracy of modelling on only the Reynolds number was insufficient and hence established cooling water correlations were used. Two alternative correlations for the cooling water-side heat transfer coefficient were considered, Equation 5.1, proposed by Sieder & Tate [89] (1936), and Equation 5.2, proposed by Gnielinski [92] (1976).

$$\alpha_{cw} = 0.027 \frac{k}{D} \mathrm{Re}^{0.8} \mathrm{Pr}^{\frac{1}{3}} \left(\frac{\mu}{\mu_s} \right)^{0.14}$$

Equation 5.1

$$\alpha_{cw} = \frac{k}{D} \cdot \frac{(f/2)(\mathrm{Re}-1000)\mathrm{Pr}}{1+12.7(f/2)^{1/2}(\mathrm{Pr}^{2/3}-1)}$$

Equation 5.2

where

$$f = (0.79 \ln \mathrm{Re} - 1.64)^{-2}$$

Equation 5.3

Equation 5.1 is a long established correlation. However, it was noted that a number of authors, e.g. [93] (1990) and [94] (1995) have discussed its accuracy and concluded that significantly more refined and accurate correlations, e.g. Equation 5.2, are available.

The range of applicability of Equation 5.1 is $0.7 < Pr < 16{,}700$, $Re > 10{,}000$ and $L/D > 10$, while Equation 5.2 is applicable for $0.5 < Pr < 2{,}000$ and $2{,}300 < Re < 5 \times 10^6$. In normal operation, the cooling water Reynolds number is approximately 19,000-20,000, well within the range of both correlations. However, during the Wilson plot tests, the Reynolds number range was 9,000-25,000. This satisfied the range of Equation 5.2 but not Equation 5.1.

Both Equation 5.1 and Equation 5.2 were developed and proposed for fully developed flows. Hence, due to the apparatus design it was anticipated that entrance effects would be significant on the tube-side heat transfer coefficient. Sieder & Tate and Gnielinski both investigated entrance effects. The results of both investigations demonstrated that developing flow enhanced the heat transfer, and that the enhancement could be described by a purely geometrical factor in the form of a length-diameter ratio. Since the enhancement was independent of flow, Equation 5.1 and Equation 5.2 were rewritten as Equation 5.4 and Equation 5.5.

$$\alpha_{cw} = K_1 0.027 \frac{k}{D} Re^{0.8} Pr^{\frac{1}{3}} \left(\frac{\mu}{\mu_s}\right)^{0.14}$$

Equation 5.4

$$\alpha_{cw} = K_2 \frac{k}{D} \cdot \frac{(f/2)(Re-1000)Pr}{1+12.7(f/2)^{1/2}\left(Pr^{2/3}-1\right)}$$

Equation 5.5

5.2.3 WILSON PLOT ANALYSIS

The objective of the Wilson plot analysis was to determine the values of the steam side resistance and establish from Equation 5.1 and Equation 5.2 which was the most representative of the apparatus cooling water system.

The total resistance to heat transfer for a row in the test condenser row can be written in the form of Equation 5.6. If the tube wall resistance is evaluated with reference to the heat flux at the outer tube surface, Equation 5.6 can be rewritten as Equation 5.7.

$$\frac{1}{\alpha_{ov}A_o} = \frac{1}{\alpha_s A_o} + \frac{1}{\alpha_{cw}A_i} + \frac{R_w}{A_o}$$

Equation 5.6

$$\frac{1}{\alpha_{ov}} = \frac{1}{\alpha_s} + \frac{D_o}{D_i\alpha_{cw}} + R_w$$

Equation 5.7

Equation 5.7 has been used as the basis for the construction of the Wilson plot diagrams, where $D_o/D_i\alpha_{cw}$ and $1/\alpha_{ov}$ are respectively used to describe the X and Y axes. Hence, if the trend of the data is extrapolated to intercept with the Y axis, i.e. $D_o/D_i\alpha_{cw}=0$, and the tube wall resistance is known, the steam side value can be estimated.

Four sets of filmwise data were obtained using cooling water velocities from 1.30-2.75m/s , see Appendix C1. Two Wilson plot analyses were conducted in parallel to estimate the steam-side resistance, establish the most representative correlation and estimate the values of K_1 and K_2.

Wilson plots were generated using Equation 5.1 and Equation 5.2 to describe the cooling water characteristics. The data can be seen in the plots of Figure 5.1 and Figure 5.2. It should be noted that these plots have been constructed using the final solution.

However the results are identical to those obtained from Equation 5.1 and Equation 5.2. A best fit line was plotted through the data using a least mean square errors technique. This line was projected back to intercept with the Y axis, the steam-side heat transfer coefficients found are tabulated in Table 5.2.

	Wilson plot steam-side heat transfer coefficients (kW/m^2K)			
	T041-T059	T135-T150	T151-T166	T167-T180
Based on Equation 5.1	52.46	240.4	64.68	69.16
Based on Equation 5.2	31.48	57.93	33.72	36.95

Table 5.2 Wilson plot results summary

The average results from the Wilson plots based on Equation 5.1 and Equation 5.2 are 125.6 and 40.02kW/m^2K respectively. At the steam conditions used, a steam-side heat transfer coefficient of 125kW/m^2K is well out-with the accepted range for filmwise condensation. The scatter of the results in Table 5.2 of the Equation 5.1 approach suggests that this equation is not accurately representing the cooling water flow characteristics. However, confirmation of this required further analysis. While there is no scientific justification for doing so, for the purpose of concluding the analysis and/or the elimination of Equation 5.1, the un-realistic value of 240kW/m^2K was neglected. The average shell-side, heat transfer coefficient based on Equation 5.1 was recomputed from the three remaining values and found to be 62.1kW/m^2K. The methodology proceeded by assuming steam-side heat transfer coefficients of 62.1kW/m^2K and 40.02kW/m^2K in the respective analyses.

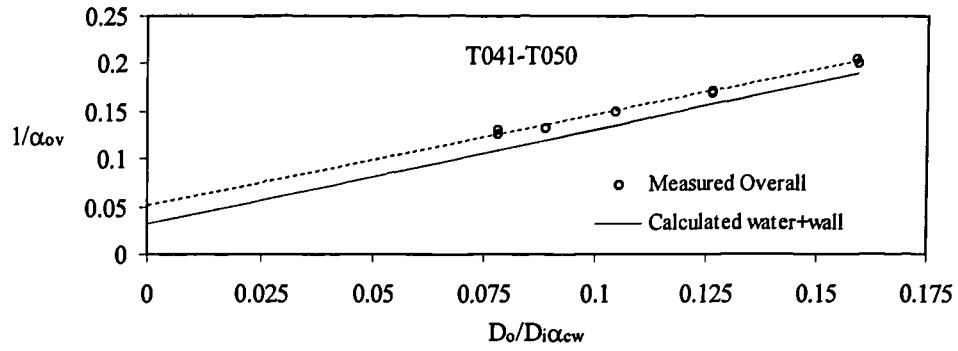

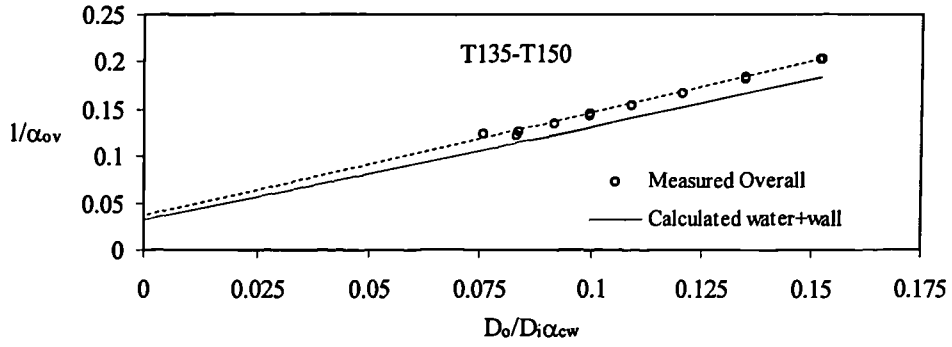

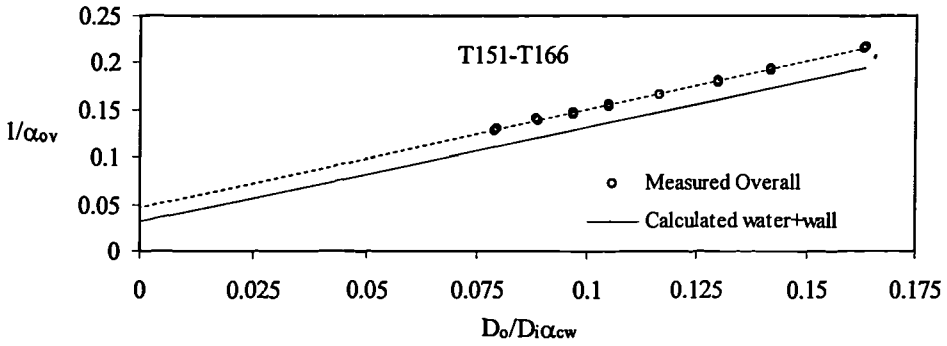

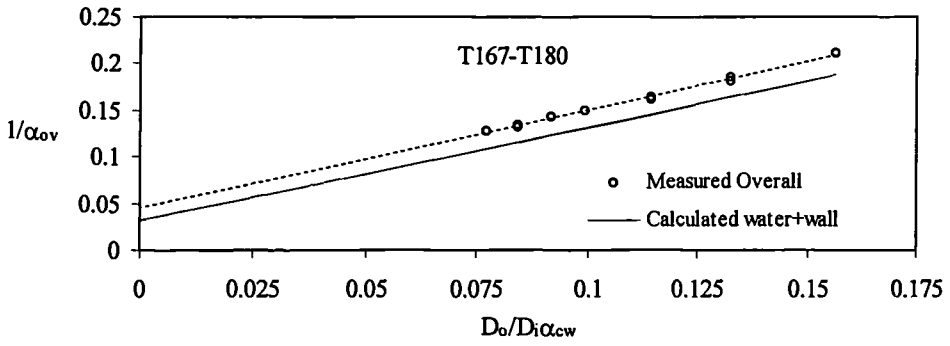

Figure 5.1 Filmwise Wilson plots, based on Equation 5.4

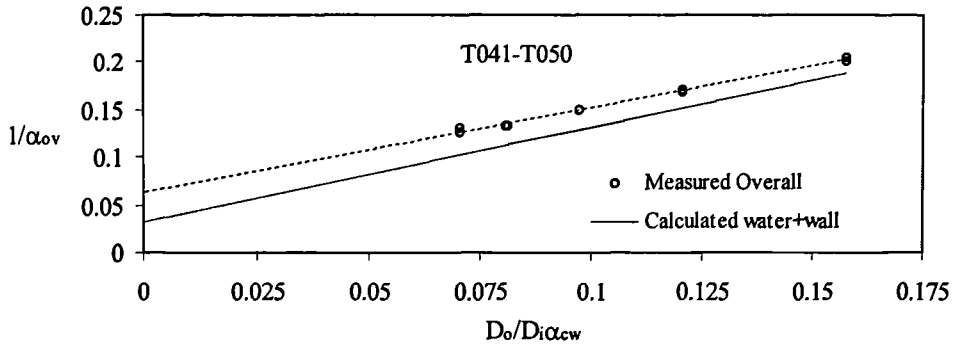

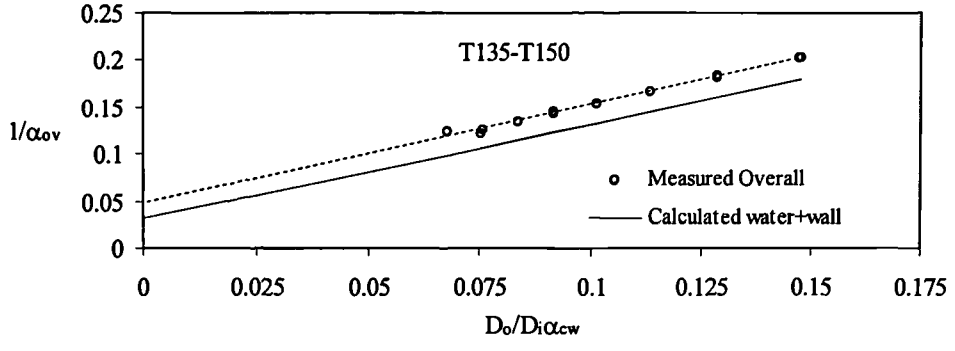

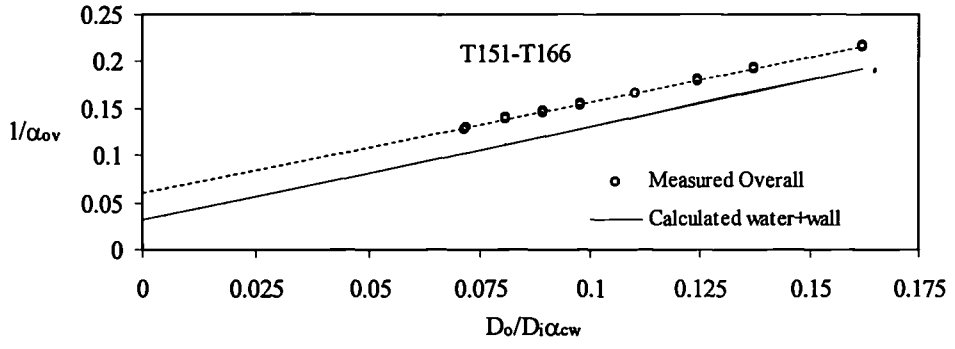

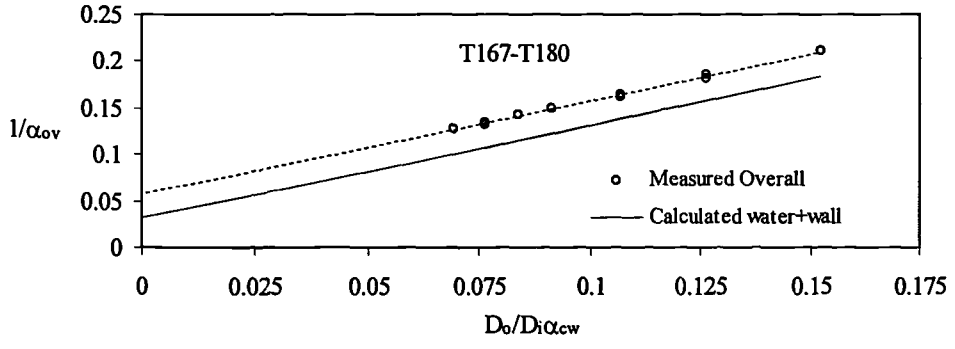

Figure 5.2 Filmwise Wilson plots, based on Equation 5.5

5.2.4 ADAPTING THE COOLING WATER CORRELATIONS

Further analysis of the water-side characteristic equations was based on the use of Equation 5.4 and Equation 5.5. These equations require the estimation of the K_1 and K_2 values. The K values were estimated by calculating the experimental water-side heat transfer coefficients using Equation 5.7 and the respective average Wilson plot steam-side value. The average under-prediction of Equation 5.1 and Equation 5.2 was then computed. It was found that values of K_1 and K_2 of 1.00 and 1.08 were required to satisfy the data. The K values and the scatter in the steam-side heat transfer coefficient were analysed by re-computing the steam-side results using Equation 5.7 and the predictions using Equation 5.4 and Equation 5.5. Appendix C2 and Appendix C3 contain tables of the results, the averages the and standard deviations. These show that, on average, the K values quoted above, result in a predicted steam-side heat transfer coefficient nearly equal to that estimated by the Wilson plot method. These results are summarised in Table 5.3.

	Based on Equation 5.1 / Equation 5.4	Based on Equation 5.2 / Equation 5.5
Direct Wilson Plot Result	62.10kW/m^{2}K	40.02kW/m^{2}K
Calculated by subtracting resistances	62.51kW/m^{2}K	44.07kW/m^{2}K

Table 5.3 Shell-side heat transfer coefficient summary

The calculated values of the tube wall plus the water side resistances were added to the Wilson plots, Figure 5.1 and Figure 5.2. These plots show the characteristics and resistances of the measured data and the predicted water plus wall behaviour. The

results shown in Table 5.3 indicated that potential for further refinement of K_2 exists. However, this was postponed and will be justified in the Section 5.2.5.

5.2.5 SELECTING THE COOLING WATER CORRELATION

Selection of the most representative cooling water correlation was based on inspection of the plots in Figure 5.1 and Figure 5.2 while simultaneously considering the mechanism of condensation heat transfer and the inherent assumptions of the Wilson plot technique. Particular attention was paid to the following considerations.

1. If a correlation accurately describes the characteristics of the cooling water-side and the shell side coefficient is unaltered by the range of cooling water velocities, then, when the overall heat transfer resistance and the predicted water-side resistance are plotted on a Wilson plot, the trends should be parallel. The gradients of the lines through the data in Figure 5.1 and Figure 5.2 have been calculated. The values are listed in Table 5.4. The gradient of the water-side plus wall prediction is unity since, for this trend, the X and Y ordinate values only differ by the constant tube wall resistance. The data gradients in Table 5.4 are scattered around a value of 1. However, the average based on Equation 5.4 is 1.033 and on Equation 5.5 is 0.972.

2. If the trends are not parallel, the mechanisms controlling the condensation process indicate that the data should tend to converge as the X axis ordinate values increases, i.e. the ratio of the data gradient divided by the prediction gradient cannot be greater than 1. The logic is thus. Since the overall inlet temperature difference remained constant, increasing values on the X axis correspond to reductions in the cooling water velocity. This results in a decrease in the overall heat transfer coefficient, a reduction in heat flux, a reduced condensation rate, a thinner condensate film and therefore a smaller shell side heat transfer resistance. The average result based on Equation 5.4 contradicts this discussion whereas the average result from Equation 5.5 is in agreement.

	Based on Equation 5.4		Based on Equation 5.5	
	α_s kW/m2K	Data Gradient	α_s kW/m2K	Data Gradient
T041-T059	52.46	0.9525	31.48	0.8859
T135-T150	240.40	1.0972	57.93	1.0447
T151-T166	64.68	1.0357	33.72	0.9615
T167-T180	69.16	1.0476	36.95	0.9967
Averages	142.23	1.0333	40.02	0.9722
Standard deviations	54.22	0.0520	10.5	0.0579

Table 5.4 Shell-side heat transfer coefficient scatter analysis

The above discussion suggests again that Equation 5.4 does not accurately model the water-side resistance. This statement is further justified by reconsidering the results and scatter of the Wilson plot steam-side, heat transfer coefficients in Table 5.4. Analysis based on Equation 5.1 (i.e. the characteristics of Equation 5.4) returns values of steam-side heat transfer coefficient which are both widely scattered and, in one case, well out-with the accepted range. In contrast, analysis based on Equation 5.2 (i.e. the characteristics of Equation 5.5) predicts values which are consistently in the accepted range and display a degree of scatter in line with the experimental accuracy. In addition, it should be recalled that the Wilson plot tests were carried out over Reynolds numbers from 9000 to 25,000. Hence, at low water velocities, the test conditions were out-with the range for which Equation 5.1 is valid. Equation 5.2 is valid down to Reynolds numbers of 2300, adequately covering the full range test conditions.

From the above it is clear that Equation 5.5 is more representative. However the K_2 value of 1.08 required further supporting analysis and discussion. The postponement of any further refinement of K_2 was based on the logic of consideration No. 2 above. If, as the physical mechanisms suggest, the trends of overall data and predicted water plus wall resistances converge as the X axis ordinate increases, then, when projecting the trends of the data back to the intercept with the Y axis, this convergent trend becomes divergent. As a result, it is possible that shell-side, heat transfer coefficients obtained directly from Wilson plot are slightly lower than the actual values. Equally, based on the same logic, it is likely that any errors in the coefficient values obtained directly from the Wilson will be biased towards under-prediction rather than over prediction. Hence, any further refinement of K_2 could not be justified due to conflicting logic. i.e. Section 5.2.4 suggests an increase in K_2, while this section suggests that an increase in K_2 was limited by the magnitude of the Wilson plot method under prediction, and if this under prediction was significant then a reduction in K_2 was required. The value of K_2 was left at 1.08 and additional data in the form of dropwise Wilson plot data was obtained to clarify the value of K_2. The analysis of the dropwise data is detailed in section 5.2.7.

The error in predicting the shell-side coefficient directly from the Wilson plots is not quantifiable. However, based on the scatter of the results a range from –25% to +45% is possible. The above analysis has shown that Equation 5.5 with K_2 = 1.08 is representative of the cooling water-side performance. Hence, the remaining analysis will be based solely on this model and K value.

5.2.6 CONFIRMING CONSTANT STEAM-SIDE COEFFICIENT ASSUMPTION

The above numerical data analysis have assumed that the steam-side, heat transfer coefficient was constant over the range of Wilson plot test conditions. Due to the range of condensation rates, and hence steam-side temperature differences, this assumption

must have been violated to some extent. However, for this work over this range of conditions, it can be shown that the use of this assumption is justified.

Wilson plot tests T041-T050 and T151-T166 were conducted at an overall inlet temperature difference of 15K. Tests T135-T150 and T167-T186 where completed at an overall inlet temperature difference of 10K. If the apparatus was capable of reliably measuring the effect of condensation rate, the average values of the measured steam-side heat transfer coefficient, shown in Table 5.5 would fall into two distinct groups. This is not the case, indicating that the changes of condensation rate within the range tested does not have a detectable effect on the heat transfer coefficient.

Test Numbers	Ranges of ΔT_s predicted by Equation 5.5 K	Range of α_s based on Fujii kW/m^2K	Measured average α_s based on Equation 5.5 kW/m^2K
T041-T050	2.69-0.71	38.59-52.53	31.48
T135-T150	1.60-0.90	43.20-49.52	57.93
T151-T166	2.56-1.28	38.99-45.49	33.72
T167-T186	1.73-0.99	42.45-48.38	36.95

Table 5.5 Constant shell-side heat transfer coefficient confirmation

Table 5.5 shows the predicted variations of the shell-side temperature differences. These values were used in conjunction with the correlation of Fujii [11] (1972) to estimate the effect of condensation rate. The range of these predicted steam-side, heat transfer coefficients are shown in Table 5.5, where it can be seen that the variation is within a band of ±15% and, in three out of four batches, within ±8%. While these results were based on the temperature difference calculated from the cooling water model, selected

by the analysis, and which is the analysis that requires validation. The variation band of ±15% is small when compared to the uncertainty band of ±40-140% associated with the prediction of the steam-side heat transfer coefficient (small error analysis results on output plots). The assumption of constant steam-side heat transfer coefficient is therefore valid, since using both methods above, it has been shown that variations due to this range of condensation rates are less than the apparatus sensitivity.

5.2.7 DROPWISE WILSON PLOT RESULTS

In addition to the four filmwise Wilson plot tests, one additional test was completed using dropwise tubes. This batch of tests was conducted at steam conditions of approximately 35m/s and 50mbar, with an overall inlet temperature difference of 15K and cooling water velocities from 1.27-2.97m/s. This test offered one significant benefit, i.e. all the current research on dropwise condensation indicates that the shell-side, heat transfer coefficient is not dependent on the temperature difference. The Wilson plot generated is shown in Figure 5.3 and, as before, includes the water-side performance based on the final solution. From this figure it can be seen that the gradient of the data and the cooling-water, and wall resistance are virtually identical, confirming that the cooling water heat transfer coefficient characteristics and values are well represented by Equation 5.2 and Equation 5.5 respectively. The figure also shows that the experimental overall results are virtually identical to the calculated water plus the wall resistance, suggesting that the shell-side resistance to heat transfer during dropwise condensation is insignificant and/or the K_2 value is at the lower limit of the possible solutions. i.e. any higher would result in negative shell-side resistance predictions.

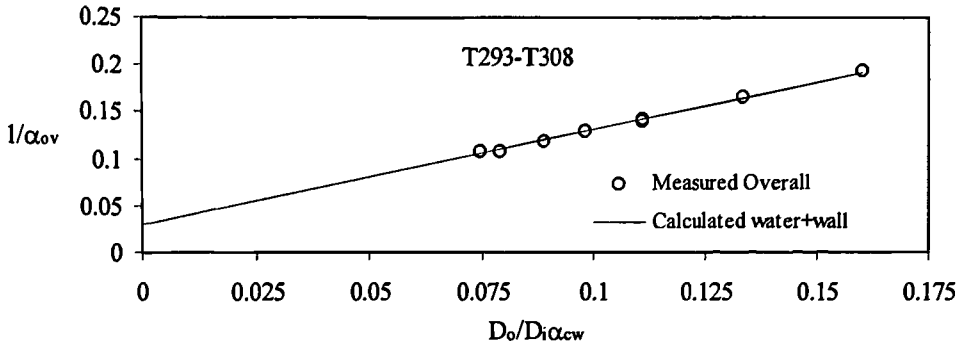

Figure 5.3 Dropwise Wilson plot constructed using Equation 5.5

5.2.8 WILSON PLOT SUMMARY

The discussion of section 5.2.7 has stated that the dropwise data indicated that the K_2 value was at the lower possible limit. The filmwise Wilson plots indicated directly a steam-side, heat transfer coefficient of 40kW/m^{2}K. Subtracting resistances using Equation 5.5 with K_2=1.08 resulted in an average shell-side result of 44kW/m^{2}K. The only possible change to the K_2 value would therefore be an increase. However, any increase in K_2 would lead to a reduction in the experimental, steam-side, heat transfer coefficient, the value of which the previous discussion stated would be above 40kW/m^{2}K and was predicted, using Equation 5.5, to be 44kW/m^{2}K. These two arguments leave minimal scope for the adjustment of the K_2 value, especially when the previous justification relating to the postponement of K_2 refinement is simultaneously considered.

Assuming a typical filmwise test condition which produces an overall heat transfer coefficient of 7.5kW/m^{2}K and a steam-side, heat transfer coefficient of 44kW/m^{2}K, the water-side, heat transfer coefficient would be approximately 9.04kW/m^{2}K. If the K_2 value were to be modified to obtain an average steam-side coefficient of 40kW/m^{2}K, the cooling water-side value would require to be increased to 9.23kW/m^{2}K, an increase of 2%. Hence,. the limits of K_2 are 1.08-1.1. The effect of this range of K_2 on the dropwise

results is as follows. If an overall heat transfer coefficient of 9kW/m^{2}K was measured, and using K_2–1.08 the steam-side coefficient was estimated to be 500kW/m^{2}K, changing K_2 to 1.1 would result in the estimated steam-side heat transfer coefficient decreasing to approximately 300kW/m^{2}K, a change, which when compared to the experimental accuracy and scatter, is not significant. Hence, the K_2 value has been estimated to a similar accuracy as the measurements. The constraints of the filmwise and dropwise data have also been simultaneously satisfied.

5.3 FIRST ROW HEAT TRANSFER ANALYSIS, FILMWISE CONDENSATION

5.3.1 FIRST ROW HEAT TRANSFER GENERAL

Heat transfer results have been obtained from all 15 rows of the test condenser. The results from the first row are particularly valuable since they were obtained at specific steam conditions and in the complete absence of condensate inundation. Data were recorded at steam velocities of 10, 20 and 33m/s, pressures of 50, 75 and 100mbar and overall temperature differences of 5, 10 and 15K, see Appendix C1 for details.

5.3.2 COMPARISON WITH SINGLE TUBE THEORIES

The first row data has been compared with the theory of Fujii et. al [11] (1972), Rose [20] (1988) and Shekriladze and Gomelauri [9] (1965). The main object was to establish which correlation best represented the present data, and hence allow both the analysis of heat transfer lower in the bundle and the recommendation of a representative flow area/correlation combination.

All three theories were originally developed for the case of an isolated tube, and are therefore applicable only to bundle conditions if an appropriate equivalent velocity can be defined. The equivalent velocity has been investigated using three definitions of flow area, inline with Briggs et al [36] (1992) and Michael et al [42] (1992)

1. maximum area, the local cross sectional area if no tubes were present
2. minimum area, the area based on the minimum gap between tubes
3. mean void area, which for a square pitch configuration is the flow area based on the ratio defined in Equation 5.8. Where the mean void area is the total area of the bundle tube plate, less the area occupied by tubes

$$\frac{A_{mv}}{A_{max}} = 1 - \frac{\pi D_o^2}{4P_t^2}$$

Equation 5.8

For this experimental configuration and relative to the free stream, the velocity ratios are 1 for the maximum area, 1.79 for the mean void area and 4 for minimum flow area.

For each of the air free data sets available, the experimental condensate film heat transfer coefficient was evaluated by subtracting the cooling water and tube wall heat transfer resistances from the measured overall value. The theories were then evaluated using the above definitions for flow area and the experimental temperature differences to determine the most representative velocity definition. The results are compared by plotting the experimental values against the predicted values. The plots generated from the theories of Rose and Fujii using the three area definitions are included as Figure 5.4, Figure 5.5 and Figure 5.6.

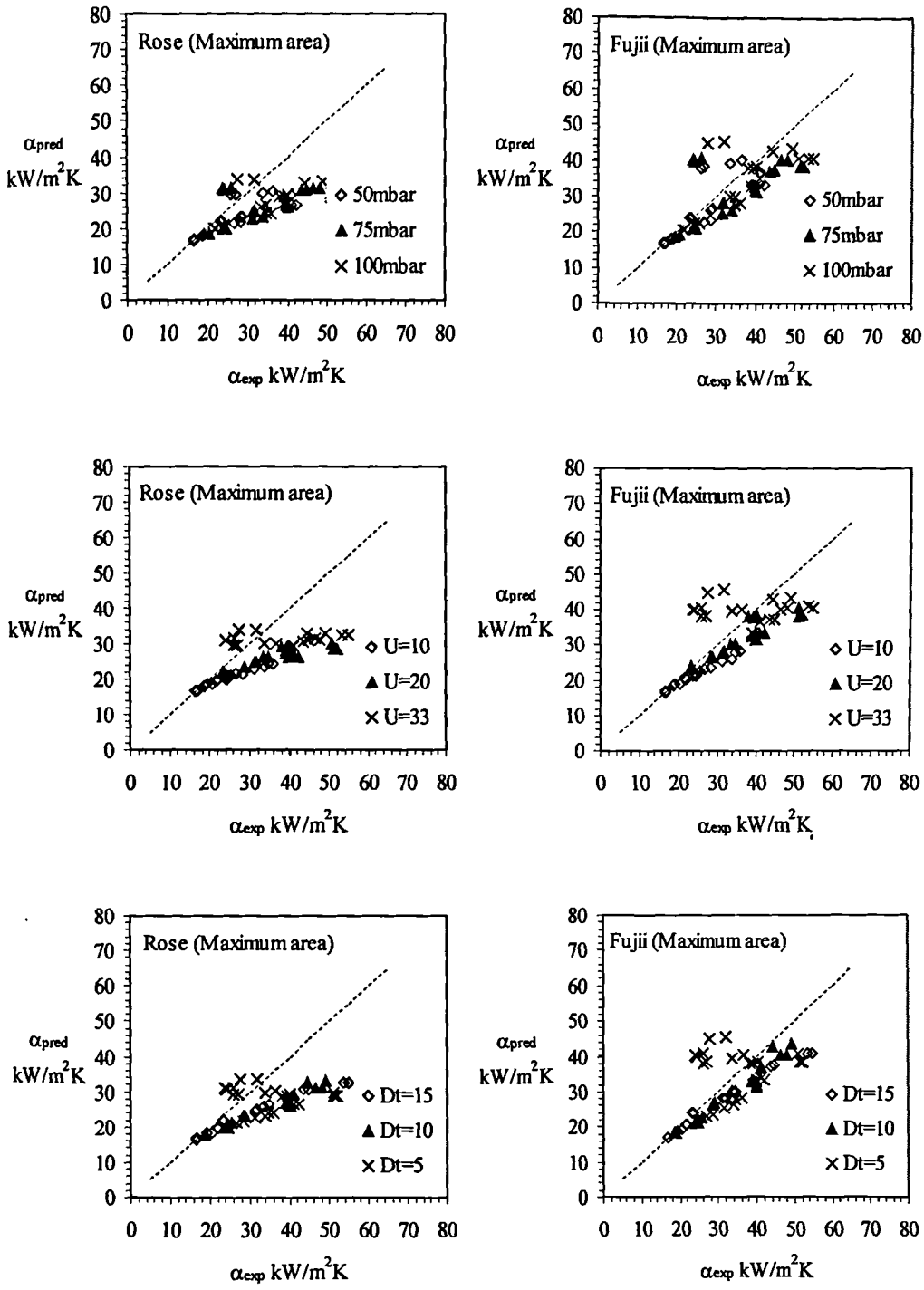

Figure 5.4 Theory of Rose and Fujii based on maximum area

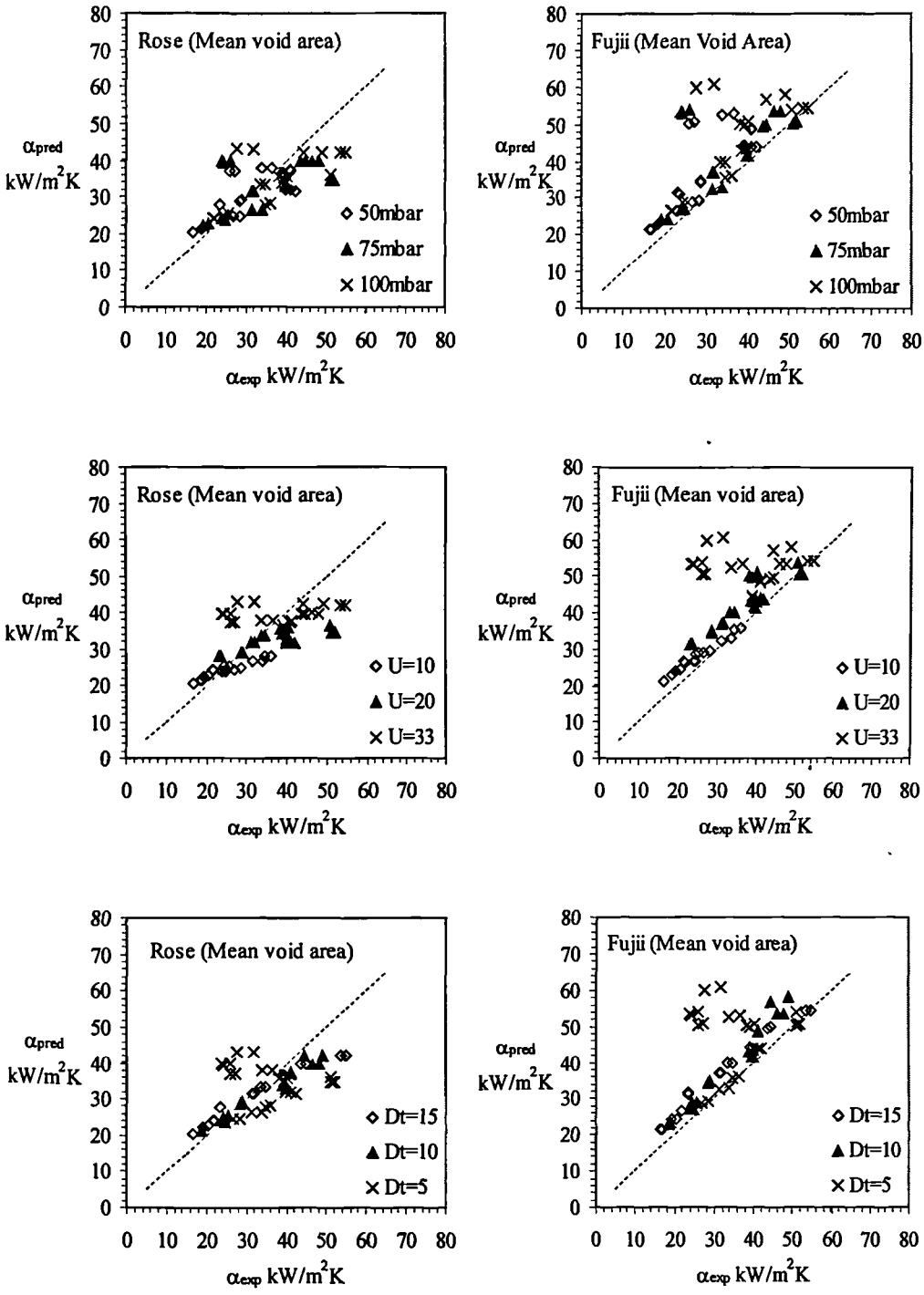

Figure 5.5 Theory of Rose and Fujii based on mean void area

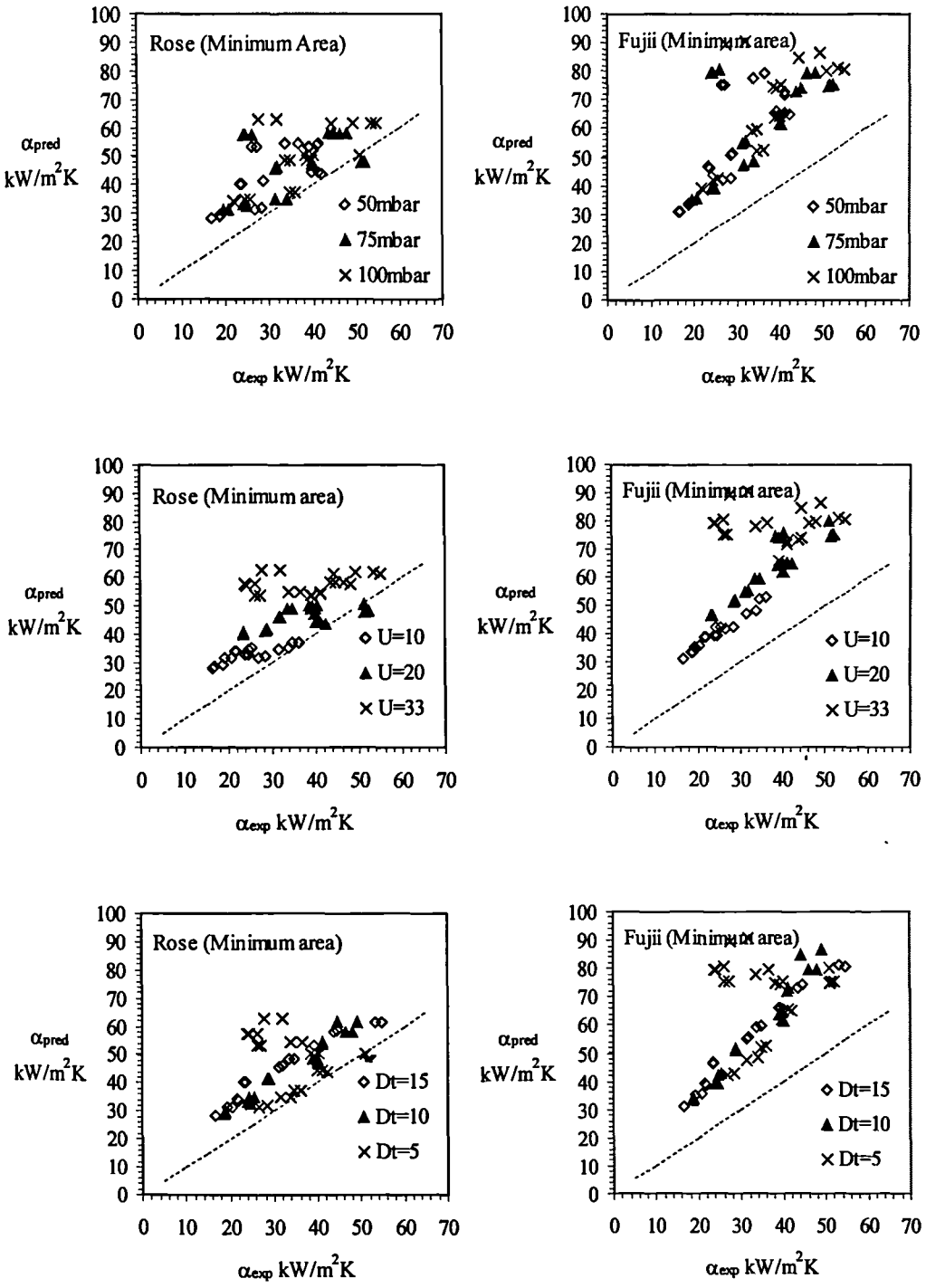

Figure 5.6 Theory of Rose and Fujii based on minimum area

When studying the plots in Figure 5.4, Figure 5.5 and Figure 5.6 it should be noted that the nine points above the general trend are all attributable to tests conducted with steam at 33m/s and an overall driving temperature of 5K, this issue is discussed further in Section 5.2.3.

Plots comparing the constant wall temperature predictions of Shekriladze and Gomelauri have been omitted, since over the range of conditions tested there are only minimal differences between this model and the theory of Rose, see Figure 5.7.

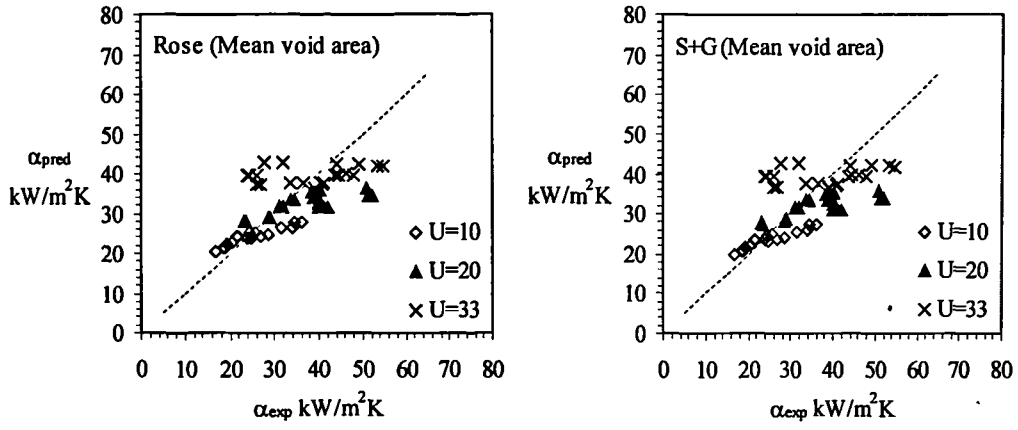

Figure 5.7 Comparison between Rose and S+G correlation results

The performance of the correlations was analysed by calculating the percentage root mean square error, where an error was calculated by dividing the difference between the predicted and experimental values by the predicted value. The error results are tabulated in Appendix C4 and it can be seen that the combination of theory and area definition which displays the least scatter, 20.3%, is that of Fujii using the maximum flow area. However, it should be noted that this value is only a marginal improvement of the scatter of Rose and Fujii using mean void area with scatter of 20.5% and 20.7% respectively. The data distribution calculated for the three combinations discussed above are virtually identical and hence the selection of the most representative combination

requires further investigation. The plots contained in Figure 5.4, Figure 5.5 and Figure 5.6 were studied. From these plots it can be seen that the correlation of Fujii follows the trends of the present data more accurately than the that of Rose. This is demonstrated by the constant temperature plots in Figure 5.4, Figure 5.5 and Figure 5.6, where it can be seen that in general the gradients of the individual series for the Fujii plot are considerably more representative of the data than those in Rose plots.

The correlation selection has been discussed and it therefore only remains to select a definition of the most representative flow area. The results of the scatter analysis for the Fujii correlation evaluated with mean void area and maximum area are virtually identical. As a result selection of the flow area was again based on inspection of the plots in Figure 5.4 and Figure 5.5. These plots indicate that predictions based on the mean void area are generally between 0-8kW/m^{2}K higher than the experimental data, while predictions based on the maximum flow area are generally very accurate at low heat transfer coefficients while at high values prediction range from approximately 0-25% lower than the data.

For the purpose of this work, the subsequent analysis of the effect of air and inundation has been based on film heat transfer coefficient predicted using Fujii and the maximum flow area. This decision was further justified by further studying the Fujii plots using the maximum flow area in Figure 5.4. These show that the performance of this combination improves at lower heat transfer coefficient values, i.e. the lower steam velocities and higher condensate film temperature differences, which are the conditions generally found lower in the test bundle and required modelling.

5.3.3 HIGH VELOCITY LOW DRIVING TEMPERATURE RESULTS

The plots comparing the experimental results with theoretical predictions of Fujii in Figure 5.4, Figure 5.5 and Figure 5.6 show that, apart from nine distinct points above

the bulk of the data, the data trends and results are in line with current theories. From inspection of these plots it can be seen that these scattered points are all attributable to tests were the velocity was a maximum, 33m/s, and the overall driving temperature was a minimum, 5K.

The magnitude of the heat transfer coefficient during forced convection film condensation is controlled by a number of factors, the most dominant of which are steam velocity and condensation rate. The present theories of Fujii et. al [11] (1972), Rose [20] (1988) and Shekriladze and Gomelauri [9] (1965), all indicate that the heat transfer coefficients increase as steam velocity increases and as condensation rate decreases, and that this behaviour may be extended without limit. The data obtained from the current configuration suggests that there may exist a finite limit to this general behaviour. From inspection of plots in Figure 5.4, Figure 5.5 and Figure 5.6 it can be see that data obtained with steam at 33m/s and a 5K overall driving temperature are of similar magnitude to data recorded at significantly lower velocities and higher temperature differences. Furthermore, the coefficients at these extreme conditions are lower, by up to 50%, than data obtained with 33m/s steam and an overall temperature difference of 10K, see Figure 5.8. It would therefore appear that the heat transfer behaviour within a tube bundle under these condition is fundamentally altered. The candidate offers no explanation for this phenomenon.

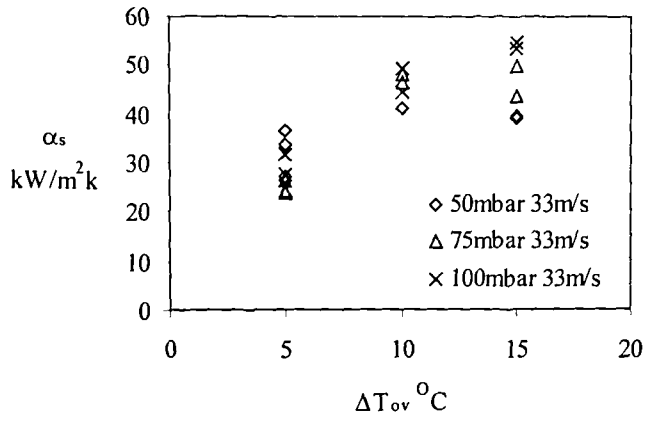

Figure 5.8 Filmwise heat transfer coefficients at extreme conditions

5.4 FILMWISE INUNDATION HEAT TRANSFER ANALYSIS

5.4.1 GENERAL

Data from all air-free, filmwise test conditions has been analysed to investigate the effect of condensate inundation, see Appendix C1 for test condition details. In line with previous workers, the effect of inundation has been described by the ratio of the experimental nth row film heat transfer coefficient to the film heat transfer coefficient which would occur without inundation, but otherwise under identical local conditions. Before proceeding, the definition of identical local conditions requires clarification. When a theoretical prediction at the nth row is calculated, this is evaluated using the predicted experimental local conditions, which includes the condensate film temperature drop. As a result, the calculated un-inundated tube value, α_n, is that which would be predicted with an increased condensate film thickness and is therefore less than a first row value calculated from only the shell-side conditions.

The correlation of Fujii, Equation 2.15, using the maximum flow area has been shown in Section 5.3.2 to be the most representative of the first row data. This correlation has been used to predict a theoretical un-inundated tube value, α_{nfujii}, the result of which has been used to calculate the inundation factor, I, defined by Equation 5.9.

$$I = \frac{\alpha_{ss}}{\alpha_{nfuji}}$$

Equation 5.9

Where α_{ss} were air free experimental shell-side values.

5.4.2 FILMWISE INUNDATION BUNDLE DEPTH DEPENDENCE

Since a number of inundation correlations indicate that the effect is dependent on only the bundle depth, an analysis of the data of this form has been completed. To establish the dependence on bundle depth, four analyses were conducted. These analyses were all based on the same methodology. However, in an attempt to isolate the sources of scatter the inundation factor, I, has been calculated with and without first row correction factors, using either all data or only data with a condensate film temperature drop of greater than 1K. First row corrections, F_{cor}, were calculated using Equation 5.10. This result, when applied, was used to normalise the data set by correcting with a factor equal to the ratio of the predicted and experimental first row results.

$$F_{cor} = \frac{\alpha_{1ss}}{\alpha_{1fuji}}$$

Equation 5.10

Figure 5.9 shows the distribution of the experimental inundation factors calculated using all data with no first row correction. From this plot it is clear that the extent of the scatter is such that no conclusion can be drawn without analysing the distribution of the data. This was done by calculating the data mean value for each row. The averages

calculated are shown as the trend labelled Un-corrected in Figure 5.11. The mean results of this trend are generally between 1.1 and 0.9, indicating that the effect of inundation in not dramatic. The trend indicates that, relative to the predicted values, the heat transfer coefficient initially increases at the second row, decreases to a minimum mid-way through the bundle and thereafter increasing to a ratio value of approximately 1.05 at row 15. This behaviour was somewhat unexpected. The decision was taken to introduce a first row correction factor and reanalyse the data. The object of the correction factor was to allow for cases where first row predictions were not equal to the first row measured value. This was achieved by calculating the correction required to make the first row prediction equal to the measured value, then applying this correction to all the subsequent rows in the data set. Figure 5.10 shows the distribution of the experimental inundation factors calculated using all data with corrections applied. The scatter of the data in this plot is less than the plot constructed from uncorrected predictions. However, as before, the scatter can be seen to be significant and the row mean values were calculated to highlight any trends. The mean values calculated can be seen in Figure 5.11 as the trend labelled corrected. Figure 5.11 shows that this correction reduced the values of the calculated inundation factors by around 10%, however, the general trend/shape of the results was basically unchanged. The indicated reduction in the inundation effect from rows 10 to 15 in Figure 5.11 was not expected. The data were re-examined and it was noted that in a number of cases, condensation ceased at some point within the bundle, due to the pressure drop reducing the steam saturation temperature to less than, or equal to the cooling water temperature.

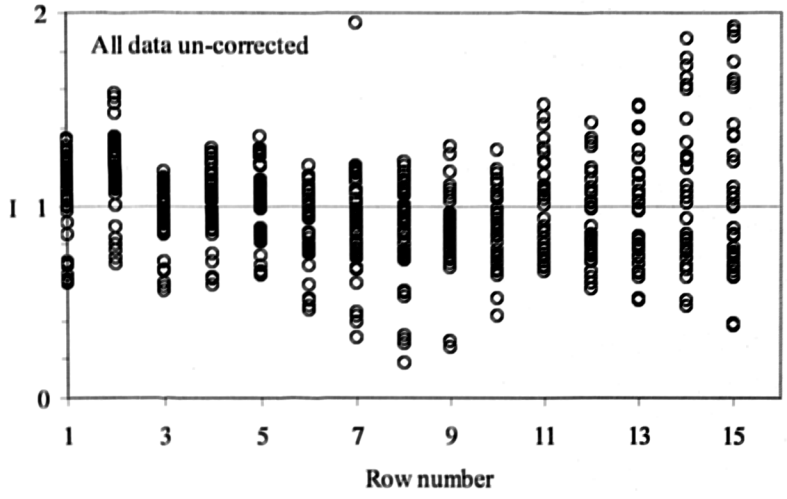

Figure 5.9 Un-corrected inundation factors

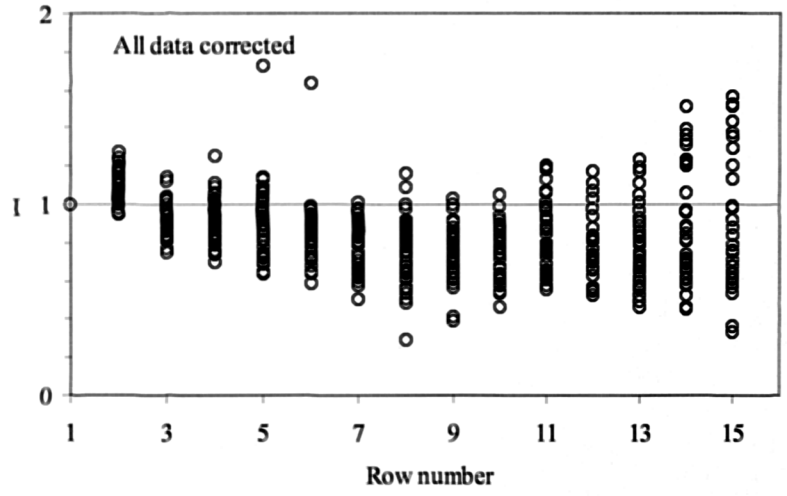

Figure 5.10 Corrected inundation factors

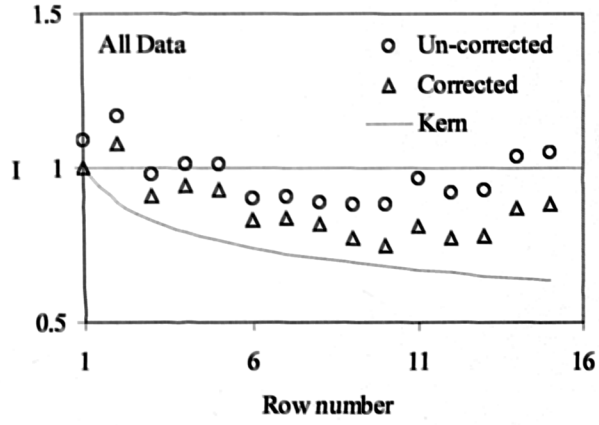

Figure 5.11 Inundation factor row average trend

The errors associated with the prediction of a shell side heat transfer coefficient were primarily a function of the temperature difference, i.e. the smaller the temperature difference the higher the error. To examine whether or not the trends were being distorted by data with significant error bands, the above analysis was repeated using only data where the shell-side temperature difference was found to be greater than 1K. Removing this data corresponded to removing data with error bands of greater than ±50%. 228 out of 765 points were removed. Plots of the same form as the previous analysis were produced, Figure 5.12 and Figure 5.13. By studying these plots it is clear that removing the low temperature difference data has reduced the scatter and that applying a first row discrepancy factor reduced this scatter further. As before, to clarify the average trend of the data a mean value for each row was calculated. These averages are displayed in Figure 5.14. Inspection of this figure shows as before, a slight increase at the second row, then a decrease to a minimum at row 10-12. However, for this case with low temperature difference data removed, beyond rows 10-12 the inundation factor remains approximately constant at 0.9 or 0.7 for the un-corrected and corrected trends respectively.

The trends of the data averages were compared with the model of Kern [46] (1958) Equation 2.47, Figure 5.11 and Figure 5.14. The Kern model was selected since it was noted that the effects of inundation displayed by the present data were small, and that of the row dependent correlations this produced the most conservative predictions. From inspection of Figure 5.11 and Figure 5.14 it is clear that for all cases, i.e. un-corrected, corrected, all data or low temperature data removed, the Kern model over-predicts the effect of inundation.

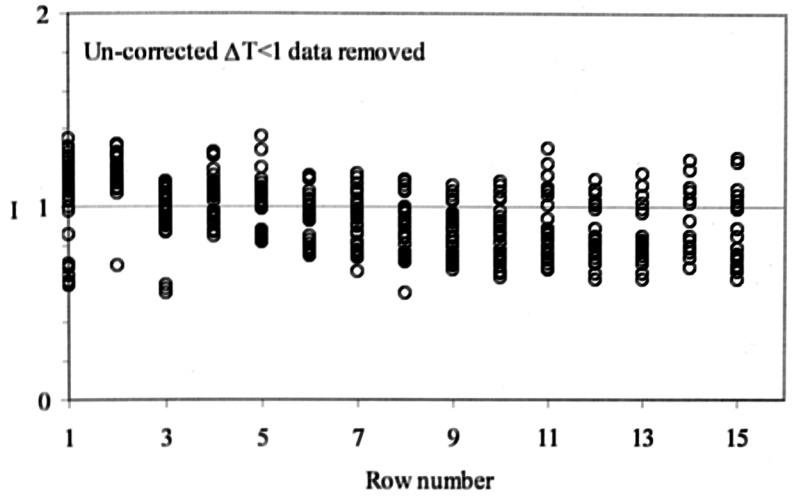

Figure 5.12 Un-corrected inundation factors

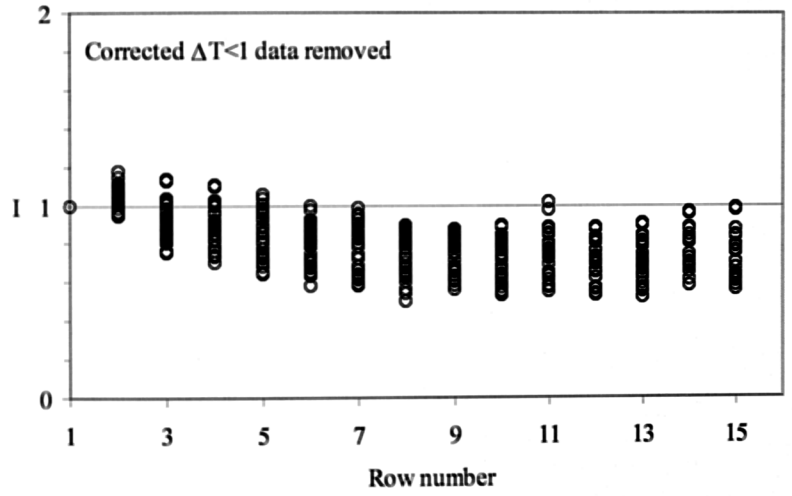

Figure 5.13 Corrected inundation factors

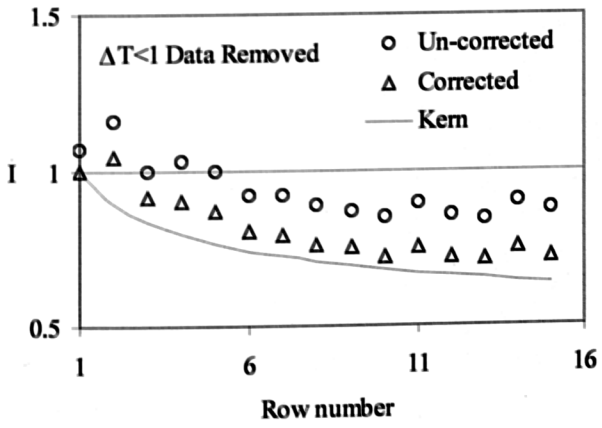

Figure 5.14 Inundation factor row average trend

5.4.3 FILMWISE INUNDATION CONDENSATE RATIO DEPENDENCE

The analysis process followed in Section 5.4.2 was repeated to investigate the dependence of the inundation factor on the condensate ratio. The condensate ratio is as used by Fuks [45] (1957) and Grant and Osment [47] (1968) which for this analysis is defined by Equation 5.11.

$$R_c = \frac{\dot{m}_c}{\dot{m}}$$

Equation 5.11

As with the row dependence analysis, plots have been generated using un-corrected and corrected data, and containing all or only data with film temperature differences greater than 1K. These plots can be found as Figure 5.15, Figure 5.16, Figure 5.18 and Figure 5.19. From inspection of these plots it is clear that at low R_c values, the values are in distinct groups, i.e. R_c=1, 2, 3, 4 and to a lesser extent R_c=5, 6 & 7. Where these groups can be clearly identified, the group number, counting from left to right corresponds to the condensing row number. As a result of these groupings at low R_c numbers, the initial trends of the bundle depth analysis are nearly identical to the row dependence analysis. The plots, Figure 5.15 and Figure 5.16 have been constructed using all the data. Both of these plots display significant scatter, however, a large proportion of the data suggests a decreasing trend on both plots. The average from batches of R_c values were calculated. The batches were R_c=1, 1-2, 2-3, 3-4 etc. The mean values for each batch of corrected and un-corrected data can be seen in Figure 5.17. This figure shows the average trend of the data. The initial trend of the mean values in Figure 5.17 is similar to that of Figure 5.11, this is due to the inherent link between to row number and the R_c values discussed above.

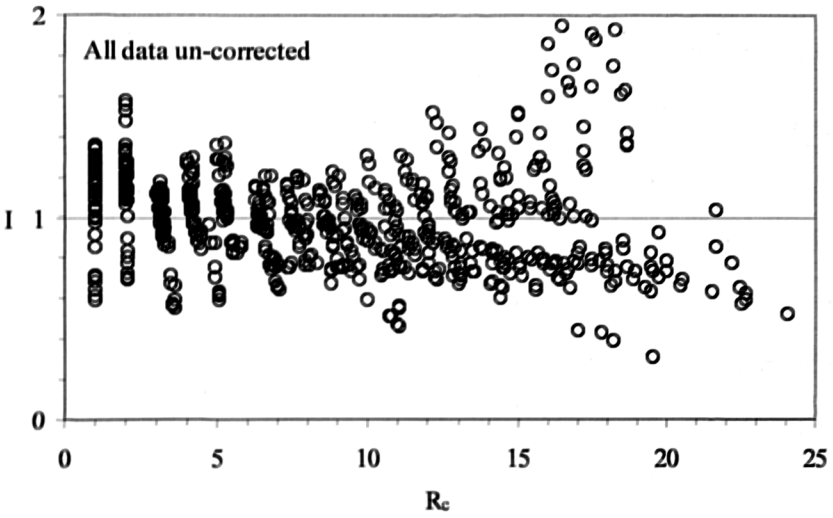

Figure 5.15 Un-corrected inundation factors

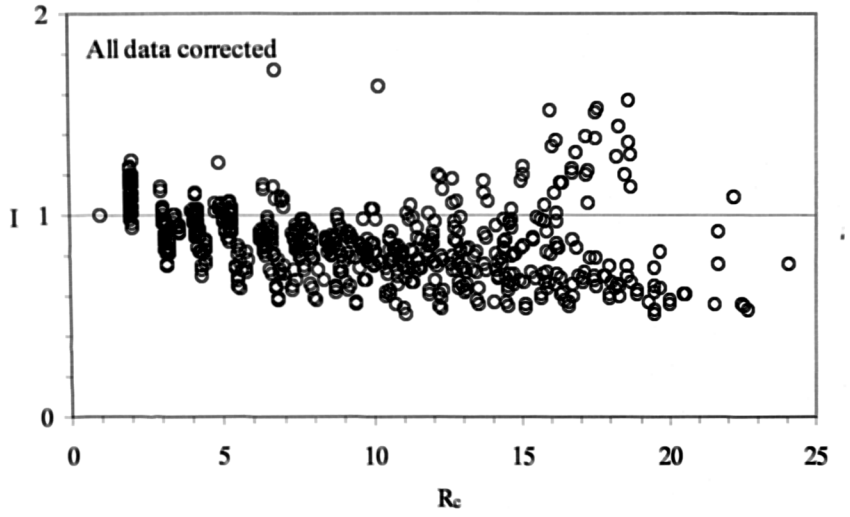

Figure 5.16 Corrected inundation factors

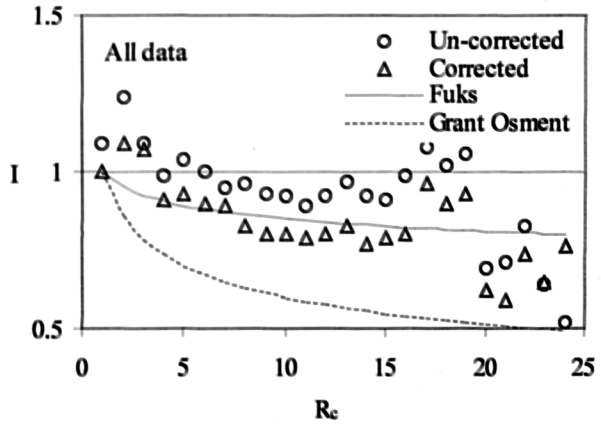

Figure 5.17 Inundation factor condensate ratio average trend

The plots were reproduced using only data with a film temperature difference of greater than 1K, these plots are included as Figure 5.18 and Figure 5.19. Mean values were computed from batches of R_c as before, the resulting trend of the data mean values can be seen in Figure 5.20. This figure indicates an initial increase in the condensate inundation factor followed by a relatively constant rate decrease as the value of R_c increases. The trends of the data averages were compared with the models of Fuks [45] (1957), Equation 2.46 with N=-0.07, and Grant and Osment [47] (1968), Equation 2.47 with N^{-}-0.223 in Figure 5.17 and Figure 5.20. The data averages shown in Figure 5.17 display considerable scatter and as a result any data trends which may exist are unclear. Despite the scatter, Figure 5.17 shows that under certain conditions the predictions of the Fuks model are in agreement with the data. This figure also shows the trend of the Grant and Osment model which, compared to the present data, can be seen to over-predict inundation effects. Comparison of correlations with the low temperature difference data removed is shown in Figure 5.20. The averages show in Figure 5.20 display a distinct trend, however the characteristics of this trend are not well represented by either of the models tested.

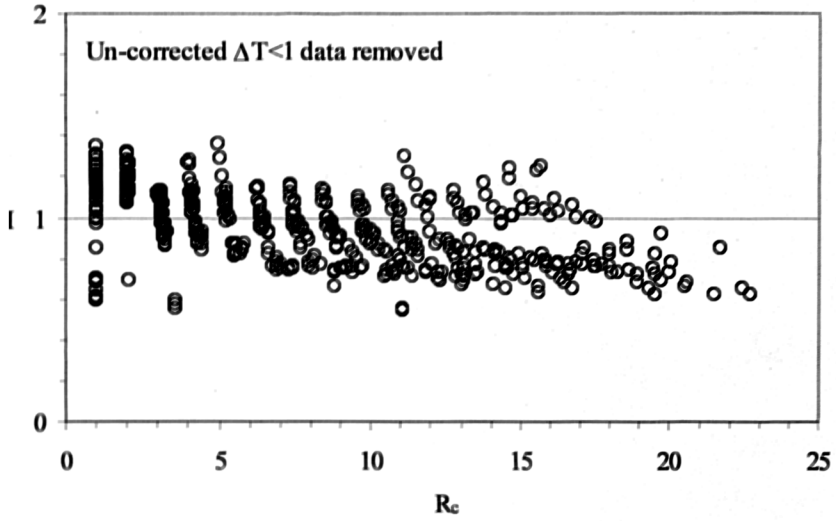

Figure 5.18 Un-corrected inundation factors

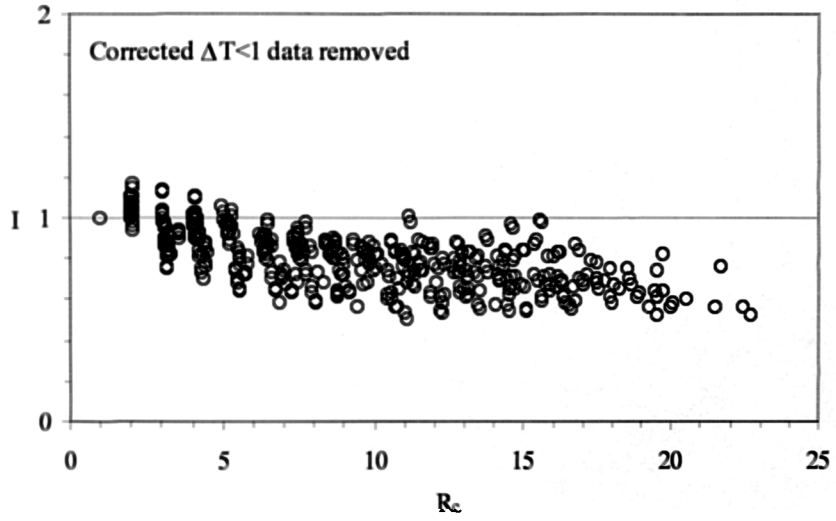

Figure 5.19 Corrected inundation factors

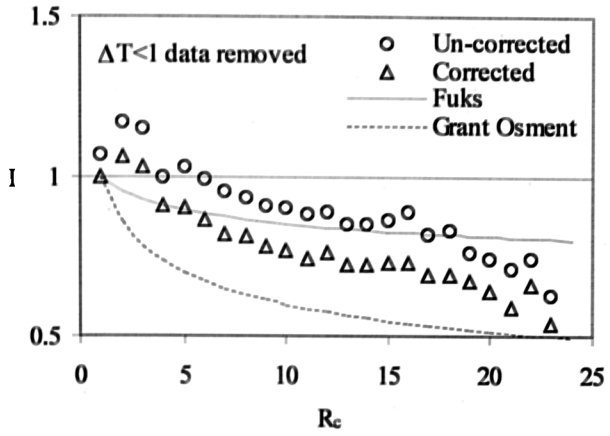

Figure 5.20 Inundation factor condensate ratio average trend

5.4.4 FILMWISE INUNDATION STEAM VELOCITY DEPENDENCE

The data were also examined for any dependence of the inundation factor on the steam velocity. This was accomplished by regenerating Figure 5.15, Figure 5.16, Figure 5.18, Figure 5.19 with different symbols corresponding to groups of steam Reynolds numbers. The Reynolds numbers were calculated based on the steam properties, the velocity at the maximum flow area and the tube outside diameter. The regenerated plots can be found in Appendix C5 and Appendix C6. From inspection of the plots in Appendix C5 it can be seen that data which displays the highest and most scattered I values is attributable to conditions of moderate R_c and steam Reynolds numbers of 2000-500. As discussed previously, some data were obtained from locations within the bundle where the steam saturation temperature was nearly equal to the cooling water temperature. Under these conditions the potential errors in the data were significant. This is demonstrated by the stark contrast in scatter between the plots of Appendix C5 and Appendix C6. These plots demonstrate the effect of removing the low temperature difference, high potential error data.

Even with suspect data removed, the scatter in the data is such that the effect of the steam Reynolds number is unclear. However, close inspection of plot 2 in both

Appendix C5 and Appendix C6 suggests that the effect of increasing R_c values on the inundation factor is more predominant at high Reynolds numbers. This behaviour is indicated by the initial rapid and distinct decreasing trends of the data with Reynolds numbers greater than 2500.

5.5 DROPWISE CONDENSATION HEAT TRANFSER ANALYSIS

5.5.1 GENERAL

Dropwise condensation data were obtained using hydrophobic tubes. These test were all conducted at a nominal bundle inlet steam pressure of 50mbar. The apparatus was run to obtain result at high, medium and low condensation rates. Detail of the local conditions can be found in Table 5.6.

Before analysing the dropwise data it should be noted that due to changes in the surface chemistry of the tube coatings, the tubes sustained dropwise condensation for only approximately 16 hours, at which point patches of filmwise condensation were observed. The failure of the tubes is reflected in the data by the reductions displayed in the last of the dropwise heat transfer coefficients results in Figure 5.22. Two sets of hydrophobic tubes were used, details of the test numbers and tube set used can be found in Appendix C1.

The sequence of the tests using the successful second batch of dropwise tubes was, low condensation rate, high condensation rate, dropwise Wilson plot and finally medium condensation rate.

5.5.2 DROPWISE FIRST ROW ANALYSIS

The shell-side heat transfer coefficients, calculated from the measured data from the first batch of hydrophobic tubes,T272-T280, are shown in Figure 5.21. These results are in general only marginally higher than filmwise results. The condensation within the

bundle was observed during these test and it was noted that the quality of the condensation was poor, i.e. the droplet departure was large and patches of filmwise condensation were present.

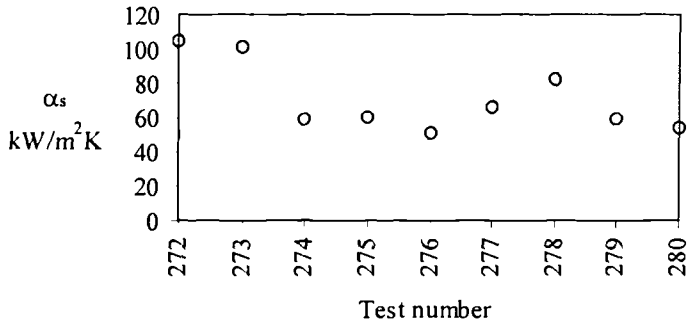

Figure 5.21 Dropwise heat transfer coefficients, first tube set

These tubes were deemed to have failed and were removed. The analysis of these dropwise results was terminated. Details of the tube failures are analysed in Section 5.5.4. At this stage the cause of failure was unknown, however, it was observed that, during this first dropwise build, the tubes had been subjected to less than ideal conditions.

Extra precautions were taken while handling and assembling the second batch of dropwise tubes and the bundle was rebuilt. The first row, air free heat transfer results from the second build as shown in Figure 5.22. This figure displays shell-side heat transfer coefficient of 999kW/m^{2}K for tests 281-302. The value 999 in the output or on graphs is not a genuine experimental value. This value was the default output from the computer program for the cases where, either the experimental coefficient was greater than 999kW/m^{2}K or, where predicted shell-side temperature difference was physically impossible, i.e. a negative value. The data shown in Figure 5.22 was obtained over three days testing which corresponds to approximately 16 hours operation.

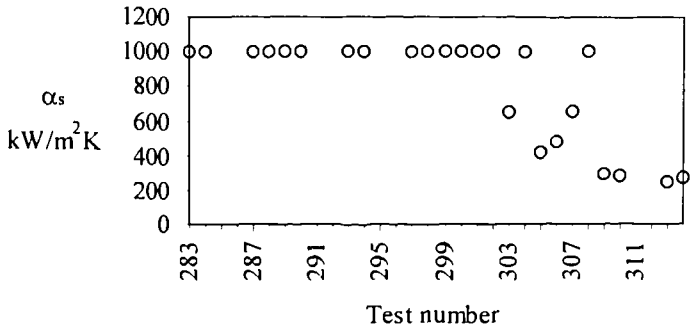

Figure 5.22 Dropwise heat transfer coefficients, dropwise tube set

From inspection of Figure 5.22 it is clear that the shell-side heat transfer coefficient during dropwise condensation is extremely high. The lower results obtained from test 303 onwards is due the presence of poor quality condensation caused by the initial stages of failure of the tube surface treatment.

Condensation rate	Inlet ΔT_{ov}	Inlet U_s	Approximate first row heat flux	Average ΔT_s	Standard deviation
High	15K	33 m/s	100 kW/m^2	-0.05K	0.040
Medium	10K	20 m/s	75 kW/m^2	0.27K	0.065
Low	5K	10 m/s	40 kW/m^2	-0.22K	0.014

Table 5.6 Dropwise condensation test summary

The average predicted first row, shell side temperature difference and the standard deviations were calculated at each condensation rate. The results are shown in Table 5.6. It can be seen that the low and high condensation rate results display a negative temperature difference prediction, while the medium rate results display an average

value of 0.27K. This is attributable to the failure of the tube coatings. The general accuracy of the results requires analysis. The error analysis described in Chapter 4 indicates that heat flux has been estimated to be within 4-8%, respectively at high and low heat fluxes. Potential errors of these magnitudes are well within acceptable limits. However, the potential errors associated with the prediction of the shell-side temperature difference are less satisfactory. The error in predicting shell-side temperature difference is controlled by the accuracy of four variables, the measured average cooling water temperature, the estimated steam saturation temperature and the predicted cooling water and wall resistances. The accuracy of these measurements and predictions have been estimated to be 0.03K, 0.1K, 1% and 1% respectively. The error analysis results can be found in the output files, however, as an approximation the accuracy of the shell-side ΔT_S in K can be described by Equation 5.12.

$$\text{Error}\Delta T_s \approx 0.02\Delta T_{ov} + 0.13$$

Equation 5.12

The resulting potential errors at low, medium and high condensation rates are therefore 0.23K, 0.33K and 0.43K respectively. These error results are significant and both cast doubt on the credibility of the results and indicate that accurate measurements in this range are not possible with the current apparatus. At this point two vital issues must be addressed. Firstly, the errors estimated above are the worst case scenario values and therefore highly unlikely to occur. In practice the errors which occur are likely to be a fraction of these values. This is borne out by the standard deviations shown in Table 5.6, the values of which are approximately 15-20% of the maximum temperature error calculated using Equation 5.12. Secondly, viewing the dropwise results relative to the

filmwise results gives a clear indication of performance. Using the same apparatus with untreated tubes gives repeatable accurate data. The change to treated tubes gives heat transfer coefficients that are so high that measurement becomes impossible.

The two high quality, dropwise average condensation results indicate shell-side temperature differences which are negative. These values are physically impossible. However, if these results are interpreted as being zero and the realistic errors of 25% of the above estimates are applied, the smallest estimates of the heat transfer coefficients are still greater than 600kW/m^{2}K. Hence, this analysis has shown that high quality dropwise condensation produces shell-side, heat transfer coefficient so large, that the apparatus cannot measure them. However, it has been shown by considering the results and the likely errors the values of heat transfer coefficient occurring are certainly greater than 500kW m^{2}K.

5.5.3 DROPWISE INUNDATION ANALYSIS

The dropwise data were analysed to investigate the effects of condensate inundation. This analysis was conducted by investigating the effects of bundle depth on both the overall heat transfer coefficient and the shell-side temperature difference. This was achieved by producing plots of the type shown in Figure 5.23, Figure 5.24 and Figure 5.25 which corresponding to the three condensation rates tested. For comparative purposes, the plots also show the trends obtained during filmwise condensation under the same local conditions. Data shown on these plots as solid symbols correspond to dropwise condensation. The open symbols correspond to filmwise condensation. Analysis of the heat transfer coefficient or shell-side temperature as a function of bundle depth shows the combined effect of inundation and reductions in vapour velocity. From inspection of the plots in Figure 5.23, Figure 5.24 and Figure 5.25 it is clear that the

combined effect of inundation and velocity reduction is significant during filmwise condensation, whereas, during dropwise condensation, their is no detectable effect.

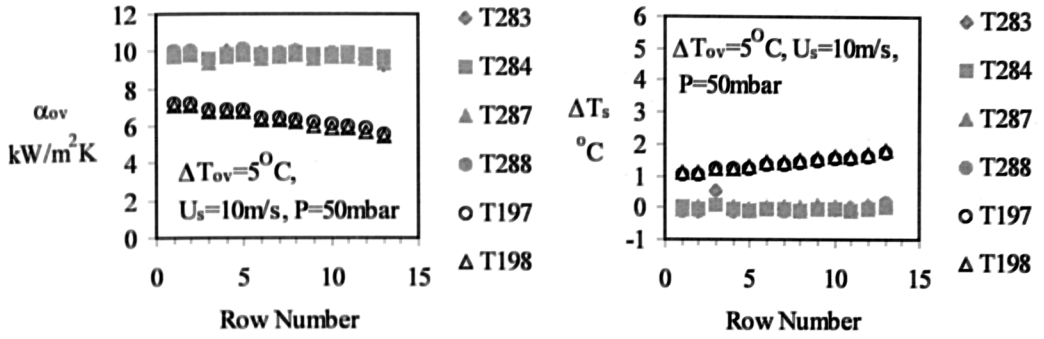

Figure 5.23 Inundation effects at low condensation rate

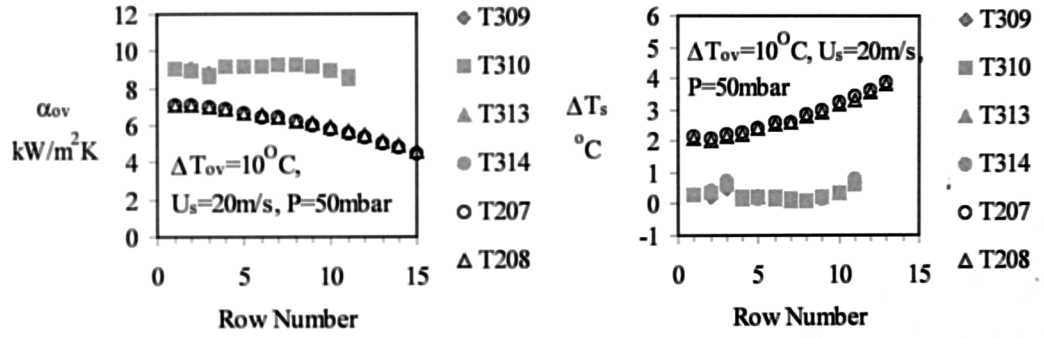

Figure 5.24 Inundation effects at medium condensation rate

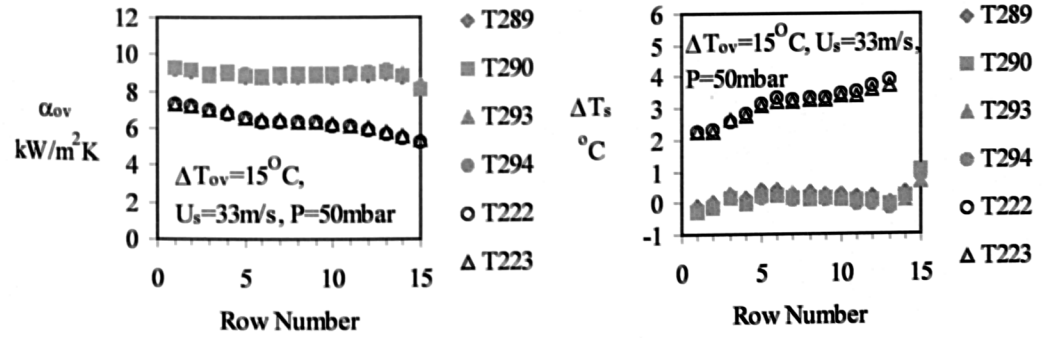

Figure 5.25 Inundation effects at high condensation rate

During filmwise condensation it is known that a reduction in vapour velocity, or the presence of condensate inundation, reduces the film heat transfer coefficient. It is also known that the combined effect of condensate inundation and reducing velocity is a combined heat transfer reduction. For the case of dropwise condensation, this type of widely accepted information is not available. However, their exists a small quantity of published work which suggests that decreasing vapour velocity leads to reductions in heat transfer coefficients, Tanasawa [65] (1991), and that condensate inundation can result in improvements in heat transfer, Rose [59] (1976). Therefore, the possibility exists that any effects of reducing steam velocity are being compensated for by enhancements caused by increasing inundation. Alternatively it is equally possible that the effects of velocity reductions and condensation inundation are so slight that the effects cannot be measured using the current apparatus.

5.5.4 DROPWISE TUBE FAILURE ANALYSIS

As indicated in Section 5.5.3 the dropwise tests were conducted using two set of hydrophobic tubes. To achieve the hydrophobic properties these tubes had been coated with an ultra-thin plasma polymer. However, under the steam conditions used for this work, the operational life of these coatings was found to be short. Of the two sets of hydrophobic tubes, the first set, failed before any data was recorded. The second set condensed dropwise for approximately 12 hours, after which the results indicated that failure was beginning to occur.

All the hydrophobic tubes used in this work were coated in a single production run, using the same equipment, materials and procedure. Furthermore, after production, the tube storage was not ordered. Hence, the 75 tubes which formed the first hydrophobic set were selected at random from the 150 tubes produced. The cause of the contrast between the operational life of the two sets of hydrophobic is not known. At the time of

failure of the first set of dropwise tubes, the cause of failure was assumed to be erosion. Hence, at the locations where filmwise condensation was occurring, it was expected that the coating had been removed. To confirm this, tube samples were sent to the Research Unit for Surfaces Transforms and Interfaces in Cheshire [95]. The surface chemistry of the tube samples was analysed. The results of this analysis showed that, in all cases, the coating had not been removed. In an attempt to trace the failure of the coatings, the analysis was extended to investigate the surface chemistry of the coatings. Since the analysis of the first samples was expected to show that the coatings had simply been removed, no unexposed reference or standard samples were included or analysed. A second batch of six unexposed tube samples were sent for analysis. Three of the samples were take from a tube which had been subjected to handling and mains tap water, while the remaining three samples were cut from a tube which, after coating, had never been handled, exposed to water or any other process. The results of the two analyses were studied. It was found that variations in the surface chemistry of the coatings were so slight that the cause of failure was not clear. The only pointer towards the possible cause of failure was found to be the surface silicon content. For the new un-handled tube, the silicon content was around 25%. For a tube subjected to handling and water, it was approximately 14%. The used tube from the bundles 12th row had 12% and the used tube from the 3rd row had 10%. The visual contrast between new and failed tubes is shown by photograph 10. These results suggested that a low Silicon content is an indicator for failure, and that silicon can be depleted by exposure to water from the local mains supply. Linking all of these factors together, it is possible that the first batch of tubes had failed before their first exposure to steam. It may be that the failure of the coatings was a result of the over-spill of cooling water which occurred on the occasions when the bundle was removed to trace air leaks.

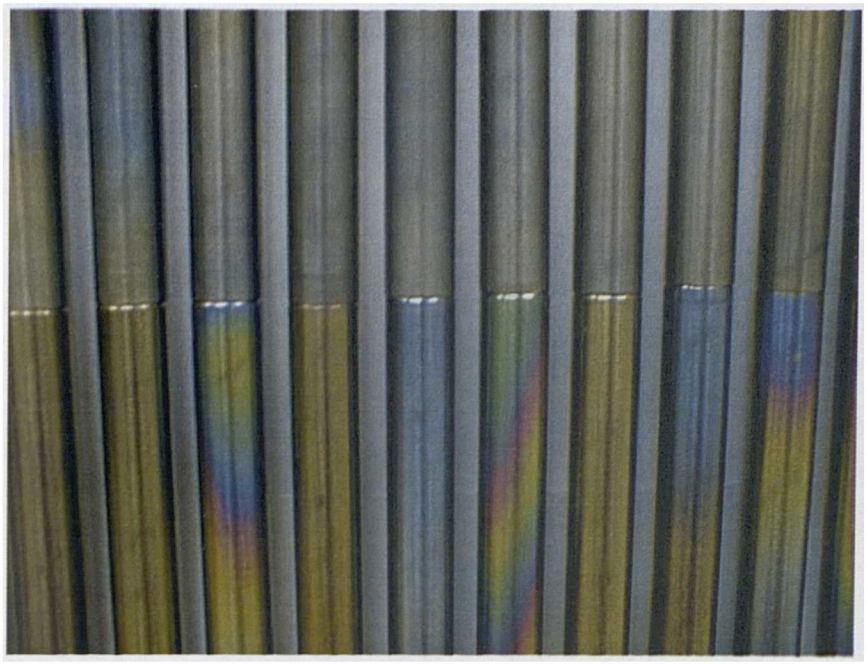

Photograph 10, Contrast between new (bottom) and used (top) plasma polymer coated tubes.

5.6 THE EFFECT OF AIR ON HEAT TRANSFER

5.6.1 GENERAL

In addition to the data obtain using pure steam, data were also recorded with steam containing air as a non-condensable gas. The data were obtained during both filmwise and dropwise condensation tests by repeating all the 50mbar conditions with steam containing approximately 1% air at the bundle inlet. For further details of the local conditions during the air tests see Table 5.1 or Appendix C1.

5.6.2 AIR EFFECTS ON FILMWISE CONDENSATION

The effects of air on the shell-side, condensation heat transfer coefficient has been analysed. This has been achieved by comparing the shell-side heat transfer results from air mixture tests with the results obtained using pure steam, at nominally the same pressure, steam velocity and overall temperature difference. For the cases where air was present, the temperature of the mixture has been assumed to be equal to the saturation

temperature corresponding to the estimated steam partial pressure. The steam partial pressure calculation was based on the measured inlet air flow rate, the local calculated steam flow rate and the measured mixture pressure. Since two sets of data were recorded for each and every test condition, the air film heat transfer coefficients have been calculated by subtracting the average of two pure steam heat transfer resistances from the air mixture average, obtained under the same conditions. The resulting air film heat transfer coefficients have been plotted as a function of row number for each of the bundle inlet conditions. These plots are shown in Figure 5.26, Figure 5.27 and Figure 5.28. From inspection of the nine plots in Figure 5.26, Figure 5.27 and Figure 5.28 it may be noted that no data is presented for the lower rows in a number of the plots. This is a result of either, condensation being prevented on the lower rows to generate the desired inlet pressure or a saturation temperature below the cooling water temperature. Where no data is presented for an upper row this is due to the measured shell-side, heat transfer coefficient with air being estimated to be higher than that without air. The plots in Figure 5.26, Figure 5.27 and Figure 5.28 show that, at positions in the bundle where the steam velocity is low and the air concentration is high, the effects of air are significant.

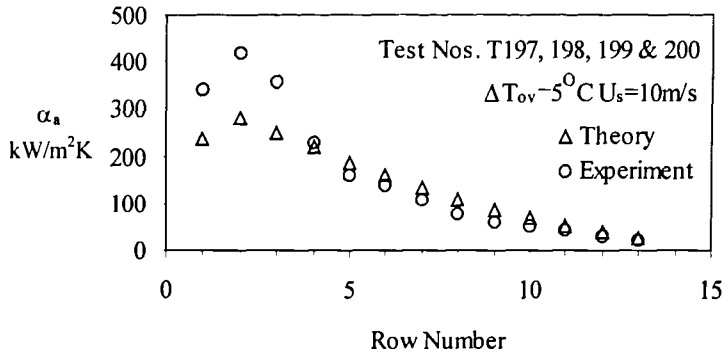

Plot 1

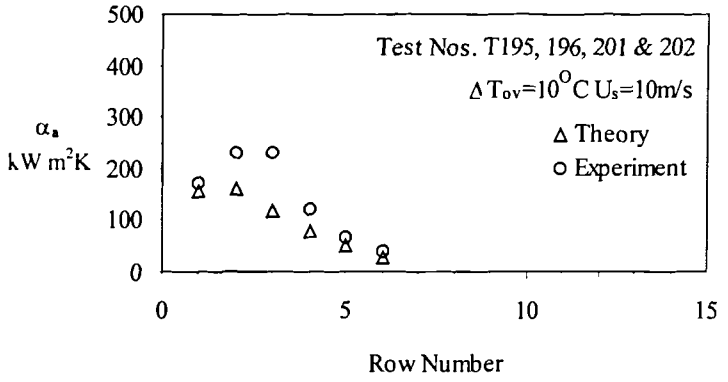

Plot 2

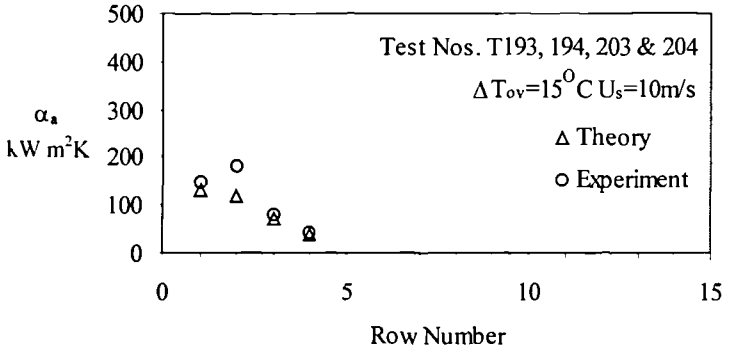

Plot 3

Figure 5.26 Air effects during filmwise condensation, steam velocity 10m/s

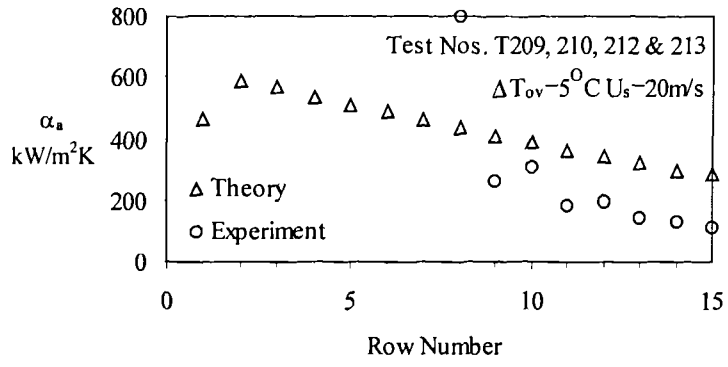

Plot 1

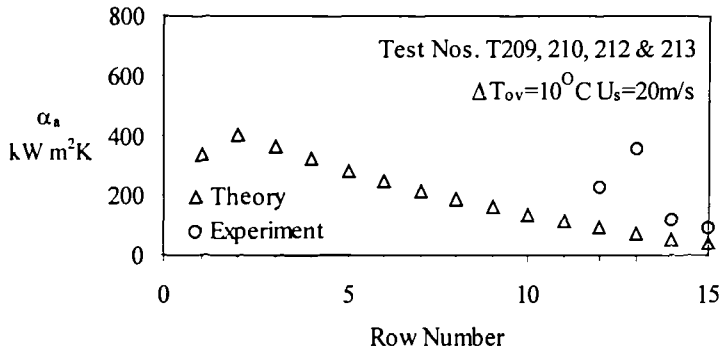

Plot 2

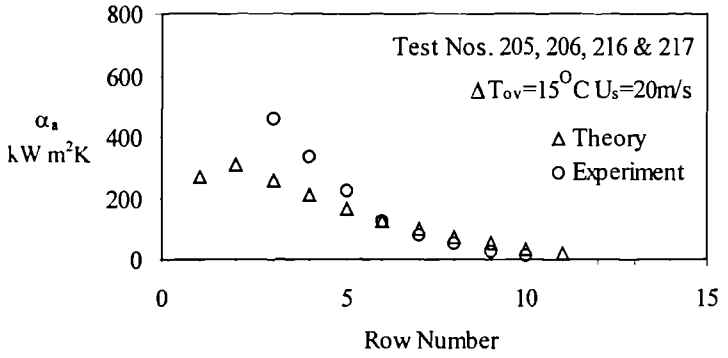

Plot 3

Figure 5.27 Air effects during filmwise condensation, steam velocity 20m/s

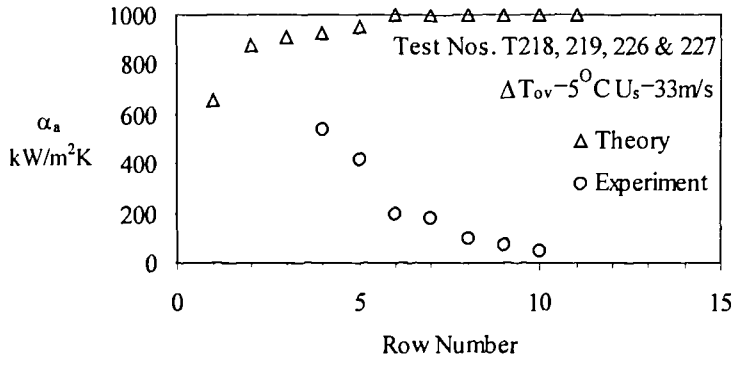

Plot 1

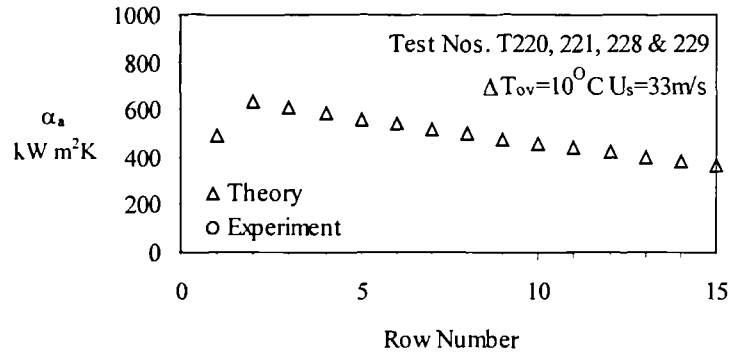

Plot 2

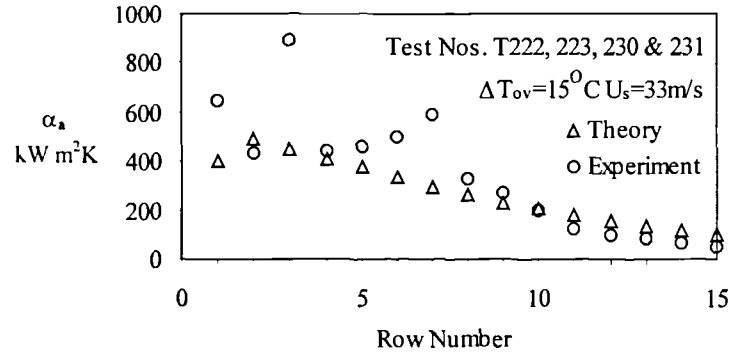

Plot 3

Figure 5.28 Air effects during filmwise condensation, steam velocity 33m/s

The experimental air film, heat transfer coefficients were compared to the theory presented by Chisholm and McFarlane [31] (1964), Equation 2.35 and Equation 2.36. This was accomplished by evaluating the model at the local experimental conditions and adding the predicted trends to the plots in Figure 5.26, Figure 5.27 and Figure 5.28. These plots show that in most cases, there is moderate to good agreement between the experimental results and the theory. However, of the plots in Figure 5.26, Figure 5.27 and Figure 5.28, there are two notable exceptions to this statement, i.e. Figure 5.28 plot 1 and plot 2. In this figure plot 2 contains only the trend of the theoretical predictions, because the value of the shell-side, heat transfer coefficient measured with air was higher than that obtained without. The measured, average, first row heat transfer coefficients at this condition were 41.1kW/m^{2}K without air and 43.8kW/m^{2}K with air, while at exit the value were 30.3kW/m^{2}K and 34.5kW/m^{2}K respectively. The most likely cause of the anomaly is an error in the steam velocity. The air and pure steam data used in this case were recorded on two different days. As a result, it is possible that, compared with the pure steam test, the steam velocity during the air mixture tests was slightly higher, and hence the heat transfer coefficient measured with air was enhanced above the pure steam value by the increased vapour velocity effects. The inlet and outlet steam velocities under these test conditions were approximately 33m/s and 25m/s respectively. Using the current apparatus, these moderate to high velocities compound the difficulties of measuring the effects of air. The difficulties arise since both the current data and the theoretical predictions indicate that, at these conditions, the effects of air are very small, e.g. heat transfer coefficients of around 500kW/m^{2}K. As discussed in the dropwise condensation analysis in Section 5.5, the errors associated with values of this magnitude are such that their measurement is outwith the capabilities of the apparatus. The previous statements relating to errors is borne out by a number of the plots in Figure 5.26, Figure 5.27 and Figure 5.28. These show that, air film, heat transfer

coefficients of above 300kW/m^{2}K produce scatter in the data that indicates that the random errors are becoming significant. In contrast to all other plots the plot 1 in Figure 5.28, displays the opposite trend to the theoretical prediction.

At this point a number of issues require consideration. Firstly, other data indicate that, at high velocities and low condensation rates, the effects of air are minimal. This is in agreement which the theoretical prediction, of α_a, the value of which, in this case, increases with bundle depth due to the increasing vapour velocity and decreasing temperature difference generated by the bundle pressure drop distribution. If the values of the prediction are accepted, then, to some extent, the discrepancy may be attributed to measurement errors which have previously been shown to be significant when the coefficient values are greater than around 300kW/m^{2}K. However, it also likely that the discrepancies displayed on Plot 1, Figure 5.28, are linked to the behaviour discussed in Section 5.3.3. The discussion in Section 5.3.3 highlighted, that the combined effect of high velocities, greater than 30m/s, and low overall temperature differences, less than 5K. gives a reduction in heat transfer rather than the predicted increase. The test data used to construct this plot can be found in Appendix C7. From an inspection of this data, it is clear that this combination of extreme local conditions, the data show no trend, displays a significant degree of scatter and also has poor repeatability. At these low to moderated values of shell-side heat transfer coefficient, this scatter is uncharacteristic. However, since it has been shown that, at these extremes, the first row heat transfer coefficient for pure steam departs from the physical trends, the presence of similar deviations using air mixtures should not be unexpected. As in Section 5.3.3 the candidate can offer no explanation for this behaviour.

However, it is worth noting that, under these test conditions, the velocity of the steam at inlet was 33m/s and 48m/s at outlet. The data at inlet conditions of U_s=33m/s and ΔT_{ov}=5K are the only data which result in an increasing velocity, and are also the only

data which defy the normal trends of a well designed condenser. Whether or not this is coincidental is unknown.

5.6.3 AIR EFFECTS WITH DROPWISE CONDENSATION

The effects of air during dropwise condensation have been analysed using the same data processing procedure as with the filmwise results. As discussed in Section 5.5.1, the dropwise tests were limited to three local conditions corresponding to high, medium and low condensation rates. Plots indicating the effects of air on dropwise condensation have been generated and can be found in Figure 5.29. The results shown on these plots indicate that as with filmwise condensation, when the steam velocity is low and the air concentrations high, the effect of air is significant. The theoretical predictions of Chisholm and McFarlane [31] (1964), Equation 2.35 and Equation 2.36, are also shown on the plots in Figure 5.29. As was the case with filmwise condensation, the agreement between the theory and the experimental results is good at low air film, heat transfer coefficients, while at higher values, where errors have been shown to be significant, the data displays increasing scatter.

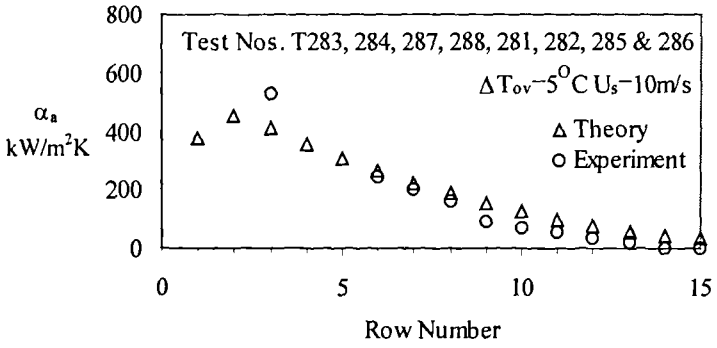

Plot 1

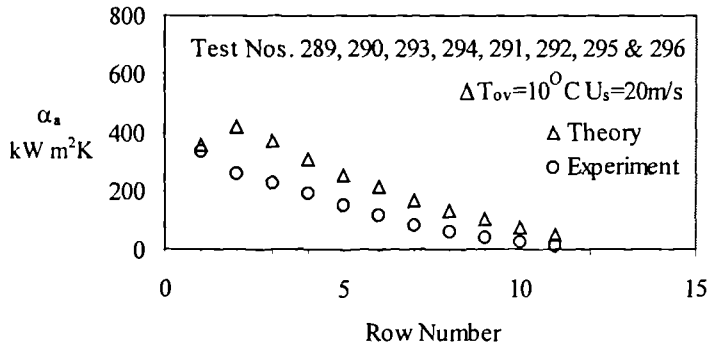

Plot 2

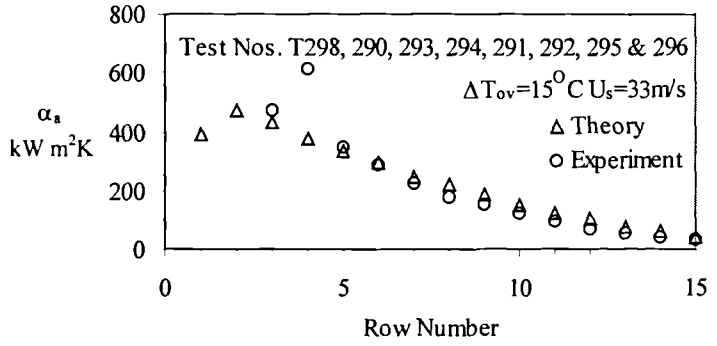

Plot 3

Figure 5.29 Air effects during dropwise condensation

5.7 OVERALL HEAT TRANSFER COMPARISON

5.7.1 GENERAL

To allow the performance of dropwise condensation to be directly compared with filmwise, the test programme aimed to test both modes at equal steam and cooling water conditions. In general this has been achieved. However, for the case where the target steam velocity with air was 10m/s, the actual velocities were 13m/s for dropwise and 9m/s for filmwise. This difference has no effect on the analysis of the data, but should be considered when directly comparing dropwise and filmwise results at this condition.

5.7.2 FILMWISE VS. DROPWISE COMPARISON

To analyse the global effect of the step change from filmwise to dropwise condensation Table 5.7 has been produced. This table shows the row average heat load adsorbed by the cell and shows that, in all cases, the dropwise bundle adsorbed more heat. This heat transfer increase was primarily a result of the dropwise heat transfer coefficients which, unlike filmwise, do not reduce with bundle depth as the steam velocity reduces and the inundation rate increases.

	Row average heat absorbed by test cell (kW)		
Dropwise	U_s=10m/s ΔT_{ov}=5K	U_s=20m/s ΔT_{ov}=10K	U_s=33m/s ΔT_{ov}=15K
0% Air	1.67, 1.70, 1.73, 1.71	3.34, 3.25, 3.27, 3.31	4.07, 4.08, 4.15, 4.13
1% Air in	1.50, 1.44, 1.52, 1.52	2.75, 2.76, 2.86, 2.80	3.76, 3.74, 3.78, 3.74
Filmwise	U_s=10m/s ΔT_{ov}=5K	U_s=20m/s ΔT_{ov}=10K	U_s=33m/s ΔT_{ov}=15K
0% Air	1.2, 1.16	2.32, 2.31	3.2, 3.22
1% Air in	1.13, 1.15	2.18, 2.17	3.18, 3.18

Table 5.7 Filmwise vs. dropwise performance summary

To compare the row by row performance of the test condenser with dropwise and filmwise condensation plots included in Figure 5.30 were produced. These plots have been generated for each of the three dropwise conditions tested, the set of three plots can be found in Figure 5.30. From inspection of and the it can be seen that the in the absence of air, particularly when compared to filmwise condensation, the dropwise overall heat transfer coefficient remains approximately constant through the entire bundle. For the case with air the dropwise overall heat transfer coefficient can be seen to drop rapidly, more so that the filmwise values This is caused by the relative values of the coefficients. During dropwise condensation the overall value are dominated by the air resistance and hence the decrease from the higher dropwise values is more rapid than from the lower filmwise results. From an inspection of the plots in Figure 5.30 it can also be seen that, in some cases, the overall heat transfer coefficient during dropwise falls below the filmwise results. This is due to the increased condensation rate through the bundle resulting in significantly higher air concentration at the lower rows. The variations in the air concentration between each dropwise and filmwise test condition are shown in Figure 5.31.

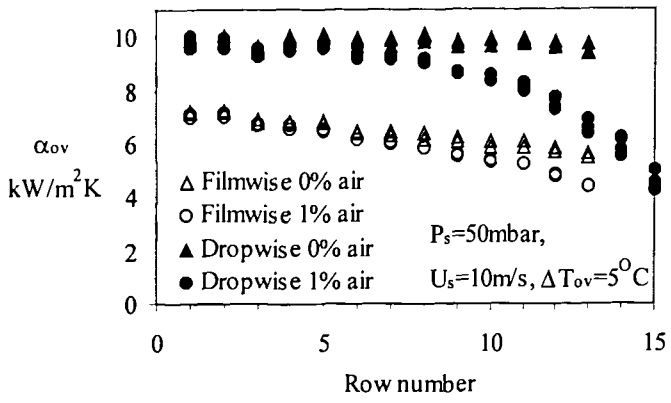

Plot 1

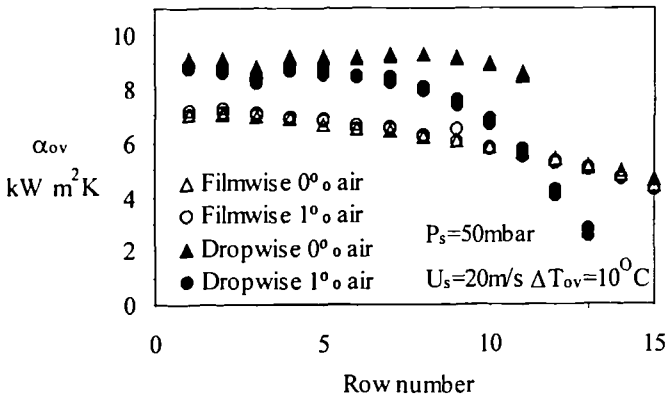

Plot 2

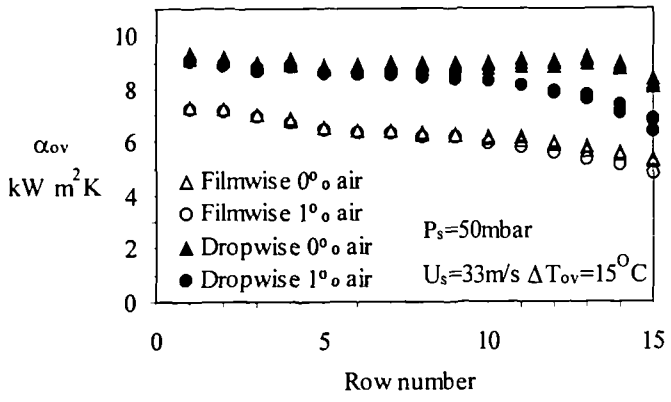

Plot 3

Figure 5.30 Heat transfer comparison between dropwise & filmwise condensation

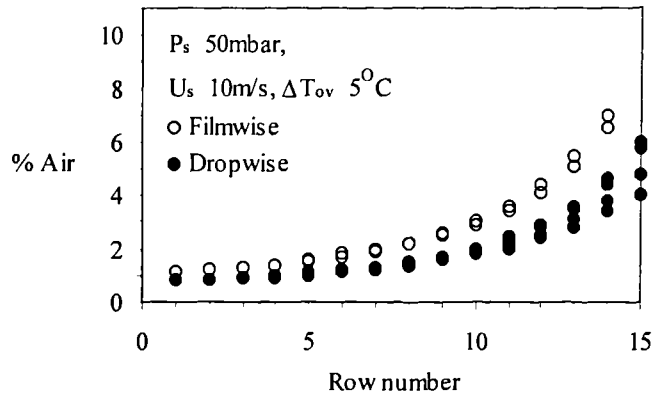

Plot 1

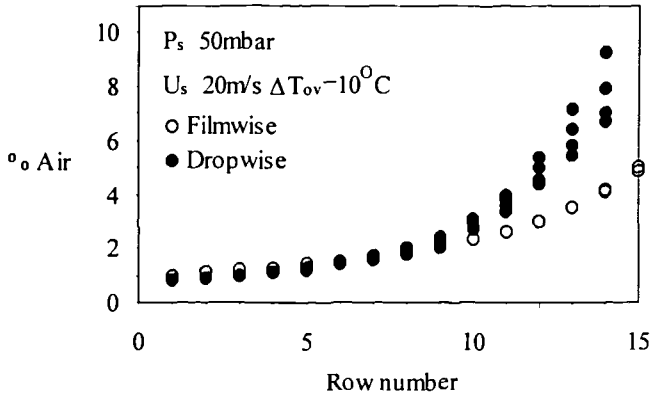

Plot 2

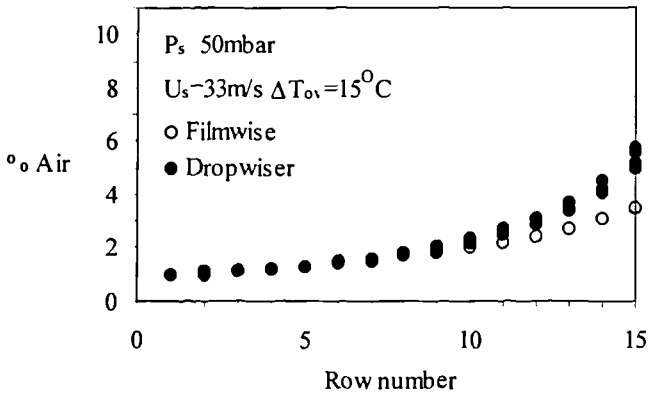

Plot 3

Figure 5.31 Air content comparison between dropwise & filmwise condensation

5.8 PRESSURE DROP ANALYSIS

5.8.1 GENERAL

As part of the procedure for collecting data, the pressure distribution within the bundle was measured. The main objective of the pressure measurements was to provide a means of determining the saturation temperature for use in the heat transfer calculations. An absolute pressure transmitter was fitted to provided this information. The range of this transmitter was 1868mbar and the stated accuracy was ±0.25% of the range (±4.67mbar). The repeatability and sensitivity of this unit was not stated. However, from experience, these values were expected to by considerably less than the accuracy. Due to these uncertainties with the absolute transmitter, a differential unit was fitted to measure the bundle pressure drop. The range of the differential transmitter was 75mbar and the accuracy was ±0.1% of this range (±0.075mbar). As with the absolute transmitter the repeatability and sensitivity of this unit was not stated. Data obtained from these two units were compared and generally gave agreement to within ±0.5mbar, confirming that the sensitivity and repeatability of the absolute transmitter is significantly less than the accuracy. See Appendix A5 for the full manufacturers transmitter specifications. Based on the results and the specifications, the sensitivity and repeatability of the transmitters was likely to have been around 1mbar for the absolute unit and 0.05mbar for the differential unit.

5.8.2 SINGLE PHASE FLOW PRESSURE DROP ANALYSIS

In addition to the pressure drop data obtained during the dropwise and filmwise test programme, three single phase test conditions were run where no condensation occurred. Data were recorded with a bundle inlet pressure of approximately 50mbar and inlet steam velocities of 26, 20 and 10m/s. During these tests, condensation was prevented by increasing the cooling water temperature to above the steam saturation

temperature using electrical heating in the cooling water reservoir tank. For further details of the single phase test conditions see Appendix C1.

The pressure drop data obtained from the both the transmitters was reduced to obtain values of bundle drag coefficient. During the data processing the effect of gravity was neglected. However, momentum pressure terms were included. Hence, the calculated drag coefficients are those attributable to friction only. Equation 5.13 shows the exact method of calculating the drag coefficient over each group of two rows between pressure tappings.

$$Cd = \frac{\overline{\rho}_m}{2 \cdot 2 \cdot \dot{m}^2_{s(gap)}} \left((P_n - P_{n+2}) + \left(\frac{\dot{m}_s^2}{\rho} \right)_n - \left(\frac{\dot{m}_s^2}{\rho} \right)_{n+2} \right)$$

Equation 5.13

The calculated drag coefficients, based on the results of the differential transmitter are shown in Figure 5.32, in which the symbols differentiate between the row 1-2 average and the averages from subsequent rows. The results from the absolute transmitter have been omitted. The main reasoning for this decision are, firstly, the results, as they should be, are in general very similar to the differential transmitter results. However, under specific conditions, were the dump condenser was operating at or near its limit, the process of venting the transmitter lines resulted in a small system pressure rise. As a result, in terms of the drag coefficient calculations, the pressure drop distribution, based on the absolute transmitter, was distorted and became unrepresentative, particularly deep into the bundle. In terms of the drag coefficient calculations this effect could have been an issue in a small number of cases. With respect to the heat transfer calculations,

the number of conditions where this system pressure rise could occur were minimal and were insignificant in terms of the total pressure the variations.

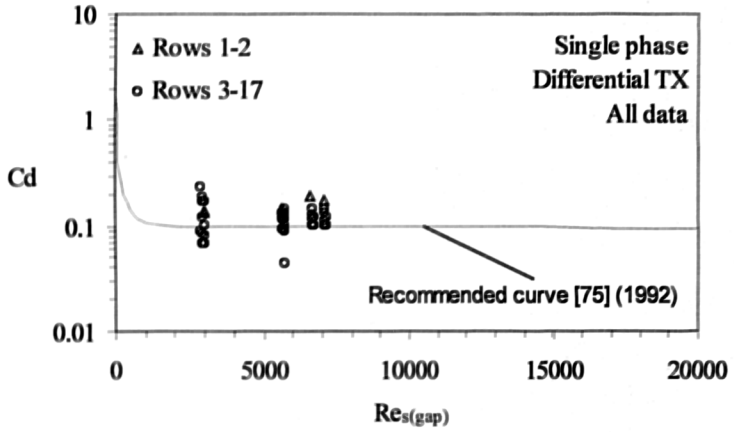

Figure 5.32 Single phase experimental and recommended drag coefficients

The recommended drag coefficients from Heat Exchanger Design Handbook [75] (1992) is shown as the continuous curve in Figure 5.32. From inspection of Figure 5.32 it is clear that the current experimental drag coefficient values are of similar magnitude to those currently accepted and in use. While the results are in line with previous workers, the data display a significant degree of scatter. Two main sources of scatter exist, errors in the pressure drop measurement and error in the estimation of the steam mass flow rate. The stated accuracy of the differential transmitter is ±0.075mbar, and since two results are subtracted to obtain each pressure drop, a error up to ±0.15mbar could occur. While this value is small, the pressure drop between tappings with a steam velocity of 10m/s is of the order of 0.3mbar. Hence, under these conditions, an error of ±50% may be possible. However, if the differential transmitter performs in a similar manner to the absolute unit, which has been shown to produce results repeatable to better than 1/10th of the accuracy band, the uncertainty band may of ±0.15mbar stated above is overly pessimistic.

Errors in predicting the steam mass flow rate also affected the results. The accuracy of the steam flow rate measurement was ±0.1kg/min, which, considering the mass flow of steam at 50mbar 10m/s ($Re_{s(gap)}$ = 3000) was 0.54kg/min, significant errors at these low Reynolds numbers may have been present. Considering the scatter at a specific Reynolds number in Figure 5.32, each of these groups of data were obtain at a fixed flow rate. As a result, the scatter of the groups must be a due to errors in the pressure drop measurements. The accuracies of the pressure transmitters have been discussed above. While it is possible that the scatter of results is due to this accuracy, this is considered to be highly unlikely. Likely sources of scatter are considered to be a combination of pressure variation due to turbulence vortex shedding phenomena, variations in the time between venting and measurement and the possibility of a condensate drop re-forming in or flowing into the pressure tapping.

From inspection of Figure 5.32 it can be seen that the drag coefficient average for rows 1-2 show significant variation. The average row 1-2 result disguises the actual relative magnitudes of the row 1 and row 2 drag coefficients. However, inspection of the curve fit drag coefficient results in output plots indicates, that around gap Reynolds numbers of 5500-7500 the first row drag coefficients were twice the second row value, and that the second row values were in line with the remainder of the bundle. The results at lower Reynolds numbers were less clear. In these cases, considering scatter and errors, it could not be shown that the first row drag coefficients were any different from those at any other row.

5.8.3 TWO PHASE FLOW PRESSURE DROP ANALYSIS

The pressure drop data obtained during filmwise and dropwise condensation have been analysed. Two analysis techniques have been used, a single phase drag coefficient method, as per the single phase analysis in which only the vapour flow is considered,

and the two phase method of Grant and Chisholm [82] (1977). For the single phase method the drag coefficients have been calculated using the method described Section 5.7.2. The experimental drag coefficients have been plotted against the tube gap Reynolds number. This plot can be found in Appendix C8, Plot 1. As before, this plot displays the experimental data and the recommended curve from Heat Exchanger Design Handbook [75] (1992). From inspection of Appendix C8 Plot 1, it is clear that the data is of similar magnitude to the recommended value at higher Reynolds numbers and displays considerable scatter at low Reynolds numbers. The sources of scatter described in the single phase analysis are equally valid for the two phase flows. However, in the condensing cases, an addition source of scatter can occur due to errors in the steam flow rate predictions. During tests where the steam flow rates were low and the condensation rates high, steam mass flow rates at the last condensing tubes could be as low as 0.1kg/min. The steam flow rate at any point in the bundle was calculated from the condensate flow rate (accuracy ±0.1kg/min) and the sum of the heat load (accuracy ±10%). Hence, at the lowest steam flow rate locations, the potential error in predicting the value could be up to 100%. In an attempt to remove data with high uncertainties it, was decided to remove data with estimated pressure errors of greater than 25%, i.e. data were the two row pressure drop was less than 0.25mbar was removed, Since low steam velocity results in low pressure drop, removing low pressure drop data removed low velocity data. The result of the cut off chosen was the removal of approximately 130 of the 900 data points shown on plot 1. The resulting plot is shown as Plot 2 in Appendix C8. From the comparison of this plot with plot 1 it is unclear whether the low Reynolds number scatter is attributable to random errors in readings of low pressures or steam velocity estimates. If the scatter were due to errors in steam velocity this would be apparent in individual data sets and would be highlighted by a gradual drift in the drag coefficient results as the bundle depth and steam velocity error increased. Inspection of

the data shows that this is not the case. Hence the scatter is primarily attributable to random pressure measurement errors.

Analysis of the data using the two phase flow method was also undertaken. This method predicted the ratio of the pressure drops between the actual two phase flow case and the theoretical case were all the mass flow occurred as a single phase vapour. Calculation of this ratio relied on the estimation of the single phase pressure drop. This was predicted using the method described in Heat Exchanger Design Handbook [75] (1992). The resulting two phase multipliers have been plotted as a function of flow quality. As before, two plots have been produce, one containing all data and the second where the high estimated error data has been removed. These plots can be found in Appendix C9. The data in both these plots displays the trend found by previous workers, e.g. Grant & Chisholm [82] (1977). The data shown on these plots is highly scattered, this is a result of the combined effects of the data scatter described in the previous section, and errors associated with the single phase estimate. An example of a typical bundle pressure distribution and the theoretical predictions of the Heat Exchanger Design Handbook [75] (1992) and Grant & Chisholm [82] (1977) is shown in Figure 5.33, The approximate inlet conditions were, steam velocity 20m/s, pressure 50mbar and overall temperature difference 10K. It should be noted that, while the theoretical models over predict the pressure loss in Figure 5.33, this is a random example and does not suggest that the models inherently over predicts.

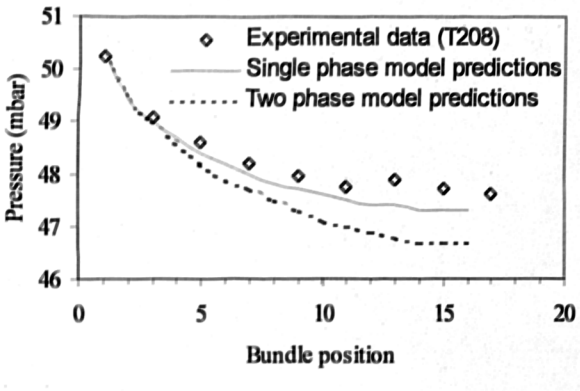

Figure 5.33 Theoretical and experimental bundle pressure distribution

The analysis described above has been repeated for the dropwise data and the same plots, which can be found in Appendix C10 and Appendix C11, have been generated. From inspection of the dropwise plots it is clear that within experimental accuracy the data is identical, with the data displaying the very similar values and scatter.

Between filmwise and dropwise condensation there was no detectable change in the steam or condensate flow within the bundle. In particular with dropwise condensation, over the range of conditions tested, no spray flow behaviour was observed. The size of droplets which actually drained from the underside of the tube during dropwise condensation were very similar to those during filmwise condensation. Note, the size of the droplets which drained from the tubes were orders of magnitude greater in size than those which departed from nucleation sites, and these did not combine with the steam flow. These droplets moved around the surface to the underside of the tube were they combined, only draining when the physical size of the forming droplet was such the it could no longer remain attached to the tube.

For the case of the drag coefficient plots, the dropwise data cover only a limited range compared with the filmwise data. This is a result of dropwise data only being available at a steam pressure of 50mbar.

CHAPTER 6

DISCUSSION

6.1 GENERAL

Following the manufacture and successful commissioning of the apparatus, an extensive experimental programme was completed. During the initial period, Wilson plot tests were conducted to establish the cooling-water-side characteristics. Single phase steam tests were also conducted to establish the adiabatic pressure drop behaviour. During the main test programme, heat transfer and pressure drop data were obtained for both filmwise and dropwise condensation of steam. For the filmwise tests, inlet conditions included steam velocities of 10 to 33m/s, steam to cooling water temperature differences of 5, 10 and 15K, air concentrations of 0 and 1% and pressures of 50, 75 and 100mbar. Dropwise data were obtained over the same steam velocities, temperature differences and air concentrations, but only at 50mbar. The data obtained are discussed below.

6.2 WATER-SIDE CHARACTERISTICS

A series of Wilson plot tests were conducted and the data were analysed. The analysis required a model for the heat transfer characteristics of the cooling water circuit. Equation 5.2 proposed by Gnielinski [92] (1976) was found to well represent the cooling water circuit characteristics. The correlation of Sieder and Tate [89] (1936), Equation 5.1, was also examined. This model was considerably less representative then the Gnielinski model. The source of the variations between the two correlations was found to be the Reynolds number dependence. The Sieder and Tate model has a Reynolds number exponent of 0.8. The Reynolds number dependence of the Gnielinski model is not apparent at first inspection, however, it can be shown that, at these experimental conditions, the exponent is approximately 0.9. The current data was

examined and was found to display a Reynolds number dependence of just over 0.9. Hence, it was clear that the cooling-water-side was best described by the Gnielinski model.

6.3 FIRST ROW FILMWISE CONDENSATION HEAT TRANSFER

Since the first row data were obtained under bundle flow conditions, i.e. a typical bundle geometry, but without inundation, this data was considered particularly valuable and was analysed separately. The first row data were compared with three established correlations using three definitions for the bundle flow area to determine the steam velocity. The correlations used were that of Fujii et. al [11] (1972), Rose [20] (1988) and Shekriladze and Gomelauri [9] (1965). The flow areas used were the maximum, minimum and mean void areas. Of these combination the correlation of Fujii using the maximum flow area, was found to represent the present data best. Statistically, there was very little difference between the performance of the Fujii correlation based on the maximum flow area and the Rose correlation based on the either the maximum or mean void areas. However, the correlation of Fujii appeared to follow the trends of the data more satisfactorily and was therefore selected as the most representative model. In general, the Fujii correlation predicted the experimental data well at low heat transfer coefficient value but under predicted by around 20-25% at higher values. The apparent, closer agreement of the Fujii correlation relative to the Rose correlation, is to some extent predictable, since, Fujii also used steam as his working fluid during the development of his correlation, while Rose developed his using data obtained for a wide range of fluids. It may therefore be the case that for design purposes where the working fluid is steam, the Fujii correlation is most representative, where as, if any other fluid has been used, the correlation of Rose with a mean void area definition may be more suitable.

The data also demonstrated that further work is required into cases where the steam velocities are high and the condensation rates are low. Under these conditions there is significant change in the condensation process. This results in over predictions of the film coefficient of up to 100%.

Not withstanding these extreme condition results, the agreement with the experimental data is satisfactory and shows that the apparatus returns results comparable to those obtained by previous workers for the first row.

6.4 FILMWISE INUNDATION

The inundation data obtained were found to display a high degree of scatter. Potential sources of scatter were examined. It was found that data obtained at low condensate film temperature differences were highly scattered. This data was removed and the scatter reduced, but was still significant. The scatter was attributed to both experimental error and to the method used to calculate the inundation factor. The method of calculating an inundation factor relied on a purely theoretical prediction of the heat transfer coefficient for a tube without inundation. While corrections were estimated in an attempt to compensate for any inaccuracies in the predicted values, the method used was considerably less than ideal, but was the best method available. The data was averaged to highlight the trends and it was found that the effects of inundation were less than those predicted by most correlations. In all cases, corrected or uncorrected, the data indicated that the heat transfer coefficient at the second row was higher than the first. The source of this increase is unclear, and may be attributable to either systematic experimental errors or to turbulence rippling thinning the condensate film and genuinely increasing the heat transfer coefficient.

None of the correlations tested could be considered to be representative of the data. However, the correlation of Fuks [45] (1957) was found in a select number of cases, to

reasonably predict the effect of inundation. The correlation of Kern [46] (1958) was found to follow the general inundation trends and produce a safe conservative estimate for design purposes.

6.5 DROPWISE CONDENSATION HEAT TRANSFER

The dropwise condensation data has shown that, when high quality dropwise condensation occurs, i.e. when the hydrophobic coatings perform well and the droplet departure size is small, the shell-side, heat transfer coefficient which results, has a value higher that can be measured using the current apparatus. The data from all 15 rows indicated that, unlike filmwise condensation, the bundle depth effects of inundation and reducing vapour velocity have minimal or no effect on the overall heat transfer during dropwise condensation. Shell-side heat transfer coefficients with pure steam were extremely high. After making allowances for experimental error, the values are certainly of the order of 500kW/m^{2}K or greater.

Since dropwise condensation results in extremely high shell-side, heat transfer coefficients, and displays no detectable, therefore no significant, variations with local flow conditions or bundle conditions. For the purpose of designing a condenser operating with dropwise condensation, setting the shell-side, heat transfer coefficient to a fixed value of 400-500kW/m^{2}K at all location should be adequate for typical condenser design situations, i.e. were the overall heat transfer resistance is dominated by combined water-side and wall resistance e.g. where the sum of these values is less than approximately 15kW/m^{2}K.

6.6 EFFECT OF AIR ON DROPWISE AND FILMWISE CONDENSATION

The effects of air on both dropwise and filmwise condensation heat transfer were analysed. In both cases, the data indicates that where the steam velocities are low and

the air concentrations high, the presence of air can introduce a significant resistance to heat transfer. The data for both dropwise and filmwise condensation were found to agree well with the prediction method of Chisholm and McFarlane [31] (1964). This suggests that the effect of air is well modelled by this method and that the presence of air introduces the same additional resistance to heat transfer for both modes of condensation.

6.7 BUNDLE PRESSURE DROP DURING DROPWISE AND FILMWISE CONDENSATION

The pressure drop characteristics of the test bundle were investigated with both a single phase steam flow and condensing flows. The data obtained were used to calculate drag coefficients and, where applicable, two phase multipliers. From the results of the drag coefficient analysis, it was clear that their was considerable scatter in the data, particularly at low Reynolds numbers. The scatter was attributed to random errors associated with the pressure drop measurements. Drag coefficient results obtained from the single phase tests, filmwise tests and dropwise tests were compared. It was found that, within the experimental scatter, their was no detectable differences and that the results were inline with previous published work e.g. [75] (1992).

The condensing data was also analysed in terms of a two phase multiplier, e.g. that proposed by Grant and Chisholm [82] (1977). However, due to the combined effects of measurement errors and accuracy of the required single phase prediction, the two phase multiplier analysis results are extremely widely scattered. The extent of the scatter is such that, beyond stating that the general trend of the two phase method is correct no particular statements can be made.

For real condenser design work the data indicates that single phase methods result in reasonable estimates of condenser pressure drops, provided only the steam flow is

considered in the calculation. This applies to both filmwise and dropwise condensation, since based both results and visual observations the drag coefficients and flow regime were, within experimental accuracy, equal.

CHAPTER 7

CONCLUSIONS

The cooling water circuit heat transfer performance was found to be accurately modelled by the correlation of Gnielinski [92] (1976).

The filmwise data obtained from the bundle first row was found to be in agreement with previous workers and has been shown to be well represented by the correlation of Fujii [11] (1972), using the maximum condenser flow area for calculation of the steam velocity. Due to the similarity between the results obtained and previous workers, the apparatus operation and data processing procedures were considered validated.

Results for the effects of condensate inundation during filmwise condensation displayed significant scatter but were often similar in magnitude to those predicted by Fuks [45] (1957) or Kern [46] (1958).

At absolute pressures of 40-50mbar on plasma treated tubes, dropwise condensation heat transfer coefficients have been estimated to be around 500kW/m^{2}K. Measurement of the exact values were found to be impossible since the dropwise process operated with shell-side temperature differences of less than 0.1K, which is outwith that which could be accurately measure using the current apparatus. No inundation effects were detected with dropwise condensation.

Over the range of conditions tested, heat transfer reductions due to the presence of air were found to be well modelled by the method detailed by Chisholm and McFarlane [31] (1964), for both filmwise and dropwise condensation.

Pressure drop characteristics during dropwise and filmwise condensation were found to be, within experimental accuracy, identical, with the measure drag coefficients being, in general, approximately 0.1. The shell-side flow distribution was unaffected by the

switch to dropwise condensation and, in particular, no spray flow behaviour was observed.

The main benefits of dropwise condensation are that high heat transfer coefficients can be achieved under high inundation and/or low steam velocity conditions, where traditionally the film resistance would have become significant, e.g. in the bundle core. For the bundle tested under identical conditions, the bundle of dropwise tubes condensed over 20% more steam than the bundle with filmwise tubes.

The present data suggests that the performance of a condenser operating entirely or partially on dropwise condensation could be modelled with existing software by setting the film coefficient for the dropwise tubes to a fixed value of around 400-500kW/m^{2}K, all other aspects of the condenser model remaining unaltered. However, since dropwise condensation does not require the high vapour velocities which are beneficial during filmwise, the optimum dropwise tube bundle geometry may utilise larger tube pitch/diameter ratios. Were the tube spacing may only be dictated by the requirement to prevent air accumulation.

RECOMMENDATIONS

Before industrial applications for dropwise condensation can be considered two main areas must be addressed. Firstly the potential benefits of dropwise condensation should be quantified by modelling a typical condenser, under typical operating conditions, using both filmwise and dropwise condensation. If the result from the model indicated sufficient benefit, a surface must be developed which can both reliably promote dropwise condensation and offer an acceptable life expectancy.

REFERENCES

1 Nusselt, Die Oberflachenkondensation des Wasserdampfes, Zeitschrift des Vereines Deutscher Ingenieure, Vol. 60, pp 541-575, 1916

2 Institution of Chemical Engineers, Symposium Series No. 75, Condensers: Theory and Practice, Pergamon Press, pp 113-130 1983

3 T. Fujii, Theory of Laminar Film Condensation, Springer-Verlag New York, Inc., 1991

4 J. W. Rose, Some Aspects of Condensation Heat Transfer Theory, Int. Comm. Heat Mass Transfer, Vol. 15, pp 449-473, 1988

5 W. M. Rohsenow, Heat Transfer and Temperature Distributions in Laminar Film Condensation, Trans. ASME., Vol. 78, pp 1645-1648, 1956

6 E. M. Sparrow and J. L. Gregg, A Boundary Layer Treatment of Laminar Film Condensation, Trans. ASME. Journal Heat Transfer, Vol. 81, pp 13-18, 1959

7 E. M. Sparrow and J. L. Gregg, Laminar Condensation Heat Transfer on a Horizontal Cylinder, Trans. ASME. Journal Heat Transfer, Vol. 81, pp 291-296, 1959

8 M. M. Chen, An Analytical Study of Laminar Film Condensation, Trans. ASME. Journal Heat Transfer, Vol. 83, pp 48-60, 1961

9 I. G. Shekriladze, V. I. Gomelauri, Theoretical Study of Laminar Film Condensation of Flowing Vapour, Int. J. Heat Mass Transfer, Vol. 9, pp 581-591, 1966

10 V. E. Denny and A. F. Mills, Laminar Film Condensation of a Flowing Vapour on a Horizontal Cylinder at Normal Gravity, Trans. ASME. Journal Heat Transfer, Vol. 91, pp 495-501, 1969

11 T. Fujii, H. Uehara and C. Kurata, Laminar Filmwise Condensation of Flowing Vapour on a Horizontal Cylinder, Int. J. Heat Transfer, Vol. 15, pp 235-246, 1972

12 H. R. Jacobs, An Integral Treatment of Combined Body Force and Forced Convection in Laminar Film Condensation, Int. J. Heat Mass Transfer, Vol. 9, pp 637-648, 1966

13 A. A. Nicol and D. J. Wallace, The Influence of Vapour Shear Force on Condensation on a Cylinder, Inst. Chem. Engrs. Symp. Ser. No. 38, Vol. 1, pp 1-19, 1974

14 V. E. Denny and V. South, Effects of Forced Flow, Non Condensables and Variable Properties on Film Condensation of Pure and Binary Vapours at the Forward Stagnation Point of a Horizontal Cylinder, Int. J. Heat Mass Transfer, Vol. 15, pp 2133-2142, 1972

15 D. W. Nobbs and Y. R. Mayhew, The Effect of Downward Vapour Velocity and Inundation on the Condensation Rates on Horizontal Tube Banks, NEL Report No. 619, pp 38-52, 1976

16 T. Fujii, H Honda and K. Oda, Condensation of Steam on a Horizontal Tube - The Influence of Oncoming Velocity and Thermal Condition at the Tube Wall, Conference Paper for the 18th National Heat Transfer Conference, ASME, San Diego, pp 35-43, 1979

17 E. S. Gaddis, Solution of the Two Phase Boundary Layer Equations for Laminar Film Condensation of Vapour Flowing Perpendicular to a Horizontal Cylinder, Int. J. Heat Mass Transfer, Vol. 22, pp 371-382, 1979

18 L. D. Berman, Influence of Vapour Velocity on Heat Transfer with Filmwise Condensation on a Horizontal Tube, Thermal Engineering, Vol. 26, No. 5, pp 274-278, 1979

19 J. W. Rose, Effect of Pressure Gradient in Forced Convection Film Condensation on a Horizontal Tube, Int. J. Heat Mass Transfer, Vol. 27, No. 1, pp 39-47, 1984

20 J. W. Rose, Fundamentals of Condensation Heat Transfer: Laminar Film Condensation, JSME International Journal, Series II, Vol. 31, No. 3, pp 357-375, 1988

21 W. C. Lee, S. Rahbar and J. W. Rose, Film Condensation of Refrigerant 113 and ethanediol on a Horizontal Tube - Effect of Vapour Velocity, Transactions of the ASME, Vol. 106, pp 524-530, 1984

22 S. B. Memory and J. W. Rose, Film Condensation of Ethylene Glycol on a Horizontal Tube at High Vapour Velocity, Proceedings of the 8th International Heat Transfer Conference, Vol. 4, pp 1607-1612, 1986

23 S. Rahbar and J. W. Rose, New Measurements for Forced Convection Film Condensation, Proc 1st UK National Conf. on Heat Transfer, Vol. 9, pp 619-632, 1984

24 S. B. Memory, E. C. Lee and J. W. Rose, Forced Convection Film Condensation on a Horizontal Tube - Effect of Surface Temperature Variation, Int. J. Heat Mass Transfer, Vol. 36, pp 1671-1676, 1993

25 Y. Q. Zhou and J. W. Rose, Effect of Two Dimensional Conduction in the Condensate Film on Laminar Film Condensation on a Horizontal Tube With Variable Wall Temperature, Int. J. Heat Mass Transfer, Vol. 39, pp 3187-3191, 1996

26 E. M. Sparrow and E. R. G. Eckert, Effect of Superheated Vapour and Non-condensable Gases on Laminar Film Condensation, A. I. Ch. E. Journal, Vol. 7, No. 3, pp 473-477, 1961

27 E. M. sparrow and S. H. Lin, Condensation Heat Transfer in the Presence of a Non-condensable Gas, Trans. ASME. Journal Heat Transfer, August, pp 430-436, 1964

28 W. J. Minkowycz and E. M. Sparrow, Condensation Heat Transfer in the Presence of Non-Condensables, Interfacial Resistance, Superheating, Variable Properties and Diffusion, Int. J. Heat Mass Transfer, Vol. 9, pp 1125-1144, 1966

29 J. W. Rose, Condensation of a Vapour in the Presence of a Non-Condensing Gas, Int. J. Heat Mass Transfer, Vol. 12, pp 233-237, 1969

30 L. Slegers and R. A. Seban, Laminar Film Condensation of Steam Containing Small Concentrations of Air, Int. J. Heat Mass Transfer, Vol. 13, pp 1941-1947, 1970.

31 D. Chisholm and M. W. McFarlane, The Prediction of Condenser Performance Using a Digital Computer, NEL. Report 161, 1964

32 E. M. Sparrow, W. J. Minkowycz and M. Saddy, Forced Convection Condensation in the Presence of Non-condensables and Interfacial Resistance, Int. J. Heat Mass Transfer, Vol. 10, pp 1829-1845, 1967

33 J. W. Rose, Approximate Equations for Forced Convection Condensation in the Presence of a Non-condensable Gas on a Flat Plate and Horizontal Tube, Int. J. Heat Mass Transfer, Vol. 23, pp 539-546, 1980

34 W. C. Lee and J. W. Rose, Forced Convection Film Condensation on a Horizontal Tube With and Without Non-condensing Gases, Int. J. Heat Mass Transfer, Vol. 27, pp 519-528, 1984

35 L. D. Berman, Determining the mass transfer coefficient in calculations on condensation of steam containing air, Thermal Engineering, Vol. 16, No. 10, pp 85-99 1969

36 A. Briggs, J. R. Cooper and J. W. Rose, Condensation from Steam-Air Mixtures on a Bank of Horizontal Tubes, 3rd UK National Conference Incorporation 1st European Conference on Thermal Sciences, Vol. 1, Hemisphere Publishing Corporation, pp 275-286, 1992

37 R. Abdullah, J. R. Cooper, A. Briggs and J. W. Rose, Condensation of Steam and R113 on a Bank of Horizontal Tubes in the Presence of a Non-condensing Gas, Experimental Thermal and Fluid Science, Elsevier Science Inc., Vol. 10 Pt. 3, pp 298-306, 1995

38 A. G. Michael, P. J. Marto, A. S. Wanniarachchi and J. W. Rose, Effect of Vapour Velocity During Condensation on Horizontal Smooth and Finned Tubes, Heat Transfer & Phase Change ASME HTD, Vol. 114, pp 1-10, 1989

39 A. Aoune and B. M. Burnside, The Influence of Tube Spacing on Vapour Shear in Condensation of Downward Flowing Vapour on a Row of Horizontal Tubes, Paper 6-PC-05, Proc. 9th Int. Heat Transfer Conference, pp27-31, 1990

40 T. Fujii, Vapour Shear and Condensate inundation: An Overview, In Power Condenser Heat Transfer Technology, editors P. J. Marto and r. H. Nunn, Hemisphere Washington DC, pp 193-223, 1981

41 D. W. Nobbs, The Effect of Downward Vapour Velocity and Inundation on the Condensation Rates on Horizontal Tubes and Tube Banks, PhD Thesis, Bristol University, 1975

42 A. G. Michael, W. C. Lee and J. W. Rose, Forced Convection Condensation of Steam on a Small Bank of Horizontal Tubes, Trans. ASME., Vol. 114, pp708-713, 1992

43 T. Fujii, H. Uehara, K. Hirata and K. Oda, Heat Transfer and Flow Resistance in Condensation of Low Pressure Steam Flowing Through Tube Banks, Int. J. Heat Mass Transfer, Vol. 15, pp. 247-260, 1972

44 B. E. Short and H. E. Brown, Condensation of Vapours in Vertical Banks of Horizontal Tubes, Inst. Mech. Eng. Proc. General Discussion Heat Transfer, pp 27-31, 1951

45 S.N. Fuks, Heat Transfer with Condensation of Steam Flowing in a Horizontal Tube Bundle (in Russian) Teploergetika, 1957, 4(1), pp 35-38, English Translation, NEL Translation No 1041

46 D. Q. Kern, Mathematical Development of Loading in Horizontal Condensers, AIChE J., Vol. 4, No. 2, pp157-160, 1958

47 I. D. R. Grant and B. D. J. Osment, The Effect of Condensate Drainage on Condenser Performance, NEL Report 350, 1968

48 G. F. Hewitt (Co-ordinating Editor), Handbook of Heat Exchanger Design, Begell House Inc. Wallingford England, ISBN 1-56700-000-2, 1992

49 E. J. Le Fevre and J. W. Rose, An Experimental Study of Heat Transfer by Dropwise Condensation, Int. J. Heat Mass Transfer, Vol. 8, pp 1117-1133, 1965

50 D. W. Tanner, D. Pope, C. J. Potter and D. West, Heat Transfer in Dropwise Condensation at Low Pressures in the Absence and Presence of Non-Condensable Gas, Int. J. Heat Mass Transfer, Vol. 11, pp 181-190, 1968

51 A. Umur and P. Griffith, Mechanism of Dropwise Condensation, Trans. ASME. Journal of Heat Transfer, Vol. 87, pp 275-282, 1965

52 J. L. McCormick and J. W. Westwater, Nucleation Sites for Dropwise Condensation, Chemical Engineering Science, Vol. 20, pp1021-1036, 1965

53 E. J. Le Fevre and J. W. Rose, A Theory of Heat Transfer by Dropwise Condensation, Proc. Third Int. Heat Transfer Conference, Vol. 2, pp 362-375, Am. Inst. Chem. Engineers, New York, 1966

54 D. W. Tanner, D. Pope, C. J. Potter and D. West, Heat Transfer in Dropwise Condensation – Part 1, The Effects of Heat Flux, Steam Velocity and Non-Condensable Gas, Int. J. Heat Mass Transfer, Vol. 8, pp 419-426, 1965

55 E. Citakoglu and J. W. Rose, Dropwise Condensation – Some Factors Influencing the Validity of Heat Transfer Measurements, Int. J. Heat Mass Transfer, Vol. 11, pp 523-537, 1968

56 R. Wilmshurst and J. W. Rose, Dropwise Condensation – Further Heat Transfer Measurements, Proc. 4th Int. Heat Transfer Conf. Paris, Vol. 6, Pt. Cs 1.4, pp 1-11, 1970

57 I. Tanasawa and J. Ochiai, Experimental Study on Dropwise Condensation, Bulletin of the JSME, Vol. 16, No. 98, pp 1184-1197, 1973

58 H. Tanaka, A Theoretical Study of Dropwise Condensation, Trans. ASME. Journal Heat Transfer, Vol. 97, August, pp 72-78, 1975

59 J. W. Rose, Further Aspects of Dropwise Condensation Theory, Int. J. Heat Mass Transfer, Vol. 19, pp 1363-1370, 1976

60 I. Tanasawa, J. Ochiai and Y. Funawatashi, Experimental Study on Dropwise Condensation – Effect of Maximum Drop Size Upon the Heat Transfer Coefficient, Proc. Sixth Int. Heat Transfer Conf., Vol. 2, pp 477-482, 1978

61 I. Tanasawa, J. Ochiai, Y. Utaka and S. Enya, Experimental Study on Dropwise Condensation (Effect of Departing Drop Size on Heat Transfer Coefficients), (In Japanese), Trans. JSME, Vol. 42, pp2846-2853, 1976

62 I. Tanasawa, Dropwise Condensation the Way to Practical Applications, Proc. Sixth Int. Heat Transfer Conf., Vol. 6, pp 393-405, 1978

63 I. Tanasawa and Y Utaka, Measurement of Condensation Curves for Dropwise Condensation of Steam at Atmospheric Pressure, Trans. ASME. Journal of Heat Transfer, Vol. 105, pp 633-638, 1983

64 S. Nagata and I. Tanasawa, Dropwise Condensation Heat Transfer of Steam Under Small Surface Subcooling, Proc. 8th Int. Heat Transfer Conf., Vol. 4, pp 1665-1669, 1986

65 I. Tanasawa, Advances in Condensation Heat Transfer, Advances in Heat Transfer, Vol. 21, pp 55-139, 1991

66 T Tsuruta, H Tanka and S Togashi, Experimental Verification of Constriction Resistance Theory in Dropwise Condensation Heat Transfer, Int. J. Heat Mass Transfer, Vol. 34, No. 11, pp2787-2796, 1991

67 M. P. Bonnar, Hydrophobic Plasma Polymer Films for Dropwise Condensation of Steam, PhD Thesis Heriot-Watt University, 1997

68 T. Furman and H. Hampson, Experimental Investigation into the Effects of Cross Flow with Condensation of Steam and Steam Air mixtures on a Vertical Tube, Proc. I. Mech. E., Vol. 173(5), pp 147-169, 1959

69 I. Tanasawa and M. Saito, Film and Dropwise Condensation of Steam on a Vertical Bank of Horizontal Circular Tubes, Proc. ASME-JSME Thermal Engineering Conf., Honolulu, Vol. 5, pp143-148, 1987

70 B. M. Burnside and Q. I. Zhao, Dropwise condensation of steam at high velocity and vacuum pressures over a small tube bank, Proc. Eurotherm Seminar 47, Heat Transfer in Condensation, Ed. C. H. Marvillet and R. Vidil, Vol. 8, pp196-204, 1995

71 O. L. Pierson, Experimental Investigation of the Influence of Tube Arrangement on Convection Heat Transfer and Flow Resistance in Cross Flow of Gases over Tube banks, Trans ASME., Vol. 59, pp 562-594, 1937

72 ESDU, Pressure Loss During Crossflow of Fluids with Heat Transfer Over Plain Tube Banks Without Baffles, ESDU Report No. 74040, 1974

73 ESDU, Crossflow Pressure Loss Over Banks of Plain Tubes in Square and Triangular Arrays Including Effects of Flow Direction, ESDU Report No. 79034, 1979

74 S. Kakac, A. E. Bergles and E. O. Fernandes (Editors),Two Phase Flow Heat Exchangers, Thermal Hydraulic Fundamentals and Design, NATO ASI Series, Series E, Applied Sciences, Vol. 143, ISBN 90-247-3693-5, 1987

75 J. Taborek, Ideal Tube Bank Correlations For Heat Transfer and Pressure Drop, Hemisphere Handbook of Heat Exchanger Design, G. F. Hewitt, pp. 3.3.7.1-3.3.8.3, 1990

76 C. R. Branan, Rules of Thumb for Chemical Engineers, Gulf Publishing Company, Houston Texas, ISBN 0-88415-162-X, 1994

77 J. E. Diehl, Calculate Condenser Pressure Drop, Petroleum Refiner, Vol. 36, No. 10, pp. 147-153, 1957

78 J. E. Diehl and C. H. Unruh, Two Phase Pressure Drop for Horizontal Crossflow Through Tube Banks, ASME Paper No. 58-HT-20, 1958

79 J. M. Chenoweth and M. W. Martin, Turbulent Two Phase Flow, Petroleum Refiner, Vol. 341, pp. 151-155, 1955

80 I. D. R. Grant and I. Murray, Pressure Drop on the Shell Side of a Segmentally Baffled Shell and Tube Heat Exchanger with Vertical Two Phase Flow, NEL Report No. 500, 1972

81 I. D. R. Grant and I. Murray, Pressure Drop on the Shell Side of a Segmentally Baffled Shell and Tube Heat Exchanger with Horizontal Two Phase Flow, NEL Report No. 560, 1974

82 I. D. R. Grant and D. Chisholm, Two Phase Flow on the Shell Side of a Segmentally Baffled Shell and Tube Heat Exchanger, ASME Paper No. 77-WA/HT-22, 1977

83 A. A. Nicol, Z. Aidoun and M. N. Musa, Condensation and Pressure Drop for Crossflow of Steam in Small Tube Banks, Proc. 7th Int. Heat Transfer Conf., Vol. 5, pp133-138, 1982

84 K. Ishihara, J. W. Palen and J. Taborek, Critical Review of Correlations for Predicting Two-Phase Flow Pressure Drop Across Tube Banks, Heat Transfer Engineering, Vol. 1, No. 3, pp23-32, 1980

85 E. E. Wilson, A Basis For Rational Design of Heat Transfer Apparatus, Trans ASME., Vol. 37, pp 47-70, 1915

86 D. E. Briggs and E. H. Young, Modified Wilson Plot Techniques for Obtaining Heat Transfer Correlations for Shell and Tube Heat Exchangers, Chemical Engineering Symposium Series, No. 92, Vol. 65, pp35-45, 1969

87 H. F. Khartabil, R. N. Christensen, and D. E. Richards, A Modified Wilson Plot Technique for Determining Heat Transfer Correlations, Proc. 2nd UK National Conf. on Heat Transfer, Vol. 2, pp1331-1357, 1988

88 R. K. Shah, Assessment of modified Wilson Plot Techniques for Obtaining Heat Exchanger Design Data, Proc. 9th Int. Heat Transfer Conf., Jerusalem, Vol. 5, pp51-56, 1990

89 E. N. Sieder and G. E. Tate, Heat Transfer and Pressure Drop of Liquids in Tubes, Industrial and Engineering Chemistry, Vol. 28, No. 12, pp1429-1434, 1936

90 A. Aoune, Experimental and Theoretical Studies of Condensation on a Horizontal tube Row with Vapour Shear, PhD Thesis, Heriot-Watt University, 1991

91 T. Fujii, Overlooked Factors and Unsolved Problems in Experimental Research on Condensation Heat Transfer, Experimental Thermal and Fluid Science, Vol. 5, No. 5, pp 652-663, 1992

92 V. Gnielinsky, New Equations for Heat and Mass Transfer in Turbulent Pipe Channel Flow, International Chemical Engineering, Vol. 16, No. 2, pp359-368, 1976

93 F. P. Incropera, D. P. DeWitt, Fundamentals of Heat and Mass Transfer, Third Edition, Wiley, New York, pp468-528, 1990

94 N. V. Suryanarayana, Engineering Heat Transfer, West Publishing Company, pp291-391, 1995

95 XPS Analysis results from Graham Beamson, Research Unit for Surfaces Transforms and Interfaces, Daresbury, 1999

APPENDIX A

APPENDIX A1 HEAT LOAD ESTIMATIONS

Area of one tube $-\frac{19.05}{1000}\times\pi\times 0.15 = 8.98\times 10^{-3}\,m^2$

$\Rightarrow$ Surface area of 75 tubes = 0.682 m^2

assume $\Delta T - 15$ K & $\alpha_{ov} = 8\ kW/m^2K$

then the heat adsorbed by the test cell ≈ 80 kW

The heat load to condense the maximum flow of steam

$m_s \times h_{fg} \approx 0.063\times 2400 = 150\,kW$

APPENDIX A2 WATER SIDE HEAT TRANSFER COEFFICIENTS

Estimation of an equivalent diameter

$$D_e = \frac{4 \times \text{FlowArea}}{\text{HeatTransferPerimeter}} = \frac{4 \times \frac{\pi}{4}\left(D_1^2 - D_2^2\right)}{\pi \times D_1}$$

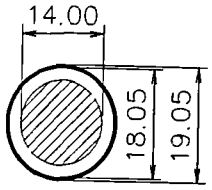

$$D_e = \frac{18.05^2 - 14^2}{18.05} = 7.2\text{mm}$$

$$\text{Nu} = \frac{\alpha D_e}{k} = 0.023\,\text{Re}^{0.8}\,\text{Pr}^{0.33}$$

$D = D_e = 0.0072$m, $k = 0.603$ W/mK, $Pr = 6.96$, $\rho = 998$ kg/m^3, $\mu = 0.001$ kg/ms

$$\therefore \alpha = 4446 \times U_{cw}^{0.8} \Rightarrow U_{cw} = \left(\frac{\alpha}{4446}\right)^{1.25} = \left(\frac{10000}{4446}\right)^{1.25} = 2.75\text{m/s}$$

$$\text{i.e. Re} = \frac{998 \times 2.75 \times 0.0072}{0.001} = 19760$$

Mass flow through annulus

$$m_{cw} = \rho U_{cw} A = 998 \times 2.75 \times \frac{\pi}{4}\left(0.01805^2 - 0.014^2\right) = 0.28\text{kg/s}$$

Total cell cooling water flow = m_{cw} x No. Tube rows = 0.28 x 15 = 4.2 kg/s

Cooling water temperature rise for a row at maximum heat load

$$\Delta T = \frac{q}{m_{cw} \times Cp} = \frac{80}{4.2 \times 4.183} = 4.55\ \text{K}$$

APPENDIX A3 CHOKING NOZZLE FLOW CALCULATIONS

Neglecting the water flow, assuming perfect gas conditions, the ratio of the specific heat capacities is 1.3 and a maximum upstream pressure 5 bar. With dry saturated steam at the inlet to the nozzle the temperature is 424.8 K (T_1) and the enthalpy is 2749 kJ/kg. At 0.05 bar the enthalpy of dry saturated steam is 2561 kJ/kg. Assuming no losses through the nozzle the steam would be superheated and require 0.077 kg of water per kg of steam to evaporate to desuperheat the steam to saturation conditions. This reduces the required steam flow through the nozzle by approximately 7%

The laws of gas dynamics state that for a choked flow, the critical pressure ratio can be predicted by

$$\frac{P_1}{P_2} = \left(\frac{\gamma+1}{2}\right)^{\gamma} = \left(\frac{1.3+1}{2}\right)^{1.3} = 1.83$$

P_2 5 bar therefore $P_1 = 2.732$ bar.

and the temperature ratio is

$$\frac{T_1}{T_2} = \frac{\gamma+1}{\gamma} = \frac{1.3+1}{2} = 1.15$$

$T_1 = 424.8$ K therefore $T_2 = 369.4$ K

also

$$Pv = mRT \qquad \rho = \frac{P}{mRT} = \frac{273}{0.4615 \times 369.4} = 1.6\,\text{kg/m}^3$$

the sonic velocity the fluid is

$$C = \sqrt{\gamma RT} = \sqrt{1.3 \times 461.5 \times 369.4} = 470\,\text{m/s}$$

APPENDIX A4 TUBE PLATE MANUFACTURING DRAWINGS

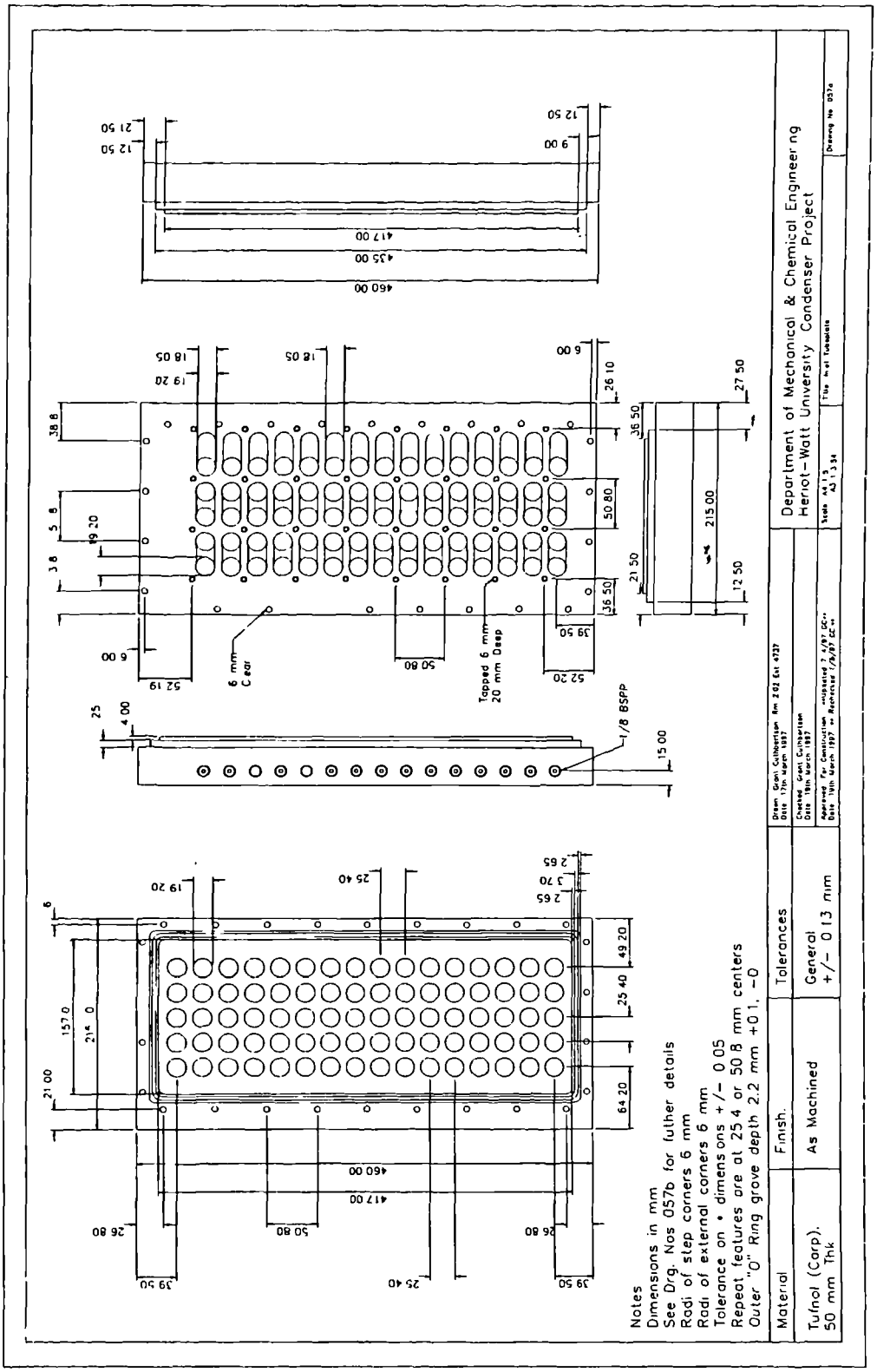

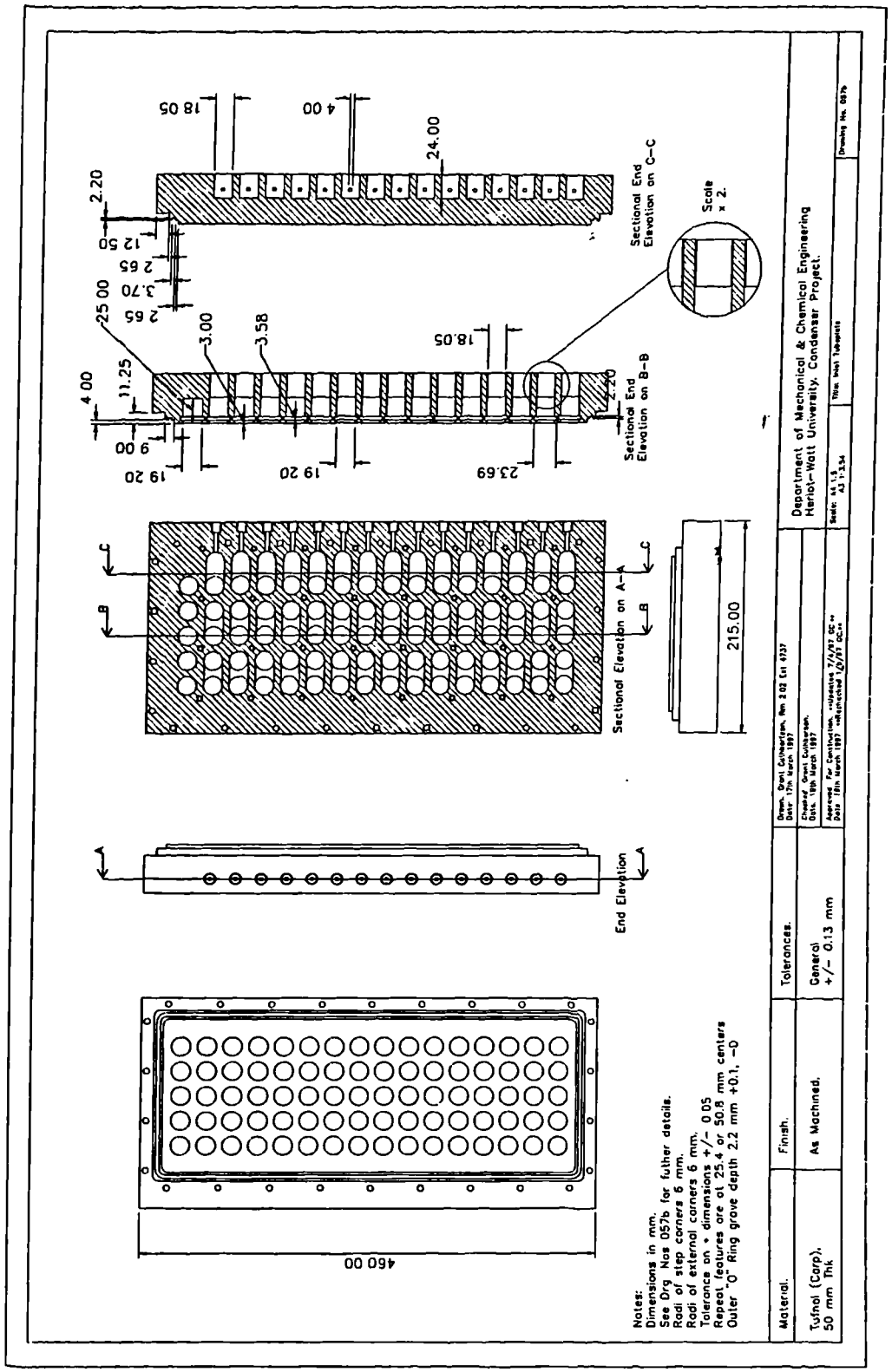
Department of Mechanical & Chemical Engineering
Heriot-Watt University. Condenser Project.
Material.
Tufnol (Carp).
50 mm Thk
Finish.
As Machined.
Tolerances.
General
+/- 0.13 mm
Notes:
Dimensions in mm.
See Drg Nos 057b for fulher details.
Radi of step corners 6 mm.
Radi of external corners 6 mm.
Tolerance on * dimensions +/- 0.05
Repeat features are at 25.4 or 50.8 mm centers
Outer "O" Ring grove depth 2.2 mm +0.1, -0
Sectional Elevation on A-A
Sectional End Elevation on B-B
Sectional End Elevation on C-C
End Elevation
Scale x 2.
215.00
460.00
24.00
18.05
4.00
2.20
12.50
2.65
3.70
25.00
3.00
3.58
11.25
9.00
19.20
23.69

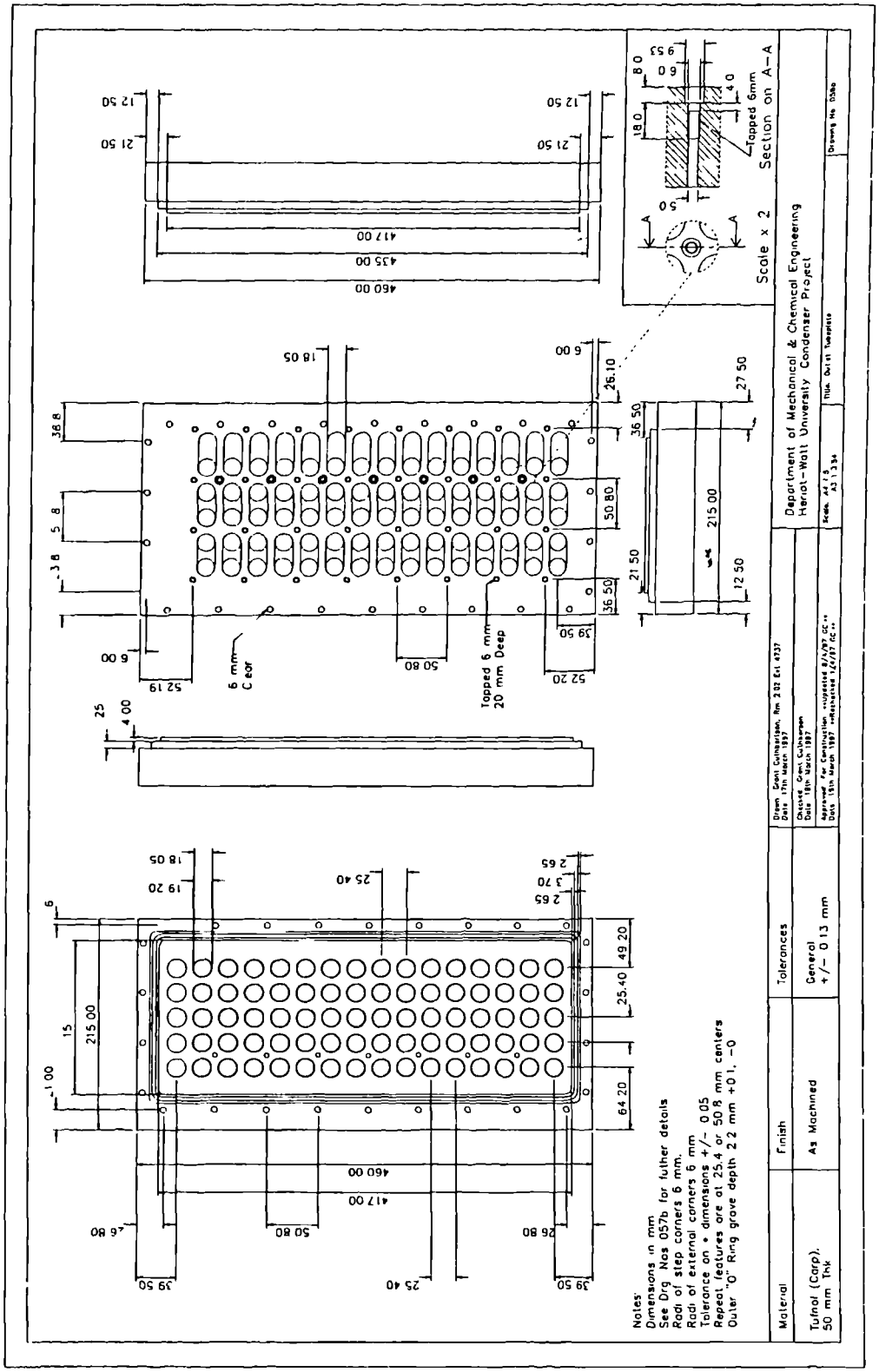
Department of Mechanical & Chemical Engineering
Heriot-Watt University Condenser Project
Scale x 2
Section on A-A
Tapped 6mm
Tapped 6 mm
20 mm Deep
6 mm
C'bor
Material
Tufnol (Carp).
50 mm Thk
Finish
As Machined
Tolerances
General
+/- 0.13 mm
Notes:
Dimensions in mm
See Drg Nos 057b for futher details
Radi of step corners 6 mm.
Radi of external corners 6 mm
Tolerance on * dimensions +/- 0.05
Repeat features are at 25.4 or 50.8 mm centers
Outer 'O' Ring grove depth 2.2 mm +0.1, -0

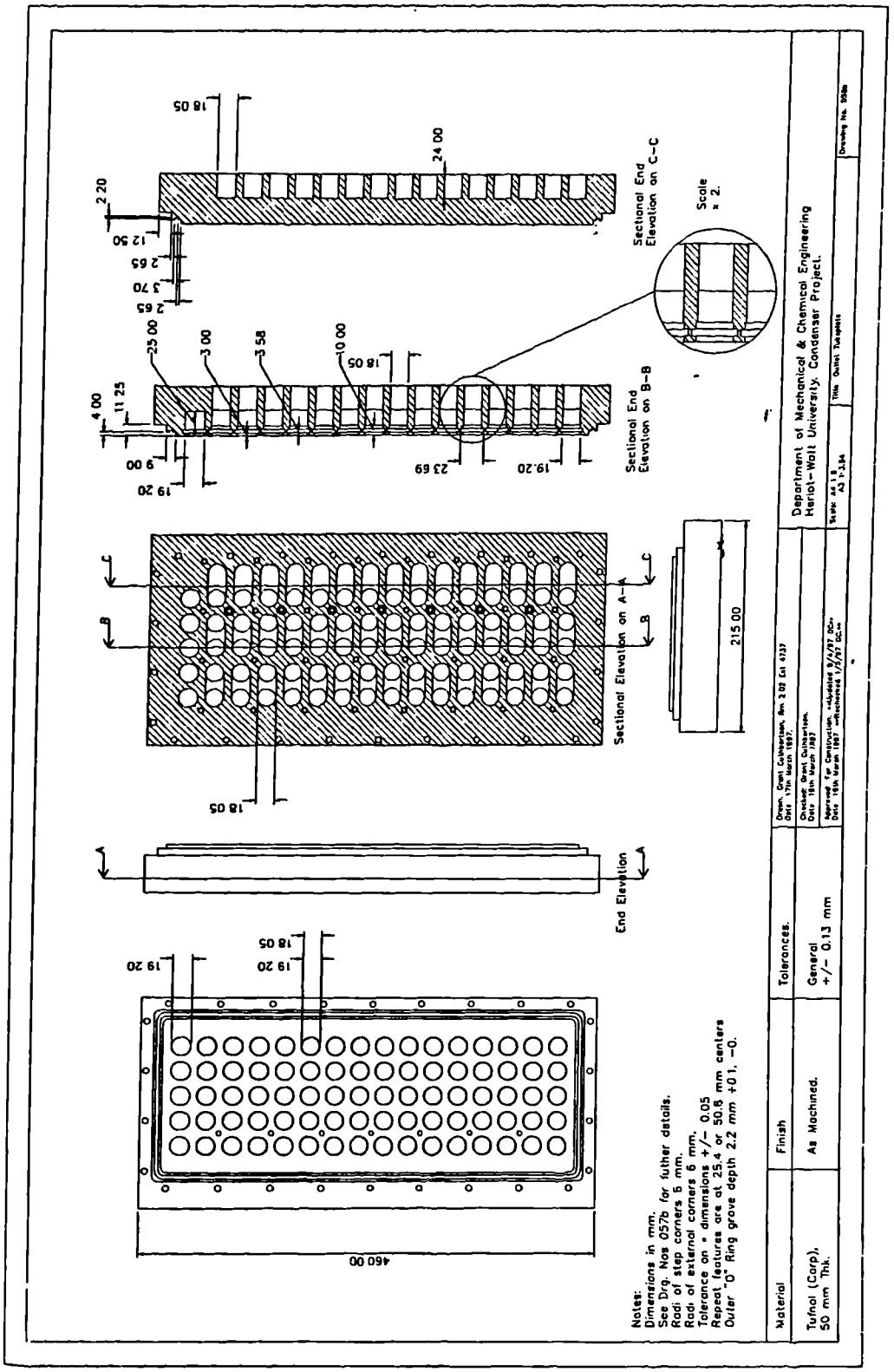
Sectional End Elevation on C-C
Scale x 2.
Sectional End Elevation on B-B
Sectional Elevation on A-A
End Elevation
215.00
460.00
Department of Mechanical & Chemical Engineering
Heriot-Watt University. Condenser Project.
Material
Tufnol (Carp), 50 mm Thk.
Finish
As Machined.
Tolerances.
General +/- 0.13 mm
Notes:
Dimensions in mm.
See Drg. Nos 057b for futher details.
Radi of step corners 5 mm.
Radi of external corners 6 mm.
Tolerance on * dimensions +/- 0.05
Repeat features are at 25.4 or 50.8 mm centers
Outer "O" Ring grove depth 2.2 mm +01, -0.

APPENDIX A5 INSTRUMENT CALIBRATIONS

APPENDIX A5.1 PLATINUM RESISTANCE THERMOMETERS

Four calibration batches were undertaken before satisfactory performance was obtained. Minor modifications were completed between each batch. Batch "D" was the final data set and this has been used to calculate the calibration constants. Calibration batches A, B and C produced inconsistent results which because of water adsorption into the probes. This difficulty was overcome by fitting a silicon sleeve over the PRT leads from the first junction box to the PRT probe, where it sealed onto the stainless steel sheath.

Calibration data was obtained using the complete data logging system and wiring in situ, except that the PRT probes were removed from their locations and placed in the calibration bath. Calibration data sets A, B & C were deleted.

The calibration bath could only accommodate twenty PRTs. As a result, each calibration batch contains three sets of data. Sets DA and DB were the original calibrations. Set DC is data for the steam outlet temperature PRT which was introduced to the rig after the other calibrations had been completed.

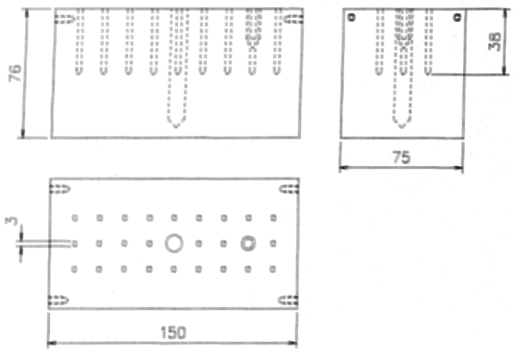

Figure A.1

The calibration equipment consisted of a 100mm x 100mm x 200mm aluminium block as shown in Figure A.1, with 20, 3mm diameter x 20mm deep holes and one 6mm x 30mm deep hole equally spaced on the top face. The PRTs were a close fit in the 3mm

holes. The 6mm hole was included to accept the standard thermometer. The block was completely immersed in the Techne RB-12A refrigerated bath with Techne TU-16D heater/stirrer. The temperature of the aluminium block in the bath was measured using a Tinsley type I platinum resistance thermometer, serial No. 218048, calibrated by the National Physical Laboratory. The ratio of its resistance to a Tinsley, type 3540B, 10 ohm grade S standard resistor, serial No. 188.129 was measured using an Automatic Systems Laboratory model F17 Resistance bridge as shown Figure A.2.

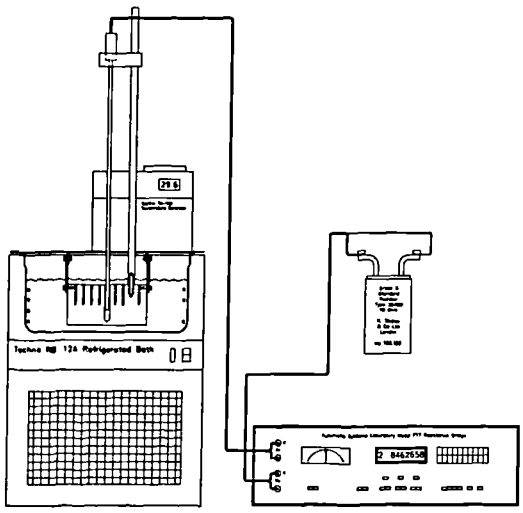

Figure A.2

The bridge measured the resistance ratio of the reference thermometer and the 10 ohm resistor R_T/R_S. The temperature was calculated from

$$T = 3337.311 - \frac{1}{2}\sqrt{6674.622^2 - 4\times(W-1)\times 1674154.4}$$

Here T is in ^{o}C, $W = \frac{R_T}{R_0} = \frac{R_T}{R_S}\times\frac{R_S}{R_0}$ and R_0 is the resistance of the reference thermometer at 0 ^{o}C = 25.2478 ohms.

The bath was initially filled with half water and half ice, the aluminium block was then completely submerged in the bath to a depth of approximately 10mm below the surface. Once the block was in position the agitating pump was started. The PRTs and the reference PRT were fitted into their appropriate locations. The system was allowed 30 minutes to stabilise. This was a generous period of time, since, after approximately 10 minutes there were no perceptible changes in the output from the resistance bridge.

The reading from the resistance bridge was entered into the computer and the calibration program was run. The program scanned the voltages on the channel numbers found in the channel list data file. The channel number followed by the voltage was then written to an output file, an example of this is included as Appendix A11. For each calibration temperature, the data logger looped through the channel list four times creating four sets of data in each calibration file.

The bath temperature was then increased. Less than five minutes was required for the bath to reach the new temperature. 15 minutes after setting the desired temperature a new value from the resistance bridge was input. The programme was run, the voltages scanned and written to file.

The data was processed using a spread sheet that calculated the average voltage of the four scans, the standard deviation for both the reference resistor and each PRT, the ratio of the PRT resistance and the standard resistor. R_T/R_S, was calculated over the temperature range.

A best fit line of the form $Ax^2 + Bx + C = T$ where x, the resistance ratio between the PRT and the standard ($x = R^T/R^S = V^T/V^S$) was calculated. Finally the calibration data was recalculated using the constants obtained and compared with the original data. The standard deviations for the calibration data were less than 0.05K, Appendix A12 shows a typical calibration data set complete with polynomial coefficients and errors. The

calibration constants obtained and used in all the experimental work can be found in Appendix A13.

In operation two voltages VS and VT were measured to obtain a value for x. The error in measuring these voltages was approximately ± 2 μV which, when worked through the equations with typical values, results in an error in the temperature measurement of approximately ± 0.005K. In practice if all the cooling water RTD's are subjected to the same cooling water flow, the standard deviation of the calculated temperatures were approximately 0.02K

APPENDIX A5.2 FLOW ROTAMETERS

The rotameters were calibrated as described in the manufactures handbook. This gave an accuracy of ± 2.5% at full flow. The procedure detailed the flow at various scale readings from which the calibration charts were generated. The values calculated are tabulated below

Size: 24. Float: Stainless steel. Fluid: Water @ 20^{O}C

Scale (cm)	0	3.4	6.6	9.7	13.8	15.5	18.3	21.9	23.3	25.7
Flow (l/min)	2.00	4.00	6.00	8.01	10.01	12.01	14.02	16.02	18.02	20.03

Size: 18x. Float: Duralumin. Fluid: Water @ 20^{O}C

Scale (cm)	1.7	5.5	9	12	15.1	17.8	20.5	23.1	25.6	28
Flow (l min)	0.22	0.44	0.66	0.88	1.10	1.33	1.55	1.77	1.99	2.21

Size: 14. Float: Stainless steel. Fluid: Water @ 20^{O}C

Scale (cm)	0	3.5	6.8	9.9	12.8	15.7	18.3	20.9	23.4	25.9
Flow (l min)	0.50	1.00	1.50	2.00	2.50	3.00	3.50	4.00	4.50	5.00

Size: 10. Float: Duralumin. Fluid: Air @ 1 Atm 20^{O}C

Scale (cm)	0.5	4.3	7.7	10.7	13.7	16.6	19.3	21.9	24.3	26.5
Flow (l min)	2.13	4.27	6.41	8.54	10.68	12.82	14.95	17.09	19.23	21.36

Size: 10. Float: Koranite. Fluid: Air @ 1 Atm 20^{O}C

Scale (cm)	0	3.8	7.9	10.1	13	16	18.6	21.3	23.8	26.1
Flow (l min)	3.41	6.83	10.24	13.66	17.07	20.49	23.90	27.32	30.73	34.15

Size: 7. Float: Stainless steel. Fluid: Water @ 20^{O}C

Scale (cm)	0	3.8	6.3	10.6	13.7	16.5	19.4	22.2	24.8	27.4
Flow (l/min)	0.10	0.20	0.30	0.40	0.50	0.60	0.70	0.80	0.90	1.00

APPENDIX A5.3 PRESSURE TRANSMITTERS

The pressure transmitters were calibrated by the manufacturer to a accuracy of ± 0.25% of the calibrated span. This equates to ± 4.5 mbar for the absolute transmitter and ± 0.2 mbar for the differential units. The full specification of these units is detailed below.

Absolute pressure unit

Wetted materials	316L Stainless steel
Range	0-750 inH_2O (1868.8 mbar)
Output	4-20 mA
Accuracy	± 0.25% of calibrated span
Stability	± 0.25% of upper range limit for six months
Temperature effect	Zero ± 0.2% of upper range limit per 100 ^{O}F
	Span ± 0.2% + 0.18% of upper range limit per 100 ^{O}F
Power supply effect	Less than 0.05% of output span per volt
Load effect	None

Differential pressure units

Wetted materials	316L Stainless steel
Range	0-30 inH_2O (74.75 mbar)
Output	4-20 mA
Accuracy	± 0.1% of calibrated span
Stability	± 0.1% of upper range limit for six months
Temperature effect	Zero ± 0.2% of upper range limit per 100 ^{O}F
	Span ± 0.2% + 0.18% of upper range limit per 100 ^{O}F
Power supply effect	Less than 0.05% of output span per volt
Load effect	None.

APPENDIX A6 SOFTWARE CONFIGURATION

Configuring a to/from object to control a 1326B multimeter.

Working in HP VEE select I/O from the main menu. Click on Instrument Manager and choose Add if not 1326 instrument exists or Edit if 1326 instrument already exists. The voltmeter configuration is as follows:

Name	Datalog
Interface	HP-IB
Address	70903

Enter advanced I/O configuration

General	Timeout(sec)	5
	Live mode	ON
	Byte ordering	MSB
	Description	hpe1326
Direct I O	Not applicable, use defaults	
Plug & Play Driver	Plug & play driver name	HPE1326 *
	Address	GPIBO::9::3::INSTR
	Perform ID query	Yes
	Perform reset	Yes
Panel driver	Not applicable, use defaults	

* Driver must be installed from drivers CD following Hewlett Packard instructions to the directory C:\VXIPNP\WINNT\HPE1326\

APPENDIX A7 COMPUTER SCREEN PRINTS

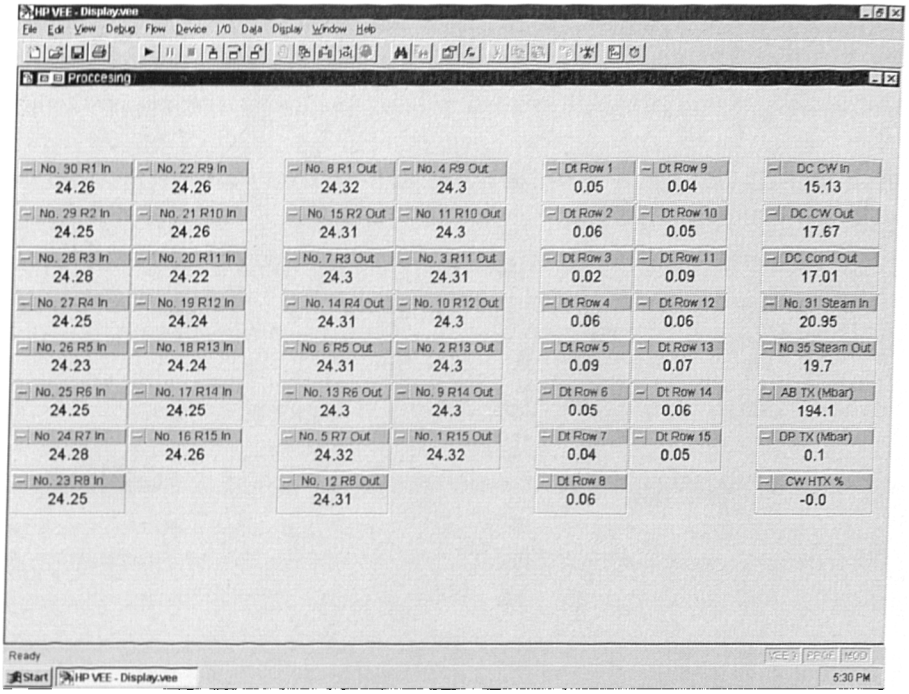

Screen 1, The display program.

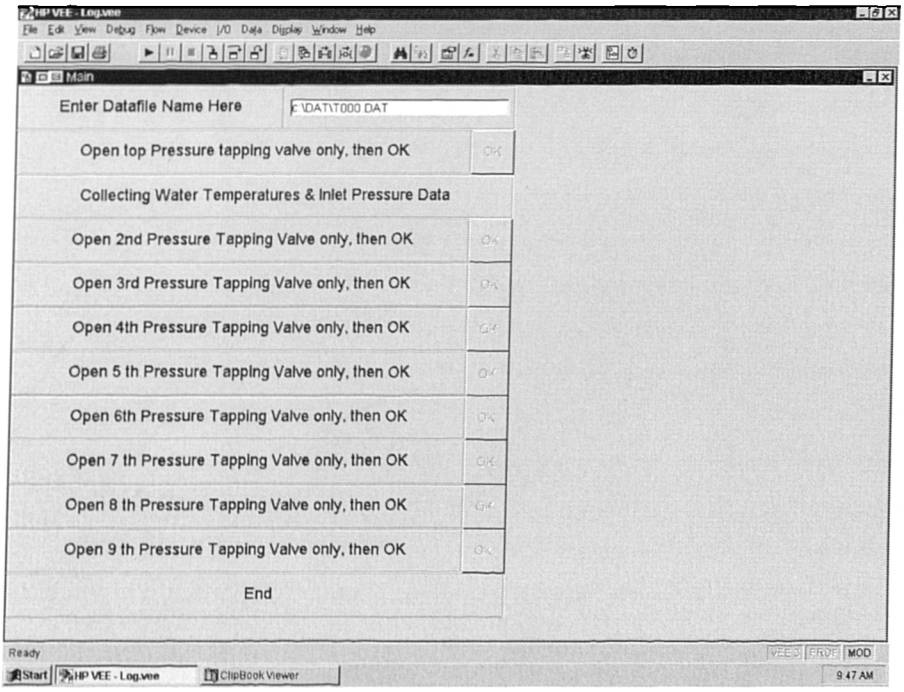

Screen 2, Data logging program.

APPENDIX A8 SAMPLE DATA FILE (T041)

Channel number	Typical value (volts)	Channel description
100	1.0027084351	Differential pressure transmitter
101	1.1074218750	Absolute pressure transmitter
102	2.2316131592	Plate HTX cooling water flow
103	0.0000030994	Redundant
104	0.2072534561	100 ohm reference resistor
105	0.2193470001	RTD 32, Dump condenser cooling water out
106	0.2179698944	RTD 33, Dump condenser cooling water in
107	0.2198429108	RTD 34, Dump condenser condensate out
108	-0.0000026226	Spare
109	-0.1632919312	Spare
110	-0.1878910065	Spare
111	-0.2053480148	Spare
112	-0.2022943497	Spare
113	-0.1973419189	Spare
114	-0.1896343231	Spare
115	-0.1844043732	Spare
200	0.2218065262	RTD 16, row 15 cooling water inlet
201	0.2217178345	RTD 17, row 14 cooling water inlet
202	0.2217540741	RTD 18, row 13 cooling water inlet
203	0.2216567993	RTD 19, row 12 cooling water inlet
204	0.2216959000	RTD 20, row 11 cooling water inlet
205	0.2216434479	RTD 21, row 10 cooling water inlet
206	0.2216329575	RTD 22, row 9 cooling water inlet
207	0.2218351364	RTD 23, row 8 cooling water inlet
208	0.2215518951	RTD 24, row 7 cooling water inlet
209	0.2218179703	RTD 25, row 6 cooling water inlet
210	0.2216968536	RTD 26, row 5 cooling water inlet
211	0.2216672897	RTD 27, row 4 cooling water inlet
212	0.2216472626	RTD 28, row 3 cooling water inlet
213	0.2216663361	RTD 29, row 2 cooling water inlet
214	0.2216959000	RTD 30, row 1 cooling water inlet
215	0.2340211868	RTD 31, Steam temp in
300	0.2231836319	RTD 1, row 15 cooling water outlet
301	0.2232913971	RTD 2, row 13 cooling water outlet
302	0.2234191895	RTD 3, row 11 cooling water outlet
303	0.2235078812	RTD 4, row 9 cooling water outlet
304	0.2236509323	RTD 5, row 7 cooling water outlet
305	0.2238521576	RTD 6, row 5 cooling water outlet
306	0.2242822647	RTD 7, row 3 cooling water outlet
307	0.2243413925	RTD 8, row 1 cooling water outlet
308	0.2233638763	RTD 9, row 14 cooling water outlet
309	0.2233800888	RTD 10, row 12 cooling water outlet
310	0.2234764099	RTD 11, row 10 cooling water outlet
311	0.2235927582	RTD 12, row 8 cooling water outlet
312	0.2237358093	RTD 13, row 6 cooling water outlet
313	0.2240247726	RTD 14, row 4 cooling water outlet

314	0.2242231369	RTD 15, row 2 cooling water outlet
315	0.2292337418	RTD 35, Steam temp out
400	-0.0000076294	Redundant
401	0.0000072718	Redundant
402	-0.0000065565	Redundant
403	0.0000015497	Redundant
404	0.0000057220	Redundant
405	-0.0000126362	Redundant
406	0.0000009537	Redundant
407	0.0000059605	Redundant
408	-0.0000050068	Redundant
409	-0.0000045300	Redundant
410	0.0000050068	Redundant
411	0.0000020266	Redundant
412	0.0000003576	Redundant
413	-0.0000011921	Redundant
414	-0.0000042915	Redundant
415	0.0000007153	Redundant
100	1.2410812378	Differential pressure transmitter
101	1.0957260132	Absolute pressure transmitter
100	1.3561630249	Differential pressure transmitter
101	1.0922927856	Absolute pressure transmitter
100	1.4780349731	Differential pressure transmitter
101	1.0889129639	Absolute pressure transmitter
100	1.4818496704	Differential pressure transmitter
101	1.0865859985	Absolute pressure transmitter
100	1.5789947510	Differential pressure transmitter
101	1.0818557739	Absolute pressure transmitter
100	1.6555633545	Differential pressure transmitter
101	1.0801086426	Absolute pressure transmitter
100	1.7122802734	Differential pressure transmitter
101	1.0790786743	Absolute pressure transmitter
100	1.7682418823	Differential pressure transmitter
101	1.0787506104	Absolute pressure transmitter

APPENDIX A9 BUILD INFORMATION

Build No.	Tests Conducted	Tubes	Configuration	36hr Pressure rise
1	T041-T150	Untreated	Inline	6mbar
2	T151-T271	Untreated	Inline	9mbar
3	T272-T280	Plasma Polymer	Inline	27mbar
4	T281-T316	Plasma Polymer	Inline	22mbar

APPENDIX A10 MANUAL RECORD SHEET

Date: Filmwise ☐ Dropwise ☐

Time: Inline ☐ Staggered ☐

Raw Data File Name: **Laboratory Temperature** ^{o}C

Processed Data File Name: **Heat Balance Error** %

Variable	Value	Units	Conversion	Units
Row CW Flow (24) [SS]		Cm		L/min
Number of Condensing Rows		Rows		
Nozzle Upstream Pressure		Bar		
Fitted Nozzle Diameter		mm		
Spray Water Pressure		Bar		
Air Flow (10) [Du] or [Ko]		cm	-	L/min
Vacuum Gauge		Bar		
Separator Outflow (10) [SS]		Cm		L/min
Dump Condenser CW Flow		Gal/min		
Condensate Out (14x) [SS]		Cm		L/min
Condensate Out (18x) [Du]		Cm		L/min
Total Condensate Out				L/min
Atmospheric Pressure		mm/Hg		
Plate HTX CW Flow		%		
Inlet Pressure		Mbar		
Cell Inlet CW Temperature		Deg. C.		
Dump Condenser Valve		Open		
Dump Condenser Valve bypass		Open		

Remarks

APPENDIX A11 SAMPLE RTD CALIBRATION DATA FILE

START
Rt/Rs – 2.5248
CAL TEMP_= 0.0019868973
CAL_DATA
104 0.2195472717
200 0.2197647095
201 0.219669342
202 0.21971035
203 0.219587326
204 0.2196865082
205 0.2196044922
206 0.2195882797
207 0.2198009491
208 0.2194871902
209 0.2197465897
210 0.2196474075
211 0.2195892334
212 0.2196063995
213 0.2195682526
214 0.2196445465
215 0.2197561264
30th_March 98
END
START
Rt/Rs_ 2.5248
CAL_TEMP_– 0.0019868973
CAL DATA
104 0.219543457
200 0.2197647095
201 0.2196712494
202 0.2197093964
203 0.219587326
204 0.2196903229
205 0.2196083069
206 0.2195892334
207 0.2198038101
208 0.2194862366
209 0.219748497
210 0.2196493149
211 0.2195892334
212 0.2196063995
213 0.2195692062
214 0.2196455002
215 0.2197599411
30th_March_98
END

START
Rt/Rs_= 2.5248
CAL_TEMP_= 0.0019868973
CAL_DATA
104 0.2195425034
200 0.2197666168
201 0.2196722031
202 0.2197093964
203 0.2195892334
204 0.2196903229
205 0.2196102142
206 0.2195911407
207 0.2198038101
208 0.2194881439
209 0.219748497
210 0.2196502686
211 0.2195901871
212 0.2196092606
213 0.2195711136
214 0.2196474075
215 0.2197599411
30th_March_98
END
START
Rt/Rs_= 2.5248
CAL_TEMP_= 0.0019868973
CAL_DATA
104 0.2195444107
200 0.2197666168
201 0.2196741104
202 0.21971035
203 0.2195863724
204 0.2196893692
205 0.2196083069
206 0.2195920944
207 0.2198038101
208 0.2194862366
209 0.2197475433
210 0.2196464539
211 0.2195892334
212 0.2196083069
213 0.2195711136
214 0.2196464539
215 0.2197589874
30th_March_98
END

Channel 200, RTD 16.

Reference Rt/Rs	2.5248	2.623275	2.723882	2.823104	2.922975	3.022541	3.120667	3.416152
Calibration temperature	0.0019	9.7993	19.8387	29.7697	39.7958	49.8218	59.7328	89.7603
Calibration data								
First scan Ch. 104	0.21954727	0.21598243	0.21244049	0.20911693	0.20582008	0.20255088	0.19954586	0.19081592
First scan Ch. 200	0.21976471	0.22445201	0.22906398	0.23351573	0.23781585	0.24186706	0.24587535	0.25699806
Second scan Ch. 104	0.21954345	0.21598053	0.21243858	0.20910739	0.20582675	0.20255184	0.19953537	0.19080829
Second scan Ch. 200	0.21976471	0.22444915	0.22906112	0.23351478	0.23781299	0.24186515	0.24587249	0.25699615
Third scan Ch. 104	0.21954250	0.2159729	0.21244144	0.20911693	0.20580959	0.20254707	0.19953727	0.19080925
Third scan Ch. 200	0.21976661	0.22444725	0.22905921	0.23351573	0.23781108	0.24186515	0.24587249	0.25699710
Forth scan Ch. 104	0.21954441	0.21597385	0.21244430	0.20912265	0.20581817	0.20254516	0.19954490	0.19080925
Forth scan Ch. 200	0.21976661	0.22444629	0.22906112	0.23351955	0.23781108	0.24186420	0.24587631	0.25699424
104 Average	0.21954441	0.2159774	0.21244120	0.20911598	0.20581865	0.20254874	0.19954085	0.19081068
200 Average	0.21976566	0.22444868	0.22906136	0.23351645	0.23781275	0.24186539	0.24587416	0.25699639
104 Standard deviation	0.0000021	0.0000048	0.0000024	0.0000063	0.0000071	0.0000032	0.0000053	0.0000035
200 Standard deviation	0.0000011	0.0000025	0.0000020	0.0000021	0.0000023	0.0000012	0.0000020	0.0000016
Calibration Rt/Rs	1.00100778	1.039222851	1.078234159	1.116683921	1.155448031	1.194109594	1.232199633	1.346865871
Calibration temp.	0.0019	9.7993	19.8387	29.7697	39.7958	49.8218	59.7328	89.7603
Polynomial coefficients		$X^2 = 9.8075$		X = 236.4904		C = -246.5542		
Temp by polynomial	0.0018	9.8039	19.8399	29.7606	39.7917	49.8257	59.7400	89.7579
Error by polynomial	0.0001	-0.0046	-0.0011	0.0091	0.0041	-0.0038	-0.0072	0.0023
Standard deviation	0.004917							

APPENDIX A13 CALIBRATION CONSTANTS

Ch. No.	Inst. Type	A	B	C
100	1	0.00000	18.68805	-18.68805
101	1	0.00000	467.2013	-467.2013
102	1	0.00000	18.68805	-18.68805
103	2	0.00000	0.000000	0.000000
104	2	0.00000	0.000000	0.000000
105	3	9.08870	239.0731	-248.2770
106	3	10.1241	236.6127	-246.5912
107	3	9.80740	236.7085	-246.6098
200	3	9.8075	236.4904	-246.5542
201	3	10.2688	235.7008	-246.1123
202	3	9.3496	237.6047	-247.1419
203	3	10.6571	234.8386	-245.5394
204	3	8.7514	240.1667	-249.0884
205	3	10.2606	235.9720	-246.3054
206	3	10.7271	234.8384	-245.6160
207	3	9.6569	237.2265	-247.1831
208	3	10.0266	236.4047	-246.3643
209	3	9.7277	236.5276	-246.4931
210	3	9.4526	237.8967	-247.4655
211	3	9.8885	236.3416	-246.2785
212	3	10.1746	236.3090	-246.5565
213	3	10.041	236.0034	-246.0703
214	3	9.7922	237.4012	-247.3113
215	3	11.2303	233.2925	-244.7683
300	3	10.5648	234.8554	-245.3982
301	3	10.0751	236.2506	-246.3656
302	3	9.6587	236.8050	-246.5038
303	3	10.1251	236.1111	-246.2808
304	3	9.8587	236.9442	-246.8520
305	3	9.0234	238.6441	-247.7224
306	3	10.0068	235.7899	-246.0698
307	3	10.6281	234.3304	-244.9257
308	3	8.8232	238.9316	-247.9107
309	3	10.5977	234.8290	-245.4836
310	3	9.6843	237.1970	-246.9779
311	3	9.9647	236.4263	-246.4493
312	3	10.3849	235.1874	-245.5962
313	3	10.2502	235.4059	-245.7424
314	3	9.2747	238.2008	-247.5701
315	3	11.5549	232.5610	-244.0123

Inst. Type:- 1 = pressure transmitter, 2 = reference resistor, 3 = resistance thermometer

APPENDIX B

APPENDIX B1 TYPICAL PROCESSED OUTPUT FILE

Input Data File Name C: DAT T270.DAT Page 1 of 2
Input information: Mode 1 Configuration 1 Number of coo_ed ro.s-15
R w CW 17.07 l/min Dump condenser CW 48.0 Gal/min Air in .0 l r.n
T tal c ndensate outflow 4.00 l/min Separator out flow .9? l rin

**********Experimental data**********

IR W	CWIN DegC	CWOUT DegC	Ts/DTcw DegC	ABTX mbar	DPTX mbar	CHECK mbar
1	.00	.00	46.50	103.49	.05	103.44
2	3 .88	34.84	3.96	.00	.00	.00
3	3 .85	34.68	3.84	96.15	7.24	96.25
4	3 .87	34.45	3.59	.00	.00	.00
5	3 .85	34.28	3.43	92.32	10.95	92.54
6	3 .84	34.12	3.28	.00	.00	.00
	3 .84	33.95	3.1	89.00	14.41	89.09
8	3 .85	33.87	3. 2	.00	.00	.00
9	3 .83	33.73	2.9	85.47	17.63	85.86
1	3 .83	33.63	2.8	.00	.00	.00
11	3 .83	33.52	2.69	82.18	20.73	82.76
12	3 .81	33.45	2.64	.00	.00	.00
13	3 .8	33.32	2.53	80.08	22.71	80.78
14	3 .79	33.24	2.4	.00	.00	.00
1	3 .79	33.19	2.4	77.66	25.34	78.15
16	3 . 9	33. 6	2.27	.00	.00	.00
1	.	.	4 .3	74.98	27.67	75.82

****

Dump c ndenser c ling water inlet=11.44 DegC, outlet=16.44 DegC
Dump c ndenser c ndensate ut 18.79 DegC.
Heat ads rbed: Cell 53.1kW Dump condenser = 76.1kW Total=129.2kW
The retical heat l ad 126.5kW Heat balance error = -2.1%
Pre sure c rrecti n .
C ling water vel city thr ugh tube annulus = 2.79 m/s

**********Further calculations**********

IR W	Pm mbar	Ps mbar	Ts DegC	q kW m2	Dt DegC	hov kW m2K	MFS Kg/min	Um m/s	AIR %	MFW Kg/min
1 1	3.49 1	3.49	46.48	.0	.0	.000	3.03	31.4	.0	.00
2	96.97	96.97	45.21	104.2	12.2	8.514	3.03	33.4	.0	.00
3	95.42	95.42	44.89	101.0	12.0	8.396	2.91	32.6	.0	.12
4	93.87	93.87	44.57	94.4	11.8	7.984	2.80	31.8	.0	.23
5	92.32	92.32	44.25	90.4	11.6	7.789	2.69	31.1	.0	.34
6	9 .77	9 .77	43.93	86.4	11.4	7.602	2.59	30.4	.0	.44
7	89.22	89.22	43.59	81.8	11.1	7.349	2.50	29.7	.0	.53
8	87.67	87.67	43.26	79.6	10.8	7.349	2.40	29.1	.0	.63
9	86.12	86.12	42.91	76.3	10.6	7.223	2.32	28.5	.0	.71
1	84.57	84.57	42.57	73.8	10.3	7.188	2.23	27.9	.0	.80
11	83.02	83.02	42.21	70.8	10.0	7.092	2.15	27.4	.0	.88
12	81.47	81.47	41.85	69.5	9.7	7.191	2.07	26.9	.0	.96
13	79.92	79.92	41.49	66.5	9.4	7.096	1.99	26.3	.0	1.04
14	78.37	78.37	41.12	64.5	9.0	7.134	1.92	25.8	.0	1.11
15	76.82	76.82	40.74	63.2	8.7	7.265	1.85	25.3	.0	1.18
16	75.27	75.27	40.36	59.8	8.4	7.134	1.78	24.9	.0	1.25
17	73.72	73.72	39.97	.0	.0	.000	1.71	24.4	.0	1.32

****

**********Experimental data analysis**********

IROW	hcw	htw	hss	Cw-Iw	Iw-Ow	Ow-B	Error Analysis(+/- %)			
	kW/m2K	kW/m2K	kW/m2K	DegC	DegC	DegC	q	Dts	hov	hs
2	15.52	32.01	54.86	7.09	3.26	1.90	4.3	32.6	5.2	36.5
3	15.51	32.01	50.50	6.87	3.15	2.00	4.4	30.6	5.2	34.4
4	15.49	32.01	38.64	6.43	2.95	2.44	4.5	24.4	5.3	28.4
5	15.47	32.01	34.54	6.17	2.82	2.62	4.6	22.3	5.4	26.4
6	15.46	32.01	31.20	5.90	2.70	2.77	4.7	20.6	5.5	24.8
7	15.45	32.01	27.38	5.59	2.55	2.99	4.8	18.6	5.7	22.9
8	15.44	32.01	27.41	5.44	2.48	2.90	4.8	18.9	5.7	23.1
9	15.43	32.01	25.77	5.22	2.38	2.96	4.9	18.1	5.8	22.5
10	15.42	32.01	25.35	5.05	2.31	2.91	5.0	18.1	5.9	22.5
11	15.41	32.01	24.22	4.85	2.21	2.92	5.1	17.7	6.1	22.2
12	15.40	32.01	25.43	4.76	2.17	2.73	5.1	18.7	6.1	23.2
13	15.39	32.01	24.32	4.56	2.08	2.74	5.2	18.4	6.3	22.9
14	15.39	32.01	24.79	4.43	2.02	2.60	5.3	19.0	6.4	23.5
15	15.38	32.01	26.46	4.34	1.97	2.39	5.3	20.5	6.5	25.0
16	15.37	32.01	24.83	4.11	1.87	2.41	5.5	19.8	6.7	24.4

**********Heat transfer & inundation predictions**********

IROW	hn	hr	hsg	hfu	Ike	Ifk	Igo	hair	Nu/	Fd
	kW/m2K	kW/m2K	kW/m2K	kW/m2K	-	-	-	kW/m2K	Re0.5	-
2	16.55	32.45	32.01	40.68	1.00	1.00	1.00	.00	1.611	.20
3	16.31	31.94	31.50	39.63	.89	.95	.84	.00	1.508	.20
4	15.45	31.15	30.77	37.55	.83	.92	.76	.00	1.176	.18
5	15.15	30.63	30.26	36.52	.79	.90	.71	.00	1.068	.17
6	14.91	30.14	29.78	35.61	.76	.89	.67	.00	.980	.17
7	14.59	29.63	29.28	34.63	.74	.87	.64	.00	.874	.17
8	14.67	29.32	28.95	34.30	.72	.86	.62	.00	.887	.18
9	14.56	28.93	28.56	33.69	.71	.85	.60	.00	.847	.19
10	14.59	28.62	28.23	33.30	.69	.85	.58	.00	.845	.20
11	14.55	28.27	27.87	32.81	.68	.84	.57	.00	.818	.21
12	14.78	28.07	27.64	32.73	.67	.83	.56	.00	.870	.24
13	14.74	27.74	27.30	32.25	.66	.83	.54	.00	.844	.25
14	14.90	27.52	27.06	32.08	.65	.82	.53	.00	.871	.27
15	15.20	27.38	26.89	32.13	.64	.82	.52	.00	.941	.31
16	15.13	27.05	26.56	31.62	.64	.81	.52	.00	.896	.32

********Other information**********Pressure drop predictions******

IROW	ReCw	PrCw	Vm	ReS	DPTX Curve	HEDH	DPTX Curve	G+C
	-	-	m3/kg	Amax	Cd	Cd	Mbar	TPM	TPM	Mbar
1	.0	.0	14.21	4005.3	.16	.28	103.5	1.109	1.539	103.5
2	26569.6	5.1	15.10	4020.4	.16	.07	99.2	1.109	.679	99.2
3	26518.5	5.1	15.34	3868.6	.09	.07	97.1	.800	.670	97.0
4	26461.9	5.1	15.57	3721.5	.09	.08	95.1	.800	.661	94.9
5	26410.3	5.1	15.82	3584.1	.10	.08	93.2	.724	.652	92.9
6	26367.6	5.1	16.07	3452.7	.10	.09	91.5	.724	.643	91.0
7	26320.1	5.1	16.34	3327.3	.10	.09	89.8	.655	.634	89.2
8	26302.7	5.1	16.61	3208.7	.10	.10	88.2	.655	.624	87.5
9	26261.1	5.1	16.89	3093.4	.11	.11	86.7	.609	.615	85.9
10	26234.4	5.1	17.18	2982.8	.11	.11	85.3	.609	.605	84.3
11	26203.4	5.1	17.48	2876.0	.08	.12	83.9	.374	.595	82.8
12	26179.3	5.1	17.79	2773.8	.08	.12	82.6	.374	.585	81.4
13	26141.2	5.2	18.12	2673.4	.12	.13	81.4	.482	.575	80.0
14	26119.5	5.2	18.46	2577.4	.12	.14	80.2	.482	.565	78.7
15	26104.0	5.2	18.81	2484.4	.11	.15	79.1	.411	.555	77.5
16	26069.3	5.2	19.17	2393.3	.11	.16	78.1	.411	.545	76.3

********** GC 1999

APPENDIX B2 PROGRAM FLOW CHART

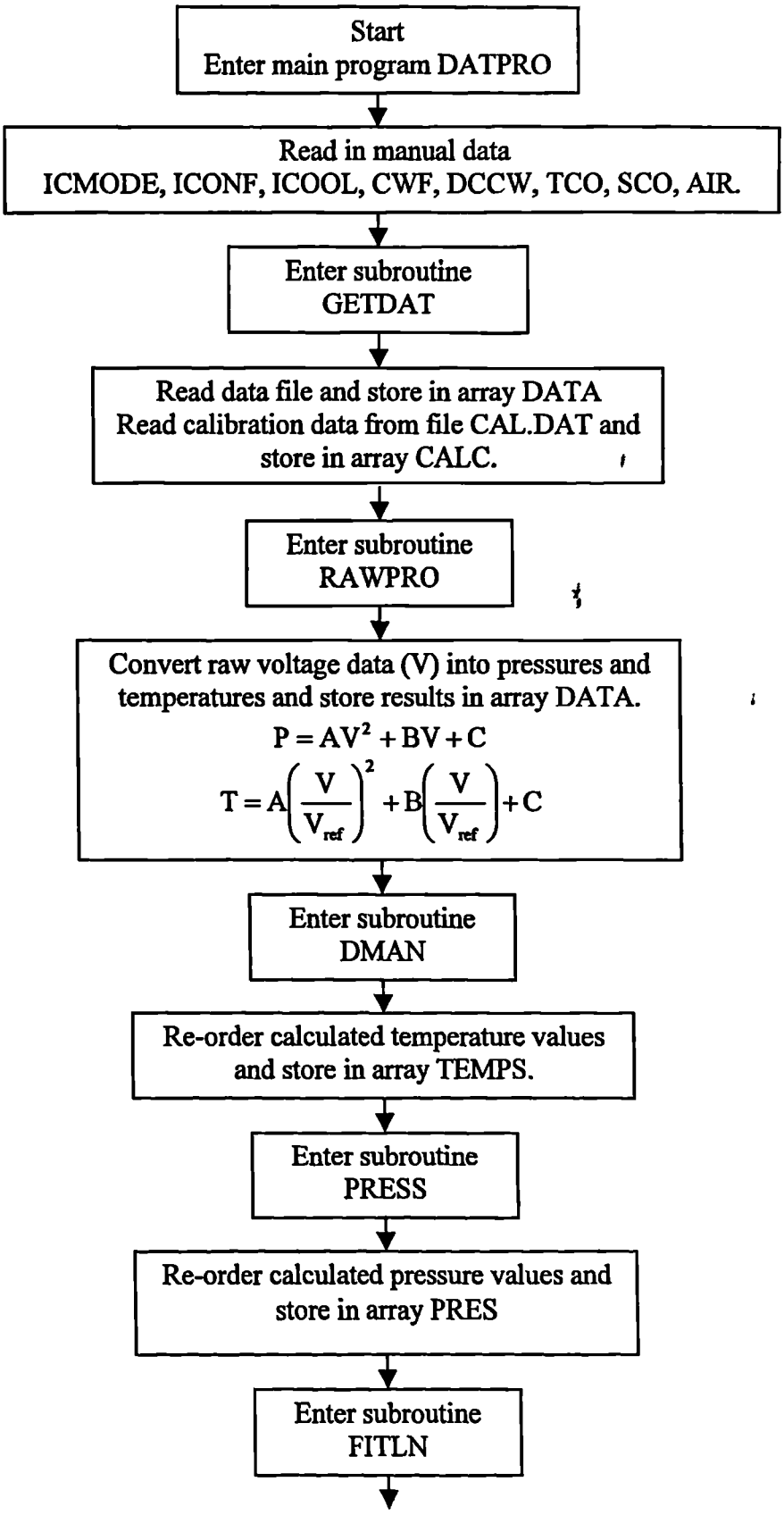

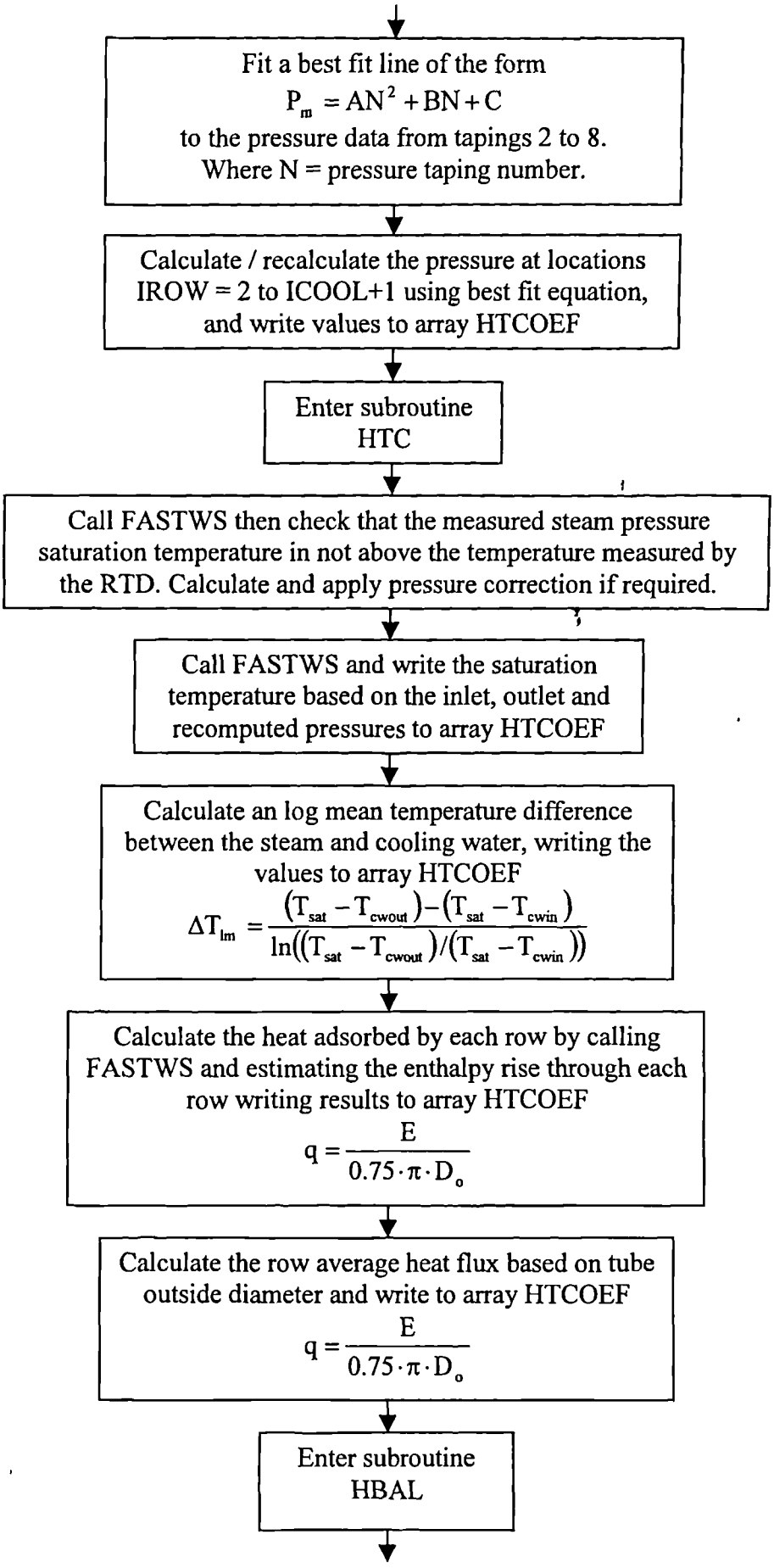
Fit a best fit line of the form
$P_m = AN^2 + BN + C$
to the pressure data from tapings 2 to 8.
Where N = pressure taping number.
Calculate / recalculate the pressure at locations IROW = 2 to ICOOL+1 using best fit equation, and write values to array HTCOEF
Enter subroutine HTC
Call FASTWS then check that the measured steam pressure saturation temperature in not above the temperature measured by the RTD. Calculate and apply pressure correction if required.
Call FASTWS and write the saturation temperature based on the inlet, outlet and recomputed pressures to array HTCOEF
Calculate an log mean temperature difference between the steam and cooling water, writing the values to array HTCOEF
$\Delta T_{lm} = \frac{(T_{sat} - T_{cwout}) - (T_{sat} - T_{cwin})}{\ln((T_{sat} - T_{cwout})/(T_{sat} - T_{cwin}))}$
Calculate the heat adsorbed by each row by calling FASTWS and estimating the enthalpy rise through each row writing results to array HTCOEF
$q = \frac{E}{0.75 \cdot \pi \cdot D_o}$
Calculate the row average heat flux based on tube outside diameter and write to array HTCOEF
$q = \frac{E}{0.75 \cdot \pi \cdot D_o}$
Enter subroutine HBAL

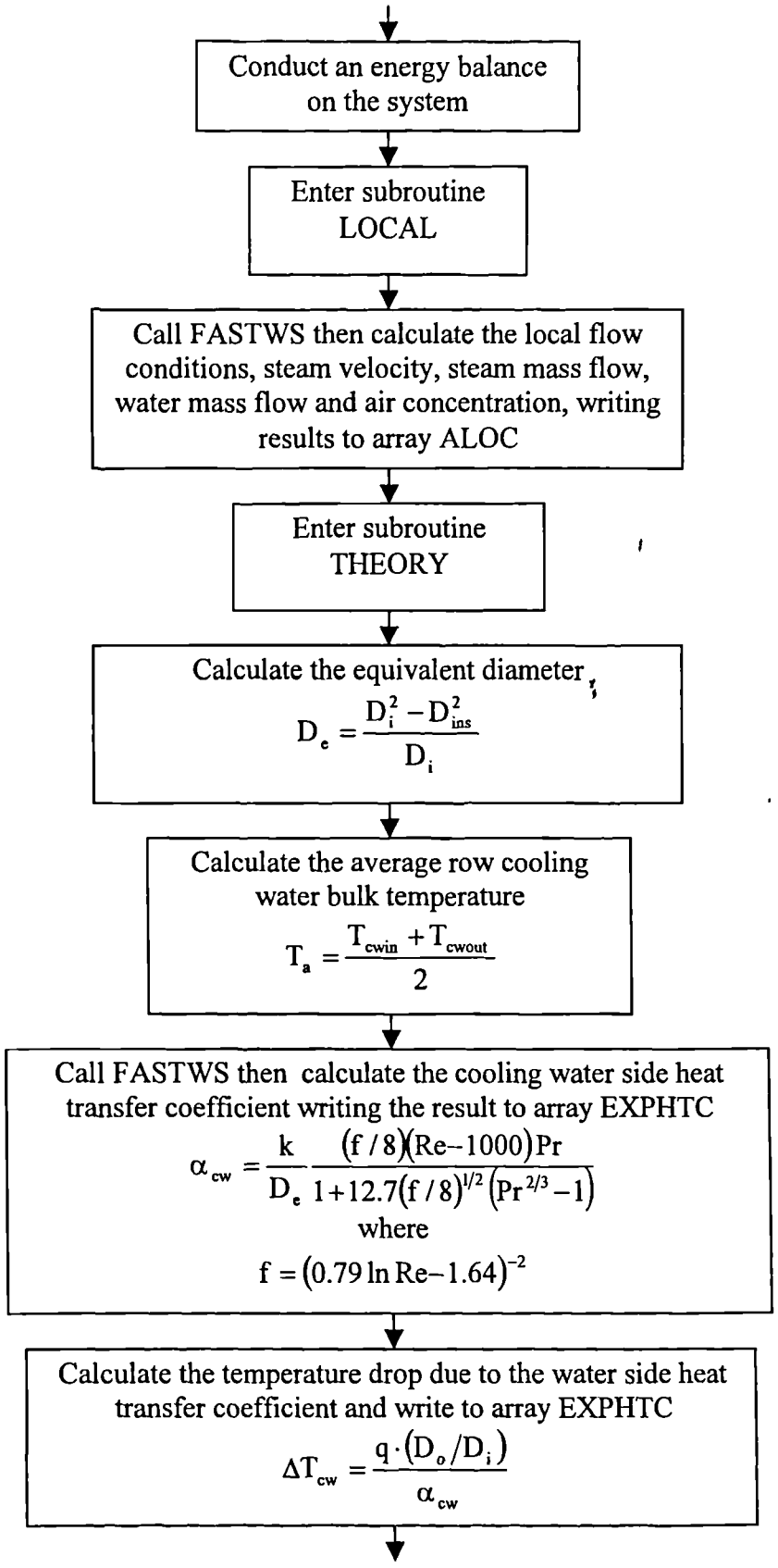
Conduct an energy balance on the system
Enter subroutine LOCAL
Call FASTWS then calculate the local flow conditions, steam velocity, steam mass flow, water mass flow and air concentration, writing results to array ALOC
Enter subroutine THEORY
Calculate the equivalent diameter
$D_e = \frac{D_i^2 - D_{ins}^2}{D_i}$
Calculate the average row cooling water bulk temperature
$T_a = \frac{T_{cwin} + T_{cwout}}{2}$
Call FASTWS then calculate the cooling water side heat transfer coefficient writing the result to array EXPHTC
$\alpha_{cw} = \frac{k}{D_e} \frac{(f/8)(Re-1000)Pr}{1+12.7(f/8)^{1/2}(Pr^{2/3}-1)}$
where
$f = (0.79 \ln Re - 1.64)^{-2}$
Calculate the temperature drop due to the water side heat transfer coefficient and write to array EXPHTC
$\Delta T_{cw} = \frac{q \cdot (D_o/D_i)}{\alpha_{cw}}$

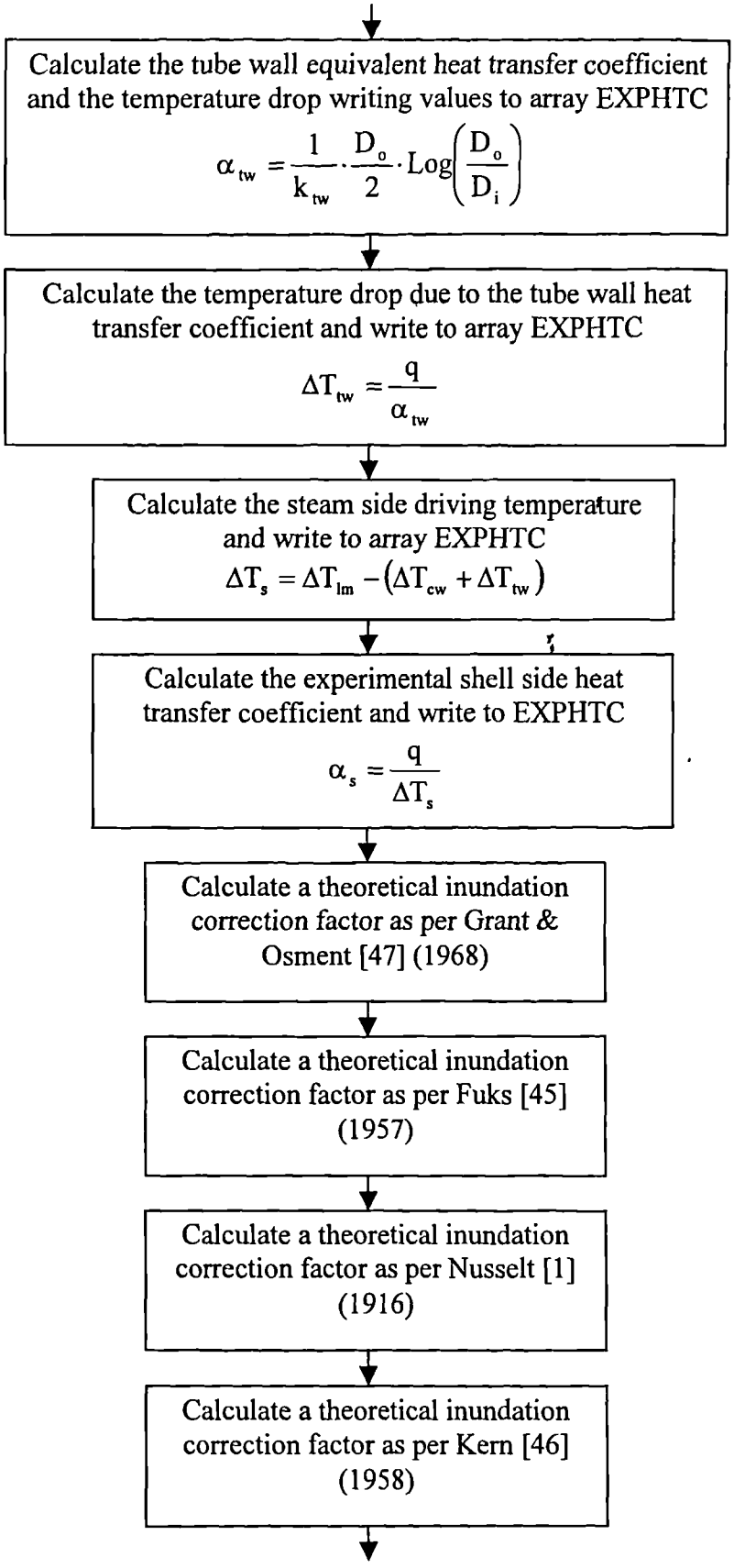
Calculate the tube wall equivalent heat transfer coefficient and the temperature drop writing values to array EXPHTC
$\alpha_{tw} = \frac{1}{k_{tw}} \cdot \frac{D_o}{2} \cdot Log\left(\frac{D_o}{D_i}\right)$
Calculate the temperature drop due to the tube wall heat transfer coefficient and write to array EXPHTC
$\Delta T_{tw} = \frac{q}{\alpha_{tw}}$
Calculate the steam side driving temperature and write to array EXPHTC
$\Delta T_s = \Delta T_{lm} - (\Delta T_{cw} + \Delta T_{tw})$
Calculate the experimental shell side heat transfer coefficient and write to EXPHTC
$\alpha_s = \frac{q}{\Delta T_s}$
Calculate a theoretical inundation correction factor as per Grant & Osment [47] (1968)
Calculate a theoretical inundation correction factor as per Fuks [45] (1957)
Calculate a theoretical inundation correction factor as per Nusselt [1] (1916)
Calculate a theoretical inundation correction factor as per Kern [46] (1958)

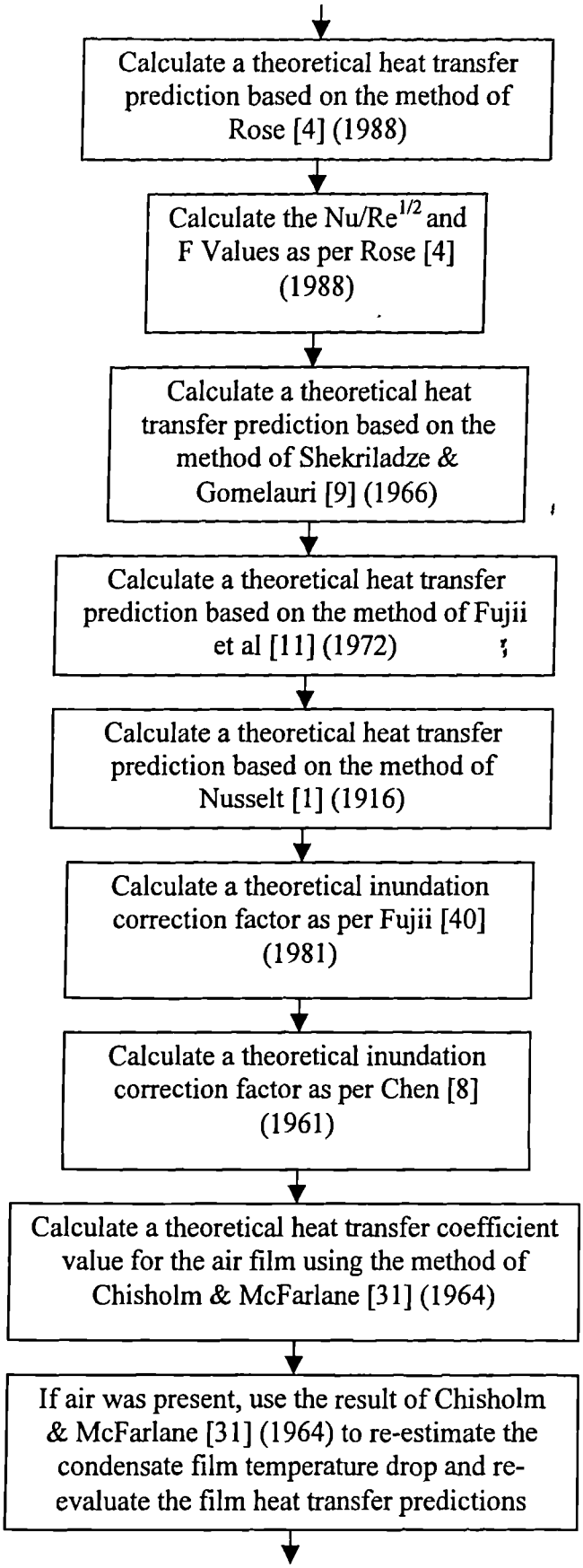
Calculate a theoretical heat transfer prediction based on the method of Rose [4] (1988)
Calculate the Nu/Re^1/2 and F Values as per Rose [4] (1988)
Calculate a theoretical heat transfer prediction based on the method of Shekriladze & Gomelauri [9] (1966)
Calculate a theoretical heat transfer prediction based on the method of Fujii et al [11] (1972)
Calculate a theoretical heat transfer prediction based on the method of Nusselt [1] (1916)
Calculate a theoretical inundation correction factor as per Fujii [40] (1981)
Calculate a theoretical inundation correction factor as per Chen [8] (1961)
Calculate a theoretical heat transfer coefficient value for the air film using the method of Chisholm & McFarlane [31] (1964)
If air was present, use the result of Chisholm & McFarlane [31] (1964) to re-estimate the condensate film temperature drop and re-evaluate the film heat transfer predictions

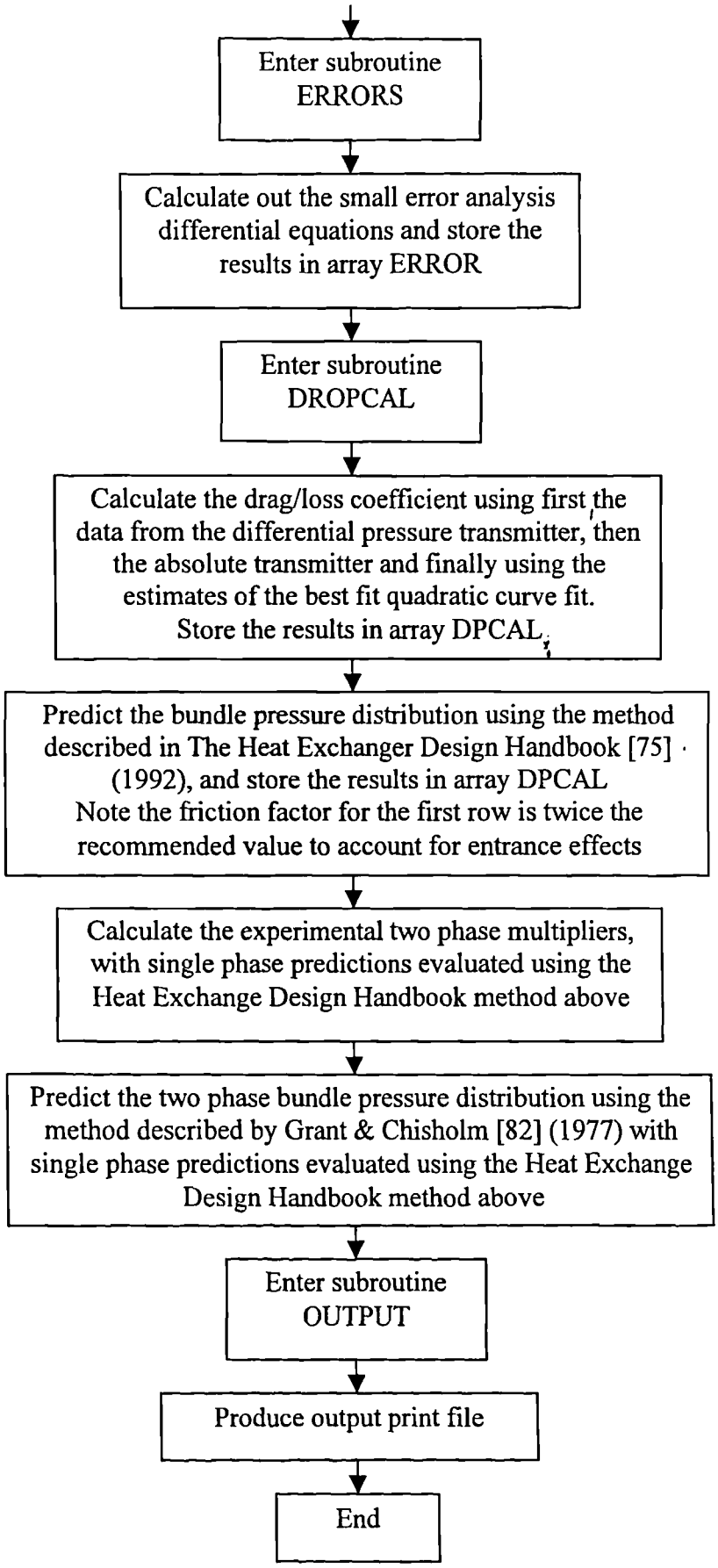
Enter subroutine ERRORS
Calculate out the small error analysis differential equations and store the results in array ERROR
Enter subroutine DROPCAL
Calculate the drag/loss coefficient using first the data from the differential pressure transmitter, then the absolute transmitter and finally using the estimates of the best fit quadratic curve fit. Store the results in array DPCAL
Predict the bundle pressure distribution using the method described in The Heat Exchanger Design Handbook [75] (1992), and store the results in array DPCAL Note the friction factor for the first row is twice the recommended value to account for entrance effects
Calculate the experimental two phase multipliers, with single phase predictions evaluated using the Heat Exchange Design Handbook method above
Predict the two phase bundle pressure distribution using the method described by Grant & Chisholm [82] (1977) with single phase predictions evaluated using the Heat Exchange Design Handbook method above
Enter subroutine OUTPUT
Produce output print file
End

APPENDIX B3 DATA STORAGE ARRAY DETAILS

Array: DATA (3,100)

Column 1 – Channel number Column 2 = Measured voltage

Column 3 – Processed variable

Array: CALC (5,100)

Column 1 – Channel number Column 2 = Instrument type code

Column 3 X^2 Quadratic coef. Column 4 = X Quadratic coef.

Column 5 Quadratic constant coef.

Array: TEMPS (5,20)

Column 1 – IROW number Column 2 = Cooling water inlet temp.

Column 3 Cooling water outlet temp.. Column 4 = Cooling water temp rise

Array: PRES (4,20)

Column 1 = IROW number Column 2 = Absolute pressure TX

Column 3 = Differential pressure TX Column 4 = Pressure check value

Array: ALOC (10,20)

Column 1 = Predicted pressure distribution Column 2 = % air concentration

Column 3 = Steam partial pressure Column 4 = Mixture specific volume

Column 5 = Mixture velocity Column 6 = Heat adsorbed by row

Column 7 = Steam mass flow rate Column 8 = Condensate flow rate

Array: HTCOEF (10,20)

Column 1 – Steam saturation temperature

Column 2 = Log mean temp. difference.

Column 3 – Row heat flux

Column 4 = Row heat transfer coefficient

Column 5 = Number of tubes in row

Array ARE (3,20)

Column 1 – Cooling water Re number

Column 2 = Cooling water Pr number

Column 3 Ave. cooling water velocity

Array: EXPHTC (10,20)

Column 1 – Tube side heat transfer coef.

Column 2 = Tube wall heat transfer coef.

Column 3 Shell side heat transfer coef.

Column 4 = Tube side temperature drop

Column 5 Tube wall temperature drop

Column 6 = Shell side temperature drop

Column 7

Column 8 =

Column 9 – Experimental $Nu/Re^{1\,2}$ value

Column 10 = Fd value Rose

Array: AHTC (15,20)

Column 1 = Film HTC Nusselt

Column 2 = Film HTC Rose

Column 3 = HTC Shekriladze Gomelauri

Column 4 = Film HTC Fujii et al

Column 5 =

Column 6 = Inundation Grant + Osment

Column 7 = Inundation Fuks

Column 8 = Inundation Nusselt

Column 9 = Inundation Kern

Column 10 = Inundation Fujii

Column 11 = Inundation Chen

Column 12 = Air film HTC Chis + McFar

Column 13 =

Column 14 =

Column 15 = Two phase steam Re No

Array: ERROR (5,20)

Column 1 – Heat flux error

Column 2 = Wall-bulk temperature error

Column 3 Overall coefficient error

Column 4 = Wall-bulk coefficient error

Column 5 –

Array: DPCAL (15,20)

Column 1 – Cd based on DT transmitter

Column 2 = Cd based on AB transmitter

Column 3 – Cd based on curve fit

Column 4 = Predicted row DP HEDH

Column 5 = HEDH predicted pressure

Column 6 = Single phase pressure drop

Column 7 – Momentum press contribution

Column 8 = 2P multiplier based on DPTX

Column 9 = 2P multiplier based on ABTX

Column 10 = 2P multiplier from curve fit

Column 11 – G+C predicted pressure

Column 12 =

Column 13 =

Column 14 =

Column 15 Steam Re number

APPENDIX B4 INPUT INFORMATION REQUIRED BY PROCESSING PROGRAM

Program input	Variable name	Typical value	
Condensation mode	IMODE	1	See note 1
Bundle configuration	ICONF	1	See note 2
Number of cooled rows	ICOOL	15	-
Row cooling water flow	CWF	22.2	cm
Dump condenser cooling water flow	DCCW	57	gal/min
Air inlet flow	AIR	4.4	L/min
Total condensate outflow	TCO	2.15	L/min
Separator outflow	SCO	0.75	L/min

Note 1 Input values for the variable IMODE are 1 or 2 only. A value of 1 indicates filmwise condensation and 2 indicates dropwise condensation.

Note 2 Input values for the variable ICONF are 1 or 2 only. A value of 1 indicates an inline bundle configuration and 2 indicates a staggered bundle configuration.

APPENDIX B5 SMALL ERROR ANALYSIS DIFFERENTIAL EQUATIONS.

Heat flux (q)

$$\dot{q}_r = \frac{\dot{m}_{cw} \cdot C_P \cdot (T_{co} - T_{ci})}{A_r}$$

$$\frac{\partial \dot{q}_r}{\partial T_{ci}} = \frac{-\dot{m}_{cw} \cdot C_P}{A_r}$$

$$\frac{\partial \dot{q}_r}{\partial T_{co}} = \frac{\dot{m}_{cw} \cdot C_P}{A_r}$$

$$\frac{\partial \dot{q}_r}{\partial \dot{m}_{cw}} = \frac{C_P (T_{co} - T_{ci})}{A_r}$$

Steam side temperature difference (ΔT_s)

$$\Delta T_s = T_{sat} - \frac{T_{co} + T_{ci}}{2} - \frac{D_o \cdot \dot{m}_{cw} \cdot C_P (T_{co} - T_{ci})}{A_r \cdot D_i \cdot \alpha_{cw}} - \frac{\dot{m}_{cw} \cdot C_P (T_{co} - T_{ci})}{A_r \cdot \alpha_{tw}}$$

$$\frac{\partial \Delta T_s}{\partial T_{ci}} = -\frac{1}{2} + \frac{D_o \cdot \dot{m}_{cw} \cdot C_P}{A_r \cdot D_i \cdot \alpha_{cw}} + \frac{\dot{m}_{cw} \cdot C_P}{A_r \cdot \alpha_{tw}} \qquad \frac{\partial \Delta T_s}{\partial T_{co}} = -\frac{1}{2} - \frac{D_o \cdot \dot{m}_{cw} \cdot C_P}{A_r \cdot D_i \cdot \alpha_{cw}} - \frac{\dot{m}_{cw} \cdot C_P}{A_r \cdot \alpha_{tw}}$$

$$\frac{\partial \Delta T_s}{\partial \dot{m}_{cw}} = -\frac{D_o \cdot C_P (T_{co} - T_{ci})}{A_r \cdot D_i \cdot \alpha_{cw}} - \frac{C_P (T_{co} - T_{ci})}{A_r \cdot \alpha_{tw}} \qquad \frac{\partial \Delta T_s}{\partial T_{sat}} = 1$$

$$\frac{\partial \Delta T_s}{\partial \alpha_{cw}} = \frac{D_o \cdot \dot{m}_{cw} C_P (T_{co} - T_{ci})}{A_r \cdot D_i \cdot \alpha_{cw}^2} \qquad \frac{\partial \Delta T_s}{\partial \alpha_{tw}} = \frac{\dot{m}_{cw} \cdot C_P (T_{co} - T_{ci})}{A_r \cdot \alpha_{tw}^2}$$

Overall heat transfer coefficient (α_{ov})

$$\alpha_{ov} = \frac{\dot{m}_{cw} \cdot C_P \cdot (T_{co} - T_{ci})}{A_r \left(T_{sat} - \frac{T_{co}}{2} - \frac{T_{ci}}{2} \right)}$$

$$\text{If } y = \frac{u}{v} \text{ then } \frac{dy}{dx} = \frac{v\frac{du}{dx} - u\frac{dv}{dx}}{v^2}$$

then

$$\frac{\partial \alpha_{ov}}{\partial T_{ci}} = \frac{-\dot{m}_{cw} \cdot C_P \left(T_{sat} - \frac{T_{co}}{2} - \frac{T_{ci}}{2} \right) + \frac{1}{2} \cdot \dot{m}_{cw} \cdot C_P (T_{co} - T_{ci})}{A_r \left(T_{sat} - \frac{T_{co}}{2} - \frac{T_{ci}}{2} \right)^2}$$

$$\frac{\partial \alpha_{ov}}{\partial T_{co}} = \frac{\dot{m}_{cw} \cdot C_P \left(T_{sat} - \frac{T_{co}}{2} - \frac{T_{ci}}{2} \right) + \frac{1}{2} \cdot \dot{m}_{cw} \cdot C_P (T_{co} - T_{ci})}{A_r \left(T_{sat} - \frac{T_{co}}{2} - \frac{T_{ci}}{2} \right)^2}$$

$$\frac{\partial \alpha_{ov}}{\partial T_{sat}} = \frac{-\dot{m}_{cw} \cdot C_P (T_{co} - T_{ci})}{A_r \left(T_{sat} - \frac{T_{CO}}{2} - \frac{T_{CI}}{2} \right)^2}$$

$$\frac{\partial \alpha_{ov}}{\partial \dot{m}_{cw}} = \frac{C_P (T_{co} - T_{ci})}{A_r \left(T_{sat} - \frac{T_{co}}{2} - \frac{T_{ci}}{2} \right)}$$

Steam side heat transfer coeficent (α_s)

$$\alpha_s = \frac{\dot{m}_{cw} \cdot C_P \cdot (T_{co} - T_{ci})}{A_r \left(T_{sat} - \frac{T_{co} + T_{ci}}{2} - \frac{D_o \cdot \dot{m}_{cw} \cdot C_P (T_{co} - T_{ci})}{A_r \cdot D_i \cdot \alpha_{cw}} - \frac{\dot{m}_{cw} \cdot C_P \cdot (T_{co} - T_{ci})}{A_r \cdot \alpha_{tw}} \right)}$$

Again

$$\text{If } y = \frac{u}{v} \text{ then } \frac{dy}{dx} = \frac{v\frac{du}{dx} - u\frac{dv}{dx}}{v^2}$$

$$\frac{\partial \alpha_s}{\partial T_{ci}} = \frac{-\dot{m}_{cw} \cdot C_P \left(T_{sat} - \frac{T_{co} + T_{ci}}{2} - \frac{D_o \cdot \dot{m}_{cw} \cdot C_P (T_{co} - T_{ci})}{A_r \cdot D_i \cdot \alpha_{cw}} - \frac{\dot{m}_{cw} \cdot C_P (T_{co} - T_{ci})}{A_r \cdot \alpha_{tw}} \right)}{A_r \left(T_{sat} - \frac{T_{co} + T_{ci}}{2} - \frac{D_o \cdot \dot{m}_{cw} \cdot C_P (T_{co} - T_{ci})}{A_r \cdot D_i \cdot \alpha_{cw}} - \frac{\dot{m}_{cw} \cdot C_P (T_{co} - T_{ci})}{A_r \cdot \alpha_{tw}} \right)^2} -$$

$$\frac{\dot{m}_{cw} \cdot C_P (T_{co} - T_{ci}) \left(\frac{D_o \cdot \dot{m}_{cw} \cdot C_P}{A_r \cdot D_i \cdot \alpha_{cw}} + \frac{\dot{m}_{cw} \cdot C_P}{A_r \cdot \alpha_{tw}} - \frac{1}{2} \right)}{A_r \left(T_{sat} - \frac{T_{co} + T_{ci}}{2} - \frac{D_o \cdot \dot{m}_{cw} \cdot C_P (T_{co} - T_{ci})}{A_r \cdot D_i \cdot \alpha_{cw}} - \frac{\dot{m}_{cw} \cdot C_P (T_{co} - T_{ci})}{A_r \cdot \alpha_{tw}} \right)^2}$$

$$\frac{\partial \alpha_s}{\partial T_{co}} = \frac{\dot{m}_{cw} \cdot C_P \left(T_{sat} - \frac{T_{co} + T_{ci}}{2} - \frac{D_o \cdot \dot{m}_{cw} \cdot C_P (T_{co} - T_{ci})}{A_r \cdot D_i \cdot \alpha_{cw}} - \frac{\dot{m}_{cw} \cdot C_P (T_{co} - T_{ci})}{A_r \cdot \alpha_{tw}} \right)}{A_r \left(T_{sat} - \frac{T_{co} + T_{ci}}{2} - \frac{D_o \cdot \dot{m}_{cw} \cdot C_P (T_{co} - T_{ci})}{A_r \cdot D_i \cdot \alpha_{cw}} - \frac{\dot{m}_{cw} \cdot C_P (T_{co} - T_{ci})}{A_r \cdot \alpha_{tw}} \right)^2} -$$

$$\frac{\dot{m}_{cw} \cdot C_P (T_{co} - T_{ci}) \left(-\frac{D_o \cdot \dot{m}_{cw} \cdot C_P}{A_r \cdot D_i \cdot \alpha_{cw}} - \frac{\dot{m}_{cw} \cdot C_P}{A_r \cdot \alpha_{tw}} + \frac{1}{2} \right)}{A_r \left(T_{sat} - \frac{T_{co} + T_{ci}}{2} - \frac{D_o \cdot \dot{m}_{cw} \cdot C_P (T_{co} - T_{ci})}{A_r \cdot D_i \cdot \alpha_{cw}} - \frac{\dot{m}_{cw} \cdot C_P (T_{co} - T_{ci})}{A_r \cdot \alpha_{tw}} \right)^2}$$

$$\frac{\partial \alpha_s}{\partial \dot{m}_{cw}} = \frac{C_P(T_{co}-T_{ci})\left(T_{sat}-\frac{T_{co}+T_{ci}}{2}-\frac{D_o\cdot\dot{m}_{cw}\cdot C_P(T_{co}-T_{ci})}{A_r\cdot D_i\cdot\alpha_{cw}}-\frac{\dot{m}_{cw}\cdot C_P(T_{co}-T_{ci})}{A_r\cdot\alpha_{tw}}\right)}{A_r\left(T_{sat}-\frac{T_{co}+T_{ci}}{2}-\frac{D_o\cdot\dot{m}_{cw}\cdot C_P(T_{co}-T_{ci})}{A_r\cdot D_i\cdot\alpha_{cw}}-\frac{\dot{m}_{cw}\cdot C_P(T_{co}-T_{ci})}{A_r\cdot\alpha_{tw}}\right)^2} -$$

$$\frac{\dot{m}_{cw}\cdot C_P(T_{co}-T_{ci})\left(-\frac{D_o\cdot C_P(T_{co}-T_{ci})}{A_r\cdot D_i\cdot\alpha_{cw}}-\frac{C_P(T_{co}-T_{ci})}{A_r\cdot\alpha_{tw}}\right)}{A_r\left(T_{sat}-\frac{T_{co}+T_{ci}}{2}-\frac{D_o\cdot\dot{m}_{cw}\cdot C_P(T_{co}-T_{ci})}{A_r\cdot D_i\cdot\alpha_{cw}}-\frac{\dot{m}_{cw}\cdot C_P(T_{co}-T_{ci})}{A_r\cdot\alpha_{tw}}\right)^2}$$

$$\frac{\partial \alpha_s}{\partial T_{sat}} \frac{-\dot{m}_{cw}\cdot C_P(T_{co}-T_{ci})}{A_r\left(T_{sat}-\frac{T_{co}+T_{ci}}{2}-\frac{D_o\cdot\dot{m}_{cw}\cdot C_P(T_{co}-T_{ci})}{A_r\cdot D_i\cdot\alpha_{cw}}-\frac{\dot{m}_{cw}\cdot C_P(T_{co}-T_{ci})}{A_r\cdot\alpha_{tw}}\right)^2}$$

$$\frac{\partial \alpha_s}{\partial \alpha_{cw}} \frac{-\dot{m}_{cw}\cdot C_P(T_{co}-T_{ci})\left(\frac{D_o\cdot\dot{m}_{cw}\cdot C_P(T_{co}-T_{ci})}{A_r\cdot D_i\cdot\alpha_{cw}^2}\right)}{A_r\left(T_{sat}-\frac{T_{co}+T_{ci}}{2}-\frac{D_o\cdot\dot{m}_{cw}\cdot C_P(T_{co}-T_{ci})}{A_r\cdot D_i\cdot\alpha_{cw}}-\frac{\dot{m}_{cw}\cdot C_P(T_{co}-T_{ci})}{A_r\cdot\alpha_{tw}}\right)^2}$$

$$\frac{\partial \alpha_s}{\partial \alpha_{tw}} \frac{-\dot{m}_{cw}\cdot C_P(T_{co}-T_{ci})\left(\frac{\dot{m}_{cw}\cdot C_P(T_{co}-T_{ci})}{A_r\cdot\alpha_{tw}^2}\right)}{A_r\left(T_{sat}-\frac{T_{co}+T_{ci}}{2}-\frac{D_o\cdot\dot{m}_{cw}\cdot C_P(T_{co}-T_{ci})}{A_r\cdot D_i\cdot\alpha_{cw}}-\frac{\dot{m}_{cw}\cdot C_P(T_{co}-T_{ci})}{A_r\cdot\alpha_{tw}}\right)^2}$$

APPENDIX C

APPENDIX C1 TEST SUMMARY

Test No	Date	Inlet conditions P_m	U_s	ΔT_{ov}	U_{cw}	Air	No. rows cooled	Comments
		mbar	m/s	K	m/s	%		
T041	7/7/98	50.19	35.0	15	2.75	0	15	1st Wilson plot
T042	7/7/98	49.96	36.2	15	2.75	0	15	1st Wilson plot
T043	7/7/98	50.42	34.6	15	2.22	0	15	1st Wilson plot
T044	7/7/98	49.85	35.0	15	2.22	0	15	1st Wilson plot
T045	7/7/98	50.34	33.7	15	1.75	0	15	1st Wilson plot
T046	7/7/98	50.16	33.8	15	1.75	0	15	1st Wilson plot
T047	7/7/98	50.17	34.0	15	1.30	0	15	1st Wilson plot
T048	7/7/98	50.33	33.9	15	1.30	0	15	1st Wilson plot
T049	7/7/98	49.68	34.9	15	3.21	0	11	1st Wilson plot
T050	7 7/98	49.05	35.7	15	3.21	0	11	1st Wilson plot
T051	8 7 98	48.26	25.6	0	2.80	0	15	Single phase
T052	8 7 98	49.35	26.7	0	2.80	0	15	Single phase
T053	8 7 98	49.65	21.5	0	2.80	0	15	Single phase
T054	8 7 98	49.97	21.3	0	2.80	0	15	Single phase
T055	8 7 98	51.65	10.8	0	2.80	0	15	Single phase
T056	8 7 98	51.79	10.8	0	2.80	0	15	Single phase
T135	19 8 98	50.84	31.3	10	2.78	0	15	2nd Wilson plot
T136	19 8 98	50.59	32.3	10	2.78	0	15	2nd Wilson plot
T137	19 8 98	50.35	31.4	10	2.48	0	15	2nd Wilson plot
T138	19 8 98	50.2	31.7	10	2.48	0	15	2nd Wilson plot
T139	19 8 98	50.44	31.4	10	2.22	0	15	2nd Wilson plot
T140	19 8 98	50.67	31.4	10	2.22	0	15	2nd Wilson plot
T141	19 8 98	50.50	31.7	10	1.98	0	15	2nd Wilson plot
T142	19 8 98	50.94	31.1	10	1.98	0	15	2nd Wilson plot
T143	19 8 98	50.49	31.3	10	1.75	0	15	2nd Wilson plot
T144	19 8 98	50.59	31.3	10	1.75	0	15	2nd Wilson plot
T145	19 8 98	50.20	31.7	10	1.52	0	15	2nd Wilson plot
T146	19 8/98	50.09	32.2	10	1.52	0	15	2nd Wilson plot
T147	19 8 98	50.84	32.3	10	1.30	0	15	2nd Wilson plot
T148	19/8/98	50.95	31.9	10	1.30	0	15	2nd Wilson plot
T149	19/8/98	50.22	32.7	10	3.14	0	12	2nd Wilson plot
T150	19 8/98	50.17	32.3	10	3.14	0	12	2nd Wilson plot
T151	16/10/98	50.98	33.3	15	2.74	0	15	3rd Wilson plot
T152	16/10/98	51.79	32.6	15	2.74	0	15	3rd Wilson plot
T153	16/10/98	50.34	33.1	15	2.45	0	15	3rd Wilson plot
T154	16/10/98	50.52	33.2	15	2.45	0	15	3rd Wilson plot
T155	16/10/98	50.22	33.0	15	2.21	0	15	3rd Wilson plot
T156	16/10/98	50.37	33.3	15	2.21	0	15	3rd Wilson plot
T157	16/10/98	50.65	32.9	15	1.93	0	15	3rd Wilson plot

Test No	Date	Inlet conditions P_m	U_s	ΔT_{ov}	U_{cw}	Air	No. rows cooled	Comments
		mbar	m/s	K	m/s	%		
T158	16/10/98	50.66	33.5	15	1.93	0	15	3rd Wilson plot
T159	16/10/98	49.73	33.9	15	1.69	0	15	3rd Wilson plot
T160	16/10/98	50.03	33.7	15	1.69	0	15	3rd Wilson plot
T161	16/10/98	50.66	32.5	15	1.51	0	15	3rd Wilson plot
T162	16/10/98	50.50	33.6	15	1.51	0	15	3rd Wilson plot
T163	16/10/98	50.52	33.4	15	1.26	0	15	3rd Wilson plot
T164	16/10/98	50.74	33.2	15	1.26	0	15	3rd Wilson plot
T165	16/10/98	49.98	34.3	15	3.14	0	12	3rd Wilson plot
T166	16/10/98	52.74	33.2	15	3.14	0	12	3rd Wilson plot
T167	19/10/98	50.81	33.4	10	2.75	0	15	4th Wilson plot
T168	19/10/98	50.51	33.6	10	2.75	0	15	4th Wilson plot
T169	19/10 98	49.95	33.5	10	2.48	0	15	4th Wilson plot
T170	19/10/98	50.03	34.9	10	2.48	0	15	4th Wilson plot
T171	19/10/98	50.33	32.7	10	2.24	0	15	4th Wilson plot
T172	19 10 98	50.17	33.0	10	2.24	0	15	4th Wilson plot
T173	19 10 98	49.96	32.7	10	1.87	0	15	4th Wilson plot
T174	19 10 98	49.71	33.1	10	1.87	0	15	4th Wilson plot
T175	19 10 98	50.19	32.0	10	1.55	0	15	4th Wilson plot
T176	19 10 98	50.65	31.7	10	1.55	0	15	4th Wilson plot
T177	19 10 98	50.19	32.4	10	1.26	0	15	4th Wilson plot
T178	19 10 98	50.01	33.1	10	1.26	0	15	4th Wilson plot
T179	19 10 98	50.16	32.6	10	3.08	0	12	4th Wilson plot
T180	19 10 98	50.28	32.9	10	3.08	0	12	4th Wilson plot
T193	26 10 98	51.60	9.4	15	2.76	0	4	Filmwise
T194	26 10 98	50.61	9.3	15	2.76	0	4	Filmwise
T195	26 10 98	50.00	9.5	10	2.79	0	6	Filmwise
T196	26 10 98	50.33	9.6	10	2.79	0	6	Filmwise
T197	26 10 98	49.19	10.2	5	2.78	0	13	Filmwise
T198	26 10 98	48.96	10.1	5	2.78	0	13	Filmwise
T199	27/10 98	50.65	9.0	5	2.78	1.1	13	Filmwise
T200	27/10 98	50.81	9.2	5	2.78	1.1	13	Filmwise
T201	27/10/98	51.98	8.2	10	2.78	1.2	6	Filmwise
T202	27/10/98	52.28	8.3	10	2.78	1.2	6	Filmwise
T203	27/10/98	51.93	8.4	15	2.79	1.2	4	Filmwise
T204	27/10/98	52.24	7.9	15	2.79	1.2	4	Filmwise
T205	27/10/98	50.02	19.3	15	2.78	0	10	Filmwise
T206	27/10/98	50.17	19.5	15	2.78	0	10	Filmwise
T207	27/10/98	50.02	19.3	10	2.76	0	15	Filmwise
T208	27/10/98	50.31	19.6	10	2.76	0	15	Filmwise
T209	27/10/98	49.86	20.6	5	2.79	0	15	Filmwise
T210	27/10/98	50.02	21.2	5	2.79	0	15	Filmwise
T211	27/10/98	49.96	21.2	5	2.79	0	15	Filmwise
T212	28/10/98	50.98	20.5	5	2.78	1.0	15	Filmwise

Test No	Date	Inlet conditions P_m	U_s	ΔT_{ov}	U_{cw}	Air	No. rows cooled	Comments
		mbar	m/s	K	m/s	%		
T213	28/10/98	51.00	20.7	5	2.79	1.0	15	Filmwise
T214	28/10/98	50.47	20.1	10	2.76	1.0	15	Filmwise
T215	28/10/98	50.20	20.2	10	2.76	1.0	15	Filmwise
T216	28/10/98	51.19	19.6	15	2.78	1	11	Filmwise
T217	28/10/98	51.16	19.6	15	2.78	1	11	Filmwise
T218	28/10/98	50.52	33.4	5	2.78	0	15	Filmwise
T219	28/10/98	50.38	33.5	5	2.78	0	15	Filmwise
T220	28/10/98	50.22	33.6	10	2.76	0	15	Filmwise
T221	28/10/98	50.35	33.1	10	2.76	0	15	Filmwise
T222	28/10/98	49.94	32.7	15	2.76	0	15	Filmwise
T223	28/10/98	50.05	32.9	15	2.76	0	15	Filmwise
T224	30/10 98	50.35	32.3	5	2.78	0	15	Filmwise
T225	30/10/98	50.50	32.2	5	2.78	0	15	Filmwise
T226	30 10/98	52.08	31.9	5	2.79	1.0	15	Filmwise
T227	30 10 98	51.78	31.8	5	2.79	1.0	15	Filmwise
T228	30 10 98	50.70	32.9	10	2.78	1.0	15	Filmwise
T229	30 10 98	50.58	32.9	10	2.78	1.0	15	Filmwise
T330	30 10 98	51.00	32.1	15	2.78	1.0	15	Filmwise
T331	30 10 98	50.97	32.1	15	2.78	1.0	15	Filmwise
T232	2 11 98	75.57	32.4	15	2.79	0	15	Filmwise
T233	2 11 98	76.28	32.1	15	2.79	0	15	Filmwise
T234	2 11 98	76.12	31.6	10	2.79	0	15	Filmwise
T235	2 11 98	75.17	31.5	10	2.79	0	15	Filmwise
T236	2 11 98	75.96	31.4	5	2.79	0	15	Filmwise
T237	2 11 98	76.65	31.6	5	2.79	0	15	Filmwise
T238	2 11/98	75.98	31.8	5	2.79	0	15	Filmwise
T239	3 11 98	76.30	20.4	15	2.79	0	15	Filmwise
T240	3 11 98	75.81	20.7	15	2.79	0	15	Filmwise
T241	3 11 98	75.52	20.8	10	2.79	0	15	Filmwise
T242	3/11/98	75.66	21.2	10	2.79	0	15	Filmwise
T243	3 11/98	75.50	20.9	5	2.79	0	15	Filmwise
T244	3/11/98	75.83	20.7	5	2.79	0	15	Filmwise
T245	3/11/98	75.81	20.7	5	2.79	0	15	Filmwise
T246	4/11/98	75.48	9.8	15	2.79	0	8	Filmwise
T247	4/11/98	75.96	9.7	15	2.79	0	8	Filmwise
T248	4/11/98	75.17	10.1	10	2.79	0	11	Filmwise
T249	4/11/98	75.18	9.8	10	2.79	0	11	Filmwise
T250	4/11/98	76.61	10.3	5	2.79	0	15	Filmwise
T251	4/11/98	76.10	10.4	5	2.79	0	15	Filmwise
T252	4/11/98	101.39	10.0	15	2.79	0	9	Filmwise
T253	4/11/98	102.85	9.8	15	2.79	0	9	Filmwise
T254	4/11/98	102.20	10.1	10	2.79	0	13	Filmwise
T255	4/11/98	102.35	9.9	10	2.79	0	13	Filmwise

Test No	Date	Inlet conditions P_m	U_s	ΔT_{ov}	U_{cw}	Air	No. rows cooled	Comments
		mbar	m/s	K	m/s	%		
T256	4/11/98	101.41	10.3	5	2.79	0	15	Filmwise
T257	4/11/98	101.64	10.3	5	2.79	0	15	Filmwise
T258	5/11/98	102.04	20.2	15	2.79	0	15	Filmwise
T259	5/11/98	101.41	20.4	15	2.79	0	15	Filmwise
T260	5/11/98	102.76	19.8	10	2.79	0	15	Filmwise
T261	5/11/98	103.14	19.7	10	2.79	0	15	Filmwise
T262	5/11/98	102.03	20.4	5	2.79	0	15	Filmwise
T263	5/11/98	102.03	20.4	5	2.79	0	15	Filmwise
T264	5/11/98	102.36	20.3	5	2.79	0	15	Filmwise
T265	5/11/98	103.64	20.1	5	2.79	0	15	Filmwise
T266	6/11/98	103.91	32.5	5	2.97	0	15	Filmwise
T267	6 11/98	102.16	33.0	5	2.79	0	15	Filmwise
T268	6 11/98	100.79	31.8	10	2.79	0	15	Filmwise
T269	6/11/98	100.95	31.7	10	2.79	0	15	Filmwise
T270	6 11/98	103.49	31.3	15	2.79	0	15	Filmwise
T271	6 11/98	101.57	31.9	15	2.79	0	15	Filmwise
T272	24 11 98	50.67	12.1	5	2.79	0	13	Dropwise set 1
T273	24 11 98	50.65	12.1	5	2.79	0	13	Dropwise set 1
T274	24 11/98	52.37	11.5	10	2.80	0	6	Dropwise set 1
T275	24 11/98	52.83	11.4	10	2.80	0	6	Dropwise set 1
T276	24 11 98	49.04	12.7	15	2.79	0	5	Dropwise set 1
T277	1 12 98	50.50	12.4	5	2.79	0	13	Dropwise set 1
T278	1 12 98	50.22	12.5	5	2.79	0	13	Dropwise set 1
T279	1 12 98	50.63	12.7	5	2.79	0	13	Dropwise set 1
T280	1 12 98	50.50	12.7	5	2.79	0	13	Dropwise set 1
T281	19 1 99	50.62	13.3	5	2.79	0.8	15	Dropwise set 2
T282	19 1 99	50.61	13.3	5	2.79	0.8	15	Dropwise set 2
T283	19 1 99	50.02	12.7	5	2.79	0	13	Dropwise set 2
T284	19 1 99	50.12	12.6	5	2.78	0	13	Dropwise set 2
T285	19 1/99	51.26	12.9	5	2.79	0.8	15	Dropwise set 2
T286	19 1/99	50.95	12.9	5	2.79	0.8	15	Dropwise set 2
T287	19 1/99	50.49	13.0	5	2.79	0	13	Dropwise set 2
T288	19 1/99	50.34	13.0	5	2.79	0	13	Dropwise set 2
T289	20/1/99	50.34	33.4	15	2.79	0	15	Dropwise set 2
T290	20/1/99	50.65	33.2	15	2.79	0	15	Dropwise set 2
T291	20/1/99	50.98	33.0	15	2.79	1.0	15	Dropwise set 2
T292	20/1/99	50.96	33.0	15	2.79	1.0	15	Dropwise set 2
T293	20/1/99	50.96	32.7	15	2.79	0	15	Dropwise set 2
T294	20/1/99	51.93	32.7	15	2.79	0	15	Dropwise set 2
T295	20/1/99	50.96	33.6	15	2.79	1.0	15	Dropwise set 2
T296	20/1/99	50.65	33.7	15	2.79	1.0	15	Dropwise set 2
T297	20/1/99	50.49	33.0	15	2.45	0	15	5th Wilson plot
T298	20/1/99	50.48	33.0	15	2.45	0	15	5th Wilson plot

Test No	Date	Inlet conditions P_m	U_s	ΔT_{ov}	U_{cw}	Air	No. rows cooled	Comments
		mbar	m/s	K	m/s	%		
T299	20/1/99	50.65	33.2	15	2.19	0	15	5th Wilson plot
T300	20/1/99	50.52	33.1	15	2.19	0	15	5th Wilson plot
T301	20/1/99	50.48	33.8	15	1.91	0	15	5th Wilson plot
T302	20/1/99	50.50	33.7	15	1.91	0	15	5th Wilson plot
T303	20/1/99	50.48	33.5	15	1.55	0	15	5th Wilson plot
T304	20/1/99	50.49	33.5	15	1.55	0	15	5th Wilson plot
T305	20/1/99	50.48	33.5	15	1.27	0	15	5th Wilson plot
T306	20/1/99	50.65	33.5	15	1.27	0	15	5th Wilson plot
T307	20/1/99	50.47	33.7	15	2.98	0	13	5th Wilson plot
T308	20/1/99	50.33	33.8	15	2.98	0	15	5th Wilson plot
T309	26/1/99	50.32	20.7	10	2.79	0	11	Dropwise set 2
T310	26/1/99	49.82	20.3	10	2.79	0	11	Dropwise set 2
T311	26/1/99	50.47	21.0	10	2.79	0.8	13	Dropwise set 2
T312	26 1/99	51.04	20.8	10	2.79	1	13	Dropwise set 2
T313	26 1 99	50.01	20.7	10	2.79	0	11	Dropwise set 2
T314	26 1/99	50.32	20.6	10	2.79	0	11	Dropwise set 2
T315	26 1 99	52.09	20.4	10	2.79	0.8	13	Dropwise set 2
T316	26 1 99	51.75	20.5	10	2.79	0.8	13	Dropwise set 2

APPENDIX C2 STEAM SIDE COEFFICENTS BASED ON EQUATION 5.4

	α_s	α_s	α_s	α_s
	T041-T050	T135-T150	T151-166	T167-T180
	kW/m^2K	kW/m^2K	kW/m^2K	kW/m^2K
	81.79	137.67	55.33	52.21
	84.00	91.09	46.23	60.50
	71.36	78.12	55.78	47.88
	75.18	86.87	50.32	50.54
	89.48	74.55	50.77	53.77
	75.60	84.87	55.61	55.01
	87.97	71.70	53.43	53.20
	72.52	70.81	55.43	56.93
	47.70	63.31	49.80	58.21
	62.31	64.35	52.60	45.23
		56.32	51.46	41.72
		55.02	48.62	43.30
		52.71	43.62	50.87
		47.94	45.40	52.33
		61.69	52.09	
		59.48	56.45	
Average	74.79	72.28	51.43	51.55
Standard deviations	11.96	20.90	3.83	5.30

Overall average steam side heat transfer coefficient 62.51kW/m^2K

APPENDIX C3 STEAM SIDE COEFFICENTS BASED ON EQUATION 5.5

	α_s	α_s	α_s	α_s
	T041-T050	T135-T150	T151-166	T167-T180
	kW/m^2K	kW/m^2K	kW/m^2K	kW/m^2K
	50.34	65.66	38.95	36.75
	51.11	52.71	34.19	40.66
	47.17	48.05	39.39	34.51
	48.79	51.23	36.57	35.87
	59.28	46.96	37.21	37.65
	52.94	50.91	39.75	38.26
	76.51	46.44	39.71	38.03
	64.59	46.09	40.82	39.93
	34.87	43.77	39.17	42.63
	41.93	44.26	40.88	35.23
		42.05	42.43	35.95
		41.31	40.51	37.12
		43.14	41.75	36.17
		39.82	43.38	36.91
		41.41	37.16	
		40.39	39.53	
Averages	52.75	46.51	39.46	37.56
Standard deviations	11.13	6.27	2.25	2.16

Overall average steam side heat transfer coefficient 44.07kW/m^2K

APPENDIX C4 FIRST ROW THEORY-DATA SCATTER ANALYSIS

Data vs. theory root mean square errors

	Maximum area			Mean void area			Minimum area		
Pressure plots	Rose	Fujii	S+G	Rose	Fujii	S+G	Rose	Fujii	S+G
50mbar	30.4	16.2	32.5	17.4	22.9	17.9	32.3	46.3	32.2
75mbar	45.4	25.8	47.9	27.3	22.8	28.5	31.2	43.9	30.2
100mbar	40.4	20.5	42.9	20.1	21.0	21.1	27.5	43.3	27.5
Averages	38.7	20.8	41.1	21.6	22.2	22.5	30.3	44.5	29.9
Velocity plots	Rose	Fujii	S+G	Rose	Fujii	S+G	Rose	Fujii	S+G
50mbar	25.5	16.1	27.6	15.4	13.7	16.4	28.3	39.9	27.9
75mbar	48.2	20.3	51.5	25.2	14.2	27.0	23.3	40.8	23.4
100mbar	38.0	25.4	39.6	23.0	32.7	22.9	37.0	52.4	37.2
Averages	37.2	20.6	39.6	21.2	20.2	22.1	29.5	44.4	32.8
Temperature plots	Rose	Fujii	S+G	Rose	Fujii	S+G	Rose	Fujii	S+G
50mbar	32.9	15.6	34.7	14.1	16.2	13.7	32.1	42.7	32.2
75mbar	36.8	15.6	39.5	12.1	13.7	13.5	25.3	41.3	25.2
100mbar	44.4	27.2	47.0	30.2	29.8	31.8	31.7	48.7	31.7
Averages	38.0	19.5	40.4	18.8	19.9	19.7	29.7	44.2	29.7
Scatter average	37.9	20.3	40.4	20.5	20.7	21.4	29.8	44.3	30.8

APPENDIX C5 INUNDATION ANALYSIS, ALL DATA

Steam velocity dependence plots

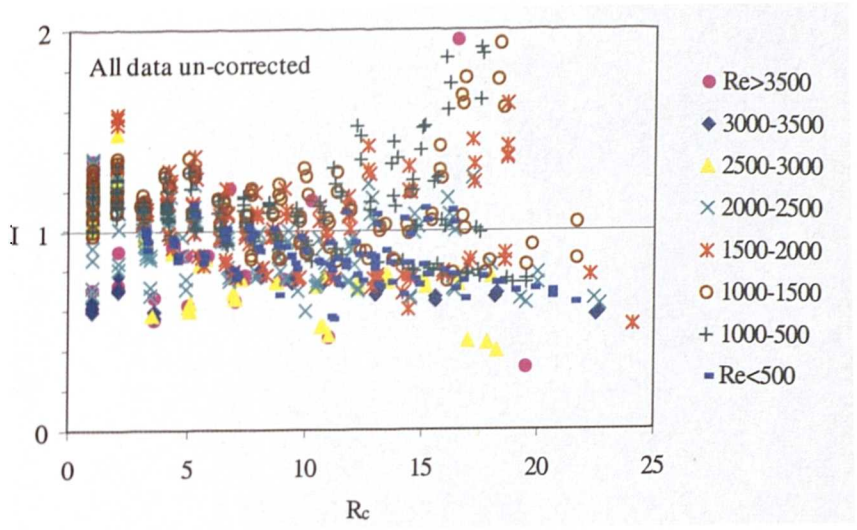

Plot 1

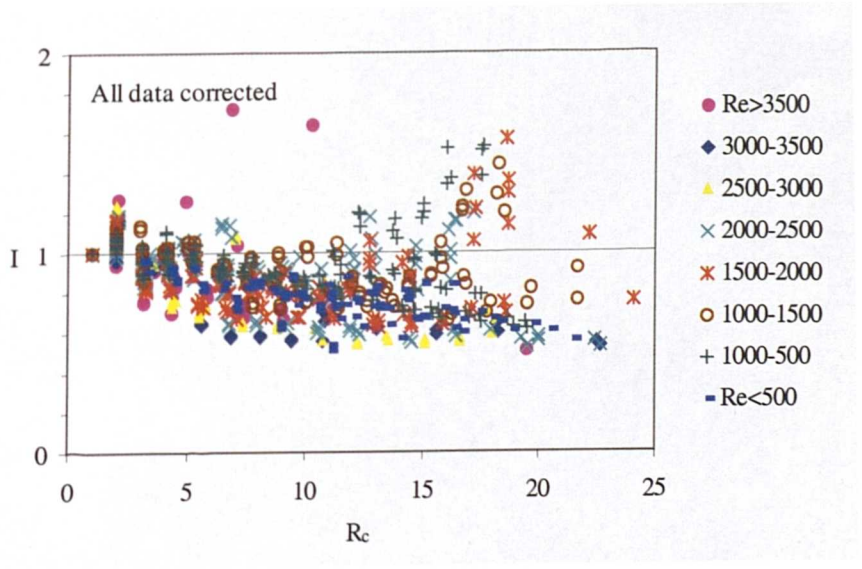

Plot 2

APPENDIX C6 INUNDATION ANALYSIS, DT<1 DATA REMOVED

Steam velocity dependence plots

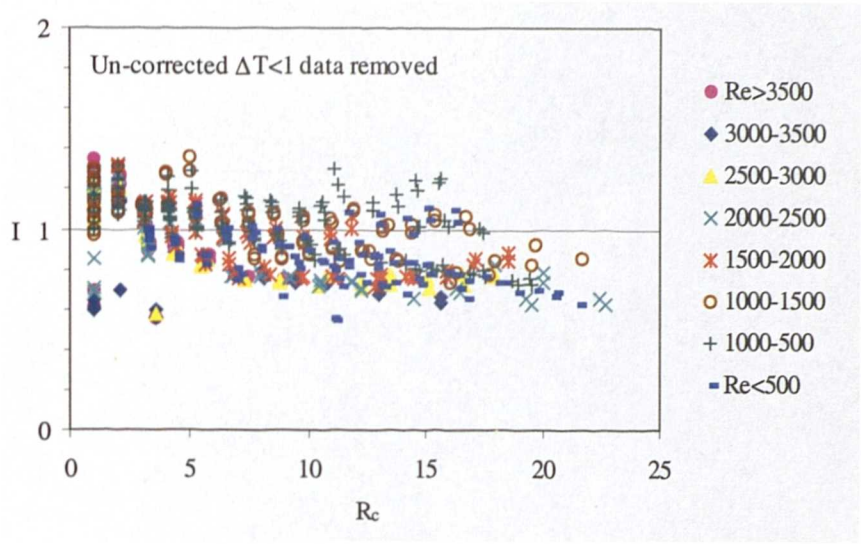

Plot 1

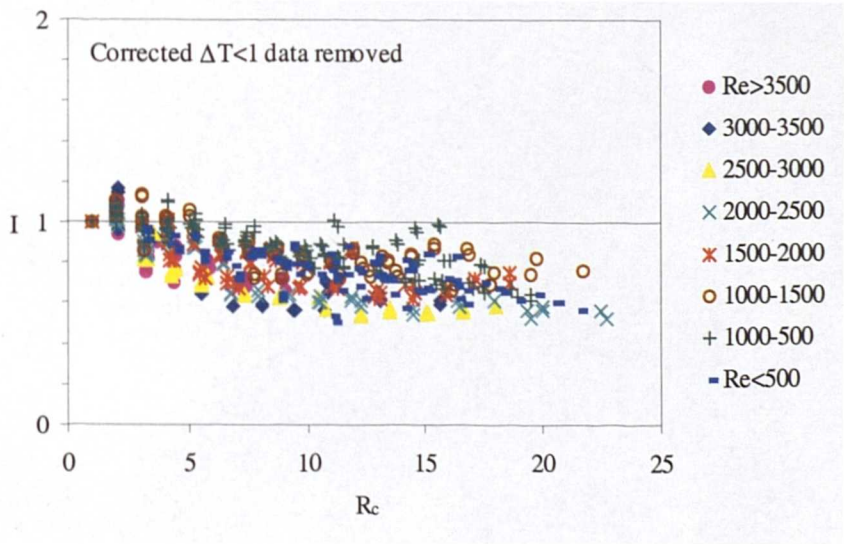

Plot 2

APPENDIX C7 HIGH VELOCITY LOW ΔT AIR ANALYSIS DATA

Shell-side heat transfer coefficients (kW/m^2K)						
Row number	T218 0%	T219 0%	T226 1%	T227 1%	Average 0%	Average 1%
1	33.74	36.62	34.62	37.79	35.18	36.19
2	41.99	46.44	42.01	45.09	44.21	43.55
3	35.13	36.19	33.95	36.26	35.66	35.10
4	37.38	42.65	34.84	39.67	40.05	37.25
5	45.31	48.36	37.00	47.17	46.83	42.08
6	36.83	40.83	30.79	34.17	38.83	32.48
7	41.81	48.41	32.88	39.16	45.11	36.02
8	59.67	64.8	34.04	41.23	62.23	37.63
9	51.64	63.54	31.03	32.41	57.59	31.72
10	42.66	31.42	20.78	22.18	37.04	21.48
11	-	-	14.53	30.42	-	22.47
12	-	-	-	-	-	-
13	-	-	-	-	-	-
14	-	-	-	-	-	-
15	-	-	-	-	-	-

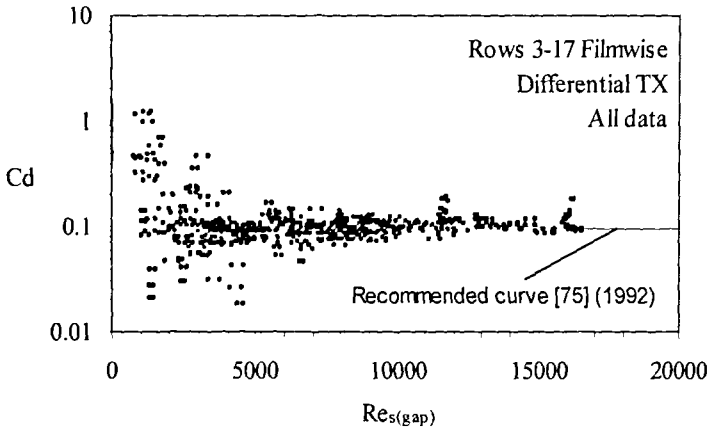
10
1
0.1
0.01
Cd
0
5000
10000
15000
20000
Res(gap)
Rows 3-17 Filmwise
Differential TX
All data
Recommended curve [75] (1992)

Plot 1

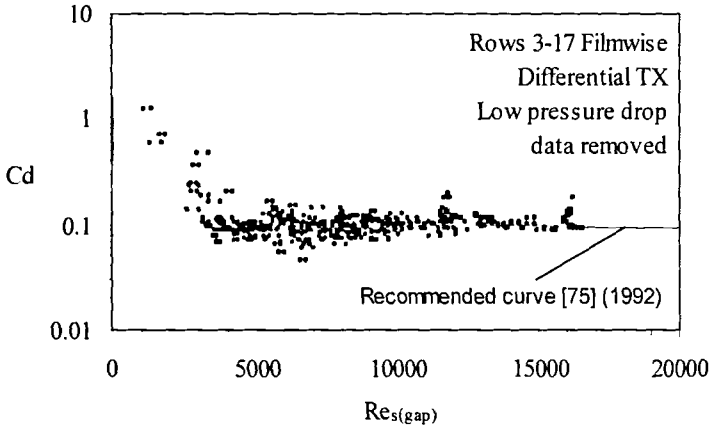
10
1
0.1
0.01
Cd
0
5000
10000
15000
20000
Res(gap)
Rows 3-17 Filmwise
Differential TX
Low pressure drop
data removed
Recommended curve [75] (1992)

Plot 2

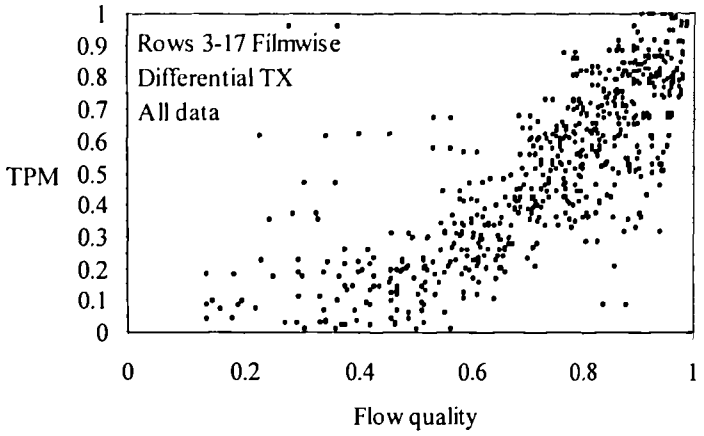
Rows 3-17 Filmwise
Differential TX
All data
TPM
Flow quality
0
0.1
0.2
0.3
0.4
0.5
0.6
0.7
0.8
0.9
1
0.2
0.4
0.6
0.8

Plot 2

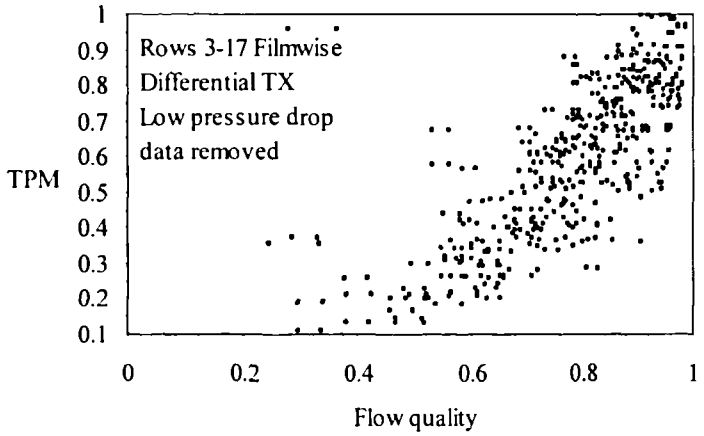
Rows 3-17 Filmwise
Differential TX
Low pressure drop
data removed
TPM
Flow quality
0
0.1
0.2
0.3
0.4
0.5
0.6
0.7
0.8
0.9
1
0.2
0.4
0.6
0.8

Plot 2

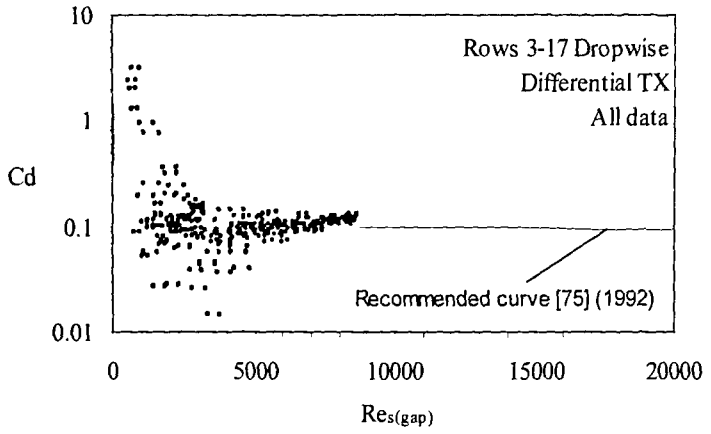
10
1
0.1
0.01
Cd
Rows 3-17 Dropwise
Differential TX
All data
Recommended curve [75] (1992)
0
5000
10000
15000
20000
Res(gap)

Plot 1

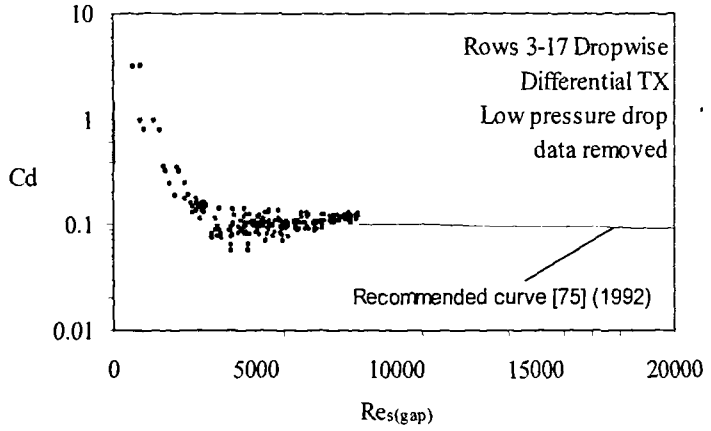
10
1
0.1
0.01
Cd
Rows 3-17 Dropwise
Differential TX
Low pressure drop
data removed
Recommended curve [75] (1992)
0
5000
10000
15000
20000
Res(gap)

Plot 2

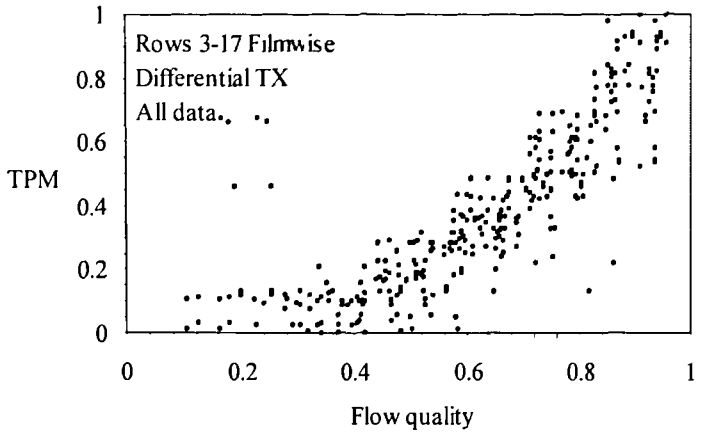
Rows 3-17 Filmwise
Differential TX
All data
TPM
Flow quality
0
0.2
0.4
0.6
0.8
1

Plot 1

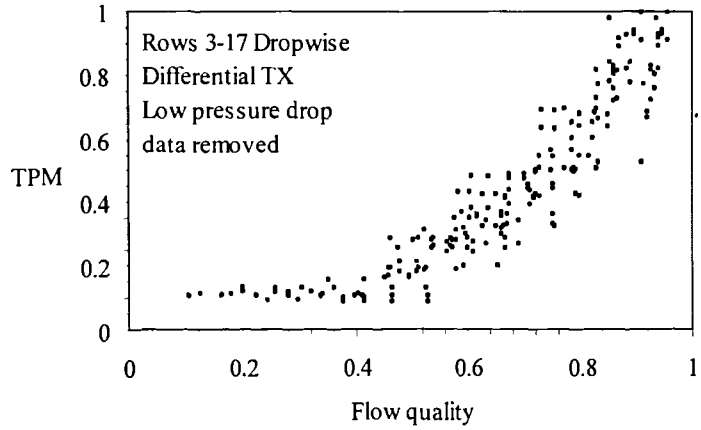
Rows 3-17 Dropwise
Differential TX
Low pressure drop
data removed
TPM
Flow quality
0
0.2
0.4
0.6
0.8
1

Plot 2